CANADIAN THESES ON MICROFICHE

THÈSES CANADIENNES SUR MICROFICHE

National Library of Canada
Collections Development Branch

Canadian Theses on
Microfiche Service

Ottawa, Canada
K1A 0N4

Bibliothèque nationale du Canada
Direction du développement des collections

Service des thèses canadiennes
sur microfiche

NOTICE

The quality of this microfiche is heavily dependent upon the quality of the original thesis submitted for microfilming. Every effort has been made to ensure the highest quality of reproduction possible.

If pages are missing, contact the university which granted the degree.

Some pages may have indistinct print especially if the original pages were typed with a poor typewriter ribbon or if the university sent us an inferior photocopy.

Previously copyrighted materials (journal articles, published tests, etc.) are not filmed.

Reproduction in full or in part of this film is governed by the Canadian Copyright Act, R.S.C. 1970, c. C-30. Please read the authorization forms which accompany this thesis.

AVIS

La qualité de cette microfiche dépend grandement de la qualité de la thèse soumise au microfilmage. Nous avons tout fait pour assurer une qualité supérieure de reproduction.

S'il manque des pages, veuillez communiquer avec l'université qui a conféré le grade.

La qualité d'impression de certaines pages peut laisser à désirer, surtout si les pages originales ont été dactylographiées à l'aide d'un ruban usé ou si l'université nous a fait parvenir une photocopie de qualité inférieure.

Les documents qui font déjà l'objet d'un droit d'auteur (articles de revue, examens publiés, etc.) ne sont pas microfilmés.

La reproduction, même partielle, de ce microfilm est soumise à la Loi canadienne sur le droit d'auteur, SRC 1970, c. C-30. Veuillez prendre connaissance des formules d'autorisation qui accompagnent cette thèse.

THIS DISSERTATION
HAS BEEN MICROFILMED
EXACTLY AS RECEIVED

LA THÈSE A ÉTÉ
MICROFILMÉE TELLE QUE
NOUS L'AVONS REÇUE

Canada

NL 339 (r. 85/09)

UNIVERSITÉ D'OTTAWA
UNIVERSITY OF OTTAWA

The University of Ottawa requires the signatures of all persons using or photocopying this thesis. Please sign below, and give address and date.

PREFACE

While extensive work has been done over many years on the electrochemistry of metals, until recently rather little knowledge has existed on electrochemical behavior of semi-metallic metal sulfides, many of which are degenerate semiconductors.

Interest in the electrochemistry of metal sulfides has been stimulated by their use in photoelectrochemistry, by their employment as cathode materials for primary and secondary batteries especially in combination with Li as anode material and in certain cases, on account of the possibilities for direct electrowinning of the metal by electrochemical treatment of its sulfide. In the case of battery materials, special interest has centered on FeS_2 and FeS particularly in development of the molten salt (450°C) Li/FeS and Li/FeS_2 secondary battery, while MoS_2 and TiS_2 have been widely studied as cathodes reversibly intercalatable by Li at ambient temperature for small rechargeable Li batteries for portable appliances, etc.

From a different point of view, interest in the electrochemical interfacial properties of mineral sulfides has arisen in relation to their separation from other material, gangue, by means of flotation in mineral processing.

In this thesis, an account is given of new work on the electrochemical surface reactivity of three mineral sulfides, galena, pyrite and pyrrhotite. In one of them, FeS_2, reduction of the

disulfide ion, S_2^{2-}, is involved and an interesting reversible surface process was discovered. This led to comparative experiments on other disulfides where the -S-S- linkage is in an organic structure as in cystine and α-lipoic acid. These were studied mainly at the Hg electrode with comparative experiments being made at Au and Pt. At PbS, on the other hand, a solution-soluble species is found to be generated in the electrochemical reaction of the mineral surface and no reversible processes are indicated, as is also found with pyrrhotite where only the monomeric sulfide ion, S^{2-}, exists in the structure.

In recent years, interest in this field of work has arisen at CANMET, Department of Energy, Mines and Resources, from whom financial support for this work has, in part, originated. In this connection, grateful acknowledgement is made to Dr. S.M. Ahmed for his interest in this work.

ACKNOWLEDGMENTS

The idea of the theme of this research was first suggested to me by Professor B.E. Conway upon my arrival: to compare mineral and organic sulfides electrochemically seemed to be an interesting topic. Since then I have been helped by numerous discussions with Professor Conway and the originally proposed theme branched out into the topics covered in this thesis. Therefore I would like to gratefully acknowledge all the help of my supervisor Professor Conway who, with typical generosity, was always prepared to give freely of his time either to deal with experimental research problems or in the discussions that arose during the preparation of the publications and this manuscript. Dr. Conway took the trouble to read this manuscript in detail and to comment on each of the Chapters.

It is also doubtful whether this work would have been completed without the help and enthusiasm of the staff of the Chemistry Department at University of Ottawa to whom I wish to express my grateful thanks:

Mr. Egon Kristof, whose suggestions helped the design and building of the cells and other glass equipment used during the work.

Mr. Joseph Halpern, who was always willing to solve any of the electrical problems which arose during the experiments and who also tried to keep the equipment in good working order.

Mrs. Eva Szabo for assistance in preparation of diagrams.

Mr. Werner Seinsch for his assistance in preparation of precision instruments.

To all my friends and colleagues in the electrochemical laboratory and this department with whom I worked over the past few years for many enjoyable and memorable moments we shared.

And to my friend Tam for his help in the very emergency instant while I was almost losing my "memory" of this thesis.

I am also thankful to Dr. Halina Angerstein-Kozlowska for occasional help and discussions.

My thanks are also due to Dr. F.C. Ho, for his help on my first touch in electrochemical experiments.

In addition, special thanks are extended to Mrs. Shui-Mui (May) Wong-Chang for her handling the word processor on "SCRIPT" of this thesis, and also to Mr. H.C. Oung, Mr. J.F. Huang, Mr. K.T. Wu, Mr. H.F. Sun, Mr. S.L. Wu and Mr. J.F. Chiang for their typing of this thesis into the terminal.

I should like to pay special appreciation to my little boy David Yun Kong for his great understanding, unexpected for his age, during the years.

Lastly, I would like to express my thanks to the University of Ottawa, Department of Chemistry, for the use of its research facilities.

CONTENTS

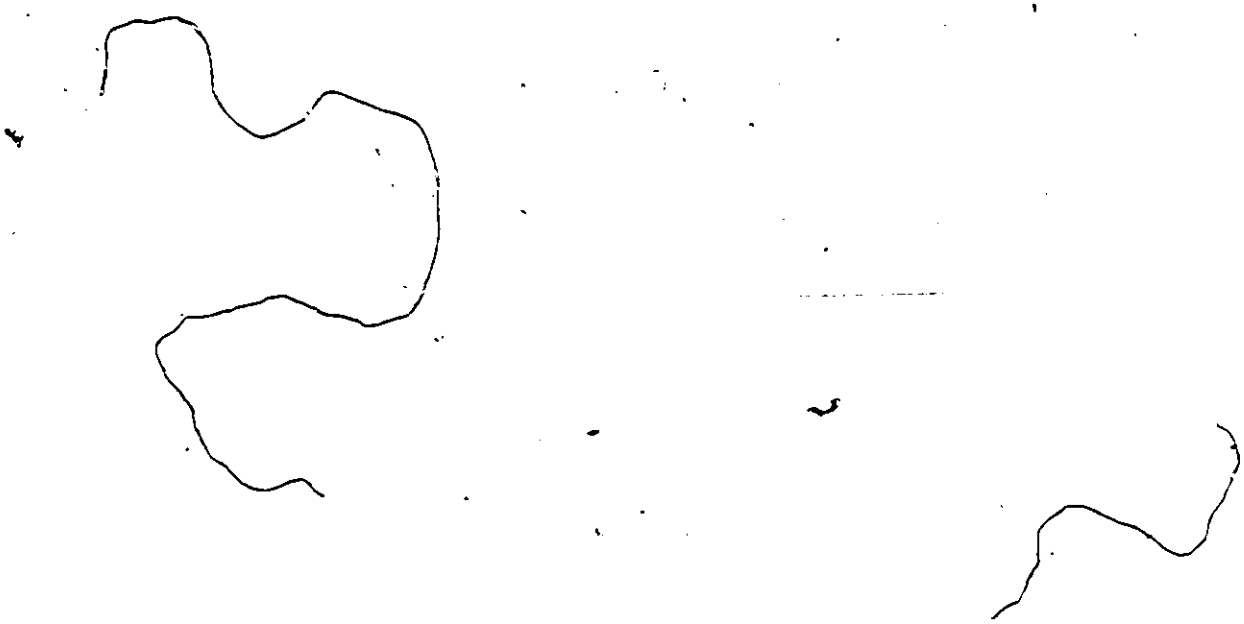

LIST OF FIGURES

BRIEF GLOSSARY OF TERMS AND SYMBOLS

α_a (= zFs/RT) for reversible charge-transfer process.

A Electrode surface area, cm^2.

$A(\omega)$ Open loop gain of the operational amplifier.

b (= zFs/RT) for irreversible charge-transfer process.

C Counter electrode.

C_{dl} Capacitance of double-layer charge distribution at electrode interface or (as a pseudo-capacitance) of an ad-layer where coverage θ is a function of potential V.

C_p Faradaic reaction capacitance.

C_O Bulk concentration of reactant.

CV Cyclic-voltammetry: the method for studying electrode reactions under controlled-potential conditions when the potential is cycled in the anodic and cathodic directions in a repetitive manner at constant voltage sweep-rate, $\pm dV/dt$; developed by Will and Knorr for the study of surface processes at noble metal electrodes.

D Diffusion coefficient.

dE The differance of Ec and Ee

d.l. Double-layer region: the potential range in a cyclic-voltammetry i-V profile over which the currents are predominantly, or only, those for charging of the double-layer capacitance.

E Potential, used in instrumentation in this thesis.

E_c Control potential in instrumentation.

E_e Existing potential in instrumentation.

E_H Potential measured with respect to that of a reversible H_2/H^+ electrode in the same solution ("Hydrogen scale").

Electrosorption: chemisorption of a radical or atom at an electrode surface as a result of a Faradaic charge-transfer process.

F Faraday constant.

Galvanostatic: controlled-current procedure.

i An experimentally measured current-density ($A\ cm^{-2}$).

i_o The exchange current-density (or reversible rete in terms of equal anodic and cathodic current-densities at the reversible potential of a process).

i_{lim} Limiting current-density due to potential-independent rate of a chemical step at an electrode in an electrochemical reaction sequence.

i_p Peak current density.

"iR" drop: potential drop near a working electrode due to passage of current (density) i across local resistance R of solution.

I Current used in instrumentation.

I Current, amp.

I_a Input current in instrumentation.

I_p Peak current.

K Absolute temperature, Kelvin.

Langmuir condition: condition for which the Langmuir isotherm

applies (approximately) to the adsorption behavior of some species.

M Molar concentration.

[O] Concentration of oxidized species of redox couple.

Potentiodynamic: controlled potential procedure used in a dynamic way with a time-variant potential.

Potentiostatic: controlled potential procedure.

q Charge for monolayer formation.

Q Charge for electrochemical reaction.

R Reference electrode.

R Resistance.

R Universal gas constant.

[R] Concentration of reduced species of redox couple.

R_{cw} Resistance in a cell between counter and working electrode.

RDE Rotating Disc Electrode.

R_i Internal resistance of power amplifier.

R_m Resistance of current meter or recorder.

R_x External resistance.

s Second.

s [= dV/dt ($V\ s^{-1}$)], sweeping-rate.

t Time.

T Temperature.

Tafel line: The linear overpotential (η) - log [current-density] relation found for many activation-controlled processes.

Tafel slope, b: The slope, $d\eta/d \log i$, of such a Tafel line.

V An electrode/solution potential difference.

V Volt, units of potential.

V_i Initial potential.

V_f Final potential.

V_P Peak potential.

V_{Pa} Peak potential for anodic sweep.

V_{Pc} Peak potential for cathodic sweep.

$V_{\frac{1}{2}}$ Half-wave potential.

W Working electrode.

z Number of electrons.

α Charge-transfer coefficient for electrochemical interfacial reaction.

α Transfer coefficient in the Tafel slope, $b = RT/\alpha F$.

β Barrier symmetry factor in an electron-transfer process.

ω Rotation speed.

ω Frequency.

η Activation overpotential = $V - V_{rev}$.

θ Coverage by an adsorbed intermediate or other species.

τ_h Holding time in CV experiment.

$(\Delta R/R)_{\parallel}$; Relative reflectivity change for parallel ($\parallel$) or perpendicularly ($\perp$) polarized light.

The other symbols used in this thesis have their usual meanings.

ABSTRACT

The work described in this thesis involves a study of the electrochemical behavior of some inorganic sulfide minerals, galena, pyrite, pyrrhotite, and some corresponding organic sulfur containing compounds: cystine/cysteine and thioctic acid. These substances present some interesting similiarities and differences to each other and also offer the possibility of examining the difference of properties which arise when the disulfide ion S_2^{2-} or monosulfide ion S^{2-} exist in the mineral crystal lattice in comparison with the situation where the -S-S- or -S-H is the main linkage of interest in the biological and organic substance.

Work was carried out by means of the potentiodynamic sweep method and its analogue, cyclic voltammetry, on single crystals of these minerals made into regular electrodes and rotating-disc electrodes which were polished suitably for the required experiments. For work with the organic sulfides in aqueous solutions, mercury pool electrodes were used together with platinum and gold rotating-disc electrodes, for control of mass-transfer. Experiments were carried out both in dilute acid solutions and at neutral and alkaline pH's with sodium borate and sodium carbonate supporting-electrolyte solutions.

At FeS_2, a reversible pH-dependent surface process is characterized and is associated with the reaction $S_2^{2-} + 2\ e \rightleftharpoons 2\ S^{2-}$. The

product ion (or SH^- in acid pH) appears to remain in the FeS_2 lattice, since there are no indications of a diffusion-controlled process involving solution-soluble species as is found, by contrast, with PbS electrodes. At pyrrhotite, $Fe_{1-x}S$, no reversible process is observed, which situation corresponds to the absence of reducible disulfide ion in this structure. Comparative behavior of galena, PbS, is presented.

Organic disulfides and thiols, e.g. cystine, cysteine and α-lipoic acid (thioctic acid), do not exhibit a directly reversible reduction/reoxidation process, but anodic and cathodic currents are observed at the Hg electrode through the mediation of Hg complexes with the -S or -SH groups, e.g. the so-called Hg cysteinate. The reactions observed are mostly diffusion-controlled but in a number of cases there is some parallel or series involvement of "surface" electrochemical processes, presumably through reaction of the Hg complexes.

The latter conclusions are reached through the results of cyclic-voltammetry experiments conducted at various potential sweep rates, the effects of electrode rotation to influence the diffusion-layer thickness and from reaction order experiments where concentration of the oxidized or reduced forms of the organic sulfides were varied. pH dependence of the reaction currents and redox potentials was also established.

Chapter I

INTRODUCTION

1.1 ORIGIN OF INTEREST IN ELECTROCHEMISTRY OF SULFIDES

Recently, there has been an increasing interest in the electrochemical properties of metal sulfides.

Mineral sulfides are usually converted to the metal by pyrometallurgical processes involving roasting in air, which produces gaseous sulfur dioxide, followed by reduction. The environmental requirements being imposed on sulfide smelters have led to a greater effort to develop hydrometallurgical routes for the treatment of sulfides in order to avoid the evolution of sulfur dioxide. Also until recent years, flotation is still a key process in concentrating sulfide ores, so that the interfacial properties of sulfide mineral crystals are of continuing interest. Other applications of sulfides are in the development of photovoltaic transducers for solar energy and as cathode materials in the development of high-energy batteries.

Cysteine or cystine are common constituents of proteins, especially keratin, where the oxidized form of the amino-acid moity, cystine, serves as a cross-linkage function through the -S-S- group, α-lipoic acid is one of most important coenzymes involving pyruvate cycles. Also the cysteine/cystine couple, α-lipoic acid and its reduced form, dithiol, provide an important redox system in protein, tissue and

metabolic biochemistry, and provide redox control in protein, or tissue structure where the -S-S- ——> 2 -SH process is involved.

1.1.1 Direct Reduction of Mineral Sulfides for Metal Winning

Metal electrowinning, electrorefining and electroplating represent major fields of molten salt and aqueous solution electrochemical endeavor. Few metals may be deposited in pure form at 100% current efficiency from aqueous solution, owing partly to the intervention of the hydrogen evolution reaction (which, if it occurred without substantial overpotential, would preclude the practical electrodeposition of many base metals). However, other factors such as oxide film formation, hydride formation, oxide deposition from stable oxycations, chemical reduction or oxidation reactions, especially those involving high and low oxidation states, with the solvent water, all impede the primary electrodeposition of many pure metals from aqueous media. Therefore, molten salts offer attractive nonaqueous environments for metal processing; molten salt systems offer distinct advantages over the only other possibility - use of organic solvents - e.g. with regard to cost, conductivity and current efficiency.

Various benefits, including wide limits of electrochemical stability, high ionic conductivity, good solvent properties for inorganic feedstocks and relatively small cathodic deposition overpotentials, have been reported, but there is still a need for studies contributing to a better understanding of mechanisms and improvements of electrolytic processes including phase relationships,

evaluation of the electrochemical series of metals in different solvents, the role of adsorbed water, viscosity and diffusion, the nature of the electrode processes involved, metal-electrolyte interaction, and such basic matters as polarization phenomena and current efficiencies.

1.1.2 Interfacial Electrochemistry in Flotation

The behavior of minerals with regard to their separation by flotation techniques is intricately connected with the local surface chemistry of the mineral and the double-layer properties of the interphase at the surface. In particular, the way in which the interfacial properties may change with potential of the surface is of some considerable importance with regard to the adhesion of air bubbles in flotation and in regard to how the air bubble adhesion may depend on the chemical condition and the charge of the mineral surface. The role of oxygen in determining the potential of the material and in changing the nature of the surface is also of considerable interest. Oxygen is also of importance in determining the chemical nature of the flotation agent itself when the latter is a substance of the xanthate or xanthogen type.

1.1.3 Metal Sulfides as Battery Cathode Materials

The storage of off-peak electrical energy from base-load plants in large secondary battery systems, for later delivery at peak demand, can increase capacity utilization and therefore decrease the cost of

electric power generation. It can also reduce the nation's dependence on fuel by providing an alternative to peak power generation by gas turbines. These applications, however, impose stringent cost, cycle life, and energy efficiency requirements on batteries which can not be met by those now commercially available.

High-temperature lithium-iron sulfide batteries offer considerable promise for electric utility load leveling and also for electric vehicle traction applications, because of their inherent high energy density and potentially low cost.

1.1.4 Organic Disulfides and Thiols

Interest in the electrochemistry of organic disulfides (cystine, α-lipoic or thioctic acid) and corresponding thiols has arisen in relation to developments in electroanalytical chemistry for the determination of protein structures. Also the possibility of a reversible redox system involving $-S-S- + 2\ H^+ + 2\ e \rightleftharpoons 2\ -S-H$ has attracted attention. Previous work indicates, however, that this direct redox process does not actually occur but that, at Hg, a reduction of disulfides and reoxidation of thiols can be made to take place but it proceeds only through one or more Hg complexes of the compounds involved at the Hg surface or with dissolved Hg-sulfide complexes in solution. Correspondingly, and rather surprisingly, the redox reaction does not proceed at Au. A more detailed review of the earlier work on this topic is given below.

1.2 REVIEW OF ELECTROCHEMISTRY OF SULFIDES

1.2.1 Previous Work on Inorganic Mineral Sulfides

1) Flotation and reduction of oxygen

In the extraction of metals from their ores, the hydrometallurgical operation receives feed from flotation. These processes play an important role in modern metallurgical operations, especially in relation to minimization of environmental pollution.

Chander and Fuerstenau (1) interpreted the natural floatability of MoS_2 and studied the molybdenite-potassium-diethyldithio-phosphate system. Hoover and Malhotra (2) investigated the wetting and spreading of hydrocarbon oils with surfactant on the faces of molybdenite; Voskanyan (3) studied the effect of electrochemical treatment of suspensions of pyrite, chalcopyrite and molybdenite on sorption of a sulfhydryl collector at the mineral surface. Almaev (4) optimized the xanthate feed in the flotation of molybdenite, chalcopyrite, and pyrrhotite at the electrode potential region for maximum recovery of the metals.

Romanov et al (5) studied hydrogen and oxygen evolution in pyrite flotation. They found that electrolytic hydrogen hardly influences the pyrite output while electrolytic evolution of oxygen led to 98% pyrite yield in the presence of K-butyl-xanthogenate. Rozhdlestvenskaya et al (6) worked on the effects of complexing agents on the electroxidation of pyrite. Studies on the relation of electrochemical and flotational behavior of pyrite were reported by Yashina et al (7) and of galena by Lamache et al (8) under varying pH

conditions. Work on pyrite and galena removal from kerogen materials was reported by Yen et al (9) and by Abramov (10), respectively, on galena and chalcopyrite while adsorption of dithiophosphates and dithiophosphonates was studied by Solozhenkin (11). Ahmed (12,13) made interesting studies on the electrocatalytic activity and mechanisms of reactions at galena, pyrite and cobalt sulfide (Co_3S_4) and of oxygen reduction at these materials in relation to xanthate adsorption and flotation; he pointed out that the catalytic activity for oxygen reduction, the electrode potentials and the xanthate adsorption, as shown by bubble attachment within certain pH limits, all varied in the order Co_3S_4 > pyrite >> PbS, indicating considerable dependence of the redox processes in flotation on the d-electron character of the sulfides. Also an heterogeneous two-site electrochemical mechanism for reduction of oxygen and oxidative adsorption of xanthate on galena was proposed.

In their investigation of the galena-xanthate-oxygen flotation system, Tolun and Kitchener (14) concluded that galena was compartively inefficient as an oxygen-reduction catalyst. Peters and Majima (15) derived polarization curves for oxygen reduction over a range of temperatures; this process exhibits a mass-transfer controlled limiting current and pyrite is in a "passive" state after exposure to air; ordinarily, the film formed on pyrite that leads to passivity is present in air and may be adsorbed oxygen or an oxygen-sulfur compound. Fuerstenau et al (16) found that the point of zero charge of pyrite is unchanged in the presence of different xanthate additions; this indicates surprisingly that adsorption of xanthate is

physical in nature and that no chemical or specific adsorption of xanthate take place. Majima and Takeda (17) confirmed that in the process of anodic polarization of pyrite in a xanthate solution, xanthate is oxidized to dixanthogen, which depresses oxygen evolution at higher potentials. At low pH, Biegler et al (18) showed that the rate of reduction of oxygen on pyrite is determined by the step $O_2 + e \longrightarrow O_2^{2-}$ while, in alkaline solution, the rates of subsequent steps

$$O_2^{2-} + 2H^+ + e \longrightarrow H_2O_2 \xrightarrow{2H^+ + 2e} 2H_2O$$

$$\downarrow$$

$$H_2O_2 \text{ (solution)}$$

become kinetically important. Nicol, Paul and Diggle (19) found that cathodic reduction of natural galena gave Pb metal and, depending on the pH, various forms of the sulfide ion; the reduction of anodically produced sulfur is possible but the rate is strongly dependent on the amount of sulfur present and the history of its formation.

Kishi et al (20) noted the rate of reduction of oxygen on some sulfides decreases in the order βNiS > CoS > αNiS > FeS; this order is the inverse for the Volmer reaction (H_2O^+ discharge) on the sulfides: the reaction sites for oxygen reduction are the metal while sites for the Volmer reaction are sulfur sites. Kitayama et al (21) examined cathodic reduction of oxygen on cobalt sulfides with various ratios of Co:S in 0.1M KOH; the activity for electroreduction increased with an increase in Co_3S_4 content. It was suggested that the direct four-electron reduction of oxygen to OH^- proceeds in parallel with the two-electron reduction to HO_2^- on electrodes containing a large fraction of Co_3S_4, whereas no four-electron reduction took place on electrodes containing none, or a small percentage of Co_3S_4. Ahmed and Gerischer (22) indicated that oxygen reduction on MoS_2 is influenced by surface orientation.

In addition, basic principles and practical application of electrochemistry to flotation of sulfides minerals were extensively reviewed by Woods (258), Poling (258), Richardson and Maust Jr. (259), Liza (260), Rogers (261) and Ahmed (262).

2) Anodic oxidation of sulfides

Electrowinning of metals from sulfide minerals by direct anodic attack (corrosive leaching behavoir) was observed by Masuko and Hisamatsu (23). The rest potentials and corresponding currents of pyrite were rather unstable and strongly dependent on the composition of the electrolyte. Wrabetz (24) and Sato (25) concluded that the metal and elemental sulfur are produced in the first step of anodic oxidation of metal sulfides. In the case of pyrite, the suggested first reaction step is

$$FeS_2 \longrightarrow Fe^{2+} + 2\ S^0 + 2\ e$$

This is followed by a second electrochemical step in which the ferrous ions are oxidized to ferric ions; the latter then seem to convert sulfur to sulfate in a purely chemical oxidation reaction, so the final reaction products are ferric and sulfate ions, as indeed was observed by Peters and Majima (15) who represented the overall anodic reaction as

$$FeS_2 + 8\ H_2O \rightleftharpoons Fe^{3+} + 2\ SO_4^{2-} + 16\ H^+ + 15\ e$$

The metal and sulfur activities are not constant and the electrode potentals will consequently also be variable due to small deviations

from the ideal stoichiometric composition. This behavior has been experimentally verified by Trampler (26) for PbS, by Noddack and Wrabetz (27) for Ag_2S and by Springer (28) for pyrite, and theoretically discussed by Sato (29). The cathodic reaction commences only below the equilibrium potential for hydrogen evolution. As Fe^{2+} and H_2S are produced as well, a preferential leaching of sulfur is expected, but apparently the development of H_2S only proceeds when hydrogen is also formed (28). Hamilton and Woods (30) studied the surface oxidation of pyrite and pyrrhotite with the linear potential sweep method. It was found that pyrite oxidized to both sulfur and sulfate. The formation of sulfur is restricted to the order of a monolayer at pH 9.2 and 13, but significant yields of sulfur and sulfate arise at pH 4.6. The proportion of sulfate formed increases rapidly with increase in potential; also, sulfur is the major product of pyrrhotite oxidation at pH 4.6, 9.2 and 13, while sulfate is formed, as well, in significant quantities, particularly in the alkaline solutions. Oxidation of pyrrhotite is strongly inhibited by the surface ferric oxide produced. Biegler and Swift (31) argued that the overall anodic reaction is a combination of two pathways leading to sulfate and elemental sulfur, the proportion of reaction in each pathway varying linearly with potential. As with pyrite, the sulfate yield increases with increasing potential but elemental sulfur is not an intermediate in the sulfate route. The mechanism suggested for this reaction involves adsorption of hydroxyl radicals and oxygen derived from water, with the second charge-transfer step being rate-determining:

$$FeS_2 + H_2O \rightleftharpoons FeS_2(O)_{ads} + 2\,H^+ + 2\,e$$

$$FeS_2(O)_{ads} + H_2O \rightleftharpoons FeS_2(HO_2)_{ads} + H^+ + e$$

or $$FeS_2 + 2\,H_2O \rightleftharpoons FeS_2(OH_{ads})_2 + 2\,H^+ + 2\,e$$

$$FeS_2(OH_{ads})_2 \rightleftharpoons FeS_2(HO_2)_{ads} + H^+ + e$$

Bailey and Peters (32) reported a study of the decomposition of pyrite in acid by pressure leaching in the presence of O_2 at high pressure and by anodization. By using ^{18}O tracer tests, they showed that the oxygen atoms in the sulfate produced by pressure leaching come from the water and not from the molecular oxygen. This observation, together with the electrochemical measurements at the elevated temperatures and pressures used in the pressure leaching experiments, are consistent with an electrochemical mechanism in which the cathodic reaction is reduction of oxygen at the pyrite surface and the anodic reaction is the sum of two reactions: one the oxidation to Fe^{3+} with production of sulfate and the other oxidation to Fe^{2+} and elemental sulfur.

Meyer (33) reported, in strongly basic solution, a semi-amorphous film was formed and a diffusion limited-plateau current, approximately proportional to hydroxide concentration, was observed. No visible film was formed in acid solution and the reaction rate increased as the pH was increased. Yashina and Olerskaya (34) noted that regions of non-stoichiometric Fe_xS_{1-x} and the the iron oxides, Fe_2O_3 and Fe_3O_4, were developed on the surface of pyrite after subjection to anodic polarization. During anodic dissolution of copper sulfide CuS,

$Cu_{2-x}S$, in sulfuric acid, Hillrichs and Bertram (35,36,37) observed the formation of metastable non-stoichiometric copper oxide. Ammou-Chokroum et al (38) noted the formation of a passive film at low potentials (0.5-0.7 V vs S.H.E.). It was an electronically conducting phase formed during anodic polarization of chalcopyrite in this potential region; pH had only a modest influence on the results. Bauer et al (39) and Jones (40) found an initial preferential release of iron from the chalcopyrite lattice during anodic dissolution. This is consistent with the reaction which was confirmed and proposed by Warren et al (41) as:

$$CuFeS_2 \longrightarrow Cu_{1-x}Fe_{1-y}S_{2-z} + X\,Cu^{2+} + Y\,Fe^{2+} + Z\,S^{o} + 2(X+Y)\,e$$

For the condition Y>X, the compound or defect structure, $Cu_{1-x}Fe_{1-y}S_{2-z}$ is an intermediate product phase which, mixed with sulfur, forms an electron conducting passive layer on the minneral surface.

Parker (42) regards the intermediates formed in oxidation of chalcopyrite as polysulfides having semiconducting properties. Ammou-Chokroum et al (38) suggested that cupric ions released at the surface react with H_2S to form CuS, the H_2S having been formed by the electroless dissolution of chalcopyrite in acid solutions. Warren et al (41) proposed that a second intermediate forming in the region 0.70 to 0.75 V vs S.H.E. may be represented by

$$Cu_{1-x}Fe_{1-y}S_{2-z} \longrightarrow (2-z)CuS_{(n-z)} + (1-y)Cu^{2+} + (1-y)Fe^{2+} + 2(1-y)e$$

One of the principal problems in electrowinning of lead from galena is the limited number of soluble lead salts which can be formed, so that this puts several restraints on the choice of the medium. Many published papers in the literature (43,44,45) report studies in perchlorate medium in which the lead oxidation is accompanied by formation of insoluble oxides. Ghali and Dandapani (46,47,48) indicated when lead sulfide is anodically dissolved in hydrochloric acid at high anodic potential, direct electrowinning is feasible and obstruction due to passivation by the products formed could be minimized by increasing the temperature, the acid and the chloride concentrations or by addition of glycine.

Mazalov et al (49) reported anodic polarization behavior of galena in relation to NaOH concentration and temperature. Gardner and Woods (50) indicated that, in acid media, Pb^{2+} ions are dissolved leaving a surface layer of sulfur; the sulfur produced by the electroanodic reaction is of an amorphous form which inhibits further oxidation of the galena surface. The surface film is, however, converted by a nucleation and growth mechanism to a crystalline form which is sufficiently porous to allow continued oxidation of the underlying galena. The predominant Pb species formed at pH 6.8-11 is considered to be PbO together with a monolayer of products of anodic oxidation, PbO + S, inhibiting the oxidation process.

Power (51,52) showed that the passive layer formed on NiS or Ni_3S_2 during oxidation is a mixture of sulfur and sulfur-rich sulfide. At higher potentials complex anion-dependent dissolution behavior, involving the formation of elemental surfur and sulfur oxyanions,

occurs. At cathodic potentials non-oxidative acid dissolution with the formation of H_2S is observed concurrently with the evolution of hydrogen and the production of metallic nickel. Price and Davenport (53) reported decomposition of nickel sulfide; Ni_3S_2, βNiS, with loss Ni^{2+} ions through the series:

$$Ni_{1.5}S \longrightarrow Ni_{1.2}S \longrightarrow NiS_2 \longrightarrow Ni^{2+} + 2\ S^0$$

The dissolution behavior of crystalline molybdenite in hypochlorite solutions has been investigated by Krishnaswamy and Fuerstenau (54); dissolution is found to be extremely anisotropic in character; especially, reaction occurs only at exposed edges of the S-Mo-S sandwich structure and proceeds along the sandwich layers; the anodic reaction is hole-limited. The possibility of an electrochemical mechanism has also been suggested with charge-transfer through the molybdenite crystal. In terms of stable products, the oxidation of molybdenite may be represented as

$$MoS_2 + 24\ OH^- \longrightarrow MoO_4^{2-} + 2\ SO_4^{2-} + 12H_2O + 18\ e$$

The general experience with anodic oxidation of sulfide minerals is that sulfur forms, as an element, and resists oxidation; when the oxidation potential is below 0.8 V S.H.E., the reaction may be written, in the case of MoS_2, as

$$MoS_2 + 8\ OH^- \longrightarrow MoO_4^{2-} + 2\ S^0 + 4\ H_2O + 6\ e$$

The sulfur formed in this manner may act as a protective layer and inhibit further reaction, particularly on the basal plane of molybdenite where the packing density is high (55).

3) Semiconductor properties and photoelectrochemical behavoir

Semiconductor properties

Spring (28) observed that the limiting photo-currents, which are characteristic for ideal semiconductors, could not be detected on pyrite, galena and chalcopyrite. Perhaps this experiment was not properly controlled or conducted or could be caused by the impurity of the materials. The polarization curve slopes for pyrite are about 120 mV per decade change of current both for anodic and cathodic processes (28); a slope of 59 mV is expected if a one electron transfer step is involved on an ideal semiconductor surface (56,57) whereas a value of about twice as much would result for the same reaction on a metal. He therefore concluded that the mineral does not behave as an ideal semiconductor in the investigated range of moderate current densities. This is in agreement with the investigations of Kunori and Ishii (58), and also Biegler (59). Biegler and Swift (60) confirmed this conclusion for pyrite. Gerischer (61) observed that at CdS under illumination the current increases to a limiting value as the potential is increased. Studies of the electrocatalytic activity of CdS toward the redox couples Fe^{2+}/Fe^{3+}, $Fe(CN^-)_6^{3-}/Fe(CN^-)_6^{4-}$ and I^-/I_3^- by Tyagai (62), and CdS, MoS_2 by Gerischer (63) have shown that the activity depends on the formation of short-lived surface states (i.e., energy levels between the conductance and valence bands arising from specific adsorption of ions and lattice defects (61,62,63)). Ahmed and Gerischer (22) found

that the current densities and rate constants for oxidation/reduction of $Cu(NH_3)_4^{2+}/Cu(NH_3)_4^{+}$, $Fe(CN^-)_6^{3-}/Fe(CN^-)_6^{4-}$ and Fe^{3+}/Fe^{2+} couples are one order of magnitude larger for the ||-c surface than for the ⊥-c surface of MoS_2.

Electrophoretic mobility measurements by Healy (64) provide some evidence for specific adsorption on ZnS and PbS. Although the anodic dissolution of the more conductive sulfides does not appear to depend on semiconductor behavior, the leaching of galena by Eadington and Prosser (65) shows effects of both light and stoichiometry (66), indicating a "semiconductor" type of behavior. Results from surface photovoltage and electrochemical studies (67) indicated that at the rest potential, the surface potential of the degenerate n-type and slightly p-type galena, was large and negative, corresponding to an electron-deficient or hole-rich charge. Phillips and Spitler (68) observed that electron/hole recombination plays a significant role in the aqueous photoelectrochemistry of MoS_2 and $MoSe_2$ single crystals.

Photoelectrochemical behavior

The stability of n-type CdS electrodes toward photoanodic dissolution in aqueous solution, using Fe(II)-EDTA as reductant, has been studied by Wilson and Park (69), and Tenne improved their stability by addition of indifferent salts such as NaCl (70), also some redox couples as $Fe(CN)_6^{3-/4-}$ (260), I^-/I_3^- (265), and S^{2-}/S_n^{2-} (271) can partly prevent photodissolution. An and She, Xiao Wang and Chang (71) have studied CdS and Cu_2S for solar cells while Rothwarf and Barnett (72) investigated CdS-Cu_2S solar cell materials and, using $Cd_{1-x}Zn_xS$ in place of CdS, reached a practically attainable efficiency of 15% and a theoretical efficiency of greater than 26% for solar energy conversion.

In recent years, work has centered mostly on layer-type structured sulfides such as ZrS_2 (73), WS_2 (74,75,76) and especially MoS_2 (22,74-91) or modified surfaces of MoS_2. Tributsch (77-79) indicated that the covalent bonding character of this layer crystal and a Mo dz^2 band which is split off from the 4d molybdenum conduction band and overlaps the sulfur 3p valence band, gives rise to reaction behavior which is very different from that found with polar metal-sulfur compounds: thus, sulfate and not molecular sulfur is the main product of the electrochemical and photo-electrochemical oxidation of MoS_2 which exists as an intrinsic semiconductor material. A parallel photochemical liberation of molecular oxygen at low electrode potentials by reaction with H_2O could be detected on freshly prepared surfaces illuminated with light at 400-715 nm. Ahmed (88) and Gerischer (80,87) first found and discussed the anisotropic photoelectrochemical effects on MoS_2 due to surface orientation and investigated the role of cleavage steps and either line or screw dislocations. The MoS_2 photoanode was found to be remarkably stablized by specific adsorption of I^- on the surface (74,76-78,86,92,93). MoS_2 was also demonstrated to be able to serve as a durable photo-anode for the photogeneration of Br_2 or Cl_2 (81).

Moreover extensive reviews on photoelectrochemistry of semiconductors has been published by Memming (263), Gerisher (264,265), Rajeshwar, Singh and DuBow (266), Harris and Wilson (267), Nozik (268), and Morrison (269).

4) Sulfides as cathode materials in high energy-density batteries

The recent work on high energy-density batteries, which are required for electric vehicle propulsion and for the storage of off-peak and solar power, has been attracting serious attention. In

considering the selection of electrode matrials and electrolytes for high energy-density betteries the following conclusions have been reached: (i) the active alkali metals with atomic weight less than zinc are to be utilized as anodes; (ii) dry organic and inorganic electrolytes, solid-electrolytes and molten-salts are required as electrolytes, and (iii) an electronically conductive, highly oxidizing solid that can react readily and in an electrochemically reversible way with the active alkali metal as the cathode is desirable.

Most researchers have aimed recently at using layer structure chalcogenides as intercalation cathodes for rechargeable Li batteries due to the ease of redeposition of the anodic metal. Whittingham et al (94-97) and Denes, Sibernagel et al (98,99) have reported, in a series of papers, the fundamental properties of Li_xTiS_2 type intercalation compounds. According to Whittingham (100) these investigations were initiated by their finding that titanium disulfide could be used as the cathode of a high energy-density reversible battery with a lithium anode (101), which, on discharge, transfers Li^+ ions to the host lattice TiS_2 in an intercalation reaction. Bichon et al (102), Chianelli et al (103) also reported the intercalated location of small alkali ions. Rickel and Schollhorn (104) found the same behavior for metallic TiS_2 in Li_xTiS_2 : the lattice changes continuously from a "CdI" to a "NiAs" structure as x varies from 0 to 1. The structure of Na_xTiS_2 was elucidated by Leblanc-Soreau et al (105) for various x values. These structure studies are used to characterize the expansion of lattices and to define their compositions and stability ranges (96). The diffusivity of Na^+ ion in $NaTi_{1+y}S_2$ has been measured experimentally by Winn (106). The

discharge rate for the electrode is related, of course, to the diffusivity of the mobile ion in the intercalation agent. The diffusivity-controlled discharge rate is critically dependent on stoichiometry of $A_xM_{1+y}X_2$ compounds (107). Cell voltage stability with $Na_xTi_{1+y}S_2$ when $0.54 < x$ has been studied by Winn and Steele (108).

Besenhard, Meyer and Schoellhorn (109) studied the cathodic reduction of MoS_2 in DMSO electrolytes containing alkali-metal cations A^+. Discharge results in the formation of ternary phases $A_{0.125}(DMSO)_y[MoS_2]^{0.125-}$ with highly mobile solvated interlayer cations. Reaction in DME electrolyte gives similar products. Basal spacings were found to be dependent on solvent type and on the ionic radius of A^+; further reduction of these compounds is associated with irreversible processes. Haering and Stiles (110) improved the dichalcogenide cathode by dopeing with Na, K, Cs and Rb. Suib et al (111) and Jacobson et al (112) studied the structural effects on the electrochemical capacity and behavior of molybdenite - TaS_2 intercalates. Kumagai et al (113) examined the charge-discharge characteristics and structural changes in various niobium sulfide cathodes for lithium-nonaqueous secondary batteries. Johnson et al (114) studied lithium titanium sulfide, Li_xTiS_2, and lithium sodium titanium sulfide, $Li_xNa_yTiS_2$, using a polymer electrolyte by varing x. Zanini el al (115) investigated the behavior of Na intercalated in TiS_2, TaS_2 and NbS_2 with β-alumina as a solid electrolyte. Eibschuetz et al (116) indicated that in lithium intercalated vanadium disulfide batteries, when some of the vanadium is replaced by iron, the reversibity of the cathode is greatly improved. The behavior of NbS_2,

TiS_2 and TaS_2 electrodes in Ag solid-state cells was investigated with kinetic, diffusion and thermodynamic studies by Patriarca et al (117).

Another family of rechargable battery systems comprises anodes of lithium or lithium alloys. Systems utilizing cathodes of sulfur or a metal sulfide, and a molten-salt electrolyte have been developed at Argonne laboratory (118-120) and by other groups (121-123). With FeS cells the examination by Mrazek and Batlles (124) showed that the reaction between an FeS electrode and potassium in LiCl-KCl electrolyte forms a Li-K-Fe-S compound, designed "J-phase". This reaction causes high polarization which results in low utilization of the active material in the cathode. Steunerberg et al (125) modified the J-phase by addition of Cu_2S to the FeS and reduced the polarization of the FeS electrode, resulting in much improved utilization of the theoretical capacity (126), but excessive swelling of the electrode still occurred (127). In the absence of potassium from these electrolyte, Shimotake and Vissers (128) using LiF-LiCl-LiI or LiF-LiCl-LiBr cells, demonstrated significantly higher performance. With FeS cells, swelling of the cathode is more controllable than in FeS_2 cells; however, the expansion of the cathodes was more than expected from the cell reaction (129). Addition of CoS_2 to FeS_2 improved the utilization of the cell reactant and lowered both diffusional and ohmic resistances significantly (130). Shimotake et al, developed another approach to solve the above problems by assembly of Li-Al/FeS or Li-Al/FeS_2 cells in the uncharged state; experimental results showed significant improvement. Inoue and Koura (123) using

x-ray and metallugical methods, as well as electrochemical measurements, characterized the discharge and charge reactions for cathodes of Al/FeS_2 molten-salt secondary cells. The Li_xFeS_2 cathode in nonaqueous electrolytes was studied at room temperature by Brec, Dugast and Le Mehaute (131). An Al/FeS_2 cell employing an organic electrolyte operating at room temperature was investigated by Takahashi and Koura (132). A Li battery embodiment using Li anodes with complex metal sulfide cathodes for nonaqueous cells has been granted a patent to Evans and Leger (133). Also McKee and Park (134) obtained patent in the U.S. for their electrode comprising MoS_2 and I_2 for use in fuel cells . Hodes, Manassen and Cahen (135) also hold a patent for use of chalcogenides coated on stainless-steel electrodes for a photo-electrochemical cell.

1.2.2 Previous Work on Organic Sulfides

Many compounds of pharmacological interest are involved in biological redox processes and the understanding of their electrochemistry may contribute to better perceptions of the role of these compounds in biochemical processes in addition to improved methods for their analysis.

Interest in the electrochemistry of organic sulfides orginates from the early observations of Brdička (136) in polarography that cystine and some proteins give rise to a "catalytic" effect on cathodic hydrogen overpotential analogous to the behavior of some alkaloids (137,138). These effects were traced to the -S-S- or -SH groups in the structure of these molecules; in fact, on the basis of

quantitative comparison of the effects of cysteine (I)[1] and cystine (II)[2], the former molecule was identified as the source of the catalytic effect, being itself produced by 2e, $2H^+$ reduction of cystine (II). Similar effects were demonstrated with glutathione and derived dipeptides. The effects of S-containing proteins arise similarly (139).

The mechanism of activation of the H_2 evolution reaction was related by Brdička (136) to loosening of the S-H bond in -SH groups in cysteine through complexing with the Co^{2+} ion, followed by discharge of the proton from the -SH complex rather than directly from water (cf. ref. 138). Protonation from water then follows in a rapid step; thus the -SH group acts as a mediator facilitating the proton discharge step in cathodic H_2 evolution.

Considerable evidence has accumulated (140-150) that S-containing molecules like cysteine and cystine, and related proteins, are strongly adsorbed at the Hg surface. Conway, Bockris and Lovreček (138) suggested that such strongly adsorbed molecules can act as "proton carriers" in the double-layer, facilating proton transfer and the kinetics of the hydrogen evolution reaction. The catalytic effects with -SH molecules are thus analogous to the similar effects observed with alkaloids (137,138) where the N hetero-atom centre in the protonated state provides a carrier of H^+ for discharge in the inner region of the double-layer at Hg. Apart from the role of Co^{2+} complexation in Brdička's work (136) this mechanism is seen to be

---

[1] See p. 48 for the chemical formula.

[2] See p. 48 for the chemical formula.

analogous to that of Brdička.

In biochemical reaction pathways (143,151), the reduction of disulfide compounds such as cyctine or 6:8 dithiooctanoic acid ("thioctic acid" system), to cysteine or 6:8 dimercaptooctanoic acid, respectively, and their re-formation by reoxidation, provide an hydrogen carrier process.

Cipris and Pouli (152) have been granted a U.S. patent for the reduction of disulfides in the presence of halide ions to form corresponding thiols by using MX_2 type cathodes, where M is Mo, Nb, Ta, Ti, V, W or Zr and X is S or Se. Wong and Wang (153) prepared cysteine from cystine by reduction on a stainless-steel electrode. Khusainov and Rafikov (154) obtained similiar results on Ag coated with anodically deposited Ag oxide.

Catalytic cathodic hydrogen liberation in solutions of cobalt(II), or nickel(II) complexed with cysteine has been investigated by Toropova et al (155) and Medyantseva (156), in solutions of a molybdenum complex by Lamache-Duhameaux (157) and in the presence of peptides containing cysteine with cobalt(II) by Kadleček et al (158).

Returning to the electrochemistry of the cystine/cysteine couple, it is to be noted that Brdička's work led to a number of further papers on the mechanism of the redox process and on the role of the Hg surface leading to specific complex-formation (140,141,143) with the -S-S- or -SH functions. Interest in this topic extends to the present time when a number of new papers have appeared in the field over the past ten years (142,159,160-162), which we shall refer to below. In addition to the electrochemical behavior of cysteine, cystine and

α-lipoc acid (thioctic acid) (III)[3] a 5-membered disulfide ring compound, has also been examined at Hg. This molecule is again one of biochemical, as well as electrochemical, interest as it is involved in the reactions of the enzyme dihydrolipoyl-transacetylase (159) that is one of the three enzymes making up the important pyruvate dehydrogenase system; it employs the -S-S- ——> 2 -SH redox again as a mechanism of H transfer.

Cystine and cysteine, despite common reference in texts on organic chemistry, are interconverted through facile reduction or oxidation processes. The interconversion of the molecules themselves as a reversible electrochemical reaction, as with the quinone/hydroquinone system, is not practically realized, e.g. at noble metals. On the other hand, at mercury, cysteine can undergo aerial oxidation to a mercury complex through the reaction

$$Hg + 2\ RSH \longrightarrow Hg(SR)_2 + 2\ H^+ + 2\ e \qquad (1)$$

or, correspondingly, it was shown by Kolthoff and Barnum (140,141) that cystine reacts according to

$$RSSR + [Hg] \longrightarrow [Hg](SR)_2$$

where [Hg] represents the surface of a mercury electrode. The complex $[Hg](SR)_2$ can then undergo electrochemical reduction to cysteine by the reverse of reaction (1). Similar surface complexes of α-lipoic acid are recognized (143,159):

---

[3] See p. 49 for the chemical formula.

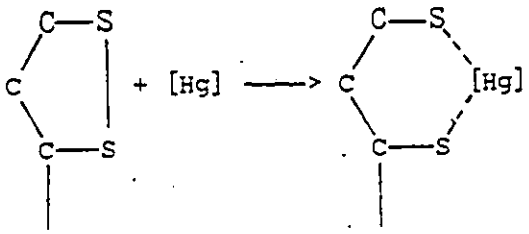

or through electrochemical oxidation of dihydrolipoic acid.

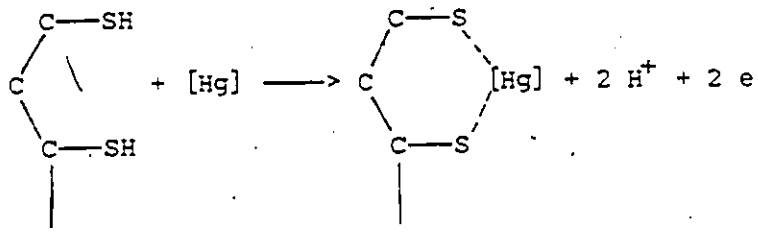

At pH 7, the dihydrolipoic acid and α-lipoic acid give (143) almost identical cyclic-voltammograms at Hg and the behavior is said to approach reversibility with either compound.

The most important conclusion of Kolthoff and Barnum (140) was that cysteine is <u>not</u> directly oxidized to cystine at Hg electrode but reacts through the formation of the surface complex "$Hg(SR)_2$". Following the early work of Brdička (136,163) on polarographic behavior of cysteine, Kolthoff and Barnum in their second paper (141) on the cysteine/cystine system studied the reduction of the latter compound at Hg. Roncato (164) attributed the two main polarographic reduction waves be observed to reversible reduction of cystine followed by irreversible reduction in the second wave; the reversible step was associated with reduction of the cystine cation and the second to reduction of neutral cystine or the anion. This work was not satisfactory as it was conducted in unbuffered solutions and it is obvious that the processes referred to above would be pH dependent.

In Kolthoff and Barnum's work (141), a strong polarographic maximum is observed in reduction of cystine which is eliminated by addition of thymol or camphor as capillary-active agents; the wave is also shifted to more negative potentials. These effects are attributed to the requirement that the cystine be adsorbed and oriented prior to reduction. Generally, the cystine waves are drawn out on the potential scale and do not correspond to the behavior expected for a reversible, 2e reduction process. Only at pH 1, with surface active agents present, does the wave have a more normal appearance.

At pH 3 and 9.2 two-step waves are observed (as found later also by other authors). The first step of the wave does not correspond to a true reduction of cystine but rather to cystine complexed with Hg, as found in the work on oxidation of cysteine (140). The second step of the wave was believed to correspond to a true reduction of cystine, presumably with the product cysteine being diffused into the solution. It is to be noted that, in this work (140), the diffusion constant of cystine in 0.1 M aq. HCl was derived as 5.3×10^{-6} cm^2 s^{-1}.

The electrooxidation of cysteine and the reduction of cystine were studied by Stankovich and Bard (142) at the hanging Hg drop electrode and at a Hg pool using cyclic-voltammetry. These authors tried to characterize the adsorption and diffusion-controlled processes that are associated with RSSR (cystine) reduction. The work of Kolthoff (140,141) has indicated that polarographic RSSR reduction is characterized by an adsorption "prewave" followed by a "diffusion" wave. The suggested mechanism associated with the prewave is reaction of RSSR with Hg with scission of the -S-S- bond giving Hg-cysteine

(140) which is the species reduced. Whether the intermediate involving Hg is a chemical intermediate or an adsorbed species remains to be elucidated.

At low concentrations (10^{-3} - 9 x 10^{-2} mM) of RSSR, a symmetrical CV peak characteristic of an adsorbed species was observed (142), with peak currents increasing linearly with sweep-rate, s. On sweep reversal, an anodic wave having the shape of a diffusion peak was observed with peak currents proportional to $s^{\frac{1}{2}}$. This, it was supposed, corresponds to reoxidation of a non-adsorbed species produced in the first wave from the adsorbed species. At higher concentrations, 0.4 mM, the characteristics of the first scan reduction waves were unchanged but on reversal to the anodic scan, a current spike superimposed on the diffusion peak was observed. It was attributed to an oxidation process associated with a compact layer of the Hg-cystine intermediate. Following this anodic sweep, a further cathodic scan showed a corresponding cathodic spike. For s > 5 V s^{-1}, the cathodic and anodic scans did not exhibit spikes and the adsorption and diffusion characteristics were as observed at lower concentrations. The sweep-rate ranges were ca. 1 to 20 V s^{-1}. In the present work, rather different sweep-rate ranges were employed and somewhat different conclusions are reached regarding the adsorption "prewave" behavior (142) which is difficult to characterize.

In addition to the adsorption prewave, Stankovich and Bard (142) observed a second reduction wave at -0.9 V SCE for which the peak currents varied as $s^{\frac{1}{2}}$, supposedly corresponding to diffusion-controlled reduction of dissolved RSSR from the bulk solution. At the

higher concertrations, it was supposed that a reduced form is also adsorbed and is oxidized in the anodic scan to an adsorbed oxidized form. These processes are associated with the "spike" currents observed.

The nature of the species involved was further investigated in these authors' work (142) by examination of the electrochemical behavior of cysteine (RSH) at Hg. With this compound, only a single, diffusion-controlled wave with oxidation peak currents linear in s was found at concentrations up to 0.1 mM and with s = 0.2 V s^{-1}. On scan reversal, the reduction peak was found to be an adsorption peak (as with RSSR) with i_p proportional to s. These results were independent of pre-equilibration time of the Hg drop in contact with the solution for times of 10 s to 2 min. For s > 5 V s^{-1} the anodic and cathodic waves were generally the same as those at lower concentrations while at lower s, two peaks appeared. The linear variation of the anodic peak current with concentration found at low concentrations up to ca. 0.3 mM is no longer observed at higher concentrations where i_p levels off with increasing concentration.

In a chemical experiment, at a stirred Hg pool, Stankovich and Bard (142) showed that a compound of cystine with Hg (mercury "cysteinate"; cf. ref 140) could be detectably formed but only at a slow rate on a pool electrode of relatively large area (not at the HMDE). It was noted that only small amounts of RSSR are evidently converted to $(RS)_2Hg$ even after 1 h. The order of magnitude of the concentration is 10^{-6} M. However, it should be noted that only extremely small quantities of an ad-species are required to cover 1 cm^2 surface of a

Hg electrode (on the order of 10^{-9} mole cm^{-2}) and give rise to currents for reduction or oxidation of an ad-species derived from cysteine or cystine. The role of the presence of an ad-species at Hg is further emphasised by the quite different behavior found at Au and Pt, as noted by Koryta et al (160-162,165-168) (and also observed in the present work).

The work on reduction of α-lipoic acid: α-lipoic acid is a cyclic disulfide structure shown earlier in Section 1.3.2. Since the 5-membered ring is closed by the disulfide bond, it may be thought that this molecule could undergo a more reversible electrochemical reduction/reoxidation reaction than cystine, as does the S_2^{2-} ion at the surface of FeS_2. This is not the case.

In studies by Moireaux et al (143) at Hg, Pt and glassy-carbon electrodes it was concluded that the redox reaction involving -S-S- $\rightleftharpoons$ 2 -S-H was highly irreversible. In fact, again, formation of a Hg surface compound is indicated, as proposed by Nygard (169):

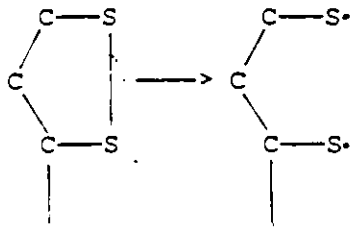

fission

(III)

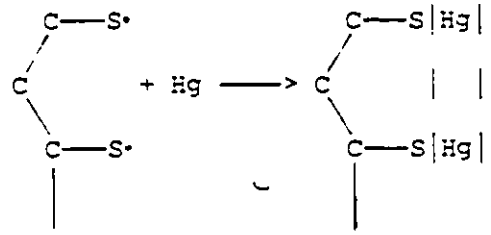

adsorption or surface compound formation

(IV)

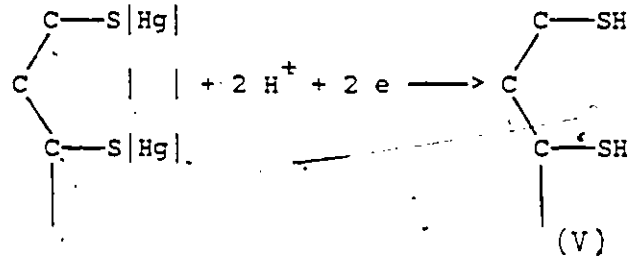

(V)

The anodic reoxidation was supposed to involve the reverse of these steps. The way the involvement of Hg is written is not consistent with Kolthoff and Barnum's conclusion (141) regarding reduction of cystine where the product cysteine is indicated as being in the form of a Hg cysteinate complex. Hence the reduced form of the cyclic disulfide would be expected also to be similarly complexed. Conversely, it could be supposed that cystine reacts first with Hg according to

$$RSSR + Hg \longrightarrow RSHgSR$$

which is then reduced to Hg cysteinate of the form RSH Hg with $2H^+ + 2e$. This chemical reaction of Hg with RSSR is actually the process suggested Stankovich and Bard (142) which they found to be "slow".

Moireaux et al (143) also proposed that the electrochemical reoxidation of the dithiol produces HgS rather than the initial material. However, no evidence for this was given nor is a mechanism for such a step shown. This paper is very confusing and inconclusive, and contains self-contradictory statements in various places concerning interpretation of their results. Products of the reaction of Hg(II) ions with the disulfide and the dithiol were said to have been isolated and it was concluded that the same product VI arose from

reaction of Hg with the disulfide, the dithiol and from 2e electrolyte oxidation of the thiol.

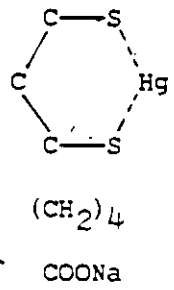

(VI)

The supposed formation of HgS is inconsistent with the conclusion given later in their paper regarding reactions to form the above Hg complex. Cyclic-voltammograms of the disulfide and the dithiol at Hg (at pH 7) had almost the same appearance, exhibiting two peaks, one smaller than the other. They concluded from electrocapillary experiments that the first wave corresponded to adsorbed (? surface-complex) reactant ("depolarizer") while the second wave is said to arise with "product adsorption". (It is unclear what is meant here as this paper (143) refers to both the disulfide, lipoic acid, and the dihydro form as "products". HgS, said to be another product, is not further referred to). Mechanistically, the following is proposed:

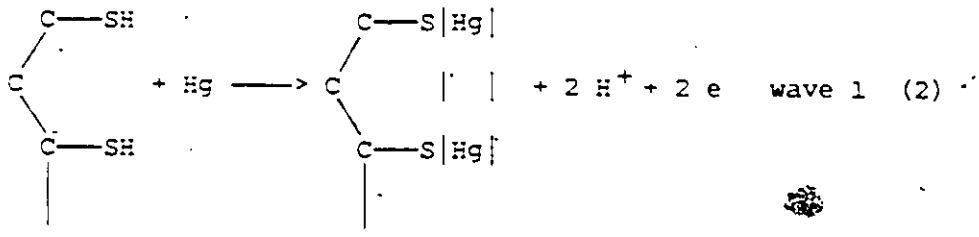

adsorbed

and

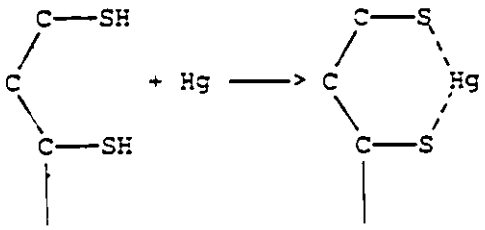

followed by

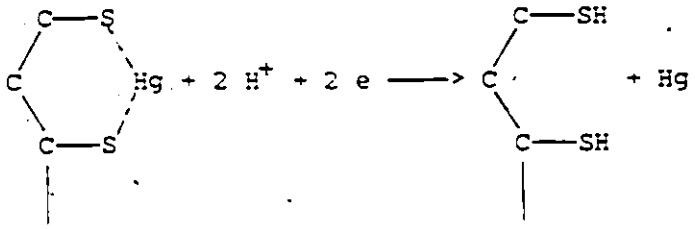

The first wave (wave 1, reaction (2)) observed is an adsorption prewave. Note that the second step is written (typically for this paper) in a chemically unbalanced form. It is said that the wave processes corresponds to the reversible redox system written above for wave 1 (reaction (2)).

Summary of electrochemical behavior of cysteine, cystine and α-lipoic acid:

i) Direct reversibility of the disulfide/thiol system is not observed with the thiols or the corresponding disulfides.

ii) A mercury-complex intermediate is involved which undergoes electrochemical oxidation, or with disulfides, reduction.

iii) Reduction of cystine and α-lipoic acid may also involve an intermediate surface compound in which scission of the -S-S- linkage already occurs chemically by reaction with Hg.

iv) Two waves are observed polarographically and in some cyclic-voltammetry experiments, but their assignment to specific electrochemical reactions is controversial. Some results exist which indicate that one of the waves is an "adsorption pre-wave" and that the cyclic-voltammetry behavior corresponds (i_{peak} vs s being linear) to a process involving an adsorbed species.

v) Under other conditions, diffusion-controlled currents are always observed and a diffusion constant has been reported for cysteine at pH 1.

vi) Some indications exist that there is no reversible redox reaction in the cysteine/cystine system at Au or Pt electrodes. This is contrary to the common belief in organic and biochemistry that the system is "reversible".

vii) Reduction of cystine at more elevated cathodic potentials at Hg gives rise to a "catalysis" of the hydrogen evolution reaction (Brdička) which is believed to be associated with formation of the Hg "cysteinate" complex (Kolthoff and Barnum) acting as a mediator in proton transfer and neutralization, through the -SH group.

viii) The exact chemical nature of the Hg complexes is unclear but in some works stoichiometric chemical formulae have been proposed. In one paper, formation of HgS is said to occur but without any proof.

1.3 STRUCTURES OF SULFIDES USED IN THE WORK

1.3.1 Structures of some Inorganic Minerals that Have Been Studied Electrochemically

1) Occurrence

Certain ore minerals occur characteristically in sedimentary rocks, some can precipitate in oxidizing depositional environments as with pyrolusite, MnO_2, or goethite, FeO•OH, while in reducing depositional environments, pyrite FeS_2 is typical. In addition to pyrite, the sulfides pyrrhotite $Fe_{1-x}S$, chalcopyrite $CuFeS_2$, galena PbS and sphalerite ZnS occur in stratiform concentrations whose genesis apparently involves sedimentary processes. Bacterial reduction of sulfate to sulfide has also been suggested for some deposits (170). Formation temperature is another important factor; the sulfides of iron, lead, zinc and copper are typical minerals of middle-temperature hydro-thermal veins.

2) Mineral Conductivity

Minerals with electrical conductivity neither as good as a metal like copper, nor as poor as an insulator like halite are defined as semiconductors. A semiconductor becomes less conductive at low temperatures (contrast metals) and has an energy gap between occupied electronic states (valence band) and unoccupied states (conduction band) usually much greater than kT.

Electrical conduction in semiconductory minerals is due to the mobility of free charge-carriers, and depends also on their concentration. The charge-carriers may be of two types: electrons in

the normally empty conduction band or holes in the normally full valence band. Three sources of free carriers may be distinguished: deviation from stoichiometry; trace elements in solid solution and thermal excitation of electrons across the energy band gap[4]. The last source is important only if the band gap is small or the temperature is high. When it is dominant, the electron and hole densities are equal and the semiconduction is termed "intrinsic". Most semiconducting minerals are "extrinsic", that is, the carriers are due to donor or acceptor defects, which represent nonstoichiometry and/or arise from impurities.

As was earlier documented by Harvey (171), the measured conductivity of natural extrinsic semiconductors varies by several orders of magnitude from one sample to another, even when measurement errors and the effects of sample heterogeneity are discounted. This variation is in response to deviations in stoichiometry and/or purity which are often as small as a few tens of parts per million.

Unless the densities of donor and acceptor defects balance very exactly, the charge carriers in an extrinsic semiconductor are predominantly of one type. The semiconduction is termed n-type or p-type according to whether electrons or holes are dominant. Most minerals occur only in one type. Typical exceptions are galena, molybdenite and pyrite, for which n-type and p-type occurrences are of comparable abundance.

---

[4] Photo-excitation may, of course, also occur and leads to well-known photo-electrochemical processes at semiconductors.

3) The mineral/solution interface

The interface between a mineral and an aqueous phase is of great technological importance. The electrical impedance of the interface is the basis of the "induced polarization" method of geophysical exploration (172,173). The electrochemical interaction between certain dissolved organic additives and the mineral surface is the basis of the floatation method for ore concentration (174,175). It is known that the space charge layer at the semiconductor-electrolyte interface is dependent on the band gap, the surface states and the concentration of point defects, which are also basic in determining the bulk electrical conductivity (176-178). Thus, future theoretical studies on charge-transfer interfacial phenomena involving minerals and aqueous solutions may benefit from knowledge of bulk electronic properties.

4) Structure and properties of pyrite

Crystal structure

The following summarises the essential crystal structure data for pyrite;

System	:	Cubic
Space group	:	205; T_h^6 ; Pa3
FeS_2 per cm^3:		2.54×10^{22}
Fe-S distance:		0.226 nm
S-S distance:		0.218, 0.366 nm
Fe-Fe distance:		0.381 nm

The crystal structure of iron pyrites, FeS_2, can be described in terms of the cubic rocksalt structure (179) as shown in Figure 1.1(a). Iron atoms are in a face-centered cubic array. A covalently bonded SS pair (S-S = 0.218 nm) (180) occupies positions corresponding to that of the anion in the rocksalt type of structure. The unit cell contains four such pairs, each oriented along one of the four distinct body-diagonals of the cell. Pyrite may thus be regarded as a derivative of the rocksalt structure type. The Fe atoms accordingly form an octahedron about the SS pair. Each sulfur atom is coordinated by three Fe atoms and one S atom in a distorted tetrahedral configuration; each Fe is octahedrally coordinated by S. Although all Fe-S distances are equal, the octahedron is not perfect, but is slightly compressed along one axis.

Bonding

In an ionic model pyrite is $Fe^{2+}(S_2)^{2-}$. The molecule-ion $(S_2)^{2-}$ would have fully occupied $2p\pi$ orbitals and an empty antibonding $2p\sigma$ orbital (181). The Fe^{2+} ion has the configuration $(3d)^6$. In the high-spin state there are four unpaired spins and hence a net magnetic moment but, in pyrite, the effective permanent molecular moment is zero (181). Evidently the Fe^{2+} is in the low-spin state, which for octahedral coordination has no unpaired electrons. The 3d orbital triplet is completely filled while the doublet is empty.

If the Fe-S interaction is strong enough to cause a low-spin configuration of the iron, it probably also involves some sharing of electrons. This is also implied by the internuclear Fe-S distance of 0.226 nm, which is much less than the sum of the ionic radii, 0.260nm.

(a)

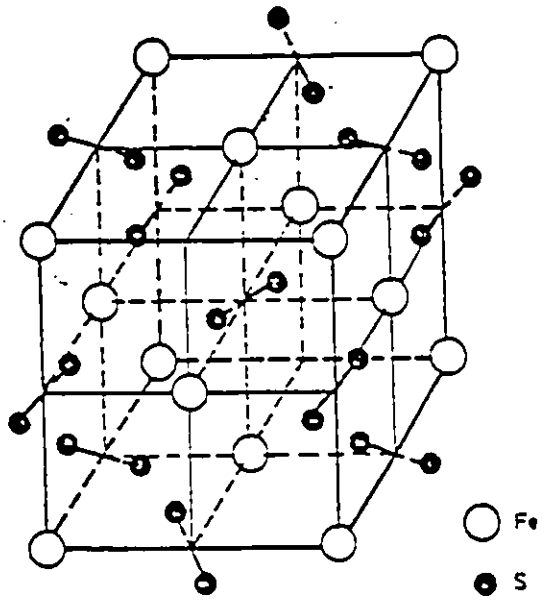

(b)

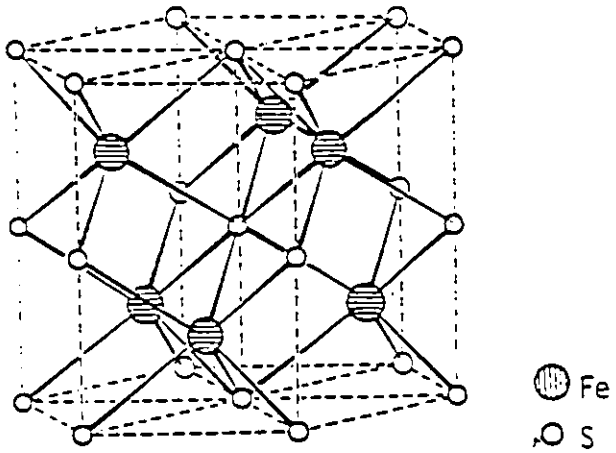

(c)

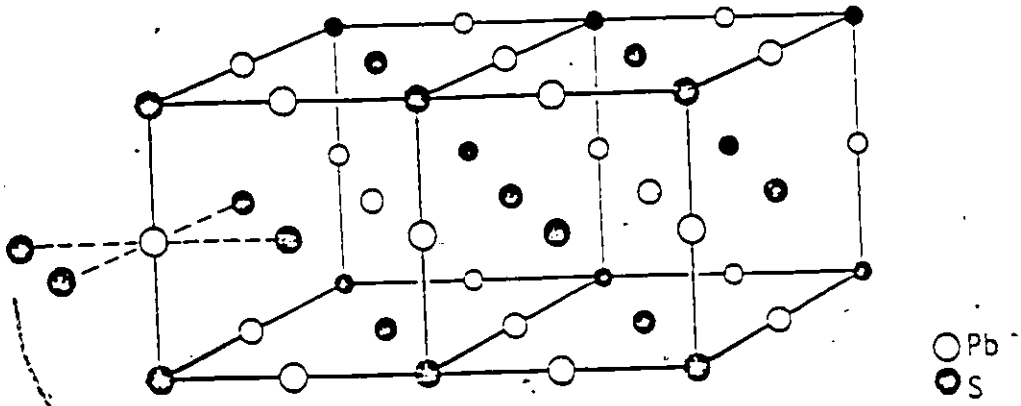

Fig. 1-1: Crystal structure of (a) pyrite; (b) pyrrhotite; (c) galena.

Band structure and Band gap

Bither et al (182) have introduced a general band model which they have used to interpret their electrical, magnetic and optical data on the pyrite-structure compounds MX_2, with M = Fe, Co, Ni, Cu, Zn and X = S, Se, Te. The conduction band in FeS_2 is derived from the e_g doublet of 3d orbitals on Fe, and in its upper part from the 4s orbital. At the sulfur atom Bither et al. consider the conduction band wave function to be an sp^3 hybrid. Each S is in tetrahedral coordination by three Fe and one S, and the wave function is supposed to have antibonding σ character with respect to each neighbor.

The valence band is derived from the t_{2g} triplet of 3d orbitals on Fe and the antibonding $2p\pi$ molecular orbitals of the $(S_2)^{2-}$ group. Since the sulfur atoms are in octahedral coordination about the iron, the overlap is relatively slight. Hence the valence band is narrow, 1 eV according to the photo-emission data of Li et al (183). They also found the occupied band derived from sulfur 3p levels to be 7 eV wide and just below the t_{2g} valence band.

From the measurements on the optical reflectivity spectrum of synthetic pyrite, Bither et al (182) found the band gap to be 0.9 ± 0.1 eV. Fukui et al (184) measured the photoconductivity spectrum of a natural pyrite at 77 K and found a sharp peak at around 0.9 eV, thus confirming the conclusion of Bither et al.

The band gap has also been estimated from the activation energy of resistivity at about 500 K, where the pyrite is presumed to be intrinsic. Marinace (185) and Sasaki (186) reported values of 1.2 eV and 1.12 eV, respectively. Bither et al (182) obtained a value of

0.92 eV for a simple synthetic crystal, while Horita (187) found 0.77 eV for a series of natural crystals.

Electrical conduction

Pyrite is found with both n- and p-type semiconductivity. Conduction electrons are nearly two orders of magnitude more mobile than holes (182,184,185,187-190), and n-type pyrite statistically has a lower resistivity than p-type as shown in Fig. 1.2 (191). Also p-type pyrite may have a negative, and n-type a positive temperature coefficient of resistivety due to thermal release of holes trapped at acceptors (185,186,190). Common donor impurities are Co, Ni and Cu (192-196), while As is the most common acceptor impurity (193). It also found that there are sulfur vacancies in high-temperature pyrite and iron vacancies in low-temperature pyrite (197,198).

5) Structure and Properties of pyrrhotite

Composition

The composition of pyrrhotite is bounded by the formulae "FeS" and "Fe_7S_8". Since the report of Carpenter and Desborough (199) was published, pyrrhotite has been regarded mineralogically as having three distinct phases: troilite, hexagonal and monoclinic pyrrhotite. Troilite is FeS with no detectable departure from stoichiometry. Monoclinic pyrrhotite is Fe_7S_8, while hexagonal pyrrhotite is complex and not completely characterized. All natural samples evidently have re-equilibrated to room temperature where the stability range is rather narrow. Arnold (200) found that a metastable solid solution of

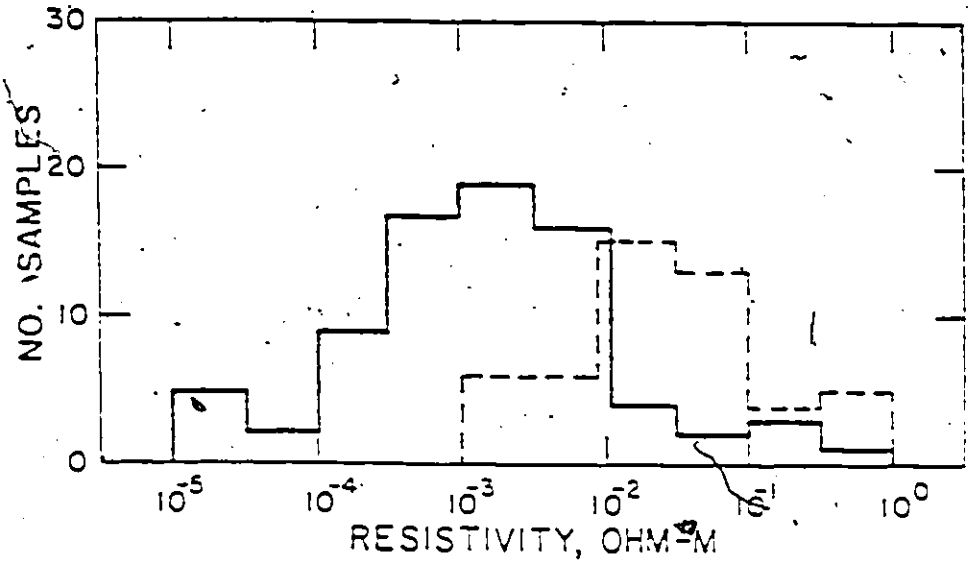

Fig. 1-2: Resistivity distribution for pyrite, as compiled by Pridmore and Shuey (1975). Solid line is for n-type, dashed line is for p-type, and samples of mixed type are omitted.

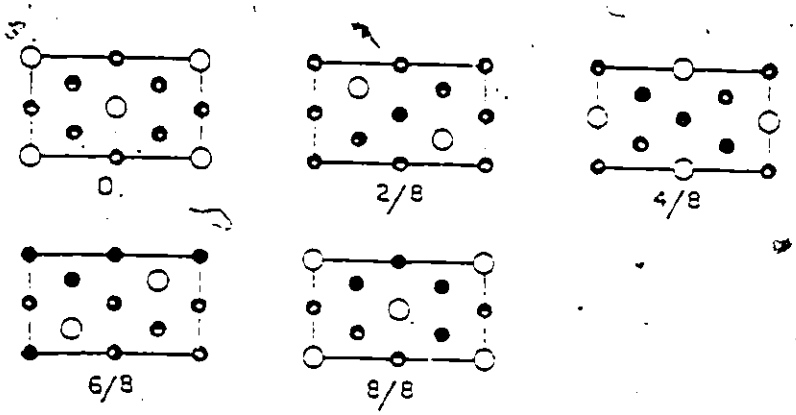

Fig. 1-3: Schematic indication of the arrangement of vacancies pyrrhotite. Solid circles indicate Fe atoms occupying octahedral sites in the NiAs-type structure, the larger open circles indicate a vacancy. Sulfur atoms are not shown.

the three phases unmixes in about two months. The majority of terrestrial pyrrhotite is an intergrowth of hexagonal Fe_9S_{10} with monoclinic Fe_7S_8 (200,201) as in Table 1.1.

TABLE 1-1

PHASES IN 82 NATURAL TERESTRIAL PYRRHOTITES (ARNOLD, (200))

phase	number	percent
troilite	3	3%
tr and h-po	4	5%
hexagonal pyrrhotite	8	10%
h-po and m-po	60	73%
monoclinic pyrrhotite	7	9%

tr : troilite; h-po : hexagonal pyrrhotite;
m-po : monoclinic pyrrhotite.

Crystal structure

The following summmarises the essential crystal structure data for pyrrhotites;

	FeS	Fe_7S_8
System :	Hexagonal	Monoclinic
Space group :	190; D^{4}_{3h}; $P\bar{6}2c$	15; C^{6}_{2h}; $C2/c$
S per cm^3 :	3.3×10^{22}	3.5×10^{22}
Fe-S distance:	0.24-0.27 nm	0.24-0.26 nm
Fe-Fe distance:	0.29 nm	0.29 nm
S-S distance:	0.35 nm	0.345nm

Pyrrhotite, $Fe_{1-x}S$, is an extremely complex derivative of the NiAs-structure type which is important in mineralogy. Troilite, stoichiometric FeS, has a structure derived from NiAs (Fig. 1.1(b)) through small displacements of Fe normal to the c axis and small displacements of S parallel to the c axis (202). The crystal structures of two other forms of pyrrhotite are known in detail.

One variety has a and b equal to twice the dimensions of the ortho-hexagonal double cell of NiAs, in which the c axis is four times larger. According to current nomenclature, this form is loosely referred to as "4c" pyrrhotite. The vacant sites (203,204) are confined to alternate layers of octahedral sites in the NiAs configuration. The arrangement of vacancies within these layers is indicated schematically in Fig. 1.3, where the larger open circles indicate the vacant sites. Sulfur atoms, as well as the intervening layers of completely filled octahedral sites are not indicated. It may be noted that the arrangement of vacancies is the same in each level.

The structure of a second variety of pyrrhotite (Fe_7S_8) is also available (205). This variety of pyrrhotite, "3c", is hexagonal with a and c equal to twice and three times, respectively, the lattice constants a and c of the NiAs substructure. The structure is somewhat analogous to that of the 4c structure in that the array is slightly distorted and the vacant sites occur again on alternate layers of sites.

Resistivity

Pyrrhotite is known as a consistently good electrical conductor, as indicated in Table 1.2. Parasnis (206) reports that ore with 75% pyrrhotite has about the same range of resistivity as pure polycrystalline pyrrhotite.

TABLE 1-2

RESISTIVITY OF NATURAL PYRRHOTITE IN OHM-M

Low	High	No. of samples	Reference
2×10^{-6}	2×10^{-5}	6	Harvey (171)
6.5×10^{-6}	1.6×10^{-4}	5	Semenov & Malchevskiy (207)
1.8×10^{-5}	5.7×10^{-5}	3	Parasnis (206)
3×10^{-6}	1×10^{-5}	5	Theodossiou (212)

Anisotropy

Hirahara and Murakami (208), Hihara (209) reported that synthetic single crystal FeS has a high resistivity along the c-axis; upon heating above the α-transition at 413 K the axial resistivity drops and the electrical anisotropy nearly disappears. Hihara (209) measured electrical anisotropy in metastable solid solutions of troilite and hexagonal pyrrhotite. His results imply that hexagonal pyrrhotite is essentially isotropic. There is no direct evidence regarding electrical anisotropy in monoclinic pyrrhotite.

Conduction and impurity effects

Pyrrhotite is always a good electrical conductor, although low troilite has a relatively high resistivity along the c-axis. Hall and thermoelectric data are difficult to interpret quantitatively, but indicate carrier concentrations around $10^{21} cm^{-3}$ for all phases (210-212). At high temperatures, conductivity varies inversely with temperature (208,209) and is fairly independent of composition. These results suggest that all pyrrhotites should be considered as low mobility metals.

Nickel, cobalt, manganese and copper are the most common impurities (193,201,202). Vaughan et al (202), found that Ni, up to 1%, has a small but measurable effect on magnetic properties, but there is no direct information about the electrical properties. Thus if $Fe_{1-x}S$ is considered to be a low-mobility metal, the indicated impurities should not have much effect.

Bonding

$Fe_{1-x}S$ is usually considered to be ionic with composition $Fe_{1-3x}Fe_{2x}\#_x S^{2-}$ where # means an iron vacancy. Tokonami et al (205) found the x-ray diffraction intensities in Fe_7S_8 to be insensitive to this. Bin and Panthenet (213) concluded from the smallness of the Fe_7S_8 spontaneous magnetization that all Fe^{3+} ions are on the sublattice with iron vacancies. The Mossbauer spectra of Fe_7S_8 (214) show no sign of Fe^{3+} even at 4.2 K. This means that even at this low temperature Fe^{2+} and Fe^{3+} ions do not have a separate existence for a time larger than the Mossbauer transition time, 10^{-7} to 10^{-8} s.

The S-S (i.e. S^{2-}-S^{2-}) distances of 0.34 to 0.35 nm are significantly less than the ionic diameter 0.368 nm, so there must be some electron sharing among the close-packed sulfur atoms. Most of the Fe-S distances are also less than the sum-of-radii 0.260 nm. Vaughan and Tossell (215) report that under pressure of 16 Kb the Mossbauer spectrum is completely changed. They interpret this as due to the conversion of Fe to a low-spin state as in pyrite.

Band structure, band gap and conduction

There is no definite information on the pyrrhotite band structures; the following is merely a speculative assessment of the available clues.

The reflectivity of hexagonal pyrrhotite, studied by Von Gehlen and Pillar (216), implies a peak in interband optical absorption below 1.9 eV, thus the threshold for interband transition must be quite low. Hall and thermoelectric effects both indicate carrier concentrations on the order of $10^{21} cm^3$, which with a resistivity of 10^{-5} ohm-m implies a mobility on the order of 6 $cm^2 v^{-1} s^{-1}$. This is too high for hopping of localized carriers, so the electronic states must be delocalized (except along the c-axis in low-FeS). Kaplan and Worrell (217) noticed that in hexagonal high-pyrrhotite solid solution the conductivity is 1/4 to 1/5 that of pure iron at the same temperature, and decreases approximately as T^{-1}. These data indicate that all $Fe_{1-x}S$ should be regarded as metallic with the Fermi level near the middle of the Fe 3d band. The interband transitions suggested by the optical reflectivity behavior are presumably d-d transitions.

6) Structure and properties of galena, PbS

Crystal structure

The following summarises the essential crystal structure data for galena:

System	:	cubic
Space group	:	225; O_h^5 ; Fm3m
Cell dimensions:		a=0.593 nm
PbS per cm^3:		1.92×10^{22}
Pb-S distance:		0.297 nm
Pb-Pb distance:		0.416 nm
S-S distance:		0.416 nm

Galena has the well-known structure of halite (NaCl), Fig. 1.1(c). The S atoms are in cubic close-packing with Pb atoms in the octahedral interstices. Each S has six Pb neighbors at 0.297 nm and twelve S next-nearest neighbors at 0.416 nm.

Bonding

The NaCl structure is traditionally associated with ionic bonding. It is expected for ionic RX compounds where the ratio of cation radius to anion radius is in the range 0.41 to 0.73 (218). The Born ionic model accounts fairly well for the observed bond energy (219), although not as accurately as in the alkali halides. In the purely ionic model, S^{2-} has a fully occupied 3p subshell, while Pb^{2+} has an occupied 6s subshell and an empty 6p subshell. The sum of ionic radii

(0.340 nm) is somewhat larger than the actual Pb-S internuclear distance of 0.297 nm, which indicates some electron sharing. Krebs (220) considers that partial covalence occurs by admixture of lead 6p orbitals into the sulfur 3p orbitals. This type of bond is appropriate for dual octahedral coordination.

Band structure

Several calculations have been made of the electronic band structure of galena, a problem rendered especially difficult by the large spin-orbit coupling in lead. The recent calculation of Overhof and Rossler (221) appears to have overcome this difficulty and produced a structure consistent with a large quantity of experimental data. The valence band is about 7 eV wide and is derived primarily from sulfur 3p and lead 6s orbitals. Thus, the full band contains eight electrons per PbS formula unit. At the top of the band the wave functions have a significant lead 6s component. This has been confirmed in PbTe (altaite) by Weinberg and Callaway (222). For the conduction band edge, the wave function has 6p character at the lead atoms. Some 15 eV below the band gap are the rather narrow bands derived from the lead 5d and sulfur 3s orbitals.

Energy gap

The energy gap between the full valence band and the empty conduction band is about 0.37 eV at room temperature. Approximately this same value was obtained from optical absorption measurements (223), photoconductivity (224) and the temperature dependence of the Hall effect and resistivity (225).

The energy gap has a temperature coefficient of about 4×10^{-4} eV K^{-1} (233), so at 77 K it is decreased to about 0.29 eV. This change is in the opposite direction from that usually found in semiconductors.

1.3.2 Structures of Organic -S-H and -S-S- Compounds that Have Been Studied Electrochemically

Cysteine; 2-amino-3-mercaptopropanoic acid. Found in hydrolysis of proteins. Oxidized rapidly to cystine; N-protected derivatives, useful in peptide synthesis.

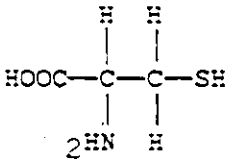

(I)

Cystine; 3.3'-dithiobis[2-aminopropanoic acid], dithiodialanine. Widely distributed in proteins, reduced to cysteine; N-protected derivatives.

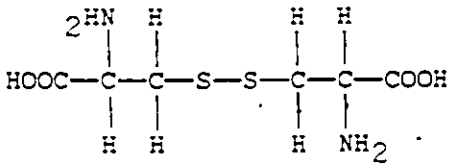

(II)

α-Lipoic acid; 1,2-dithiolane-3-pentanoic acid, thioctic acid. Natually occuring isomer, which is a growth factor for many bacteria and protozoans. Used to treat liver disease and in cases of Amanita toadstool poisoning (liver necrosis).

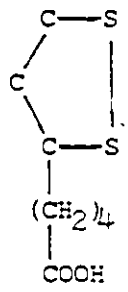

(III)

1.4 AIMS OF THE WORK

The electrochemical behavior of materials is intricately connected with local surface chemistry of the substance involved and the double-layer properties of the interphase at their surfaces. In particular, the way in which the interfacial properties may change with potential of the surface and the condition of its environment, is of considerable interest.

The use of electrochemical techniques and complementary optical methods for the study of reactivity and electrical properties of mineral sulfide surfaces is a field of importance in electrochemical surface science and in the surface chemistry of minerals.

These methods and techniques give: (a) a general idea of the electrochemical reactivity of the material, both in the anodic direction for oxidation processes and in the cathodic direction for reduction of any oxidized surfaces formed in the previous anodic polarization and for cathodic products developed on the surface initially; (b) information on whether the electrochemical polarization leads to formation of any solution-soluble species on account of oxidation or reduction of the surface at various potentials over the

range scanned in the experiment. This turns out to be a useful approach in distinguishing various types of processes that occur on the surface as a function of electrode potential; (c) information concerning different states of the surface that may be formed over different ranges of potential with regard to how the production of a changed state of the surface is related to the properties of the interface; and (d) indication of any reversible electrochemical processes, involving the surface or the bulk of the substance, that are of special kinetic and practical significance.

The combination of these new lines of information on the electrochemical bahavior of mineral surfaces as a function of potential are very useful and important in industrial applications as well as in basic scientific research in the fields of surface science of mineral crystals, battery cathode development, corrosion studies, mineral separation and semiconductor photo-chemical energy conversion and associated interfacial phenomena.

Interest in the electrochemical behavior of organic sulfides arose comparatively with respect to the work on FeS_2, $Fe_{1-x}S$ and PbS. In particular, the question of interest was whether some organic disulfides could be reversibly reduced to thiols like the S_2^{2-} ion evidently is in the surface of FeS_2 (in that case: $S_2^{2-} + 2\ e \rightleftharpoons 2\ S^{2-}$). Also, the role of chemisorption or surface compound formation of disulfides and thiols at the Hg electrode is of interest in their electrochemistry (cf. refs. 140,141,143) including their so-called catalytic effects on the cathodic H_2 evolution reaction at Hg.

Accordingly, in this work, some attempts were made to investigate possible reversibility of disulfide reduction at Hg and comparatively at Au, and to characterize the role of mass-transfer and surface reactions in the electrochemistry of the processes involved. All will be seen from the results, the processes are of unexpected complexity but some progress can be made in elucidating the electrochemistry by conducting cyclic-voltammetry experiments at limiting conditions of pH and with selected compounds having appropriate structures.

Chapter II

EXPERIMENTAL

2.1 GENERAL:CHOICE OF METHODS

In the present work, emphasis is given to the study of the electrochemical reactivity of two iron sulfides (pyrite and pyrrhotite) and lead sulfide (galena) over certain potential ranges in solutions at various pH's, and comparatively, of several organic sulfides under similiar conditions. Because, on the one hand, surface reactions of the mineral crystals were to be investigated and on the other, reaction of organic sulfides at concentrations limited by low solubilities, steady-state methods were not generally applicable in the work, since steady currents, at various potentials, would not be maintained. Thus, limited solubility of reagents places an unavoidable restriction on methods available for use in the work, e.g. steady-state polarization experiments without diffusion limitation conditions, are not feasible. Hence some transient method(s) was (were) required. For convenience, and on account of it good resolution of successively occuring processes and its capability for distribution between both reversible and irreversible processes, and of surface and diffusion-controlled reactions, the method of cyclic-voltammetry was used predominantely in the present work. The following experimental techniques were therefore used in the study of

this topic: (a) Cyclic-voltammetry and voltammetry after potentiostatic holding of the electrode potentials at various controlled values. (b) An examination of how the current-voltage curves which result from voltammetric studies depend on mass-transfer at the interface or surface processes at the sulfide mineral interfaces. This was achieved by use of rotating-disc electrodes. (c) Procedures (a) and (b) were complemented by scanning electron microscopy and X-ray emission analyses.

Scanning electron microscopy was used to view the changes of the surfaces of FeS_2 and $Fe_{1-x}S$ before and after controlled potential cycling. X-ray emission analyses were performed in the electron microscope on the samples before and after the electrochemical experiments in order to determine changes in the Fe:S ratio in the surface region of the electrodes and to detect any changes of surface morphology.

Approach (a) gives a general idea of the electrochemical reactivity of the sulfides, both in the anodic direction for oxidation processes and in the cathodic direction for reduction of any oxidized surface species formed in the previous anodic polarization and for products in a reduced state developed on the surface initially or after cathodic potential scans. Method (b) gives information on whether the electrochemical polarization leads to formation of any solution-soluble species on account of oxidation or reduction of the surface at various potentials over the range scanned in the experiment. Interesting effects are observed when, at some sulfides, a solution-soluble species is formed while at others a species remaining fixed or

adsorbed to the surface is produced. This approach turned out to be a useful one in distinguishing various types of processes that occur on a sulfide surface as a function of electrode potential. Method (c) is very useful as it provides a means of making an analysis of the surface region (25 to 40 nm depth) of sulfide materials before and after electrochemical treatment and also to observe directly, by means of scanning electron microscopy, the morphology of these surfaces after various treatments.

The combination of these three methods has led, in the present work, to interesting and new information on the electrochemical behavior of mineral sulfide surfaces as a function of potential.

The previously published work (140-143) has indicated the possible role of Hg surface complexes with several organic sulfide adsorbates such as cysteine and cystine. In the present work cyclic-voltammetry were employed to characterize: (a) the various stages of oxidation and reduction of sulfide adsorbates at Hg; (b) the potentials at which these various processes take place in anodic and cathodic potentiodynamic sweeps; (c) the effect of sweep-rate on the various peak currents; (d) the relation between current peaks on cathodic sweeps and those on anodic sweeps, to establish conjugate pairs that correspond with one another (this is achieved by conducting cyclic-voltammograms from progressively increasing potentials in successive cycles) and (e) time effects in the cycling regime with holding the potential constant at some point. Also, the dependence of peak currents on the sulfide compound concentration was investigated in relation to distinguishing bulk diffusion from surface reaction control of the current.

Some comparative experiments have to be made at Au, Pt and Pb electrodes, including the effects of electrode rotation.

2.1.1 Cyclic-Voltammetry Experiments

Cyclic-voltammetry has become a very useful and frequently employed technique for initial electrochemical studies of new systems and has proven valuable in obtaining information about fairly complicated electrode reactions, especially these involving adsorbed species or surface compounds.

Some principal aspects of the electrochemical behavior of a system can be obtained through a series of stepwise changes of potential to successively increasing potentials (V) with recording of current (I) vs time response curves to give a three-dimensional I-t-V surface Fig. 2.1 (227). However, the accumulation and analysis of these data can be cumbersome; also it is not usually possible to distinguish or idenitfy the presence of various species from the recorded I-t curves alone. Thus derivation of well-resolved I-V curves is needed. More information can be obtained in a single experiment by sweeping the potential with time and recording the I-V curve directly. Usually the potential is varied linearly with time at a sweep-rate s, with the current being simultaneously recorded as a function of potential, Fig. 2.2. Reversing the direction of the potential scan after the peak current of the reaction process has been passed is a usual procedure. Thus the potential is scanned reversely beyond the peak and then reversed again in a further linear sweep, or in a continuous repetitive manner ("cyclic-voltammetry"). Such a technique provides

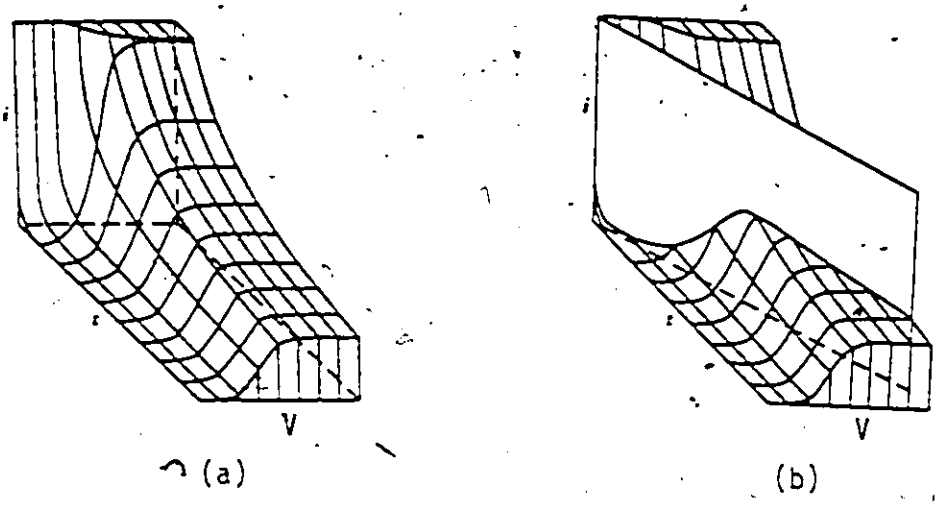

Fig. 2-1 (227):
(a) Representation of a portion of the i-t-V surface for a Nernstian reaction. Potential axis is a units of 60/n mV.
(b) Linear potential sweep across this surface.

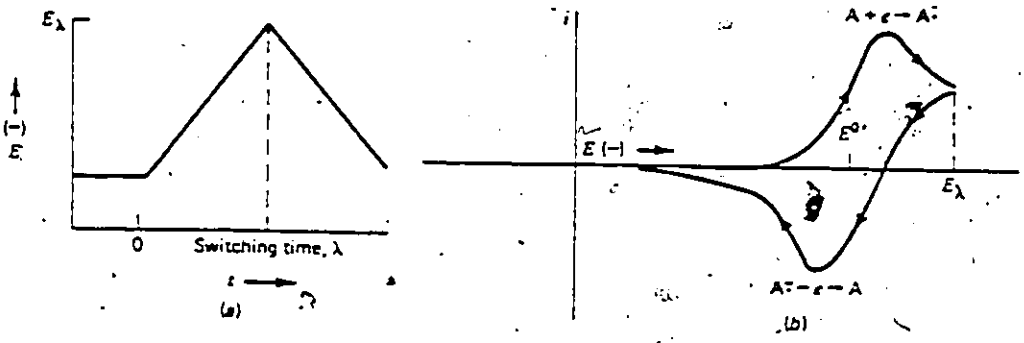

Fig. 2-2: (a) Cyclic potential sweep. (b) Resulting cyclic voltammogram.

information concerning the behavior and characteristics of the electrochemical process and also gives insight into any complicating side processes such as pre-electrochemical and post-electrochemical chemical reactions, as well as kinetic considerations such as slowness of charge-transfer steps or the development of limiting currents due to a pre-electrochemical chemical step such as dissociation, chemisorption or isomerization. The resulting I vs V relation is shown in Fig. 2.2.

The complete electrical circuit utilized in the cyclic-voltammetry experiments is illustrated in Section 2.2 on "electrical instrumentation".

2.1.2 Rotating Disc Electrode (RDE) Experiments

Conventional magnetic stirring is not a very efficient or controllable means of varying the rate of mass-transfer to a small electrode and is seldom used in voltammetry. However, the rotating disc electrode provides a quantitatively controllable mass-transfer rate and is one of the most useful and easy ways of providing hydrodynamic flow control at an electrode.

The disc rotates precisely about a central vertical shaft. Only the bottom surface of the disc is used as an electroactive surface. Electrical connection is made through a control conductor by means of a brush or axial contact.

The electrode is connected to a ASR2 rotator device made by Pine Instrument Company, Grove City, Pa, U.S.A., and the rotation speed ω is controlled by change of the applied voltage through a ASR Speed

Control which has been calibrated to an accuracy better than 1% of the dial reading.

The preparation of the RDE's used in the present work is described in Section 2.9 on "Working Electrodes".

2.1.3 Scanning Electron Microscopy and X-ray Emission Analysis

Great depth of focus, the possibility of direct observation of the external form of real objects, the ability to switch rapidly over wide ranges of magnifications and the ease of operation and sample preparation make the scanning electron microscope a very important and widely used tool for the characterization of solid surfaces in electrochemistry and materials science.

In present work, the Semco Nanolab 7 scanning electron microscopy, which was interfaced with a Microspec WDX-210 wavelenth dispersive x-ray spectrometer, was used to obtain electron micrographs and elemental ratios in the surface regions of the specimens. Especially, indications of morpholgical changes of the surface of sulfides, due to cyclic electrochemical processes, were sought.

2.2 ELECTRICAL INSTRUMENTATION

2.2.1 Basic Principles of Potentiostatic Control

Usually, potentiostats consist of an operational amplifier with high-impedance inverting (-) and non-inverting (+) inputs, coupled with a rapidly responding power amplifier with a low impedance output, as shown in Fig. 2.3.

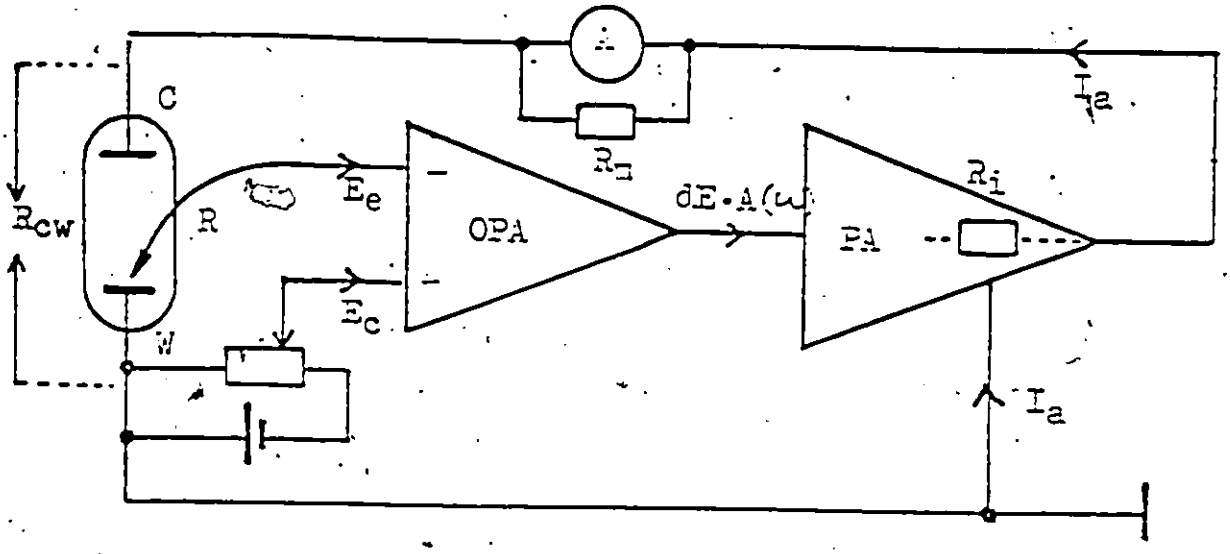

Fig. 2-3: Schematic diagram of potentiostat with electrochemical cell.

The control potential E_c (controlled by manual adjustment or by means of a function generator or minicomputer) applied to the non-inverting (+) input of the operational amplifier is compared with the existing potential E_e of the inverting (-) input. The difference of these two voltages, dE, is greatly amplified by a factor $A(\omega)$ and applied to the input of the power amplifier as the controlling variable $dE.A(\omega)$. $A(\omega)$ is the open loop gain of the operational amplifier which usually depends on frequency.

The power amplifier supplies the output current I_a (up to 1 or 10 A in most instruments) which is required in the controlled system (an electrochemical cell) so that the existing voltage E_e between the reference electrode R and the working electrode W is made almost equal (within 0.2 to 1 mV) to the control voltage E_c.

The difference dE between E_c and E_e becomes smaller as the differential voltage gain $A(\omega)$ of the operational amplifier increases, and also as the output current and the sum of the resistances in the output circuit of the power amplifier decrease.

This sum of the resistances consists of the internal resistance R_i of the power amplifier, the resistance of a current meter or recorder R_m inserted into the output circuit and the terminal resistance R_{cw} of the electrochemical cell between the counter electrode and working electrode, determined mainly by the electrolyte conductance and the cell geometry.

Using the quantities defined above, the difference between the control voltage and the actual voltage is given by

$$dE = E_c - E_e$$
$$= [I_a/A(\omega)](R_i+R_m+R_{cw}).$$

Ideally, dE is close to zero or very small, due to I_a or R being small and $A(\omega)$ being large. Thus there is almost no current passing through the reference electrode, which is maintained therefore at its equilibrium potential.

2.2.2 Circuit

A Servomex LF-141 waveform generator is used to adjust the control potential E_c of the Wenking potentiostat in a preset way and the current density is automatically recorded (after conversion of current to voltage by means of a decade resistance box) vs potential using an Omnigraphic 2000 X-Y recorder. This arrangement gives direct plots of cyclic voltammograms. A block diagram of the circuits is shown in Fig. 2.4. For sweep-rates that correspond to slewing speeds of the recorder greater than full-scale in 1 to 2 s, an oscilloscope, in an X-Y mode, must be used to record the cyclic voltammogram. Alternatively, fast digital acquisition systems can be used for recording conjugate X, Y signals with the cyclic voltammogram being constructed subsequently.

2.2.3 Use of Potentiostats in the Galvanostatic Mode

A potentiostat can be used as a galvanostat by modifying the connections to the electrochemical cell. Instead of controlling the potential difference across the cell, the instrument controls the current through the cell independently of the electrochemical reaction proceeding within it.

The control of current is achieved by inserting an external resistance R_X into the return current line from the working electrode to the potentiostat. Passage of current produces a voltage drop IR_X at R_X to ground as the cell current flows through it. This drop is then applied to the inverting input of the operational amplifier and compared with the control voltage E_c at the non-inverting input. Any deviations between the voltage E_e across R and the set voltage E_c are greatly amplified in the operational amplifier and used to correct the cell current to a value identical with the desired output current of the power amplifier. Feed-back response times are commonly on the order of 1 to 10 μs, depending on the impedance of the instrument and that of the cell and external circuit. These consideration apply also to voltage control in the potentiostatic mode.

From the equation

$$dE = [I_a/A(\omega)](R_i+R_m+R_{cw})$$

it is found that the relative deviation of the controlled cell current I_a from the expected current, calculated by $I=E_c/R_X$ with $dI=I-I_a$, is again inversely proportional to the gain $A(\omega)$:

$$dI/I_a = [1/A(\omega)][(R_i+R_m+R_{cw}+R_X)/R_X]$$

For accurate control of the current it is seen from the above equation that R_X should be comparable in magnitude with the sum of the other resistances.

The controlled current or the potential can be adjusted either manually or by means of a preadjusted function generator. The block diagram is shown in Fig. 2.5.

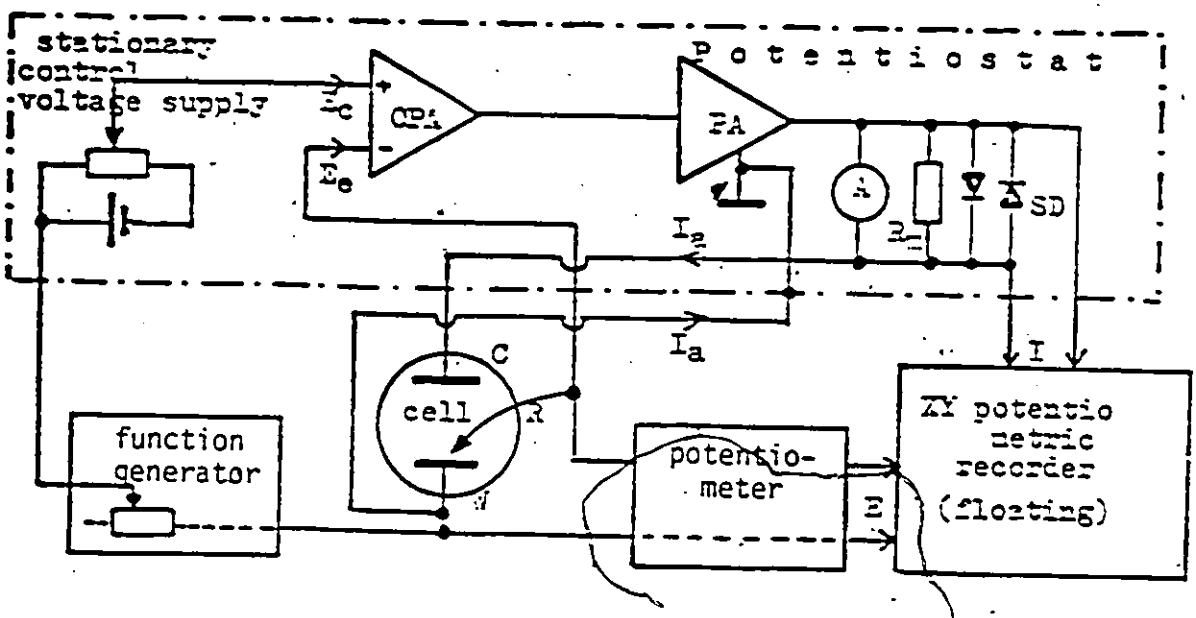

Fig. 2-4: Block diagram for recording current-density vs potential curves.

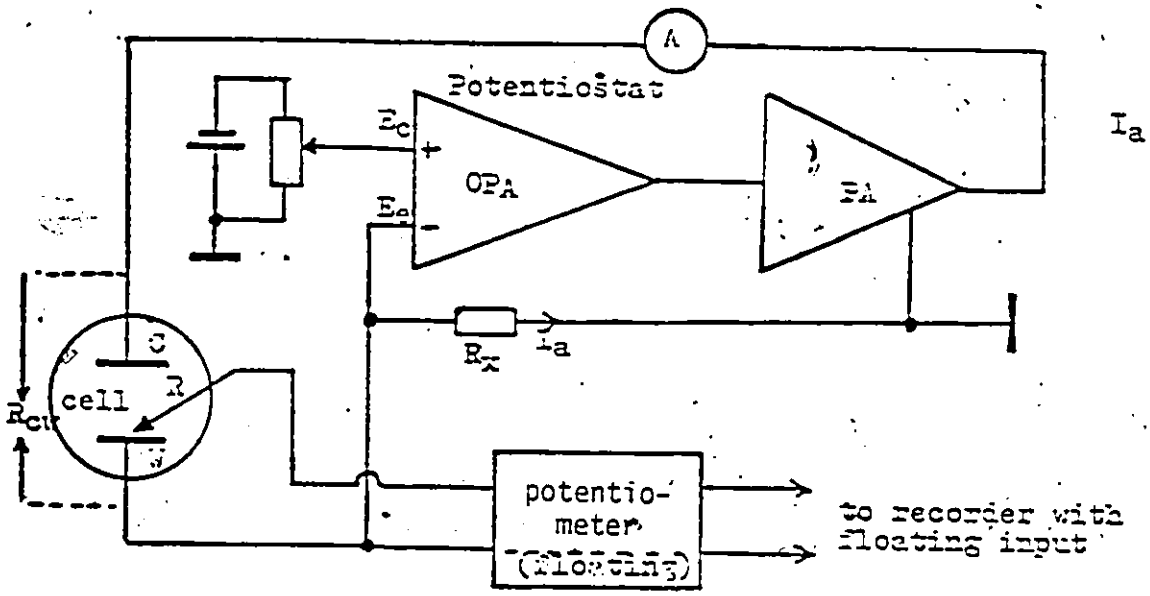

Fig. 2-5: Schematic diagram; galvanostatic principle with potential recording.

2.3 CHOICE AND PREPARATION OF SOLUTIONS

The choice of solvent in an electrochemical investigation usually is dictated by circumstances and focused on the particular system and the information that can be gleaned from the electrochemical study.

The solvent properties of electrochemical importance include: protic character (acid-base properties); anodic and cathodic voltage limits (related to redox properties and protic character); mutual solubility of the solute and solvent; and physico-chemical properties of the solvent (dielectric constant and polarity, donor or solvating properties, liquid range, viscosity, and spectroscopic properties). Practical factors also enter into the choice and include the availability and cost of the solvent, ease of purication, toxicity, and general ease of handling.

There are several ways in which the solvent-supporting electrolyte system can influence mass-transfer, the electrode reaction (electron transfer) and the chemical reactions which are coupled to the electron transfer. The diffusion of an electroactive species will be affected not only by the strength of the solute-solvent interactions which determine the size of the solvent sphere; the solvent also plays a crucial role in proton mobility.

The use of an indifferent or "inert" supporting electrolyte is indispensable in electrochemistry and affects the solvent medium in several ways: (a) it regulates cell resistance and mass transport by electrical migration; (b) it may control or "buffer" the level of hydrogen ion activity in solution: (c) it may associate with the electroactive solute, as in the complexing of metal ions by certain

ligands; (d) it may form ion-pair or micellar aggregates with the electroactive species; (e) it largely determines the structure of the double-layer; and (f) it may impose positive or negative voltage limits because of its redox properties.

2.3.1 Preparation of Inorganic Aqueous Solutions

Pyro-distilled water was used for all solutions. The quality of this water have been discussed elsewhere by Conway and co-workers (228). The use of this type of water is desirable for most surface electrochemical work.

1) Perchloric acid solutions.

$HClO_4$ solutions were utilized very often in this work. The acid solutions were made up volumetrically from BDH Aristar $HClO_4$ (a very high purity grade) and pyro-distilled water. The electrochemical purity of these solutions was found to be excellent as indicated by the i-V behavior of a platinum electrode in a cyclic voltammetry experiment. $HClO_4$ was chosen as the supporting electrolyte for most of the work at acid pH's as it can be obtained very pure and also its anion is only weakly specifically adsorbed at Hg and other metals.

2) Hydrochloric Acid solutions.

Hydrochloric acid solutions used in the experiments were prepared volumetrically from BDH Aristar grade HCl and pyro-distilled water.

3) Potassium chloride solutions were prepared volumetrically from 2X recrystallized KCl, dried at 423 K in vacuo. A.C.S. analytical grade KCl was used with double-distilled water.

4) Sodium perchlorate solutions were prepared volumetrically from BHD "AnalaR" Grade $NaClO_4$ H_2O and double-distilled water.

5) Disodium hydrogen orthophosphate and sodium dihydrogen orthophosphate solutions were prepared volumetrically from BHD "AnalaR" Grade Na_2HPO_4 $12H_2O$ and/or NaH_2PO_4 with double-distilled water to make up buffer solutions at various pH's.

6) Sodium borate solutions were prepared volumetrically from BHD "AnalaR" Grade $Na_2B_4O_7$ $10H_2O$ with double distilled water to make up buffer solutions at various pH's.

7) Sodium carbonate solutions were prepared volumetrically from BHD "AnalaR" anhydrous Na_2CO_3 and double-distilled water to make up solution at pH 11.

8) Buffer solutions. All buffer solutions were prepared from the stock solutions made individually, as indicated above;

pH		
0	1M $HClO_4$	
1	0.1M $HClO_4$	
2	88ml 0.2M KCl	+ 12ml 0.2M HCl
3	0.001M $HClO_4$	+ 0.1M $NaClO_4$
5	20ml M/15 Na_2HPO_4	+ 980ml M/15 NaH_2PO_4
7	692ml M/15 Na_2HPO_4	+ 308ml M/15 NaH_2PO_4
9	0.1M $Na_2B_4O_7$	
11	0.1M Na_2CO_3	

Most of the solutions were prepared from perchloric acid, sodium perchlorate or other sodium salts in order to minimize specific adsorption, this being small with Na^+ cation and ClO_4^- anion at sulfides (175). The probable adsorption of Na^+ ion on sulfides in strongly basic solution prevented this study from being satisfactory in high pH solutions.

All solutions used were deoxygenated by bubbling a slow stream of purified N_2 gas through them prior to the experiments for 30 minutes and during the experiment itself (as indicated).

9) Pyro-distilled water

Recently, it has been found to be difficult to prepare pure water free from organic, surface-active contaminants by means of distillation, even from alkaline potassium permanganate.

The organic contaminants commonly present in domestic and industrial water supplies are steam-volatile and are hence not removed by distillation. Conway and co-workers (228,229) have developed a pyro-distillation technique for further purifying regular Barnstead distilled water, which meets the requirements for use in electrochemical studies, particularly on surface processes that are very sensitive to adsorption of impurities. The principle involved is pyrolysis of organic impurities by passage of the steam through a column of silica at 1023 K in a stream of oxygen. The hot column contains a 90% Pt/Rh gauze which provides an efficient zone for the catalytic oxidation of organic trace impurities. The pyro-distillation apparatus is shown in Fig. 2.6.

At first, directly-distilled water from a regular aqueous $KMnO_4$ distillation is syphoned into the boiling flask through a glass tube system. The pyro-distillation was then operated so as to recycle the water as steam through the catalytic furnace for 48 hours with passage of purified O_2 at about 1 $cm^3\ s^{-1}$. The setup was provided with a Soxhlet type overflow syphon which returns 100 cm^3 volumes of condensed pyro-distilled H_2O back to the distilling flask every hour. The distillation was continued for 48 hours before the purified H_2O was collected for use in an experiment.

The purity of such water for electrochemical measurements has been discussed by Conway et al (228) in terms of surface purity and H adsorption behavior at Pt in solutions prepared from pyro-distilled H_2O in comparison with ordinary distilled water at University of Ottawa. The specific conductance of this water was too low to be measured. The conductivity of the pyro-distilled water was consistently less than 10^{-7} $ohm^{-1}cm^{-1}$.

2.3.2 Choice and Preparation of Organic Sulfides

The compounds chosen were those having an -S-S- linkage between two similar parts of the molecule as with cystine (a disulfide), or a cyclic -S-S- linkage as in α-lipoic acid (thioctic acid). In the case of cystine, the reduced form of the molecule, cysteine, was also examined comparatively.

All solutions of cysteine, cystine and α-lipoic acid (from Fluka) were made up in pyro-distilled water at appropriate concentrations by weight and the pH's were adjusted with suitable supporting electrolytes (see p. 66).

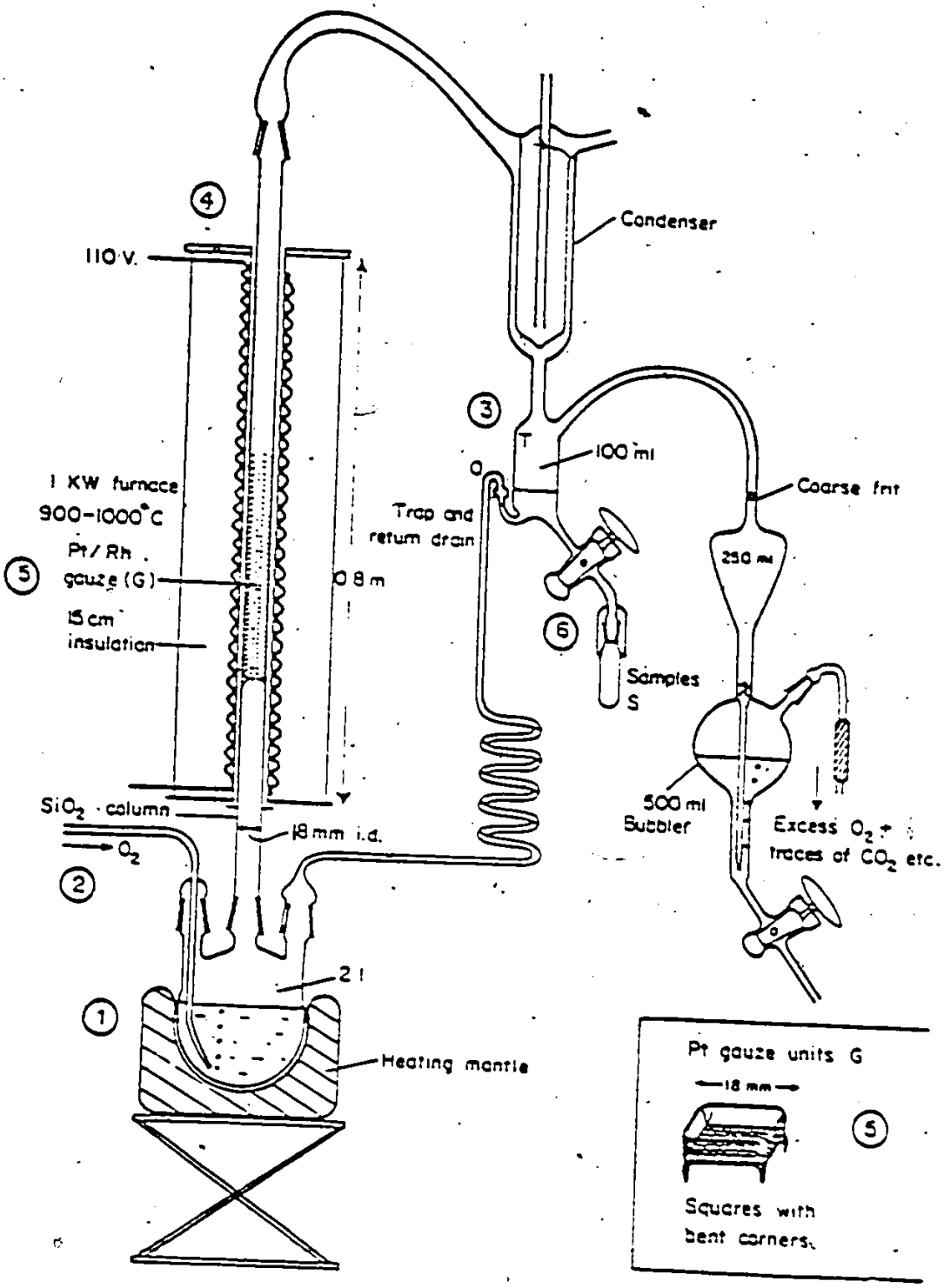

Fig. 2-6: Pyrodistillatio apparatus.

2.4 ELECTROCHEMICAL CELLS

The electrochemical cells used in this work were fabricated from pyrex glass as shown in Figs. 2.7. and 2.8. The cumulative experience has been that substantially "cleaner" results can be obtained by simplifying the cell design as much as possible.

The reference electrode compartment is separate but is connected to the solution and electrode in the working electrode compartment by a Luggin capillary whose tip is placed close to the working electrode in order to minimize the error in the measured potential associated with IR drop in the solution between the tip of the Luggin capillary and the working electrode.

2.5 CLEANING OF GLASSWARE

All electrochemical cells, including those used for optical reflectance and photo-effects, were soaked in concentrated CrO_3-H_2SO_4 mixture for 24 hours before use, followed by thorough rinsing in double-distilled water. The cells were then filled with pyro-distilled water and allowed to soak overnight. Prior to use, the cells were filled with the appropriate solution and allowed to soak for 30 minutes. The cell was then emptied, rinsed a second time, and filled with the solution required for the experiment.

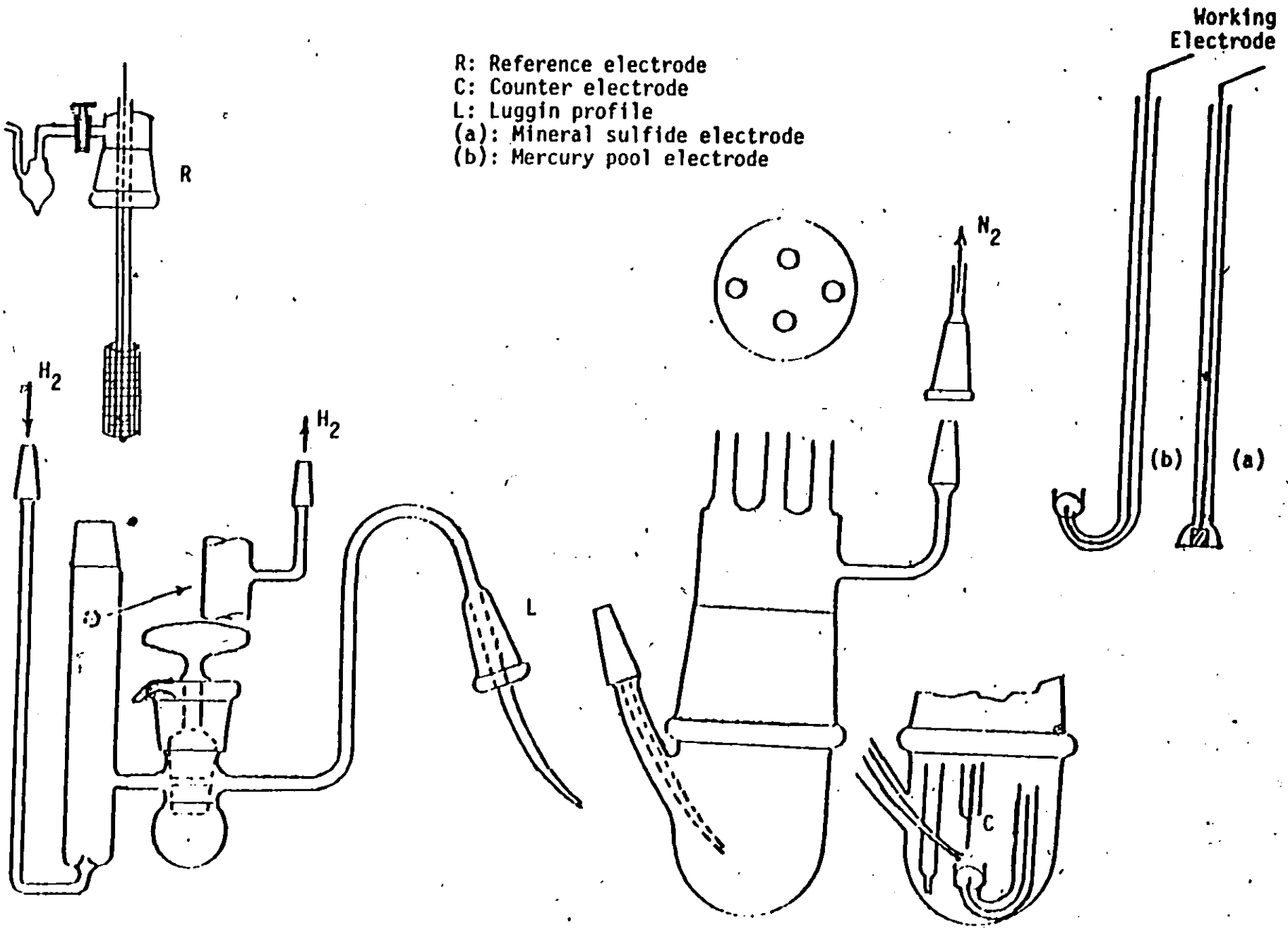

Fig. 2-7: Schematic designs and set-up of experimental cells.

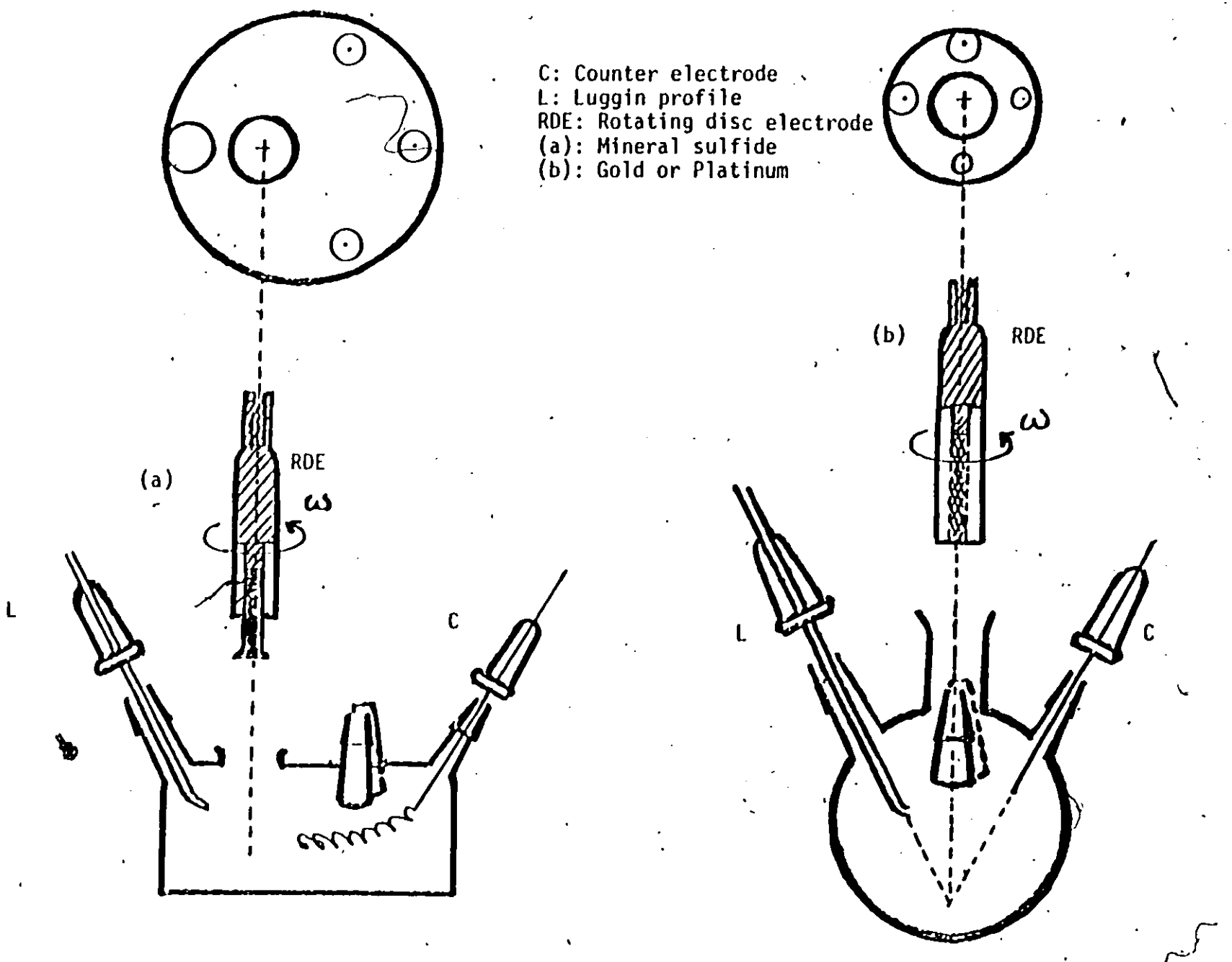

Fig. 2-8: Schematic designs and set-up of rotating electrode experiments.

2.6 PURIFICATION OF GAS

Since oxygen is chemically very reactive with many substances and electrochemically reducible, it is necessary to remove traces of oxygen from hydrogen gas (for the reference Pt/H_2 electrode) and from the nitrogen gas used for deoxygenation of the solutions prior to conducting experimental runs.

The standard procedure for purification of H_2 and N_2 as used in this laboratory was employed [5]. The gases are passed through a gas train (230-232) consisting of molecular sieves (BDH type 4A), partculate $Mg(ClO_4)_2$ as desiccant, Cu turnings at 623 K followed by three activated charcoal traps cooled by liquid N_2 as shown in Fig. 2.9. In the H_2 train, a tube containing palladized asbestos at 623 K is included for complete removal of traces of O_2 The H_2 used was electrolytic grade.

2.7 REFERENCE ELECTRODE

The hydrogen electrode established at Pt is universally adopted as the primary standard with which all other electrodes are compared. Because of its high degree of reproducibility and comparative ease of preparation, it was used throughout this study. The activity of the H_2 electrode is assured by the electrodeposition of platinum black upon a bright Pt metal substrate. The hydrogen electrodes used were periodically checked against a standard calomel electrode (see below).

Prior to making the Pt electrodes, the platinum wire and gauze used for their construction were degreased under reflux with acetone in a Soxhlet apparatus for 12 hours.

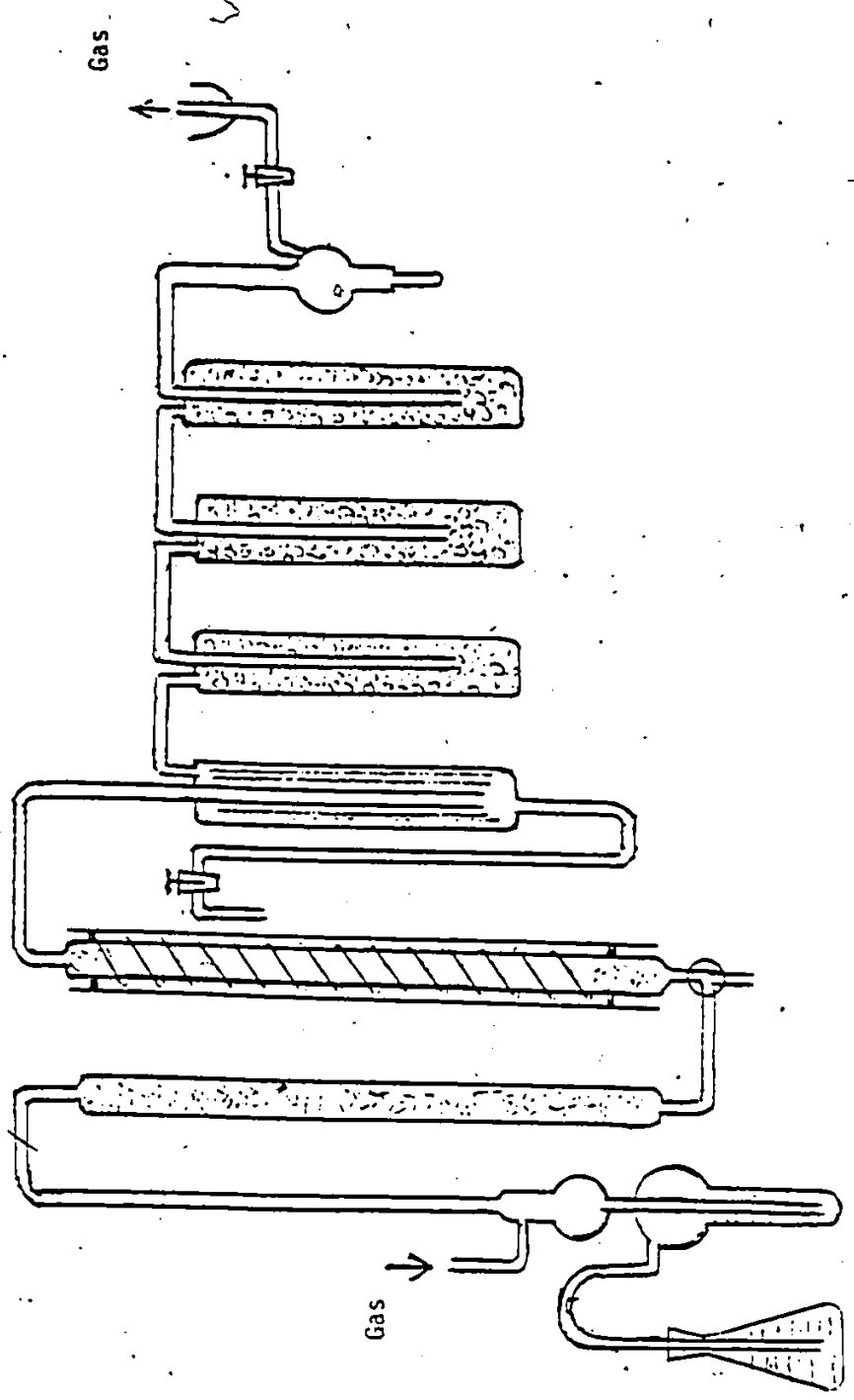

Fig. 2-9: Set-up of gas train for purification of H_2 and N_2.

The gauze was spot-welded to the short wire, then the latter was sealed into a soft glass tube to make an electrode as in Fig. 2.7:R.

Before platinization, the electrodes were cleaned by brief immersion in a warm solution of 50% aqua-regia (three volumes of 12 M hydrochloric acid with one volume of 16 M nitric acid and four volumes of pyro-distilled water). This mixture also can be used to strip the platinum black from used electrodes. The electrodes are then washed in 16 M nitric acid, rinsed with pyro-distilled water, cathodized in 0.01 M sulfuric acid and given a final thorough rinse with pyro-distilled water. The cathodization step is designed to remove surface oxides and should be carried out promptly before platinization.

Feltham and Spiro (233) have surveyed platinizing procedures and recommend a solution of 3.5% chloroplatinic acid (H_2PtCl_6) with 0.0005% lead acetate, with electrolysis at a current density of 5 mA cm^{-2}, so that there is only a slight evolution of gas (H_2 and Cl_2); good stirring is necessary. The direction of the current was reversed every minute and the plating was allowed to proceed until a moderately thick coating of grayish-black platinum was obtained. The electrode was then repeatedly washed with distilled water, followed by several washings in pyro-distilled water and stored in pyro-distilled water. If dry electrodes are exposed to air for a prolonged period, their catalytic activity is lost and they must be replatinized before use.

The active surface of the platinized electrode should be covered completely by the solution. When in use, it should be supplied with pure hydrogen gas at the rate of 1 to 2 bubbles per second from a jet about 1 mm in diameter.

Electrolytic grade hydrogen (available commercially in cylinders) is a convenient source of H_2 gas. It typically contains 0.15 to 0.20% of oxygen and 0.03 to 0.05% nitrogen. The potential of a hydrogen electrode will be biased by the partial pressure of dissolved oxygen in the solution because the oxygen is readily reduced at the catalytically active surface (234,235). Therefore, oxygen should be removed from the hydrogen gas, as described above.

The most convenient method for producing a supply of dry oxygen-free H_2 gas employs heated copper gauze (or BTS) with a palladized asbestos catalyst in conjunction with molecular sieves in a system such as was described in Section 2.6 on purification of gas. The output gas will have an oxygen and water content each below 1 ppm in a carefully built system.

For this Pt/H_2 reference electrode, the electrolyte in the reference compartment was saturated with H_2 gas for at least 30 minutes prior to the experiments.

A saturated calomel electrode (SCE) was used as a calibrating reference electrode to check the H_2 electrodes used. It was satisfactorily reversible and gave stable potentials.

2.8 COUNTER ELECTRODE

The counter electrode, whose only function in a cell is to provide a means of passing the electrolytic current, should work without introducing any high resistance in the circuit or any new species in the solution which could interfere with the study of the process to be investigated at the other (working) electrode. An electrode made from

the same material as that to be used as the working electrode, and passing current by the reverse of the investigated reaction, would therefore form the ideal counter electrode. In this way, no contaminants would be produced from the counter electrode. Under such conditions the electrolyte concentration in the cell would remain constant under conditions of stirring. However, it is not often that such a counter electrode can be made and used. Therefore, a counter electrode made from relatively inert materials such as Pt can usually be used with various working electrode materials.

In present work, the counter electrode was made from Pt wire and the same pretreatment and platinization procedure were used as described in the previous section on reference electrodes. It is important that the counter electrode wire has a perfect leak-proof seal to its glass holder. Again, soft glass is used for this purpose.

2.9 PREPARATION OF WORKING ELECTRODE

The working electrodes were of galena (PbS), pyrite (FeS_2) and pyrrhotite ($Fe_{1-x}S$) and were prepared from the natural minerals in the following manner. A small portion of mineral about 4 mm^2 in area and 15 mm height was cut from the crystal by a diamond saw and washed in an ultrasonic cleaner with a cleaning detergent and then in distilled water.

The washed piece of crystal was then clipped with a copper clipper which was soldered to a copper wire. The whole system was inserted into a glass tube which was filled with some unset Araldite epoxy adhesive. The epoxy was then allowed to solidify completely. From

the end of this electrode a thin layer was then cut off to expose a crystal surface towards the outside. For making rotating electrodes out of the mineral specimens, the electrode, as prepared above, was fitted into a Teflon insert plug and the wire soldered on to a specially made rotating electrode holder capable of being fitted into the Pine instrument Co. apparatus. The Teflon insert plug secured the glass tube and rotating holder as shown in Figs. 2.7(a) and 2.8(a).

Prior to being placed in the cell, the electrode was polished with an alumina polishing suspension from Buehler on a rotating polishing equipment and washed in an ultrasonic cleaner to remove all the polishing material.

Galena crystals were contributed from Dr. S.M. Ahmed, CANMET, Department of Energy, Mines and Resources.

Cubic pyrite crystals (Spain) were obtained from Ward's exhibition minerals.

Pyrrhotite crystals (Blue Bell, B.C.) were contributed from the Mineralogical Section of the National Museums of Canada.

2.10 ROTATING Pt AND Au DISC ELECTRODES

The electrodes used for all the experimental runs with organic sulfur-containing compounds were mounted in Teflon holders provided with the Pine Instrument Co. rotating electrode assembly.

2.11 MERCURY POOL ELECTRODE (FOR WORK ON -S-S- AND -S-H ORGANIC COMPOUNDS)

A cup to contain Hg was made from glass tubing and provided with a conducting lead as shown in Fig. 2.7(b).

For each run, a certain amount of freshly purified Hg was taken from the middle of a bulk volume of Hg, with an unused pipette and transferred into the cup.

The electrode was then mounted in the cell at a fixed geometric position.

2.12 pH VARIATIONS AND TEMPERATURE

All experiments were carried out at a variety of pH values from the range of acidic, neutral to alkaline using buffer solutions.

The temperature was kept at 298 K throughout the various programmes of experiments.

Chapter III

RESULTS AND DISCUSSION

3.1 REVIEW OF CYCLIC-VOLTAMMETRY

3.1.1 Introduction

The cyclic-voltammetry proceduce employs a relatively fast change of potential at a static electrode surface, rather than a dropping Hg one, but is applicable to any other type of electrode configuration, including these that are rotated (rotating-disc electrode as employed in part of the present work). The method finds its origins in fast-sweep polarography techniques developed by Sevčik (236) and by Delahay and Perkins (237). Since this procedure has been extensively employed in the work described in this thesis, a brief account is given below of the characteristics of this method with its application to diffusion and surface reaction controlled processes at electrodes and the types of results that are expected from it.

3.1.2 Method

The potential V is modulated according to a linear program of variation in time, t, at a sweep-rate s ($V\ s^{-1}$):

$$V = V_i \pm st$$

where V_i is some initial potential that may or may not have been held constant for some time t before the sweep was initiated. The method may utilize only a single sweep ("potentiodynamic sweep" or "linear potential sweep") between two potentials, V_i and V_f, (a final potential) or may be arranged to give a repetitive response by varying the potential in a continuous back and forward way (anodic and cathodic or vice versa) between V_i and V_f values. It is this embodiment of the method that is referred to as "cyclic voltammetry", abbreviated here by the letters CV.

3.1.3 Kinetic and Other Conditions

As with any electrode process, two principal conditions may arise:

1) reversible and irreversible kinetic behavior of the electrode reaction; and

2) activation (i.e., reaction kinetic) or diffusion-control of the rate or current at the electrode (the other conditions are those that normally obtain in polarographic experiments).

A third situation can arise:

3) where the electrode process involves only, or primarily, a surface phase or adsorbed layer of the electrochemically reactive material; then characteristic CV behavior arises that can be distinguished from that under conditions of bulk diffusion-control. In this regime, both reversible and/or irreversible behavior may also be observed as, of course, may generally be expected.

3.1.4 Characteristics of the Current Response - Diffusion Control

Characteristic current reponse behavior in CV has been evaluated for the various combinations of conditions referred to above and can be summarized as follows.

First, a CV I vs V profile, resulting from the linear variation of potential over a range where some Faradaic oxidation or reduction reaction can take place, has the form of a curve exhibiting a maximum (peak) current (I_p) at a characteristic peak potential (V_p). For diffusion-controlled rates, I_p is linear in $s^{\frac{1}{2}}$ according to the equation

$$I = zFAC_O\sqrt{\pi Da}\cdot\chi(at)$$

for a z-electron reaction proceeding at an electrode of area A; C_O is the bulk concentration of reactant, D is its diffusion constant, at = zFst/RT = (zF/RT)(V_i-V_f) for reversible conditions and χ(at) is a function of (at) arising from solution of Fick's laws for the boundary conditions obtaining for the particular diffusion flux and elctrode geometry involved. χ(at) depends on potential and gives rise to the characteristic form of the I vs V profile. χ(at) has been evaluated by Nicholson and Shain (238) and by Delahay and others (239). For irreversible conditions,

$$I = zFAC_O\sqrt{\pi Db}\cdot\chi(bt)$$

where b is analogous to a but applies to irreversible charge-transfer according to bt = αzFst/RT where α is the charge-transfer coefficient for the electrochemical interfacial reaction. χ(bt) is a similar

function to $\chi(at)$ and like $\chi(at)$ depends on potential in a characteristic manner.

For the diffusion-control regime, the following quantitative characteristics of the I vs V profiles are to be noted:

i) Difference between anodic and cathodic peak potentials

$$\Delta V_p = V_{p,c} - V_{p,a} = 2 \times (0.028/z) \text{ V at 298 K.}$$

ii) Difference between V_p and the half-wave potential, $V_{\frac{1}{2}}$,

$$V_p - V_{\frac{1}{2}} = -1.1 \times (RT/zF)$$

iii) For the irreversible case, peak shift $\Delta V_p(s)$ is 0.03 V for a 10-fold change of s at 298 K when $\alpha z = 1$, or generally

$$\Delta V_p(s) = (RT/\alpha zF)(1/2)\ln[\alpha zFs/RT]$$

iv) V_p is independent of reactant concentration.

It is to be noted that for both reversible and irreversible conditions, I_p varies with $s^{\frac{1}{2}}$. In other respects, the reversible and irreversible CV curves differ somewhat in shape, as is illustrated later in Fig. 3.2, for reasons that are discussed below in Section 3.1.5.

Secondly, the maximum in the CV profiles arises because some time is needed for the concentration gradient to become adjusted to the sweep-rate; thus the reactant concentration near the electrode surface is initially higher than later in the sweep while the rate of the electrode process is varying with potential. In the reversible case, the potential is related to the concentration of oxidized [O] and

reduced [R] species of the redox couple by the Nernst equation ($V = V_r + (RT/zF)\ln([O]/[R])$ as in polarography while in the irreversible case it is determined by a Tafel type relation involving α. Eventually the O form, in a cathodic sweep, is completely consumed at the electrode interface and the diffusion-controlled limiting current I_{lim} is approached, as in a polarographic wave.

The combination of these effects in the non-steady state leads to the peaked current vs potential profile.

In some experiments in the regime of diffusion-control, it is useful to assist the mass-transfer limitation, or eliminate it, by conducting the CV at rotated disc electrodes as was done in some of the work to be reported later in this thesis.

3.1.5 Characteristics of the Current Response - Surface Reaction Control

In the case of a reaction involving only a surface phase, there is, of course, no diffusional mass-transfer process involved (once the surface phase has been formed and provided the solution concentration is anything but extremely dilute). Then the $\chi(at)$ or $\chi(bt)$ functions that derive from integration of equations arising from Fick's laws do not enter into the equation for the current. Rather, the ad-species is deposited at the electrode at a rate proportional to the free surface site fraction, $1-\theta$, and the desorption stripping at a rate proportional to θ, each rate depending on a time-dependent charge transfer factor, $\exp(\pm\alpha VF/RT)$. The reversible case arises when, at any potential, both backward and forward (anodic and cathodic, or

vice-versa) current components involving the factors $\exp(\pm\alpha VF/RT)$ and $\exp[\mp(1-\alpha)VF/RT]$ determine the I vs V relation of the CV profile while the irreversible case arises when only one or other of these factors is involved, corresponding to the back-reaction rate being negligible.

The behavior of the irreversible case is distinguished from that of the reversible case in the regime of surface reaction control by:

i) I_p being 27% lower than that for the reversible I_p value (for a given degree of molecular coverage at saturation, $\theta=1$)

ii) Asymmetry of the shape of the I vs V profile in comparison with that for the reversible reaction case; and

iii) The peak potential, V_p, varying with log s rather than being independent of s, as with a Tafel relation; unlike the case of diffusion-control, the currents, including I_p, for a surface reaction process are linear in s rather than its square-root as shown in Fig. 3.1. This is an important distinguishing characteristic of a surface process in CV compared with a diffusion-controlled one. In the present work, some mixed cases are encountered, as will be treated later, where both diffusion and surface reaction processes appear to take place in a consecutive and parallel relationship. Usually this shift of V_p is log in s, as with the Tafel relation in log I.

iv) The peak potential is shifted from the reversible value due to a polarization effect as with an irreversible polarographic wave.

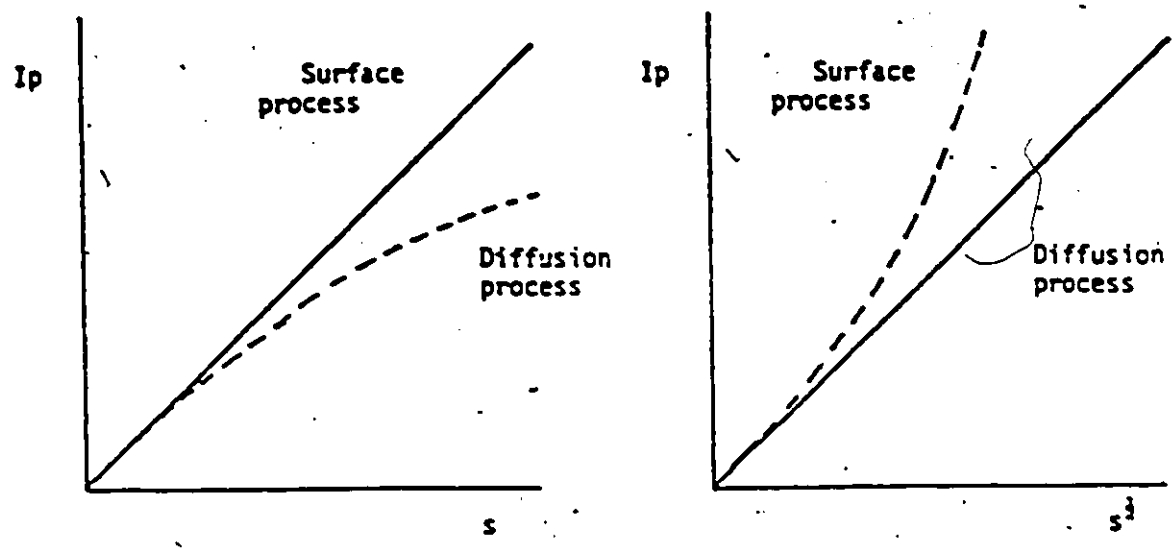

Fig. 3-1: sweep-rate dependence of peak currents for a surface reaction and a diffusion-controlled electrochemical reaction.

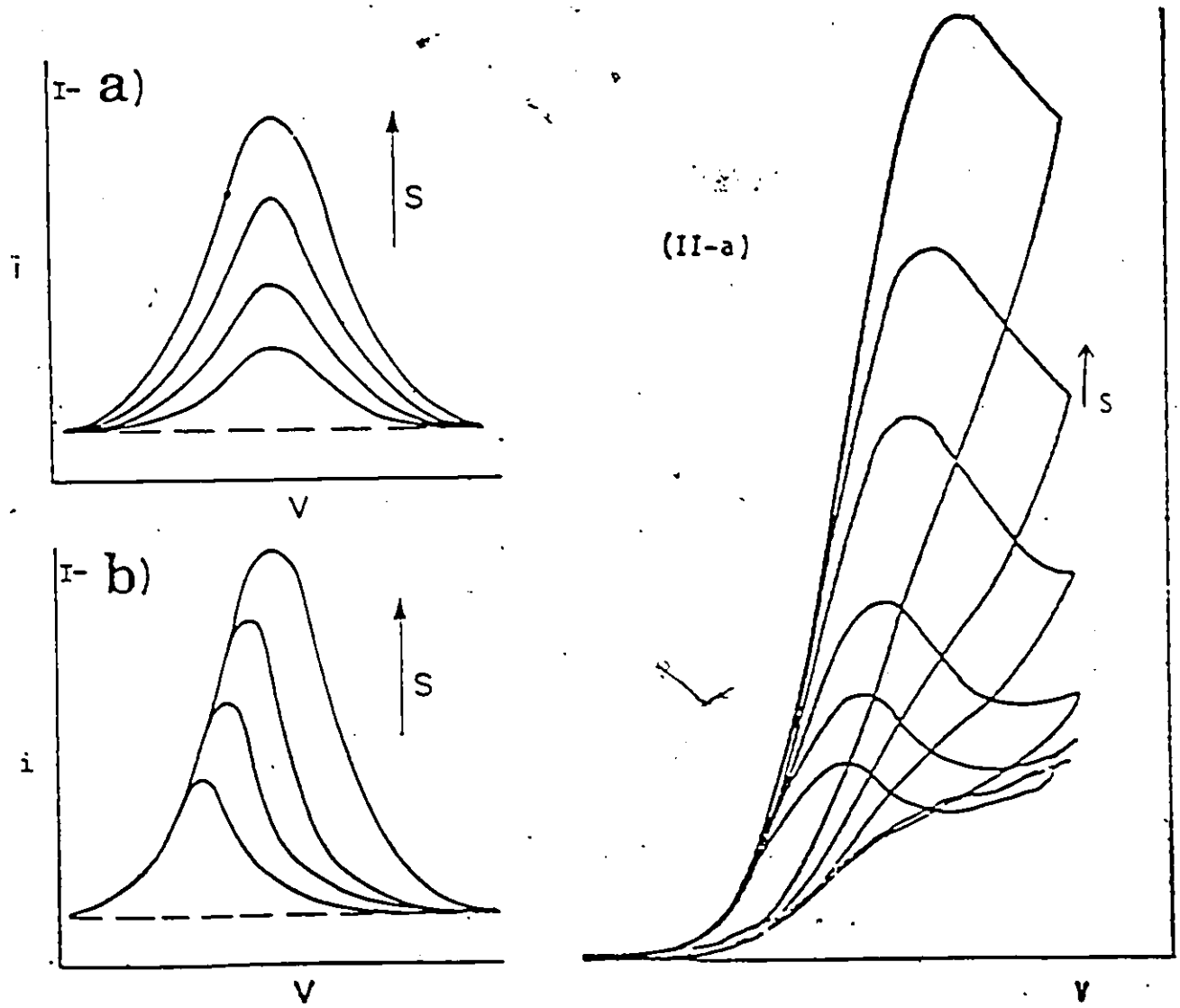

Fig. 3-2: (I-a) Shapes of i vs V profile with increasing s for a surface process involving a 2-d array of adatoms on an electrode eg H on Pb.
(I-b) Shapes of i vs V profiles with increasing s for a surface process involving consumption of a 2-d surface phase on an electrode.
(II-a) Electrochemical reaction involving diffusion process.
See (II-b) on next page.

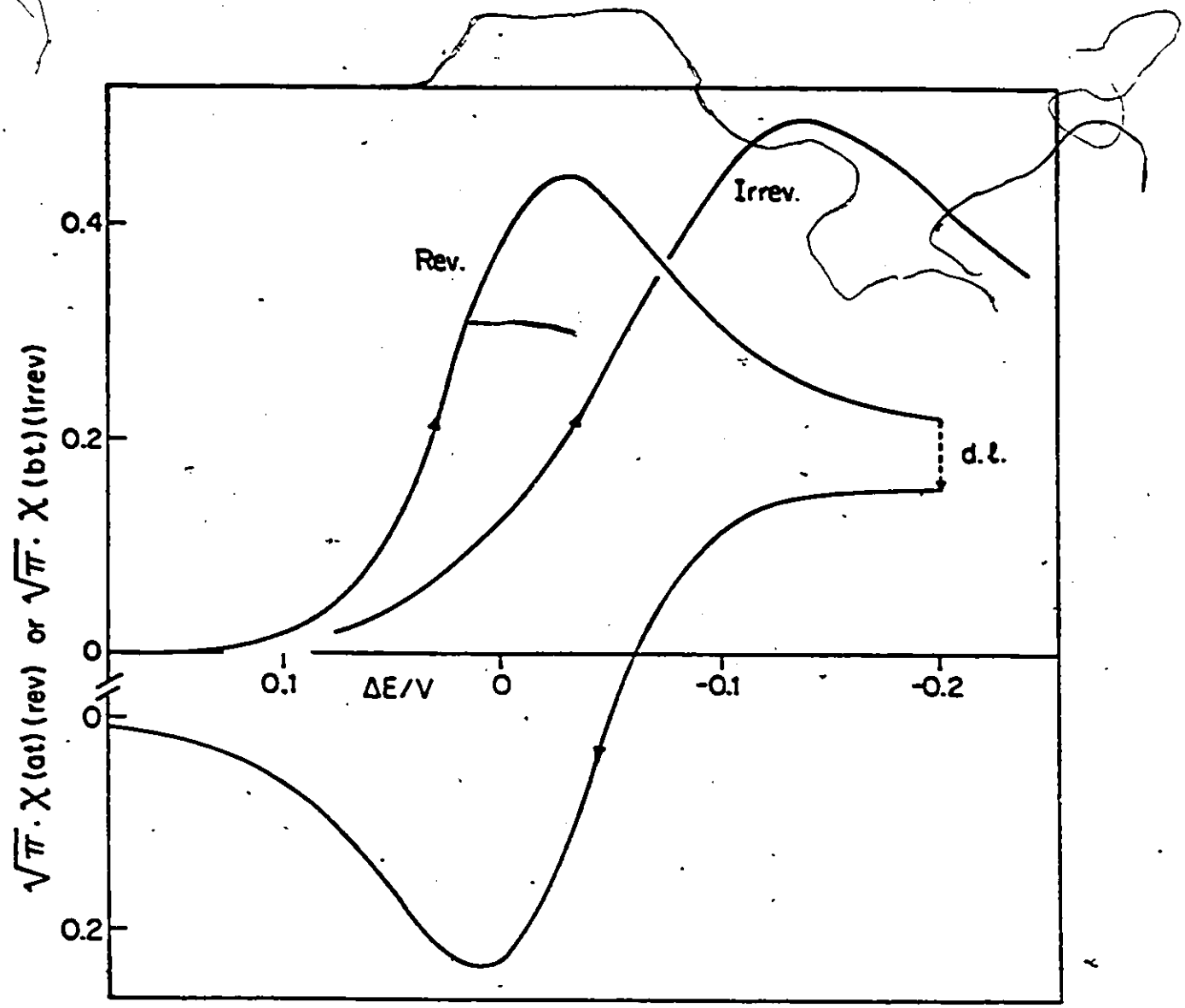

Fig. 3-2(II-b): Quantitative plots of cyclic-voltammetry current functions, $\pi^2\chi(at)$ and $\pi^2\chi(bt)$, for a reversible and an irreversible diffusion-controlled process, respectively, plotted from Nicholson and Shain's solution of the Fick diffusion equations for a 1e electrode process at a plane electrode (transfer coefficient α taken as 0.5 for the irreversible case; irreversible curve positioned on ΔE axis arbitrarily, depending on rate constant. ΔE for reversible case is $E-E_{\frac{1}{2}}$, the half-wave potential.)

3.1.6 General Form of i vs V Profiles

In general, the CV I vs V profiles for diffusion and surface reaction controlled currents are found to be somewhat similar in their peaked shape and overall form. The differences arise from the nature of involvement of concentration of the reactant species. In the diffusion-controlled case, reactant material is consumed from the diffusion layer, eventually depleting the solution completely at the electrode interface (limiting current condition). However, during the sweep, depending on its duration measured by s^{-1}, reactant material continues to diffuse into the boundary region so that the charge under the I vs V(t) profile increases with diminishing s. In the case of a surface reaction there is a finite quantity of material in the surface phase which is eventually consumed during passage of the the sweep so that the current goes to zero apart from the residual double-layer charging current $C_{dl}(dV/dt)$ that passes at all potentials, as also in the diffusion-control case.

In the surface reaction case, since the consumable reactant quantity is fixed, determined by the geometry and thickness of the surface phase, the charge, Q, under the cyclic-voltammogram ($Q = \int i dt = \int (i/s) dV$), the total charge measured is independent of sweep-rate, provided the reaction is 100% coulombically efficient, i.e. parasitic or impurity currents are insignificant.

In both cases, the rising side of the curve is associated with the exponential increase of current with V, while the descending current side is associated with consumption of the reagent - either from the diffusion layer or from the surface phase, although, of course, the

potential continues to increase. In some easily recognizable cases, the potential of the electrode surface phase remains almost constant during its consumption while for a Langmuir-type adsorbed layer the potential varies as $\ln(\theta/1-\theta)$. Refer to Fig. 3.2; in the first case, for a surface phase, the ascending current sides of the profiles at increasing sweep-rates are almost coincident (I) but fall away to the descending side at various currents as the sweep-rate is varied. For the Langmuir ad-layer, however the curves fall more symmetrically above each other (II) with increasing sweep-rate, especially in the reversible reaction case.

Referring again to the first case where ascending current curves are almost coincident at various sweep-rates, this behavior arises because a regular Faradaic current passes for essentially a bulk phase process where the thermodynamic potential does not change during its consumption (except at the very last stages). This situation applies to multilayers or thick films. In the Langmuir ad-layer case, however, only a monolayer or submonolayer is involved where the thermodynamic potential is $f(\theta)$ and hence changes during the sweep. The resulting I vs V profiles are therefore different for these two cases and both are different from the diffusion case.

Examples of all three types of behavior have been encountered in the course of the present study of the electrochemistry of mineral and organic sulfides.

3.1.7 Complications due to Pre- and Post-Electrochemical Reactions

Other complications may arise in the CV study of electrode reactions and reflect kinetic complexity of the reaction pathway; e.g. chemical reactions may precede or follow the potential-determining charge-transfer reaction and product species may be either adsorbed or formed directly into solution without adsorption. Also, two or more kinetically separate electron transfer processes may take place. The consequences of complications of these kinds for the shapes and other characteristic features of CV I vs V profiles have been worked out by several authors, e.g. by Nicholson and Shain (238) and Delahay (240) for the regime of diffusion-controlled processes and by Kozlowska, Conway and Klinger (241), and by Laviron (242), in various papers for the surface reaction control cases. In favorable cases, kinetics of the pre- or post-electrochemical chemical steps may be evaluated.

3.1.8 IR Drop Effects

At high s values, and/or with relatively reversible surface reactions, the currents generated in the CV experiment may be sufficiently large in relation to the resistance R of the solution between the Luggin probe of the reference electrode and the surface of the working electrode, that significant IR drop, increasing with s, arises. Then an instrumental IR compensation technique must be used or a calculated correction applied, e.g. as recently treated in papers by Laviron (243)' and by Tessier and Conway (244). In most of the experiments in the present work, which was conducted at relatively low sweep-rates, these problems did not arise.

PART I -- INVESTIGATIONS WITH INORGANIC SULFIDES

3.2 LEAD SULFIDE (GALENA)

3.2.1 Cyclic-Voltammetry with PbS

The electrochemical behavior of galena (PbS) mineral crystals was studied in some detail in collaboration, in part, with Ho in this laboratory.

The general form of the cyclic voltammogram obtained at PbS electrodes at pH 9 in sodium borate buffer is shown in Fig. 3.3. For convenience of discussion of the results, the current peaks are designated A_1, A_2 (anodic) and C_1, C_2 (cathodic) to correspond with the peaks.

With successive cycling of PbS electrodes in 0.1 M $Na_2B_4O_7$ aqueous solutions over the potential range -0.45 to +0.35 V vs E_H, the currents on the voltammograms progressively diminish in the A region but increase in the A_2 region (see Fig. 3.3). This behavior is not due simply to surface area changes.

The currents in the C_2 region, which are generated after taking the potential into the A_2 region, also increase with cycling in proportion to the increases which occur in the A_2 potential range. At the more negative potentials in the cathodic sweep, currents in the C_1 region decrease with cycling as they do in the conjugate A_1 region. The charge for the C_1 process should include any reduction charge passed at the beginning part of the next successive anodic sweep (i.e., without holding at -0.45 V) since it is found that the direction of the current is not immediately reversed upon reversal of the sweep

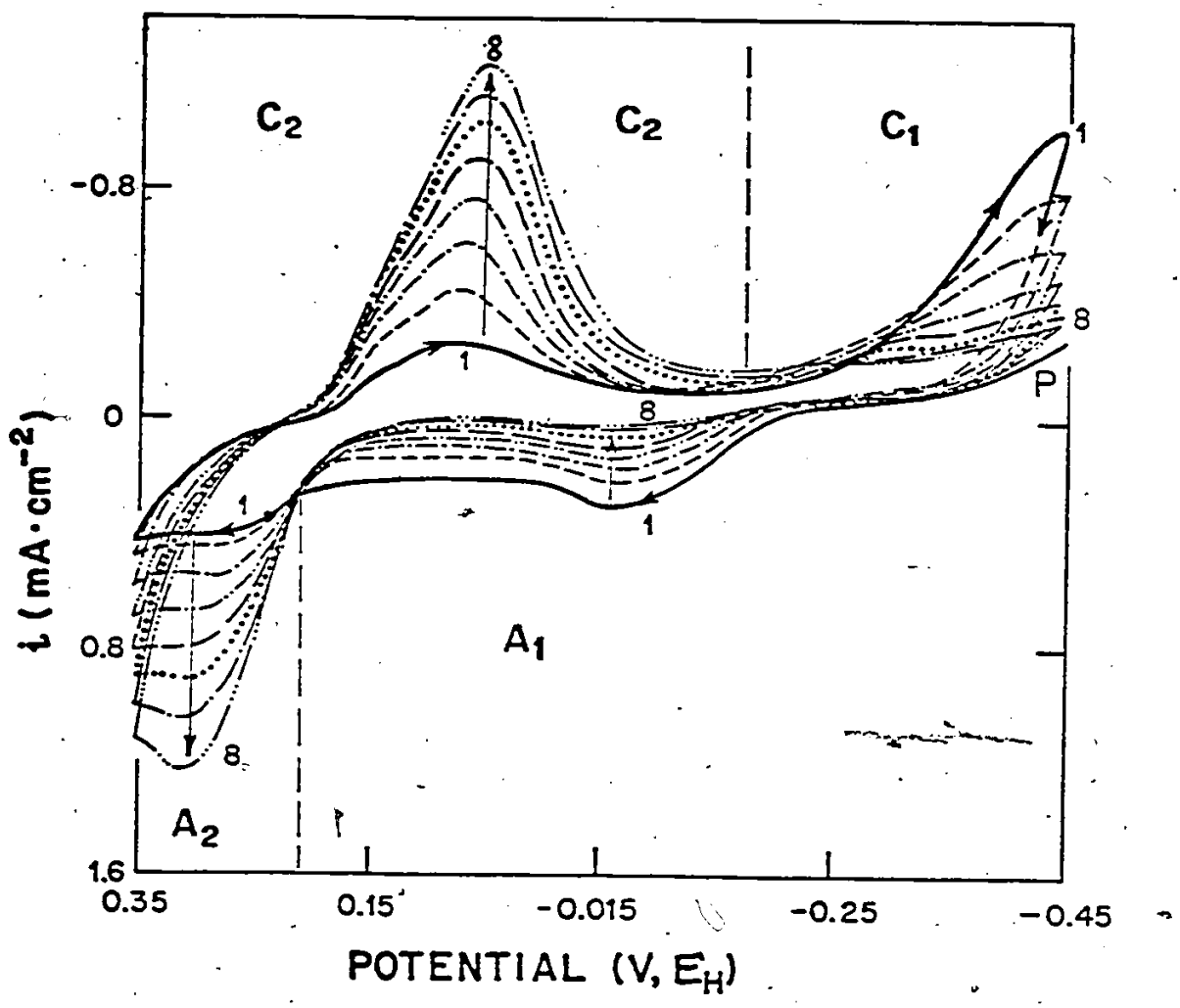

Fig. 3-3: Potentiodynamic current-potential profiles for a series of eight successive sweeps at a PbS electrode in 0.1 M aq $Na_2B_4O_7$ at 298 K at a sweep rate s=32 mV s^{-1}. The anodic and cathodic cycles are divided into two regions by the vertical line to distinguish corresponding anodic (A_1 and A_2) and cathodic (C_1 and C_2) processes.

direction at -0.45 V. This means [cf. Refs. (245,246)] that the C_1 process is not a reversible surface reaction.

The gradual increase of currents with cycling in the A_2 and C_2 regions arises from a transitional state formed in the plateau region where a surface species is further oxidized from state A_1 to state A_2. The longer the residual species formed anodically in the A_1 region is left on the surface, the greater is the quantity of the transitional species and therefore the larger is the current for the process A_2. The effect is not simply due to a progressive increase of area of the electrode since (a) curve 1 can be reproduced by holding at P (Fig. 3.3) and (b) the currents in region A_1 decrease rather than increase with cycling, which would be the case if the real area of the electrode had increased.

The dependence of anodic and cathodic charges passed in the four regions on the number of sweep cycles (Fig. 3.4) is shown in Fig. 3.5(b), and discussed below.

3.2.2 Irreversibility-Characteristic of the A_1/C_1 Region

1) Charges and the charge balance ratio, Q_c/Q_a

The cathodic/anodic charge ratios Q_c/Q_a, for each i-V profile of Fig. 3.4. are shown in Fig. 3.5(a). For sweep d in region C_2, Q_c almost balances the value of Q_a. However, for sweep a the Q_c passed in region C_1 is always greater than the Q_a over region A_1 in successive sweeps. This disparity is due, it is believed, to some continuing irreversible reduction of the surface to S^{2-} species ($PbS + 2e \longrightarrow Pb + S^{2-}$) which are not fully reoxidized in the A_1 region. Further evidence for this is provided in 2).

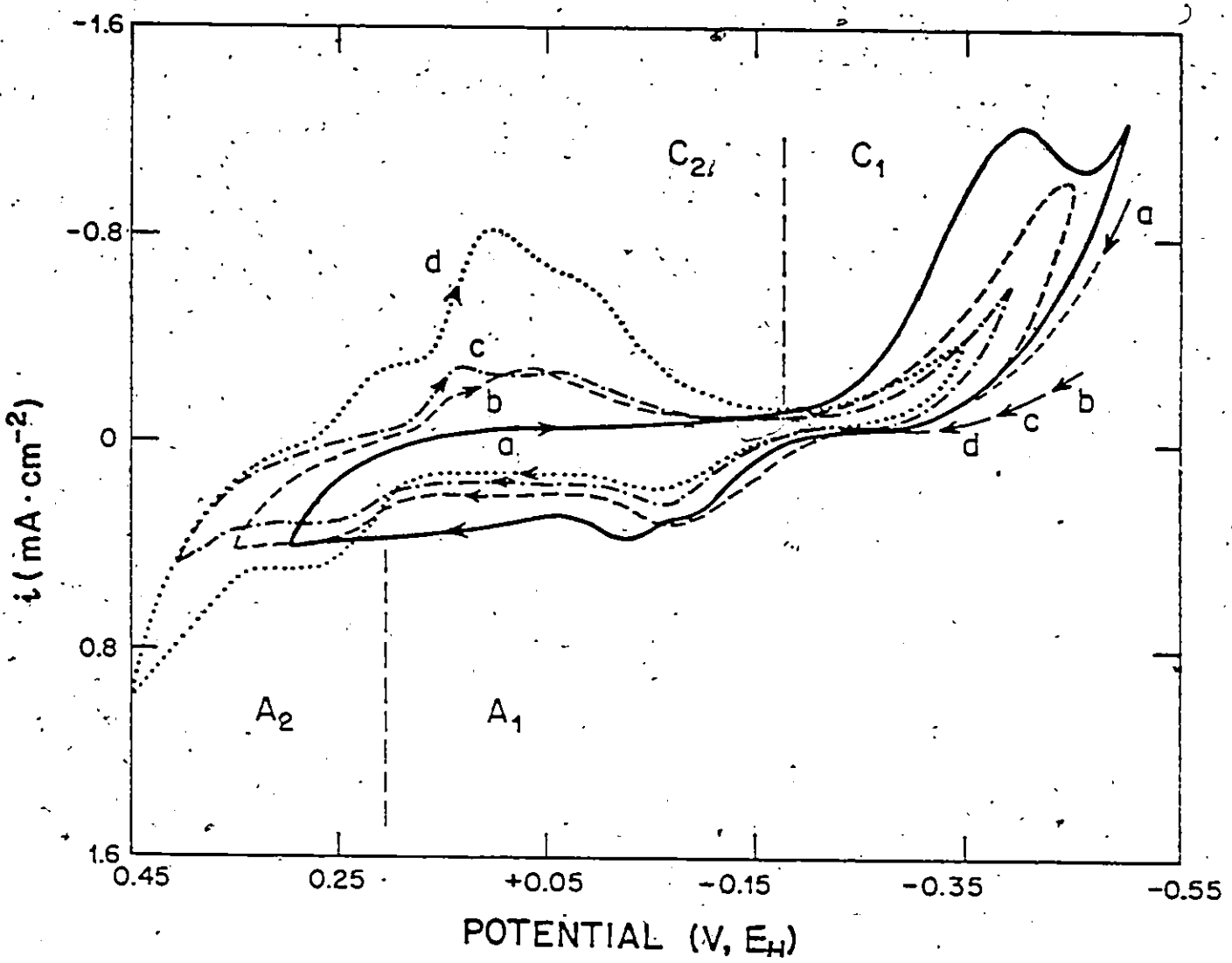

Fig. 3-4: Potentiodynamic current-potential curves for a PbS electrode in 0.1 M $Na_2B_4O_7$ over four different potential ranges at s=32 mV s^{-1}.

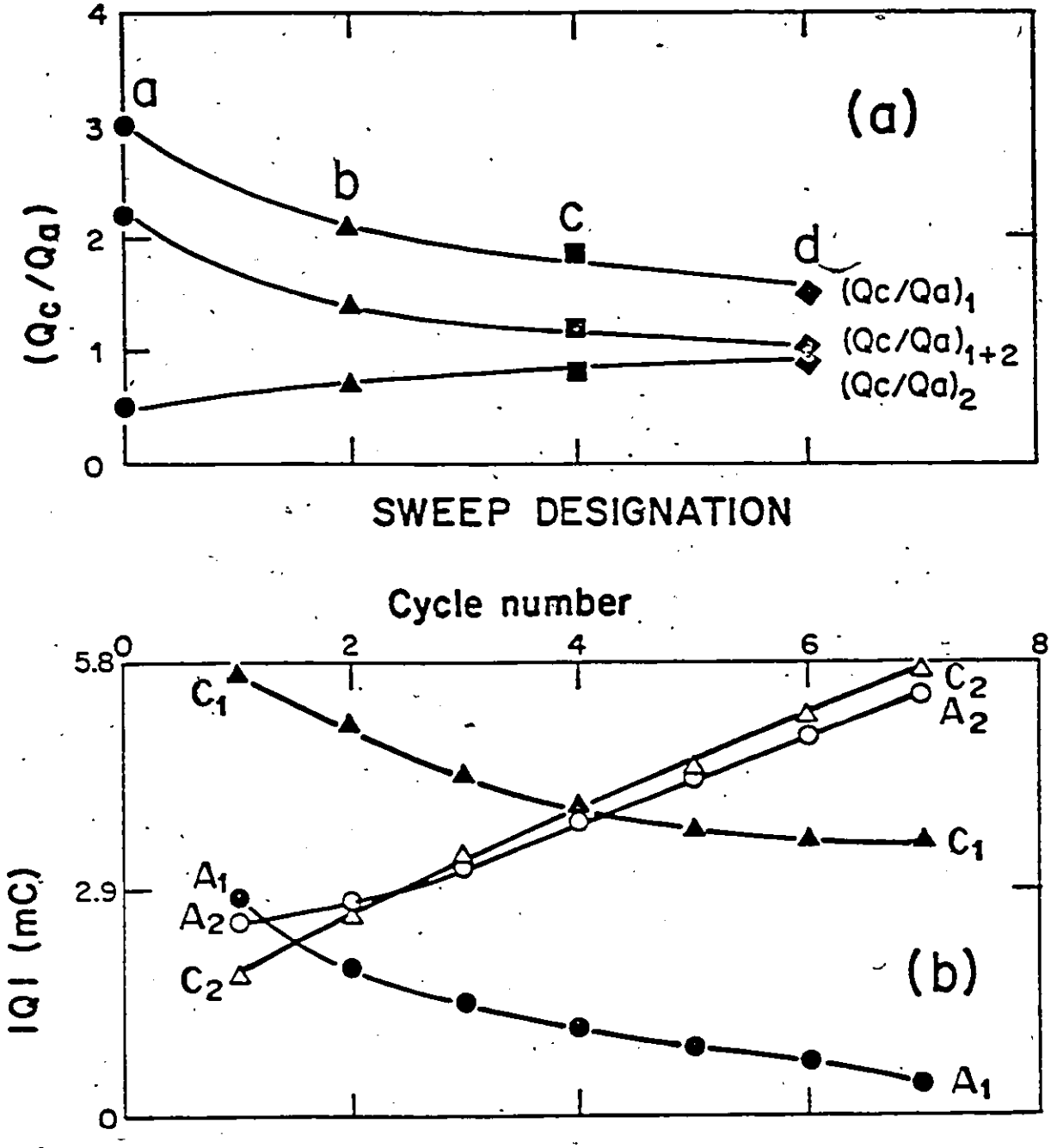

Fig. 3-5: (a) Ratios of cathodic, Q_c, to anodic, Q_a, charges for the four curves in Fig. 3-4. Subindices 1 and 2 represent the charges passed in regions 1 and 2, respectively, while subindex (1+2) represents the sum of the charges. (b) Dependence of charges passed in the four regions on the sequential number of the sweep (1 to 8).

The trends of charges passed, Q, in relation to the number of cycles, for the four regions of Fig. 3.3, are illustrated in Fig. 3.5(b) and allow a preliminary comment to be made on the hysteresis in the i-V curves of Fig. 3.3. Because of the close charge balance of regions A_2 and C_2 in each run, it can be assumed that the process associated with peak C_2 is the reverse of that in A_2. The problem of lack of balance between the charges passed in C_1 and A_1 can be eased by reference to the fact (Fig. 3.5(b)) that the charge for C_1 is uniformly greater than that for A_1, independently of the number of cycles. This implies that another type of species is irreversibly produced, independently of the prehistory of the electrode in the C_1 region.

The decline of both C_1 and A_1 with number of cycles in Fig. 3.5(b) can be understood if a comparison is made with the reduction of a surface species such as $PbSO_4$, previously studied in this laboratory and elsewhere. Thus, the explanation would be that, if an insoluble product exists on the electrode and can only be reduced in a relatively slow process (as is the case with $PbSO_4$ on Pb), any residual species, which is left on the surface because of the short duration of the cathodic sweep, will provide smaller reactive area for the anodic process on the next sweep in the opposite direction. This explanation is consistent with the fact that curve 1 (Fig. 3.3) can be reproduced again after the potential has been held at -0.45 V until the current drops to the reproducible residual steady-state value at P (Fig. 3.3) before the next anodic sweep is initiated. However, from the results of the rotating electrode experiments discussed below and

shown in Figs. 3.11, 3.12, 3.13, 3.14, it seems that the species involved in the A_1 region is not generated in a dissolution-precipitation process as in the case of $PbSO_4$ at Pb. Thus, $PbSO_4$ is not generated at potentials in the A_1 region.

2) Current-Potential Behavior in the A_1/C_1 Region

A more detailed study of the initial anodic peak (the P-A-B region of Fig. 3.6(a)) and the shallow multipeak region which follows it, i.e., the plateau region indicated in Figs. 3.3 and 3.4, is helpful for further understanding of the electrode behavior. Current-potential profiles in six linear potential sweeps at 5, 10, 20, 50, 100, and 200 mV s^{-1} are shown in Fig. 3.7(a). Corresponding relative reflectivities, $(\Delta R/R)_{\|}$, vs V curves are plotted in Fig. 3.7(b) The initial conditions, at -0.4 V, were as stated previously for each anodic sweep.

The anodic peak potentials for the process in the A_1/C_1 region move to more positive values as the sweep rate is increased. The currents, i_V, at +0.1 V and the peak currents, i_p, in Fig. 3.7(a) are linear in square-root of sweep rate (Fig. 3.8(a)). The anodic peak potentials vary with log s as shown in Fig. 3.8(b), indicating an irreversible process. It should be noted that before each anodic sweep was initiated, the potential was kept at P with N_2 stirring until the same initial conditions were reproduced in each run. The dependence of the currents or charges on $s^{\frac{1}{2}}$ in the P-A-B region is hence not the result of reoxidation of any solution-soluble species produced and reduced, respectively, in the immediately previous anodic and cathodic sweeps. However, the residual current which passes cathodically at P could

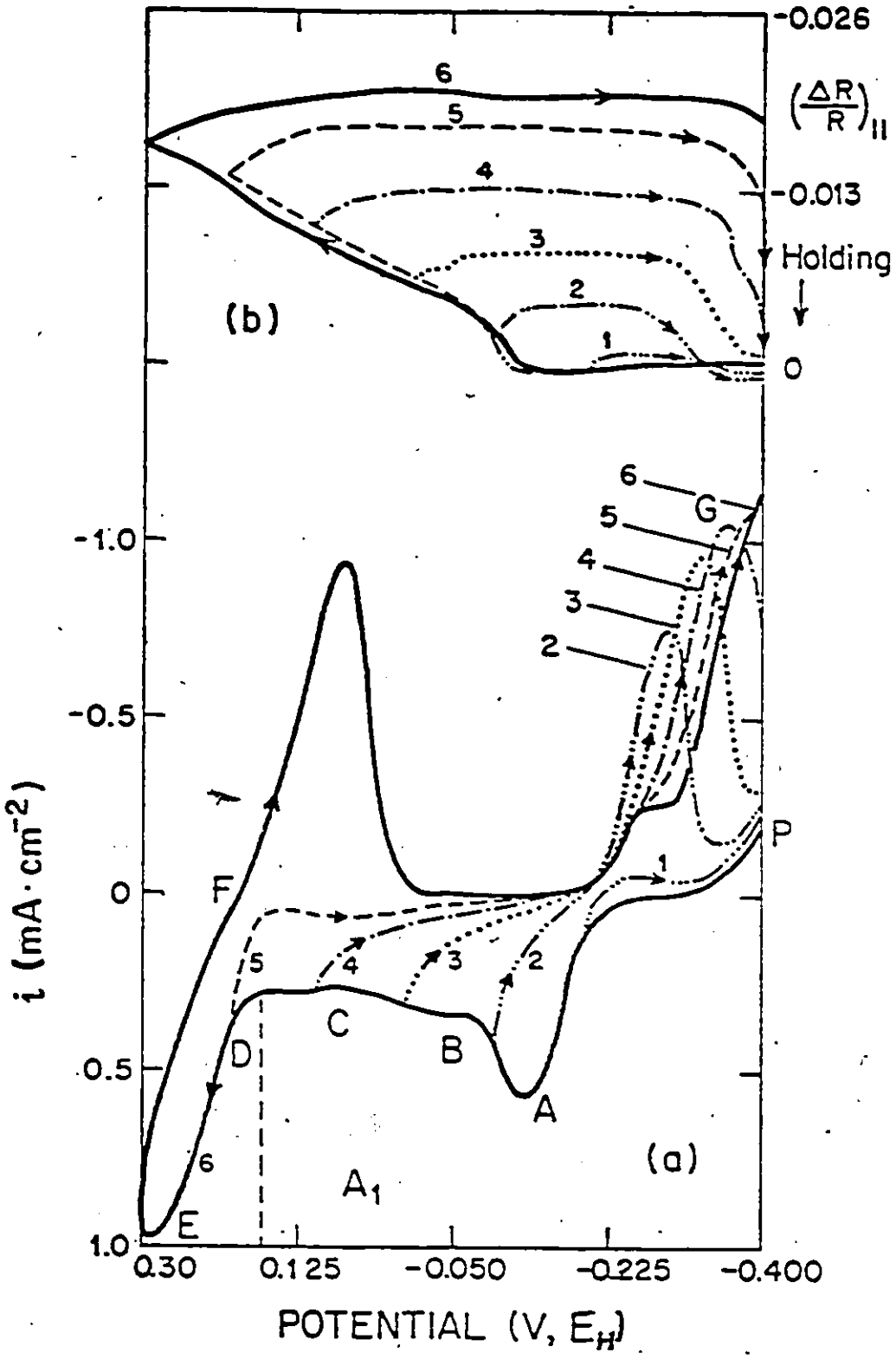

Fig. 3-6: (a) Six potentiodynamic current-potential profiles (1 to 6) for a PbS electrode in 0.1 M aq $Na_2B_4O_7$ taken successively from an initial potential of -0.4 V (E_H) at P to various anodic limits. Letters A to G designate regions of the profile referred to in the text. (b) The $(\Delta R/R)_{II}$ vs potential relations are for the same conditions corresponding to i-V profiles 1 to 6 in (a).

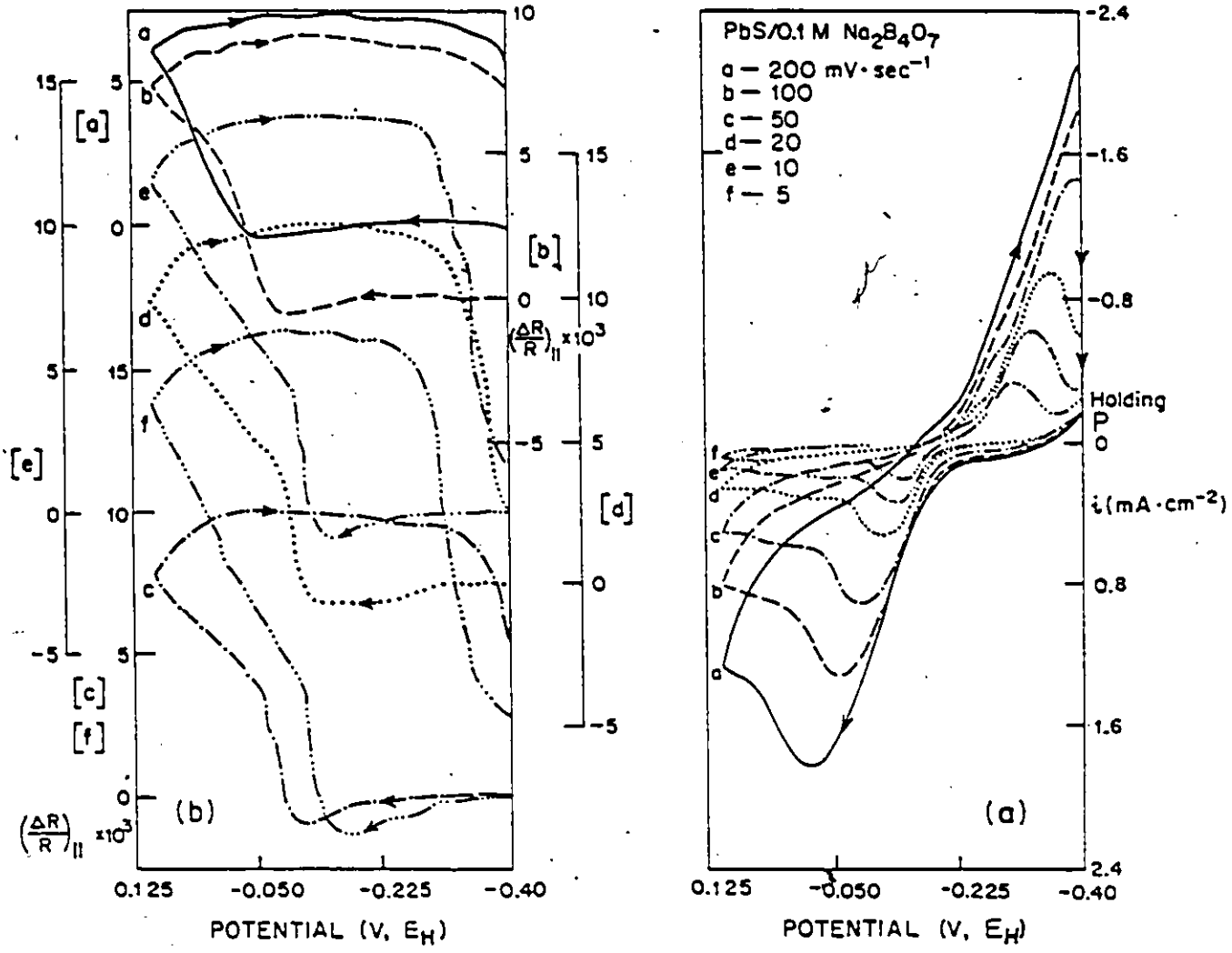

Fig. 3-7: (a) Series of potentiodynamic i-V profiles at PbS in 0.1 M aq $Na_2B_4O_7$ over the A_1/C_1 region showing the sweep-rate dependence of the anodic and cathodic peaks s=5,10,20,50,100,200 mV s^{-1}. (The potential is held at -0.40 V at P at the end of each cathodic sweep before initiating the next anodic sweep to reproduce initial conditions.) (b) Series of $(\Delta R/R)_{II}$ vs potential profiles corresponding to the current-potential curves of Fig. 3-7(a).

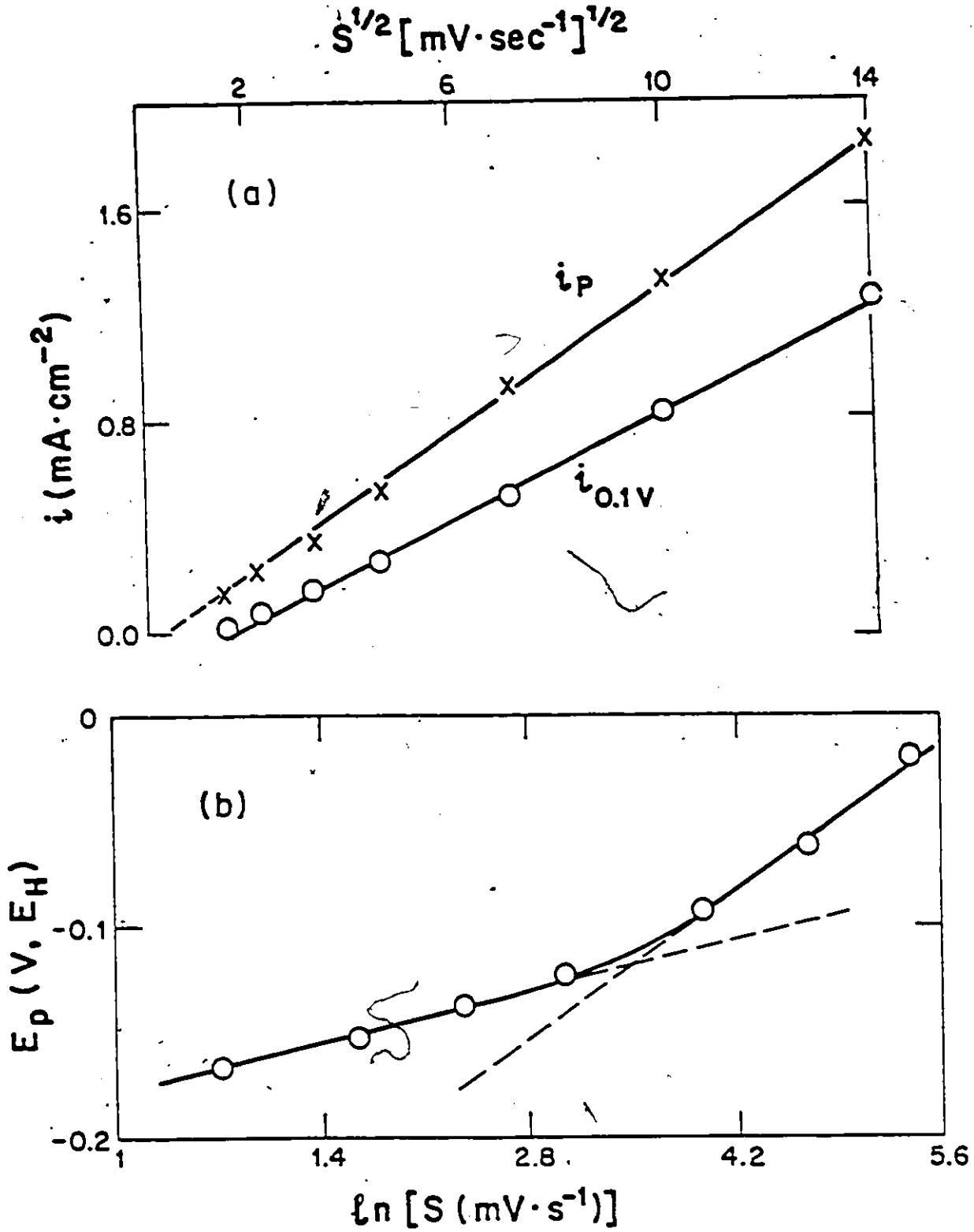

Fig. 3-8: (a) Linear plots of current i_V at V and the peak currents, i_p, vs $s^{\frac{1}{2}}$ for the PbS electrode in 0.1 M aq $Na_2B_4O_7$. (b) Dependence of the anodic peak potential V_p on ln s.

produce a reduced species reoxidizable in a diffusion-controlled process in the following anodic sweep. The situation is evidently complex, since if a steady state is established at P, subsequent anodic sweep i-V profiles taken from P after various times, τ_h, of holding at P become independent of τ_h (Fig. 3.9) if $\tau_h >$ ca. 60 s; they are actually almost independent of τ_h for shorter holding times, < ca. 60 s.

The anodic charges Q_a in four runs at sweep rates of 200, 50, 20, and 5 mV s^{-1} are plotted vs potential over the range -0.46 to +0.1 V in Fig. 3.10 and depend on the sweep rate. The dashed lines in this figure represent the charge that continues to pass on the following cathodic sweep before the zero-current line is reached, for the six sweep rates in these experiments. There are three different regions of the Q-V curves which can be seen most clearly in curve f for s = 5 mV s^{-1}. A linear relation arises at the third stage, i.e., in the region after the first anodic peak, and can be discerned in all the curves.

3) Experiments with a rotating disc electrode related to the mass-transfer behavior in the A_1/C_1 region (cf. Fig. 3.3).

It was considered important to establish whether solution-soluble species are involved in the electrode processes characterized by the i-V profiles of Figs. 3.3, 3.6(a), and 3.4. Several experiments were therefore conducted with the rotating-disc PbS electrode described earlier, by introduction of the rotation at various potentials during the sweep and also throughout the sweep in the anodic and cathodic directions. The rationale of these experiments was that if a solution-

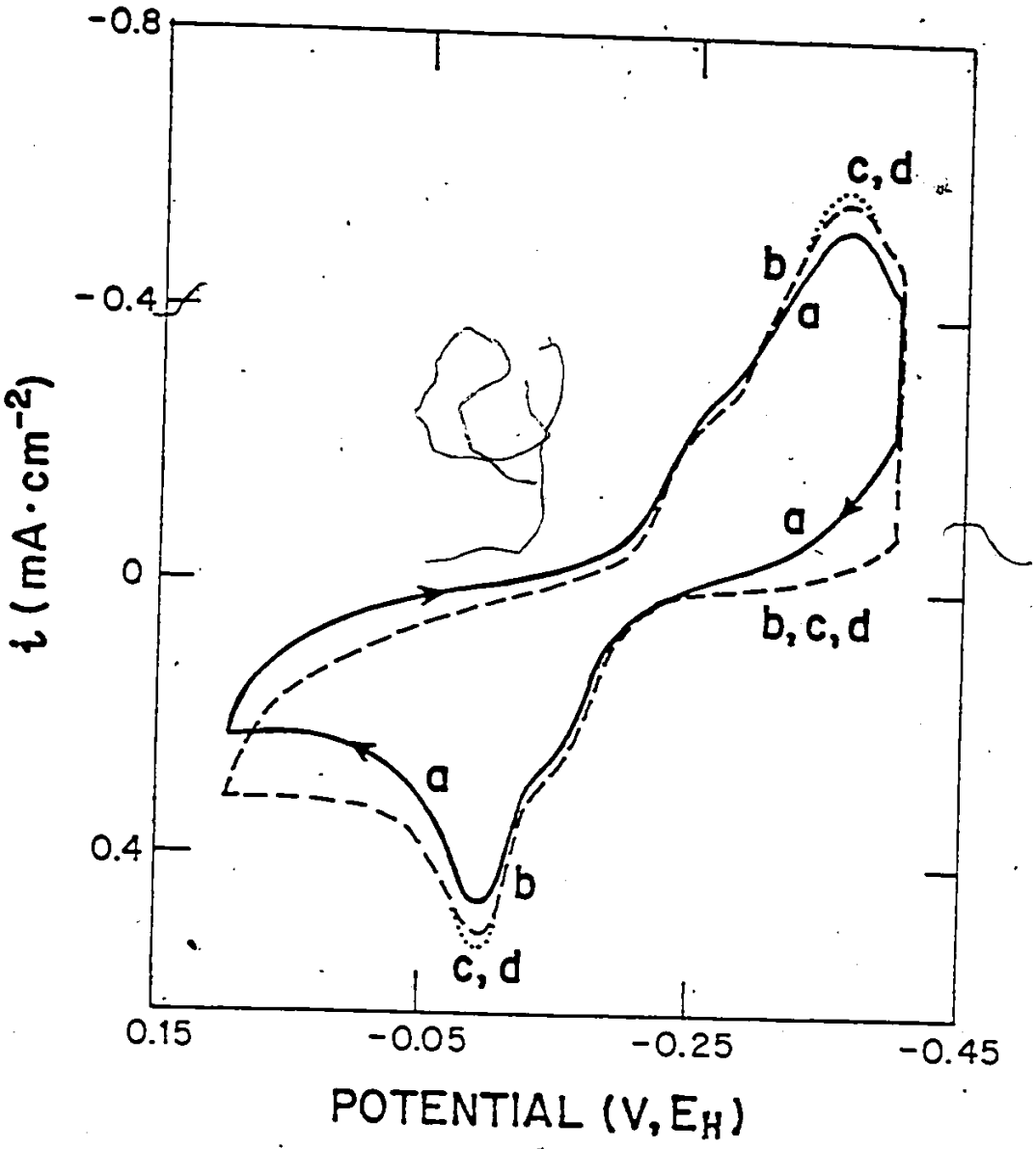

Fig. 3-9: Anodic and cathodic potentiodynamic i-V profiles at PbS in 0.1 M aq $Na_2B_4O_7$ after holding the potential constant at P for various times: curve (a), with holding for τ_h=6 s; curve (b), τ_h=60 s; curve (c), τ_h=1800 s; curve (d), τ_h=3 h, sweep rate is 20 mV s^{-1}.

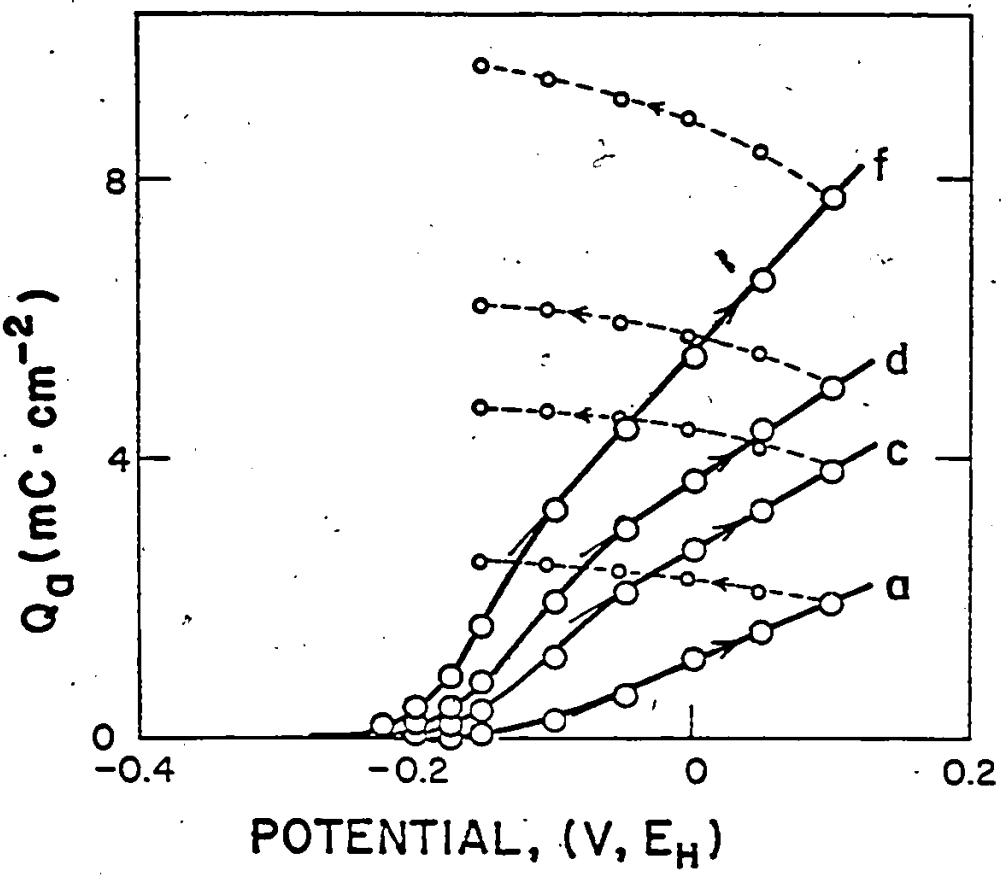

Fig. 3-10: Dependence of anodic charge Q_a in the sweeps (a) 200 mV s^{-1}; (c) 50 mV s^{-1}; (d) 20 mV s^{-1} and (f) 5 mV s^{-1}, on potential, i.e., for various sweep rates. Forward (→) curves are for the anodic sweeps and backward (←) are for the remaining anodic charge passed in the beginning of the next cathodic sweep (see i-V profiles of Fig. 3-7(a)).

soluble species or intermediate is produced, e.g., in the cathodic process, which gives rise to the residual current over the potential range -0.40 to -0.45 V, it could be spun away from the electrode, thus much diminishing any reoxidation current peak that could arise from it in a succeeding anodic sweep. The behavior in regions A_1 and A_2 and the correspondng C_1 and C_2 regions (Fig. 3.3) was investigated.

Figures 3.11(a) and (b) show the i-V profiles that arise in the A_1/C_1 region, with and without rotation of the electrode at 1600 rpm. The numbers on the curves refer to first, second, and third, etc., successive sweeps and "r" indicates whether the electrode was rotated or not. Curves 1, 2, and 3 of Fig. 3.11(a) show, first, the situation if the electrode is not rotated during the anodic sweep but is held at -0.05 V at the end of the anodic sweep for times τ_h = 0.30 or 60 s, respectively. The quantity of material reducible in the cathodic sweep evidently increases with τ_h.

In Fig. 3.11(b) it is clear from lines r1 for a repetitive anodic/cathodic sweep that over the range -0.45 to -0.05 V, electrode rotation eliminates the anodic and cathodic peaks that otherwise arise in this region (Fig. 3.11(a), cf. Fig. 3.7). If, however, the electrode potential is held (as in Fig. 3.11(a)) for some time at -0.05 V, it is found that on the cathodic sweeps, marked 2 and r2 on Fig. 3.11(b), a peak is still generated whether the electrode was rotated (curve r2) during the holding period or not (curve 2), but in the latter case the cathodic peak is enhanced by the holding, owing to an increase in quantity of reducible species remaining available at or near the electrode surface, as in Fig. 3.11(a) after holding.

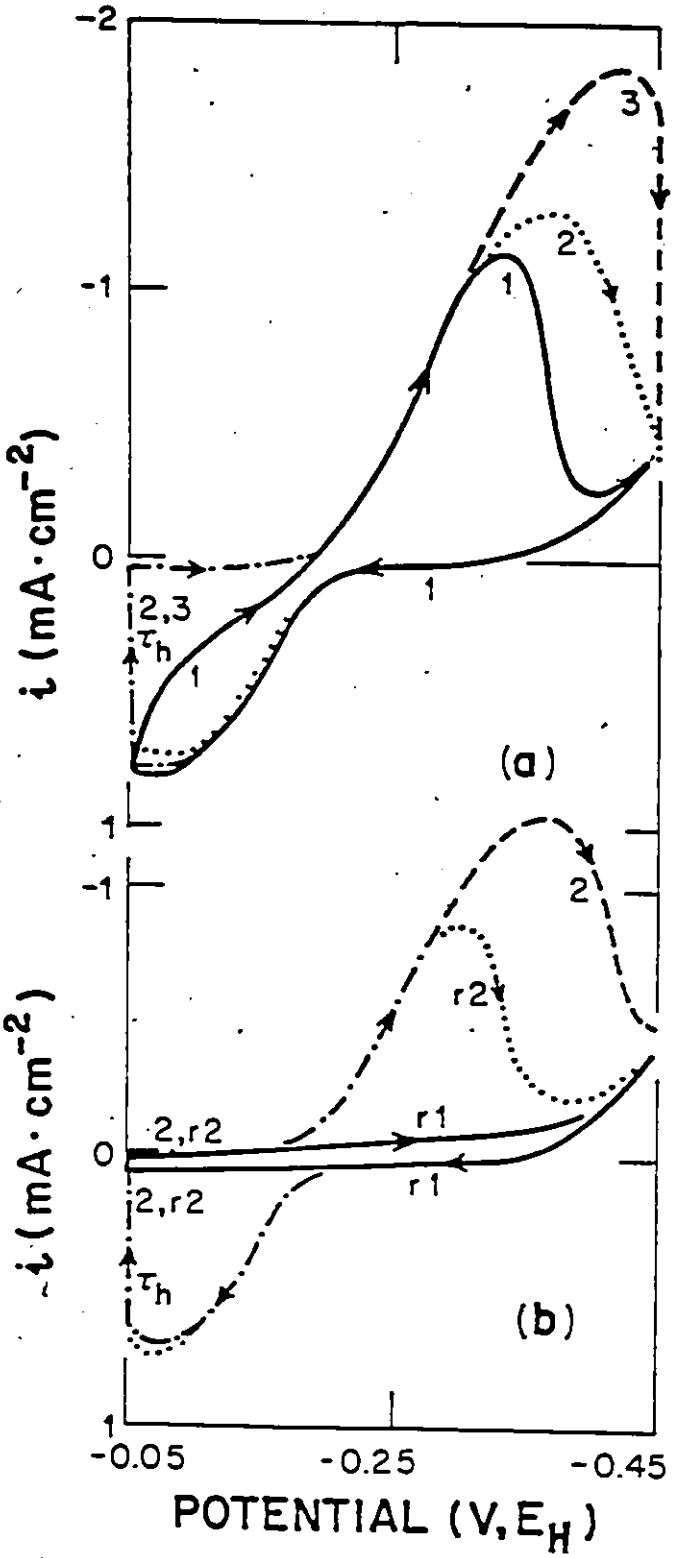

Fig. 3-11: (a) Potentiodynamic i-V profiles for a PbS electrode in 0.1 M aq $Na_2B_4O_7$ over the A_1/C_1 region. Curve 1, repetitive sweep; curve 2, with holding at -0.05V, τ_h=30 s; curve 3, with holding at -0.05V, τ_h=60 s. (b) As in (a) but showing the effect of electrode rotation at 1600 rpm: Curve 1, rotation in repetitive sweep; curve 2 , after holding at -0.05V, τ_h=30 s without rotation; curve r2, with rotation at 1600 rpm at -0.05V during 30 s holding and during the following cathodic sweep.

If the sweep is restricted at the cathodic end to a potential of -0.40 V (Fig. 3.12), no A_1 anodic peak arises in either a stirred or an unstirred solution. This proves that the species oxidized in the A_1 peak does not originate by oxidation from the surface itself at potentials more positive than -0.20 V but rather arises from the effect of holding (residual cathodic current) at P.

The rotation experiments (Fig. 3.11(b)) and the restricted range experiment (Fig. 3.12) prove that the anodic peak in the A_1 region is due to oxidation of a species produced during holding at P which can be spun away from the electrode and hence is rendered unavailable for reoxidation. However, the behavior in the A_1 region is not simply that of a solution-soluble species generated at P as might as first seem to be the case. This is indicated by the fact that the cathodic current peak (curve r2 in Fig. 3.11(b)) can still be generated after stirring during the holding period τ_h at -0.05 V and its profile initially follows that of curve 2 (Fig. 3.11) for the unstirred solution where a greater quantity of the cathodically reducible species is generated. This latter observation means that curves 2 and r2 are not simply i-V profiles for diffusion-controlled reduction of different quantities of species produced in the solution in the anodic A_1 region. The maintenance of an appreciable cathodic peak (curve r2) after rotation at -0.05 V for τ_h s (>0) means that a surface film is generated on the PbS surface in the potential range -0.20 to 0.0 V (and beyond) but this process requires the solution-soluble species generated at -0.45 V at P. Further evidence for this is given by the results in Fig. 3.13, where rotation is commenced (indicated by r↑ in

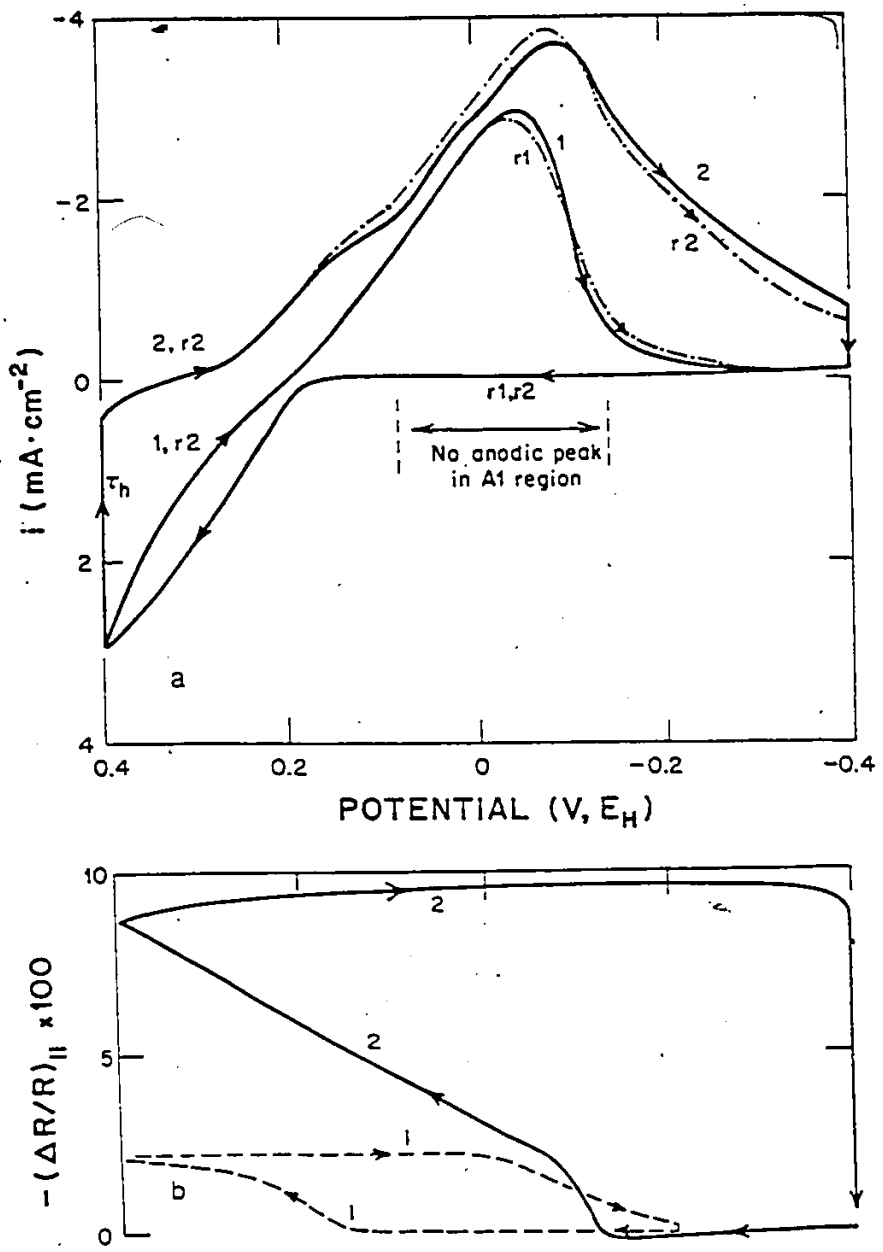

Fig. 3-12: (a) Potentiodynamic i-V profiles for a PbS electrode in the A_2/C_2 region from -0.40 V (E_H) to +0.40 V, where the A_1, C_1 processes are absent: Curve 1, anodic and cathodic sweep without rotation; curve r1, with rotation on the cathodic sweep from +0.40 V at 1600 rpm; curve 2, r2, with and without rotation at 1600 rpm after holding at +0.40 V with τ_h=60 s. (b) $(\Delta R/R)_{II}$ changes in the anodic and cathodic sweeps taken only over the A_2/C_2 region (curve 1) in comparison with $(\Delta R/R)_{II}$ changes over the whole potential range -0.40 to +0.40 V (curve 2).

Fig. 3.13) at three successive potentials in the A_1 region during the anodic sweep; the cathodic peaks (curves r1, r2, r3 and r4) depend on the potential at which rotation was commenced in the anodic sweep.

The conclusion that the A_1 peak [and the plateau region (Fig. 3.3) which follows it] is in part associated with formation of a film is supported by the reflectance results.

It could be surmised that the species that is generated cathodically at P and gives rise to the first peak in the A_1 region and to the behavior shown in Figs. 3.11 and 3.13, is the S^{2-} ion formed in the reaction.

$$PbS + 2e \longrightarrow Pb \text{ (in surface)} + S^{2-} \text{ (solution)}$$

Some support for this supposition is afforded by the results shown in Figs. 3.14(a) and (b). Fig. 3.14(a) shows the regular behavior of the PbS electrode without and with rotation (curve 1 and r1; cf. Fig. 3.11(b)) over the potential range -0.45 to -0.05 V in the presence of added S^{2-} ion (as Na_2S) at a concentration of 10^{-5} mol dm^{-3} (Fig. 3.14(b)). It is clear from this figure that added S^{2-} ion reproduces the behavior of the PbS electrode itself and, in the presence of excess S^{2-}, rotation of the electrode (curve r1, Fig. 3.14(b)) no longer eliminates the anodic peak and its conjugate cathodic peak, as in Fig. 3.11(b) (curve r1). This is as expected since the added S^{2-} is present throughout the solution at a significant concentration (and not just initially near the surface in the diffusion boundary-layer region).

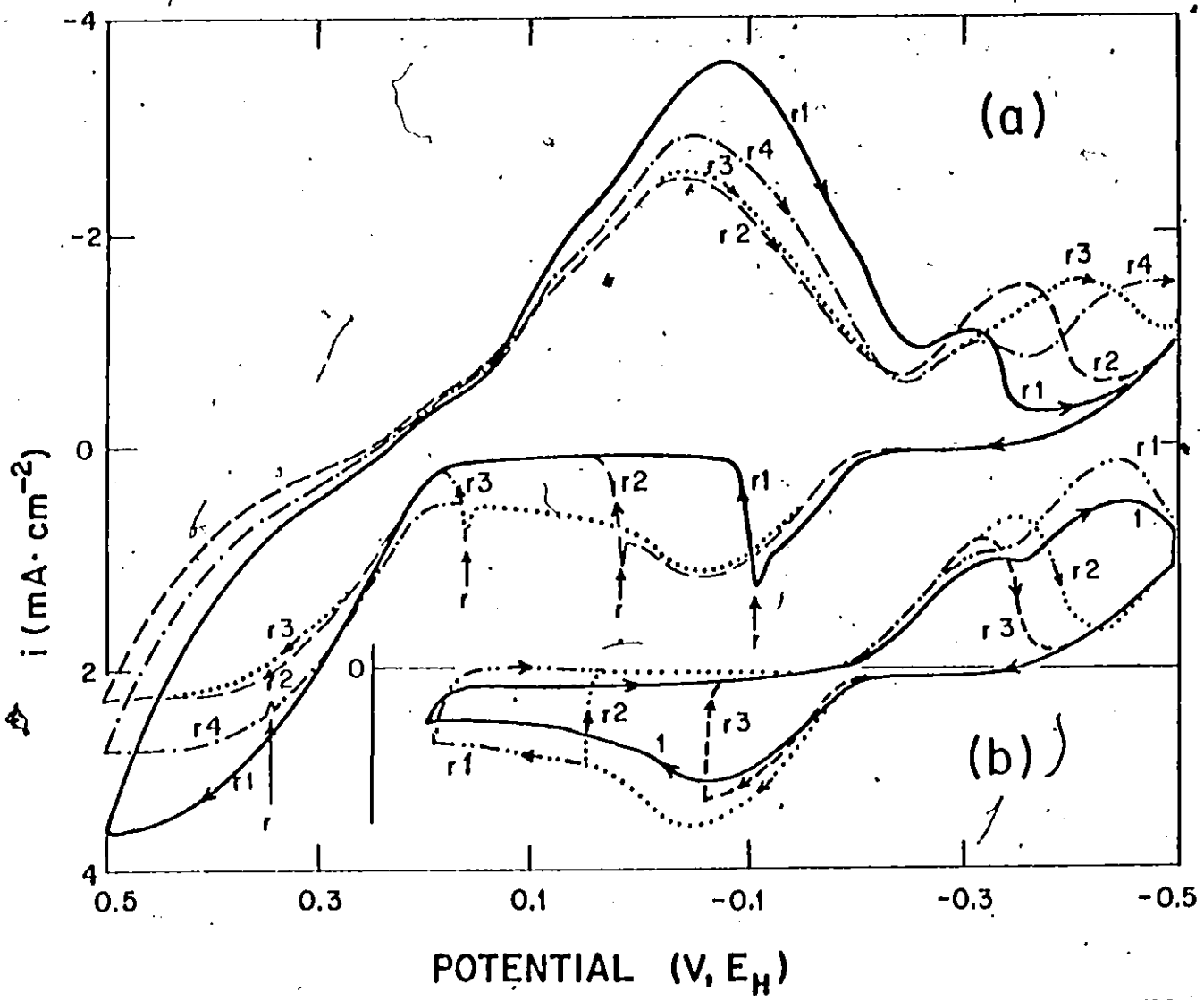

Fig. 3-13: (a) Potentiodynamic i-V profiles for a PbS electrode over the full potential range for A_1, A_2, C_1, C_2 processes with rotation of the electrode initiated at various potentials on the anodic sweep indicated by rt and maintained during the cathodic sweep. (b) As in (a) but over the restricted potential range -0.50 to +0.20 V (A_1 region).

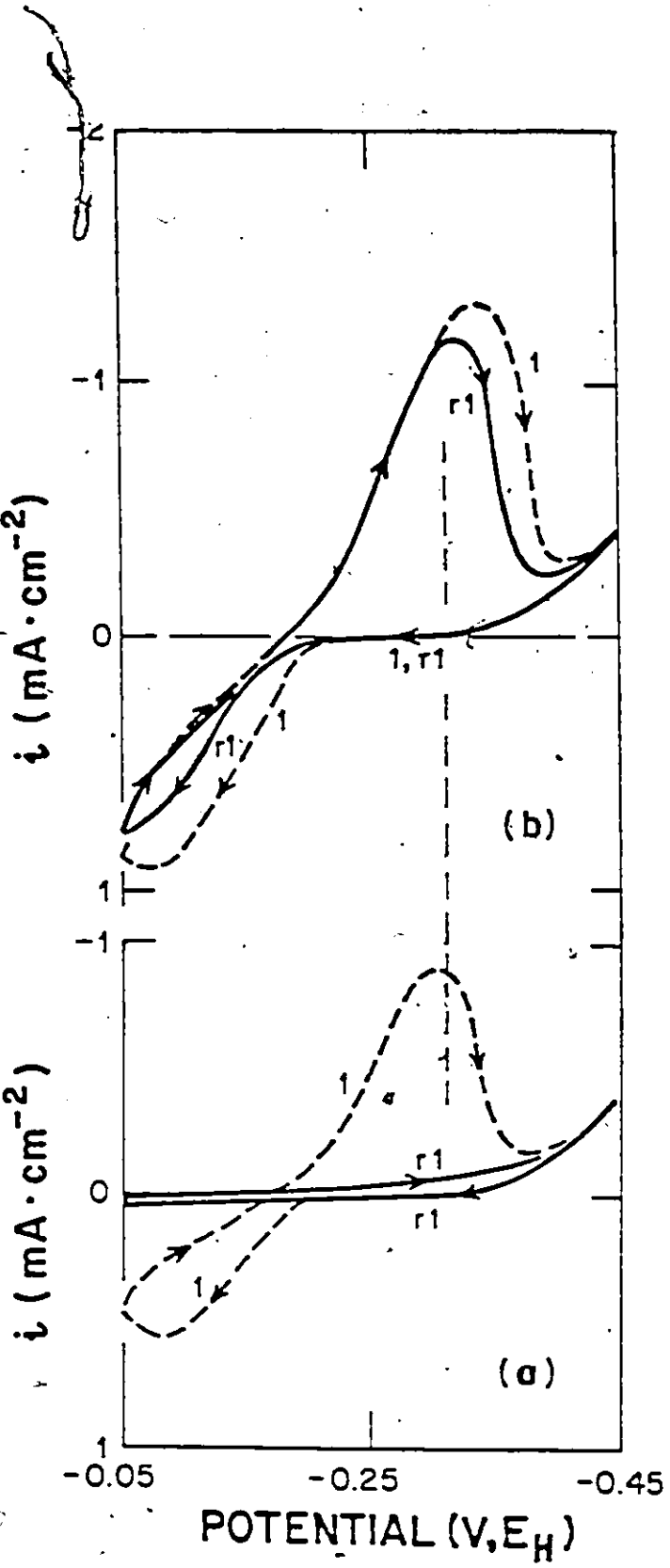

Fig. 3-14: Effect of added S^{2-} ion at 10^{-5} M (as Na_2S) on the electrochemical behavior of the PbS electrode in the A_1/C_1 region: (a) Reference curves for PbS in the absence of added S^{2-} ion, as in Fig. 3-11(a): Curve 1, sweep without rotation; curve r1, with rotation at 1600 rpm. (b) In the presence of added S^{2-} ion: Curve 1, without rotation; curve r1, with rotation at 1600 rpm.

Since Fig. 3.12 shows that no anodic process due to oxidation of PbS itself occurs in the A_1 region, it can be suggested that the species which generates the change of surface state of the PbS indicated by the cathodic peak behavior in Figs. 3.11(a), (b) and 3.13, and by the reflectance change (Figs. 3.6(b) and 3.15) is S adsorbed or deposited on the surface in a step such as

$$S^{2-} + PbS \longrightarrow PbS, S_{ads} + 2\,e$$

Alternatively, polysulfide ions produced in a step such as

$$2\,S^{2-} \longrightarrow S_2^{2-} \text{ (or higher species)} + 2\,e$$

and adsorbed on the electrode could account for the behavior.

3.2.3 Behavior in the A_2 Region with Rotation

The results obtained for the A_2 region, with and without rotation, are shown in Fig. 3.12 where i-V profiles taken from -0.40 V are recorded. Under these condition, no complications arise from the behavior of the species generated at less positive potentials which has been described in Sections 3.2.1 and 3.2.2. From curves 1 and r1 (without and with rotation), it is clear that no significant stirring effects arise since the cathodic i-V profiles are almost identical. Similarly, after holding at +0.40 V for τ_h = 60 s, the cathodic curves, although different because of further oxidation of the electrode, are almost unaffected by the stirring (curves 2, r2).

The processes associated with the A_2/C_2 region therefore appear to be connected directly with changes of the PbS surface itself although

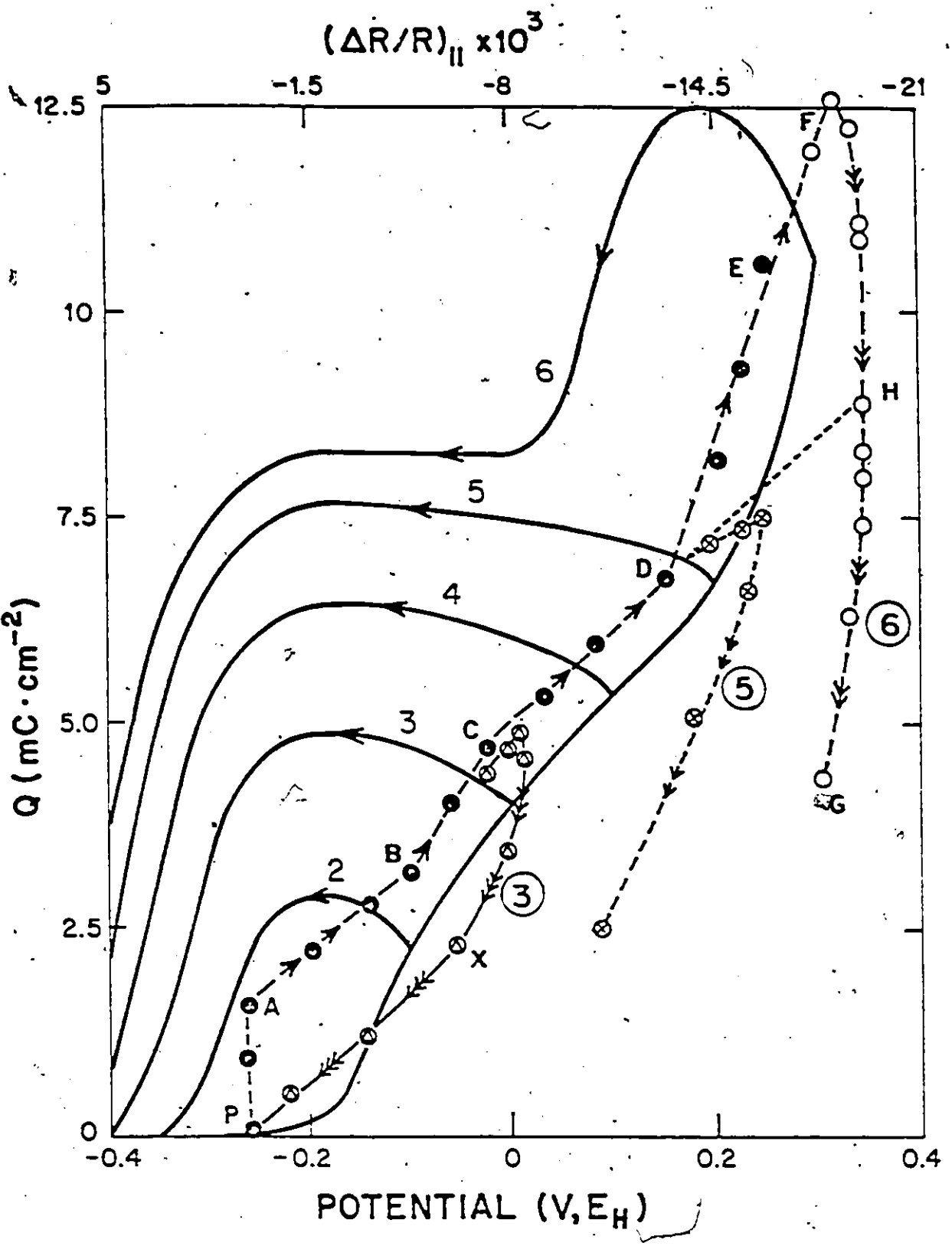

Fig. 3-15: Dependence of $(\Delta R/R)_{\parallel} \times 10^3$ on charge in surface oxidation and reduction of a PbS electrode (dashed lines with circled points) in comparison with the cathodic and anodic charge-potential relations (heavy lines 2 to 6 derived from Fig. 3-6(a)) obtained from the ciclic voltammetry data in 0.1 M aq $Na_2B_4O_7$. Curves 3, 5 and 6 for the $(\Delta R/R)_{\parallel}$ data correspond to curves with the same numbers in the charge-potential profiles. Letters A to G correspond to those in Fig. 3-6(a) designating ranges of potential sweeps.

some influence from the material deposited (adsorbed?) in the A_1 region is evident from the family of curves in Fig. 3.13 referred to earlier. The anodic i-V profile in the A_2 region and the subsequent cathodic profiles in the C_2 region depend significantly on the history and condition of the electrode in the A_1 region. This is not surprising, since if surface processes are involved in the A_2/C_2 region (Fig. 3.12), they will most likely be influenced by whatever species (S or polysulfide ion) are deposited or adsorbed in the A_1 region. The charges involved in the A_2/C_2 region closely balance each other in each run, indicating that a more or less reversible process exists (chemically speaking) and corresponds to ca. 8e/atom on a plane PbS surface, i.e., to 8/z monolayers, where z is the electron number per site involved in the process.

Supported by the reflectance experiments, it seems, in the A_2 region, reasonable to suppose that surface oxidation of the PbS occurs, and with progressive cycling (Fig. 3.3) an increasingly thick, probably porous, layer of an oxidation product is built up. The state of this layer is somewhat dependent on the surface species that is generated in A_1 from solution-soluble S^{2-} ions formed at the cathodic end of the sweep at P, as discussed earlier.

It seems likely that the product formed in the A_2 region in borate solution would be $Pb(OH)_2$ formed in a reaction such as

$$PbS + 2\ OH^- \longrightarrow Pb(OH)_2 + S\ (\text{lattice surface}) + 2\ e \quad (3)$$

since the surface becomes passivated after the initial passage of anodic current in the A_2 region and other anodic processes occur at

higher potentials, possibly involving S left in/on the PbS surface. Reaction (3) probably would occur in more than one step.

The probable formation of $Pb(OH)_2$ is supported by ancillary experiments carried out in 1 M aq NaOH in which $Pb(OH)_2$ would be soluble. Under such conditions, a regular exponentially increasing anodic current (without passivation) is observed in the A_2 region with a stirring-dependent, and hence diffusion-controlled, cathodic current in the cathodic sweep. This is presumably due to reduction of solution-soluble $(PbO_2)^{2-}$ ions produced in the previous anodic sweep under the alkaline solution conditions.

Other, more complex processes evidently occur at higher positive potentials and could involve the participation of sulfur with the formation of lead thiosulfate and ultimately $PbSO_4$ (247), or possibly Pb_3O_4, as can be seen from the Pourbaix diagrams for PbS (247) and Pb (248) itself.

3.2.4 Conclusions on Behavior of PbS

Based on the above discussion, the following conclusions are made:

Over the potential range ca. -0.45 to 0.5 V vs E_H, PbS in borate solution undergoes several principal electrochemical reactions: (i) reduction to solution-soluble S^{2-} ions at the most cathodic potentials; (ii) reoxidation of these ions at ca. -0.25 V in a diffusion-controlled process, coupled with the formation of an adsorbed or deposited film having a substantial negative relative reflectance change (this film is only formed in unstirred solutions); and (iii) surface oxidation of the PbS at more positive potentials

probably giving a film of $Pb(OH)_2$ the properties of which are, however, dependent on the material deposited (S?) in the A_1 region in the same sweep conducted in unstirred solutions.

The behavior in the cathodic sweep is determined by (i) reduction of the anodically formed $Pb(OH)_2$ film; (ii) reduction of S or polysulfide ion species produced from S^{2-} in the anodic sweep and (iii) reduction of the film material derived from S^{2-} in the anodic sweep in the A_1 region. When the surface film species derived from S^{2-} remains on the surface (i.e., in unstirred solutions), its presence modifies the further oxidation of the PbS surface in the A_2 region.

3.3 COMPARISON OF ELECTROCHEMICAL REACTIONS OF PYRITE FES_2

3.3.1 Reversibility-Characteristic of Cyclic-Voltammetry Behavior in 0.1 M $HClO_4$ (pH 1)

The behavior of FeS_2 in response to single-cycle, anodic/cathodic, linear variation of potential with time at various sweep rates, s, is shown in Fig. 3.16 for the potential range -0.1 to 0.5 V E_H, using pH 1 aqueous $HClO_4$. The general features of the curves of Fig. 3.16 are unchanged if the starting potential is -0.2 instead of -0.1 V E_H. For FeS_2, as with PbS, the anodic/cathodic cycle was always initiated after 60 s holding of the potential at the negative starting voltage (-0.1 or -0.2 V for FeS_2). This enabled a reproducible electrochemical state of the electrode to be established prior to each cycle at a given sweep rate.

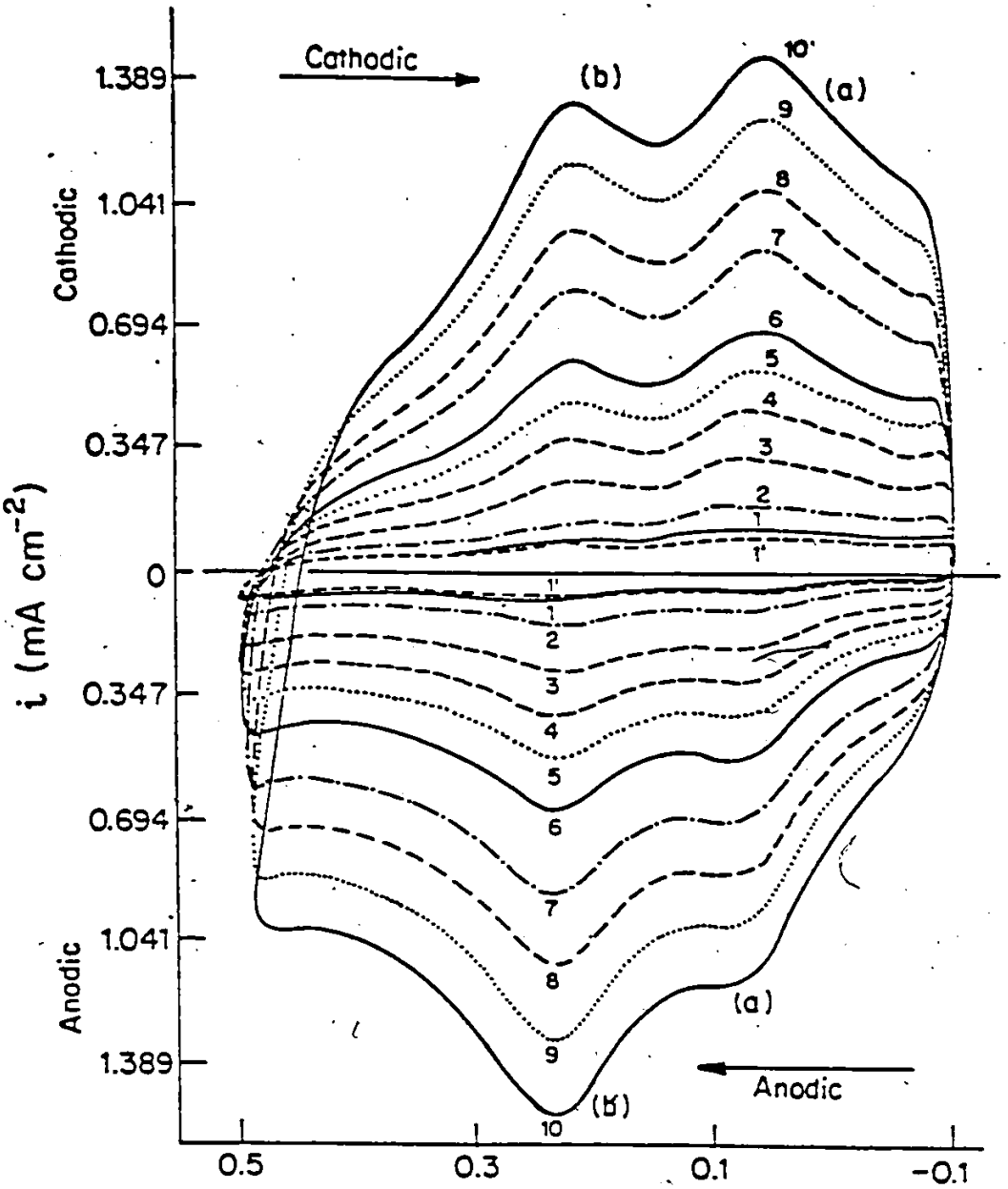

Fig. 3-16: Cyclic voltammetry i vs V profiles for FeS_2 in 0.1 M $HClO_4$ at 298 K. Curves 1-10 for s x 10^2 = 3,6,12,24,30,42, 54, 66 and 78 V s^{-1}, respectively. Curves 1 and 1' are for s = 0.03 V s^{-1}, before and after the series of cycles 2 to 10, respectively.

The most striking and significant feature of the current density i vs potential V profiles for FeS_2 (Fig. 3.16) is that two distinguishable peaks arise in the anodic sweep which remain almost at the same potentials as s is varied from 0.6 to 0.01 V s^{-1}. Also, similar peaks appear on the cathodic sweep but are displaced a little negatively by ca. 0.02 V. Thus, an almost reversible oxidation/reduction process occurs at the FeS_2 surface. The i vs V profiles over the range of potentials shown in Fig. 3.16 are not influenced by electrode rotation (contrast the behavior of PbS), and so are not associated with a solution-soluble species. This is also indicated by the almost identical values of anodic and cathodic peak potentials in Fig. 3.16. Such behavior could not arise in a process in which small quantities of solution-soluble products were generated and would thus respond according to the behavior of a diffusion-controlled reaction, viz., where anodic and cathodic peak potentials are well separated (see i on p. 83).

After a number of anodic/cathodic cycles (1-10 in Fig. 3.16), the electrode surface becomes less active and currents at a given s are diminished (curve 1' in comparison with 1 in Fig. 3.16).

If the potential range of the anodic sweep at FeS_2 is progressively extended to more positive values than that in Fig. 3.16, an increasingly irreversible i vs V profile results (Fig. 3.17(a)). Initially, almost reversible anodic [1(an) and 2(an) Fig. 3.17(a)] and cathodic [1(cath) and 2(cath)] peaks are observed. As the sweep is taken to more positive potentials, a further region of [3(an), Fig. 3.17(a)] surface oxidation, leading eventually to much larger Faradaic

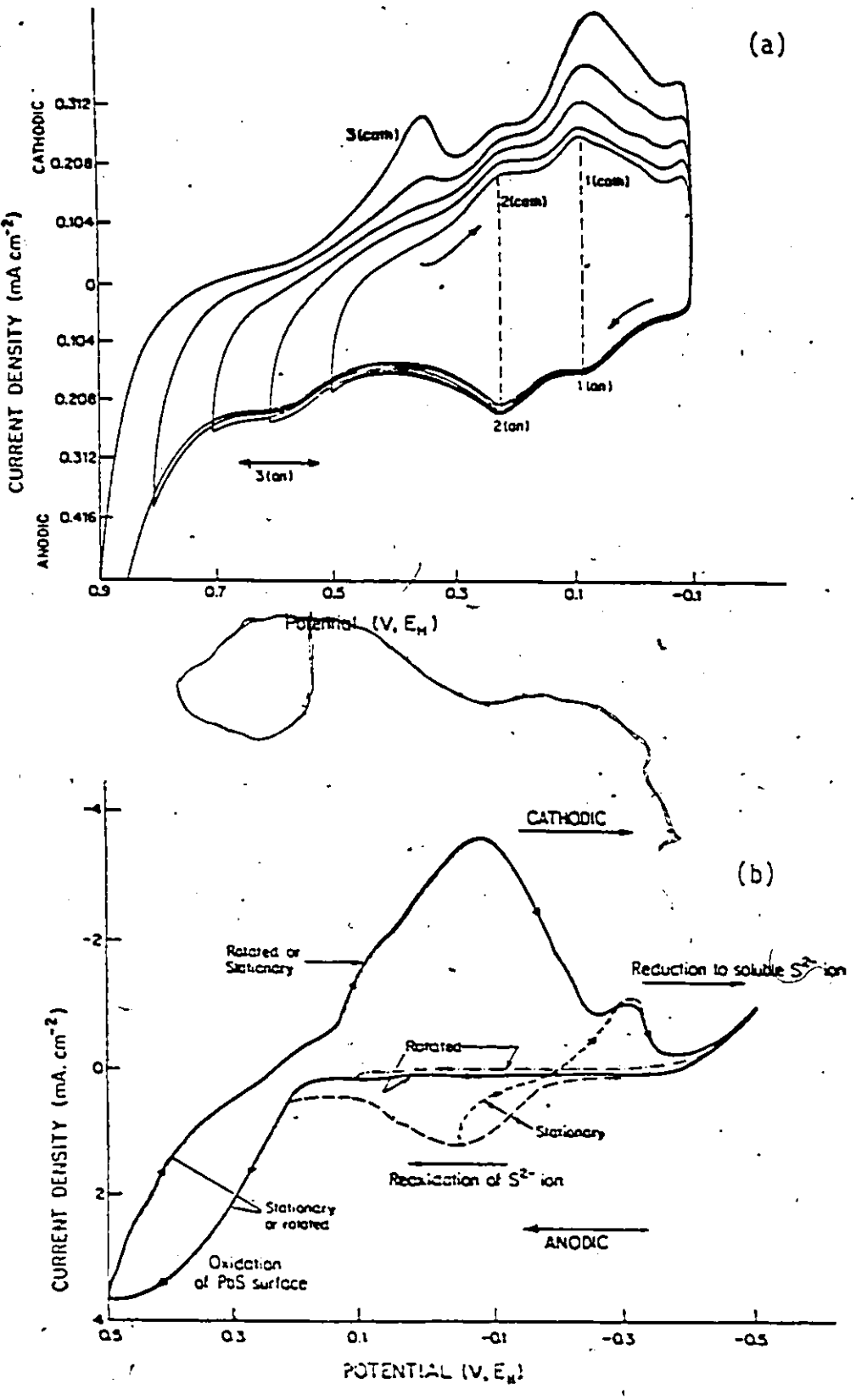

Fig. 3-17: (a) Cyclic voltammetry i vs V profiles for FeS_2 in pH 1 aq $HClO_4$ taken to successively more positive potentials beyond the reversible region. (b) Comparative i vs V profile for anodic and cathodic sweeps at a PbS electrode with and without electrode rotation (0.1 M $Na_2B_4O_7$).

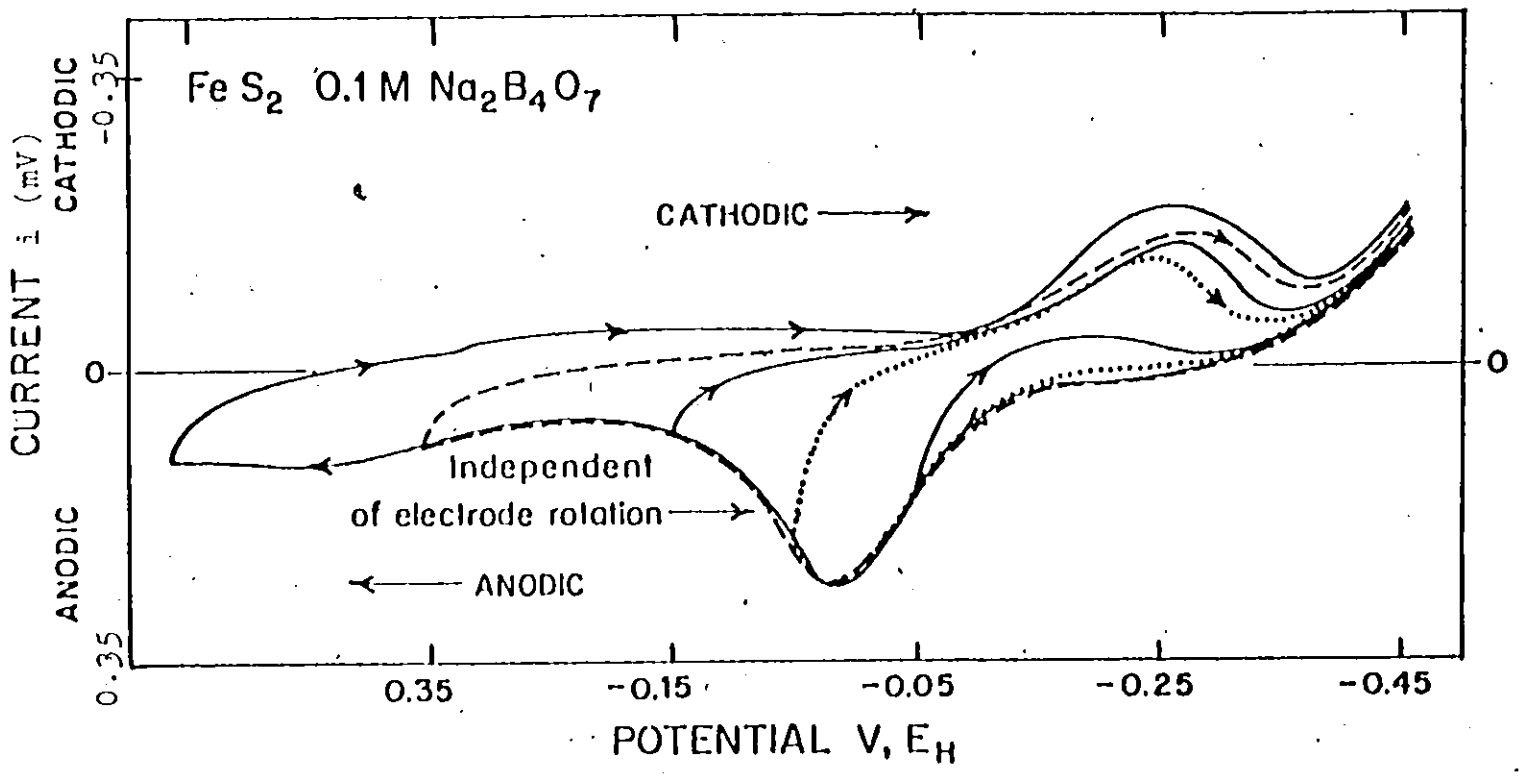

Fig. 3-17: (c) Cyclic voltammetry i vs V profiles for FeS_2 in aq 0.1 M $Na_2B_4O_7$ taken to successively more positive potentials beyond the active region.

currents, arises. On reversing the sweep, the reduction peak, 3(cath), corresponding to the oxidation process 3(an) arises at substantially less positive potentials, so the processes 3(an), 3(cath) are much more irreversible than the first two, 1 and 2. The cathodic currents arising after oxidation beyond 0.5 V also add to those in the region 2(cath) and 1(cath), increasing the peak heights at ca. 0.22 and 0.07 V. Over the wider potential range, the behavior of FeS_2 (Fig. 3.17(a)) is more similar to that of PbS over a comparable potential range, where, in both cases, strongly irreversible processes are observed.

Figure 3.18 shows the relationship between peak currents of Fig. 3.16 and s for the two main peaks, a and b of Fig. 3.16. The potentials for these peaks (Fig. 3.18) are almost independent of s and thus (249) correspond to almost reversible behavior of an anodic and cathodic surface process involved in the oxidation and reduction of the FeS_2 surface. The fact that the cathodic and anodic peaks do not match each other in Fig. 3.16 exactly, yet the peak potentials in Fig. 3.16 are independent of s, means probably that there is a small but significant resistance of the material, giving an ohmic potential drop which is in one direction in the anodic sweep and in the other in the cathodic, thus leading to a small separation between the curves.

A different approach to the investigation of reversibility of the several surface processes in Fig. 3.16 as the potential is changed was made by reversing the sweep in the cathodic direction at various potentials, as shown in Fig. 3.19. It is evident that, below 0.5 V (contrast Fig. 3.17(a)), the peaks developed in the anodic sweep are

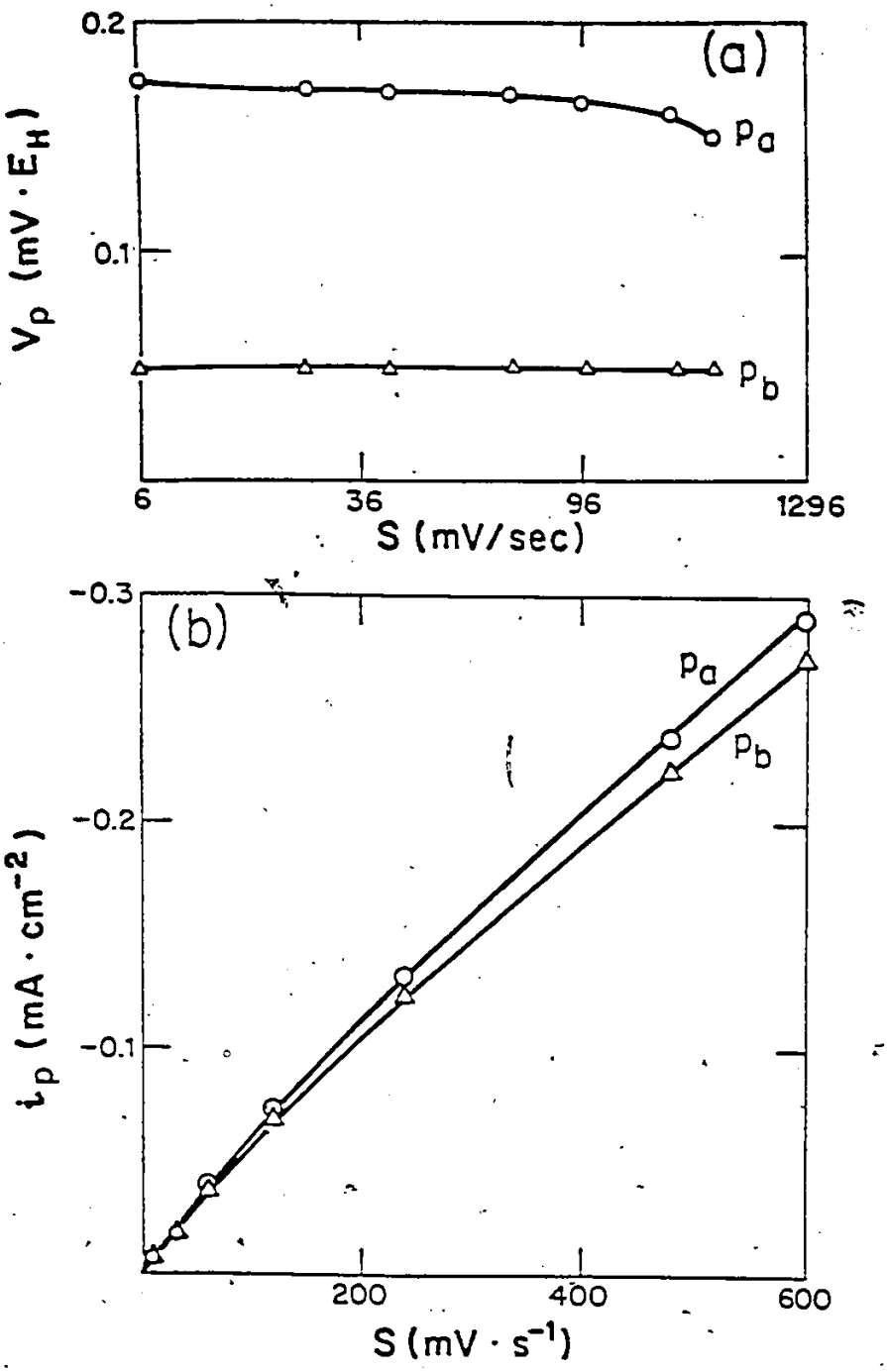

Fig. 3-18: (a) Peak potentials; V_p, of Fig. 3-16 as f(s).
(b) Peak currents, i_p, of Fig. 3-16 as f(s).

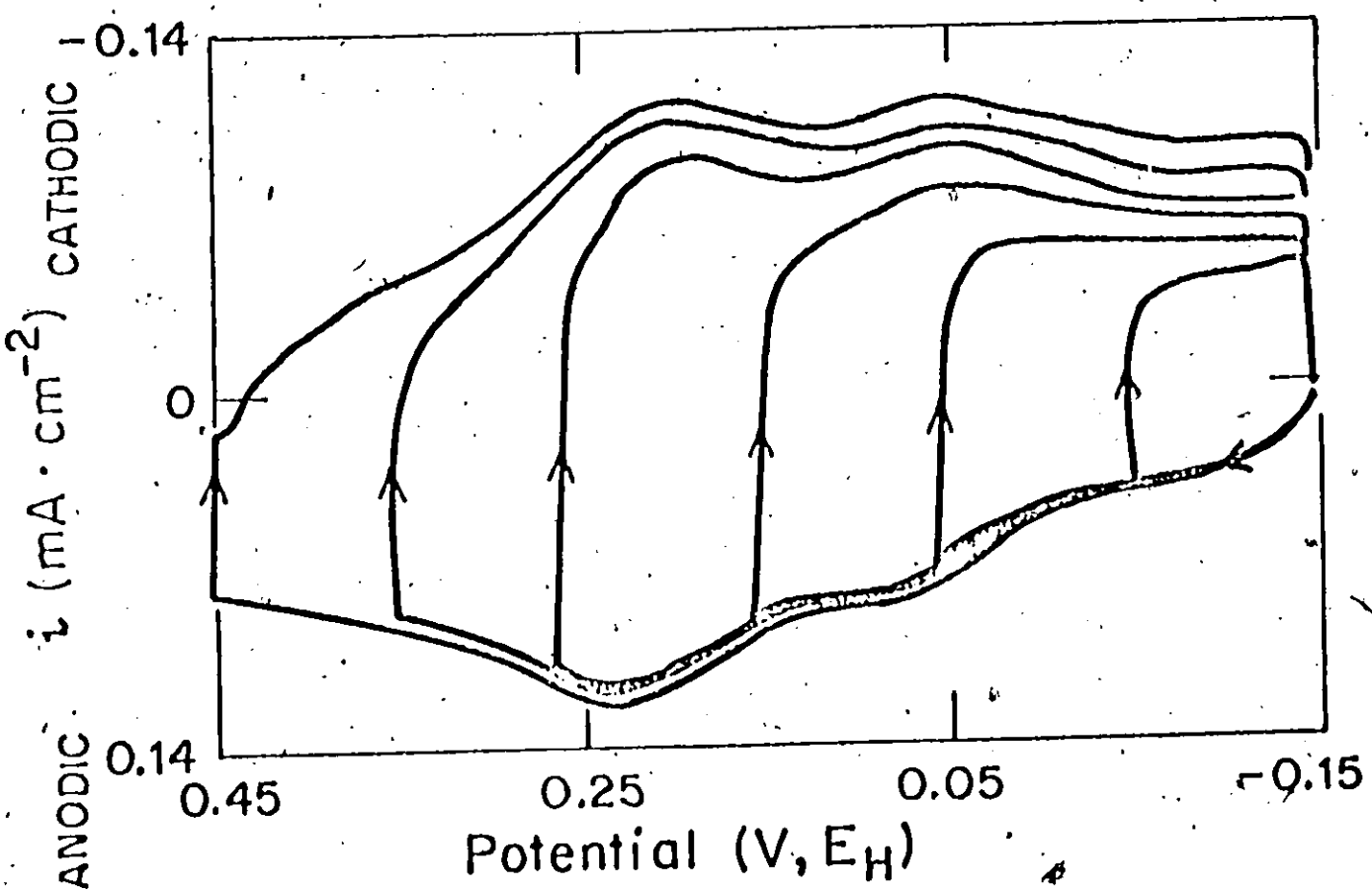

Fig. 3-19: Behavior of FeS_2 electrode upon reversal of direction of anodic sweep at successively increasing anodic potentials over the reversible region in single-cycle anodic/cathodic voltammetry, showing development of cathodic peaks conjugate to anodic ones (0.1 M $HClO_4$).

matched successively by corresponding peaks in the cathodic direction as the sweep is changed in direction at various potentials. This behavior is typical of a more or less reversible surface process as shown in previous work in this laboratory for Ru and Pt electrodes (250,251). However, the system cannot be directly compared with Pt or Ru since either new oxygen or hydrogen species are electrochemically deposited or desorbed at those metals in cyclic-voltammetry experiments but, here, chemical changes of an existing surface of a molecular material are involved. The type of behavior shown in Figs. 3.16 and 3.19 also demonstrates that the i vs V profiles are not those for diffusion-controlled process involving solution-soluble species (see below), or a solid-state diffusion process.

3.3.2 Charges for the Electrochemical Surface Processes

The significance of the currents in the cyclic-voltammetry profiles of Fig. 3.16 can be deduced by evaluation of the charge associated with the peaks. The charges in the anodic or cathodic peaks are found to be comparable with these for the monolayer processes of surface oxidation of Pt (252) (to Pt/OH at 1.1 V E_H) or electrosorption of H. Thus, Fig. 3.20 shows oxidation isotherms of FeS_2 in terms of the charge passed per square centimeter of surface as a function of potential, derived from successive anodic/cathodic sweeps taken to +0.45 V E_H; charges of ca. 300-400 $\mu C\ cm^{-2}$ are involved (cf. the charge of 210 $\mu C\ cm^{-2}$ for OH monolayer oxidation of Pt or deposition of H at Pt).

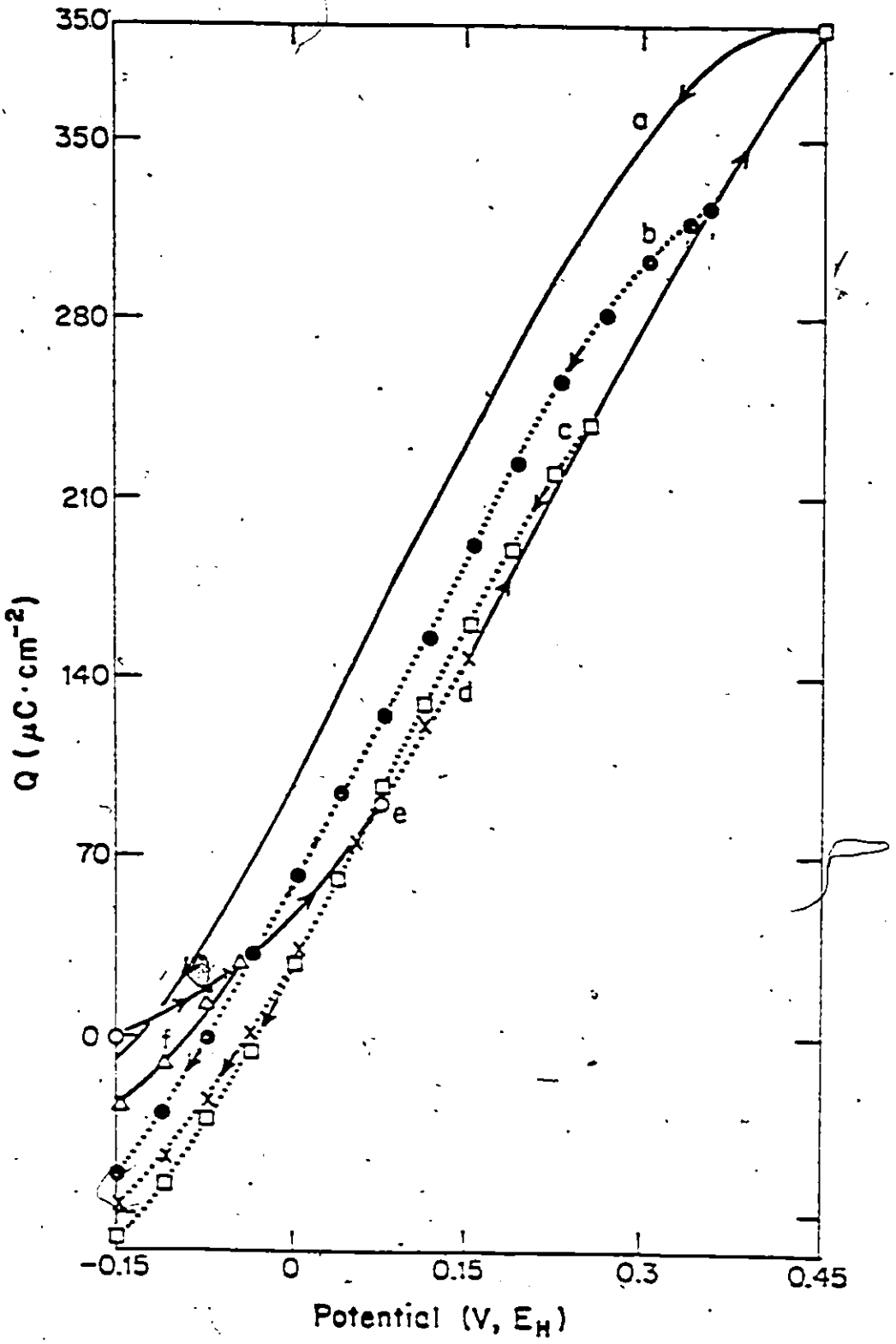

Fig. 3-20: Charge vs potentials for oxidation and reduction of an FeS_2 surface to various potentials, a, b, c, ..., f, from Fig. 3-19 (0.1 M $HClO_4$).

Unfortunately, no unambiguous real area measurement can be made electrochemically at FeS_2 or FeS, since a potential region neither for pure double-layer charging nor for H adsorption, as at Pt, is observed. Since SEM photographs (Fig. 3.23) show significant surface roughness, the figure of 300-400 $\mu C\ cm^{-2}$ could correspond to a one electron "per site" surface process at a less than ideally smooth surface.

The values of surface oxidation or reduction charge observed in the case of FeS_2 are of interest in relation to the behavior of lead sulfide because, in the latter case, the extents of surface oxidation are relatively greater than at FeS_2 and a different order of magnitude of oxidation charge is involved.

In Fig. 3.21 are shown the ratios of the cathodic charge, Q_c, to the anodic charge, Q_a, which are involved in the cyclic-voltammetry curves of Fig. 3.16 up to various potentials. It is seen that there is some excess of cathodic over anodic charge passing at the lowest potentials but the values in curves (a) and (b) for two peaks, as far as they can be resolved, tend toward a ratio of unity at the higest positive potentials. This disbalance of cathodic and anodic charge is often observed when some anodic or cathodic dissolution occurs and suggests that there may be some solution-soluble sulfide ion species generated at the more negative potentials, as was found in the case with lead sulfide.

This corresponds, of course, to reduction of the sulfide with some evolution of H_2S or formation of sulfide ion (SH^- at pH 1) under the acidic conditions when the potential is in a region where reduction

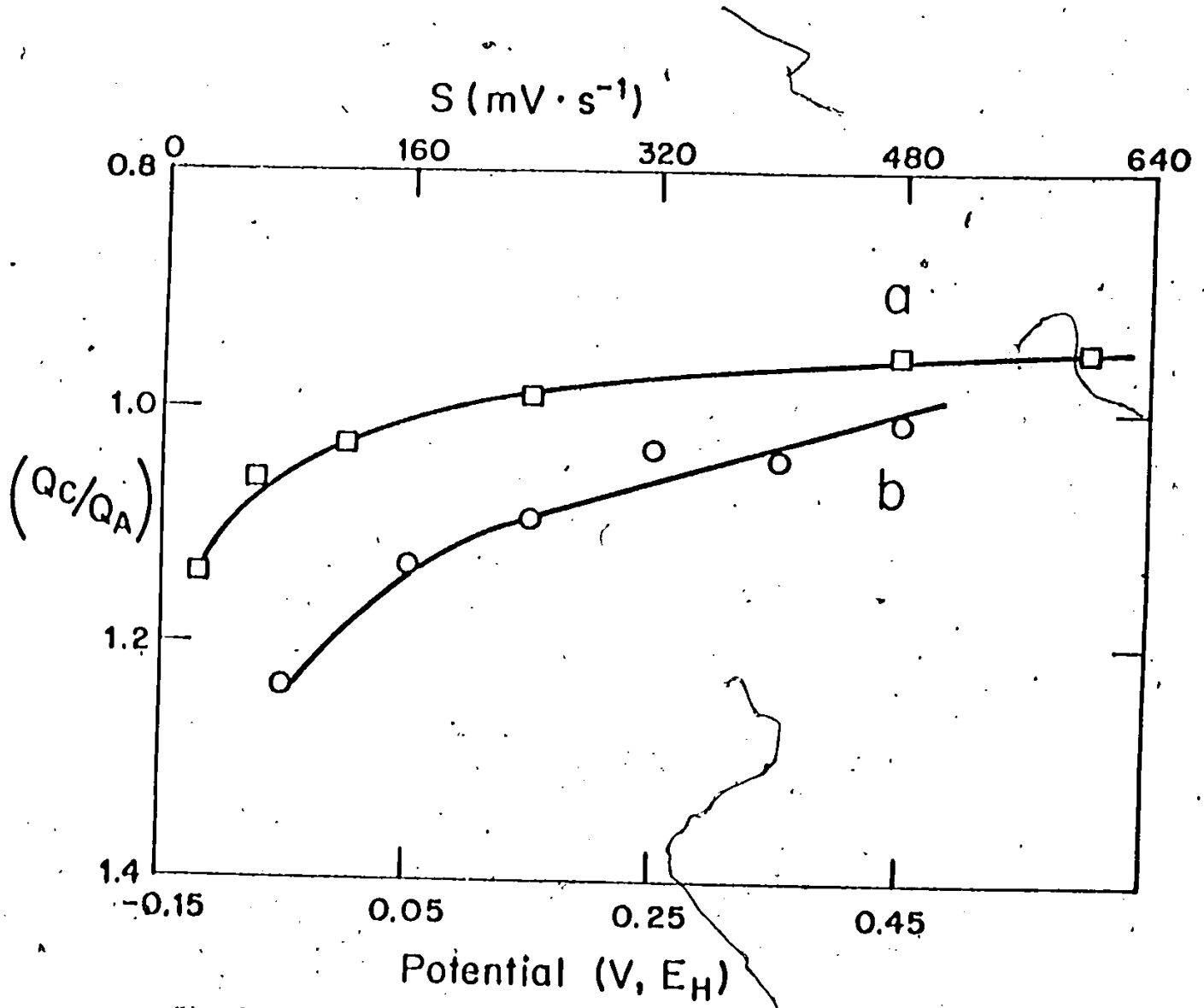

Fig. 3-21: Cathodic/anodic total charge balance for curves (a) and (b) in the reversible surface oxidation and reduction of FeS_2 in 0.1 M $HClO_4$ shown in Fig. 3-16. (a) Q_c/Q_a as f(s), (b) Q_c/Q_a as f(potential in anodic sweep).

can occur. Actually, H_2S can be smelled when the potential is held cathodically for some time.

Experiments at rotating FeS_2 disc electrodes show, however, that the peaks on the anodic sweep, after a previous cathodic sweep taken to -0.45 V with 60 s holding at this potential, is completely uninfluenced by electrode rotation. In this respect, the behavior is surprisingly different from that for PbS (see Figs. 3.17(a) and (b) for comparison). This result indicates either that solution-soluble reduction products are not significantly formed in the previous cathodic sweep and on holding at -0.45 V in the case of FeS_2 or, if formed, they are unreactive. Similar behavior is found with $Fe_{1-x}S$.

An important and further indication that the currents observed in cyclic voltammetry of FeS_2 are mainly associated with surface processes follows from the relation between the peak current i_p and s, shown in Fig. 3.18. Fig. 3.22 (see below) shows other plots of i_p vs s for the two peaks ((a) and (b)) at five pH values (see below). All the i_p vs s plots are evidently linear and extrapolate almost through zero. This behavior indicates again that surface reactions are involved rather than diffusion-controlled processes associated with any dissolved species in solution or with solid-state mass-transfer processes, e.g., as arise at the nickel/nickel oxide or the lead/lead chloride electrodes.

3.3.3 Capacitance Behavior as a Function of pH in the Range 1-11

In addition to experiments carried out at ca. pH 1, i vs V profiles for FeS_2 were also recorded at pH 3,7,9 and 11 at various sweep-rates. In going towards alkaline pH, the oxidation and reduction currents significantly increase but the i vs V profiles become somewhat less reversible than at pH 1 (Fig. 3.16). However, as mentioned above, i_p values for all conditions (Fig. 3.22) are linear in s. The smaller reversibility may be connected with the fact that in the neutral and alkaline solutions the state of S in the surface is more ionic than in acid medium where the disulfide species may be protonated in the interface. In alkaline solution it may be kinetically less easy to reduce the disulfide ion on account of its greater anionic character in the surface than under acid solution conditions.

An interesting feature of the lines in Fig. 3.22 is that their slopes increase with pH. Since the relation between i_p and s is given, for a surface process, by

$$i_p = C_p s \quad /$$

where C_p is the Faradaic reaction capacitance associated with the surface electrochemical reaction, the results of Fig. 3.22 indicate that the capacitance increases in a major way with pH, e.g., from ca. 400 $\mu F\ cm^{-2}$ at pH 1 to ca. 2×10^4 $\mu F\ cm^{-2}$ at pH 11, depending on which current peak is taken. A Langmuir monolayer, it may be noted (253), gives rise to a capacitance maximum at half-coverage (or half oxidation/reduction of an electroactive monolayer) having a value $C_p = qF/4RT$, where q is the charge for monolayer formation; with

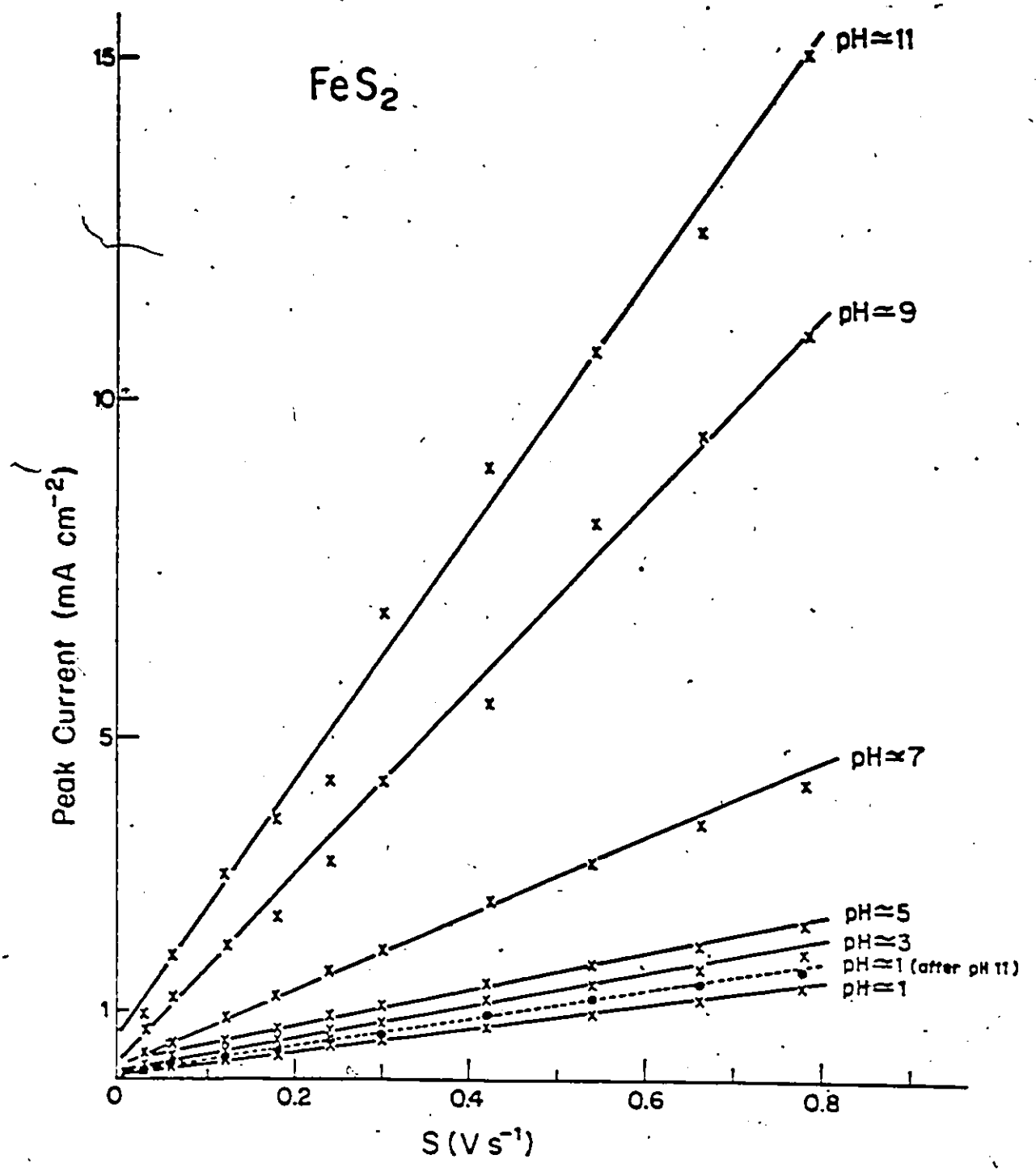

Fig. 3-22: Plots of the peak currents in the reversible regions for FeS_2 vs sweep rate over a range of pH values. Relations for pH 1 are shown before and after going to pH 11. Conditions as for Fig. 3-16.

$q = 210\ \mu C\ cm^{-2}$ (as at Pt), $C_p = 2200\ \mu F\ cm^{-2}$ for Langmuir adsorption. Changes of C_p can arise with changing lateral interactions in a monolayer (253) (C_p decreasing as they increase), e.g., if the electroactive surface species becomes more ionized at lower pH. This does not seem chemically feasible in the present case with FeS_2.

A pH effect on the surface reaction capacitance could arise from a greater reactivity of S_2^{2-} species in the surface of FeS_2 under alkaline conditions where S_2^{2-} ions can exist in the surface layer. Under acid conditions these will tend to be protonated.

Since C_p depends on the real surface area of the electrode material (determined by the value of q), the results of Fig. 3.22 could most easily be interpreted as due to an increase of surface area with cycling at high pH, due to a greater reactivity of the surface under the latter conditions.

This does not seem to be the case, however, since an interesting result found is that an electrode giving a large and increased capacitance at pH 9-11 relative to that at pH 1, gives only the smaller capacitance again when returned (in this case without repolishing) to solutions at pH 3 or 1, as shown in Fig. 3.22.

One other possibility for the results exhibited may be the effect on the properties of semiconductors of different values of pH.

Further information on the state of FeS_2 and FeS surfaces was obtained by scanning electron microscopy.

3.3.4 SEM and X-Ray Emission Analysis

A series of FeS_2 electrodes that had been subjected to 10 anodic/cathodic cycles at pH 1 and 11 were examined in a Semco Nanolab scanning electron microscope provided with a wavelength-dispersive x-

Fig. 3-23-1: SEM photograph of (a,b,e) FeS_2 and (c,d,f) $Fe_{1-x}S$ electrode surface before and after cycling in 0.1 M aq $HClO_4$ in the potential range as Figs. 3-16 and 3-24. (a,c) uncycled, (b,d) cycled and (e,f) held at cathodic end form 20 min.
(a,b)

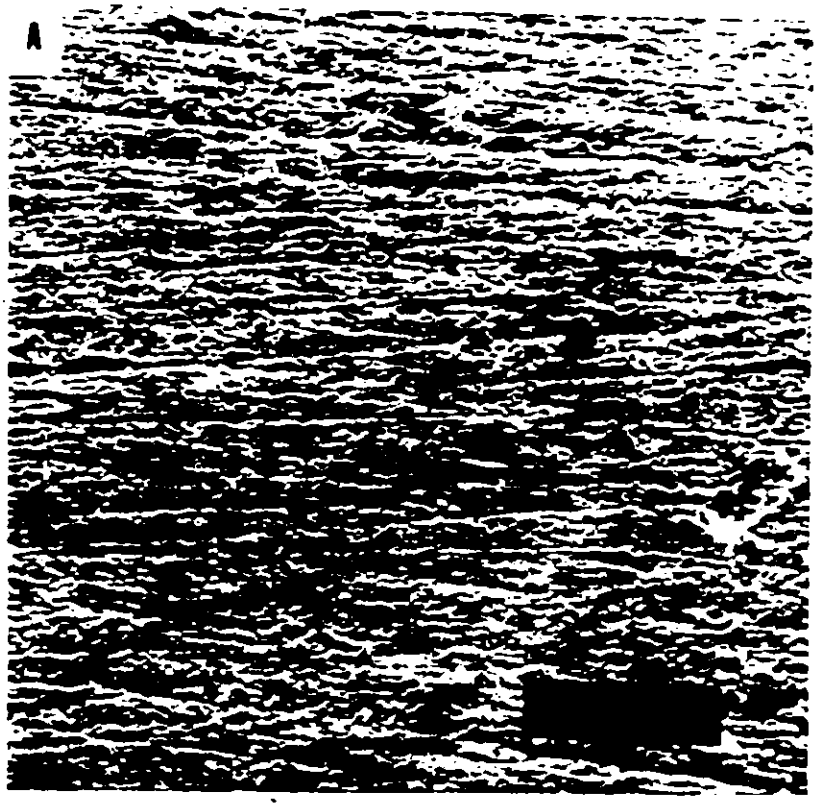
A

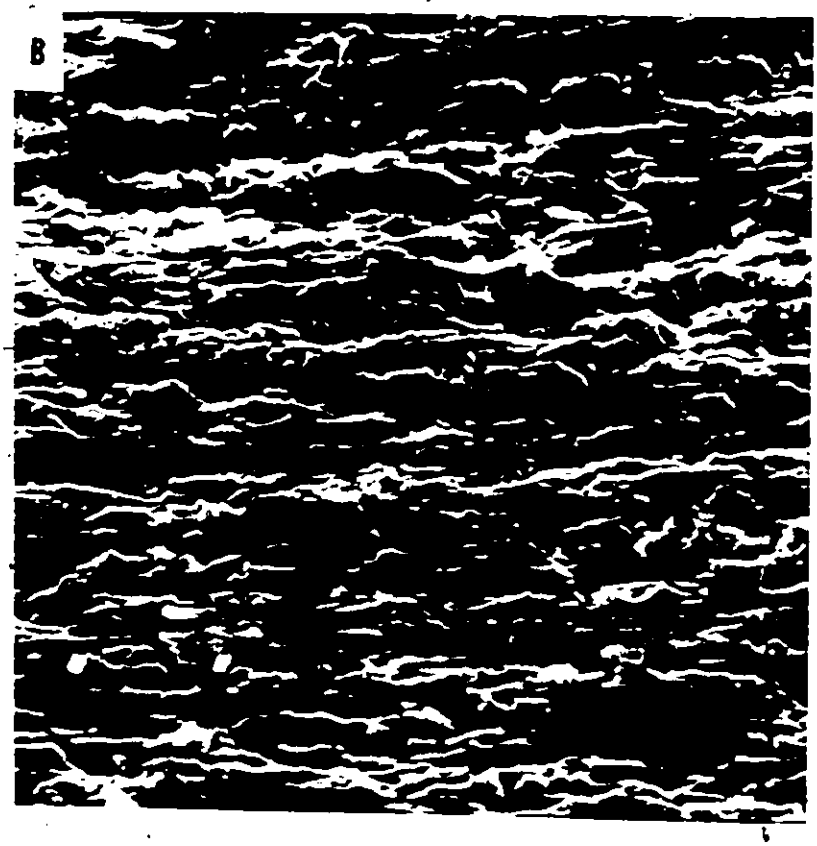
B

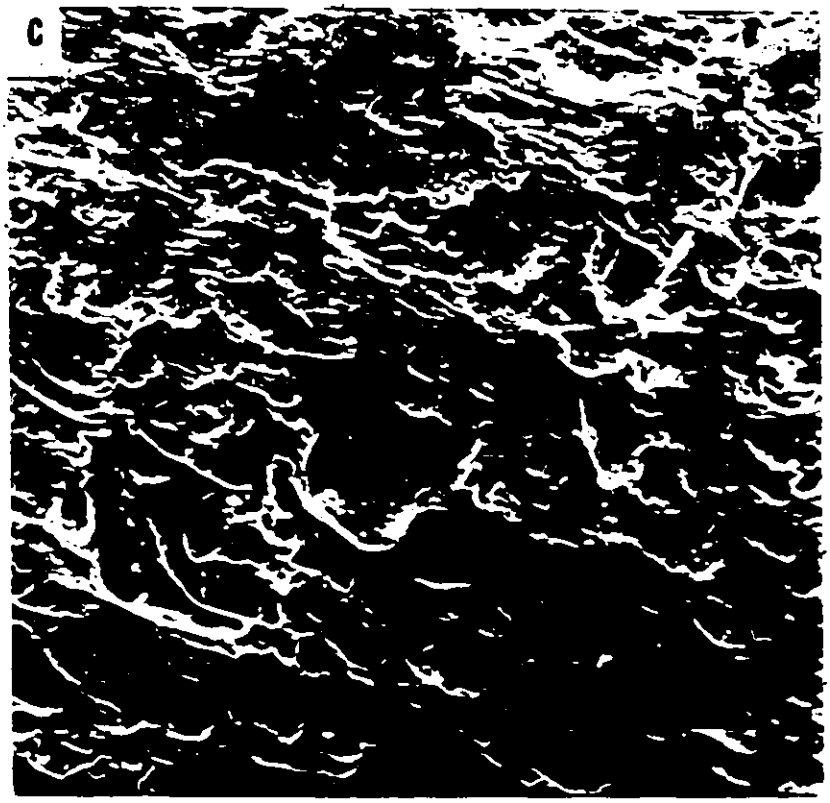
C


D

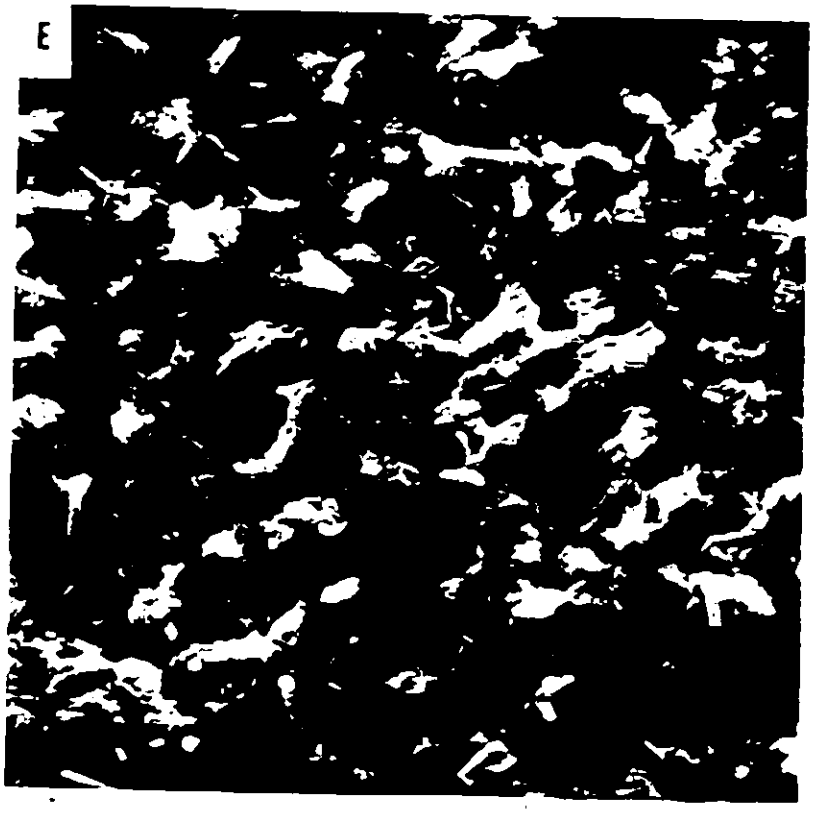
E

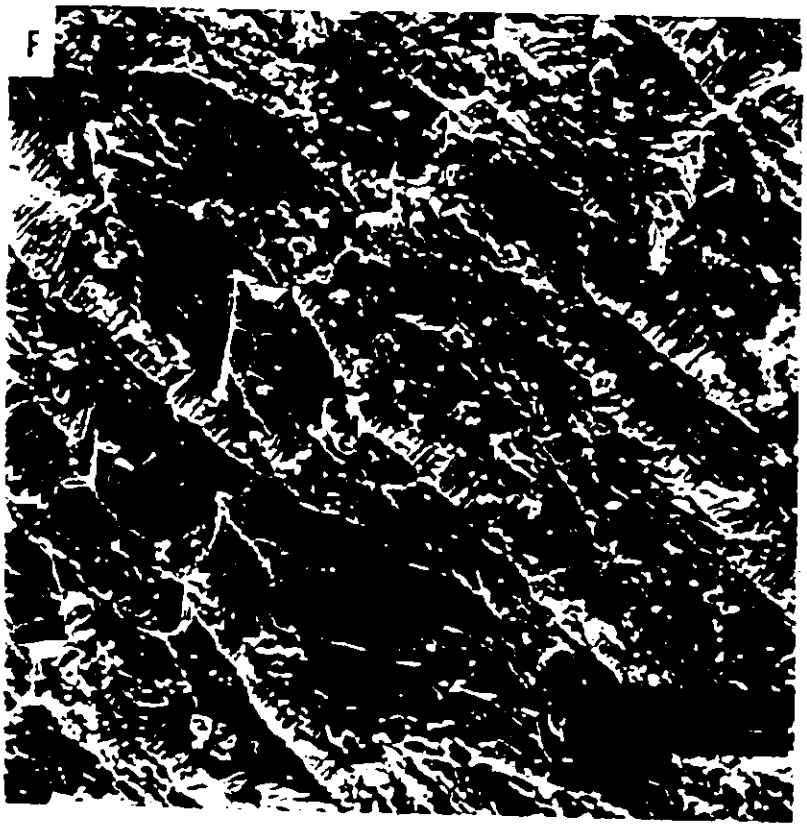
F

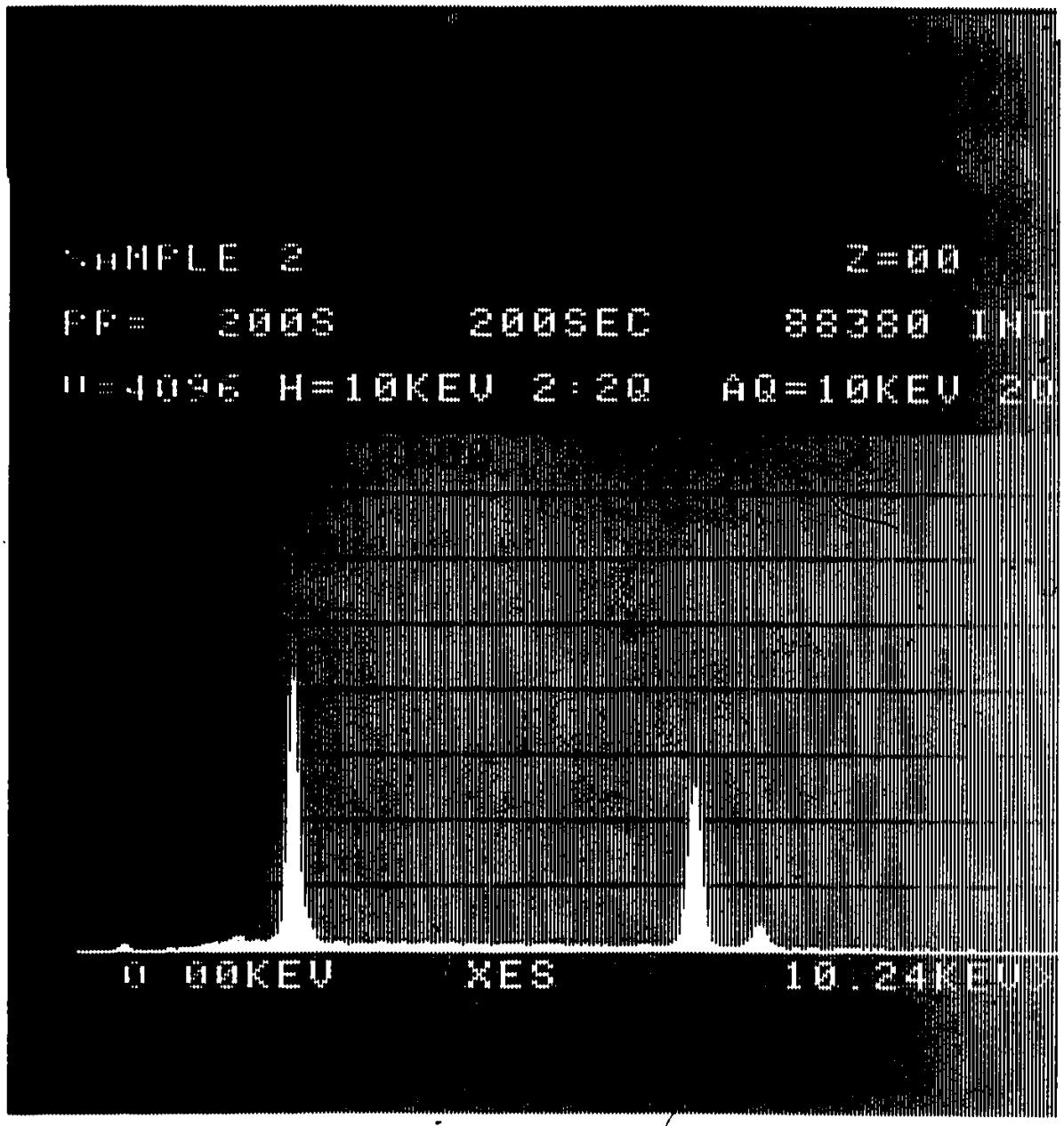

Fig. 3-23-2: X-ray emission surface analysis results of $Fe_{1-x}S$ in acidic aq solution held at cathodic end.

ray emission attachment. Figure 3.23 shows the state of the FeS_2 surfaces before and after the electrochemical cycling and holding at cathodic end. It is clear that some change of roughness of the surface takes place. Also, the Fe:S ratio in the surface region[5] of the specimens is substantially changed; at FeS_2, S is relatively enhanced while at $Fe_{1-x}S$ (Section 3.4) it is relatively depleted, as shown below:

Fe/S signal ratio in FeS_2	Before cycling	1.81 ± 0.13;
	After cycling	1.30 ± 0.03;
	Holding at -0.10 V	0.05 ± 0.01.
Fe/S signal ratio in $Fe_{1-x}S$	Before cycling	2.64 ± 0.1;
	After cycling	3.44 ± 0.1.
	Holding at -0.40 V	0.63 ± 0.03

Also by comparing SEM photographs of (a) an FeS_2 electrode cycled 15 times in pH 1 solution from -0.1 to +0.5 V with (e) one held at -0.1 V for 20 min, and from x-ray surface analysis results, it is found that holding at the cathodic end for 20 min probably produces Fe on the surface which is then lost in solution while the sulfur remains as a porous surface structure species. The cathodic holding causes a diminution of the Fe:S ratio. This is another aspect of the surface processes that iron sulfides undergo electrochemically.

---

[5] It is to be noted that the x-ray emission that is utilized for analysis arises from within a region down to several hundreds of A below the surface as well as from the surface, depending on electron beam energy.

3.3.5 Behavior after Holding the Electrode Potenial Constant for Controlled Times

A useful approach in cyclic-voltammetry studies as we have seen with PbS electrodes, is to hold the electrode potential at certain fixed values for well-defined periods of time, τ_h, and then follow the succeeding current-voltage profile upon applying a cathodic (or anodic) potential sweep at some controlled rate. Results of this procedure were obtained for different holding times, τ_h = 3 to 1000 s at FeS_2. There is a significant time effect in the degree of surface oxidation achieved at 0.35 V E_H, corresponding to superimposition of a slow process on the faster one revealed in Fig. 3.16.

Oxidation charge-potential relations may be evaluated for the holding experiments. They are of a shape similar to those of Fig. 3.20 but correspond to substantially (10-25%) higher charges being passed as a function of potential. This, of course, is on account of the time allowed for more extensive formation of the products of oxidation of the FeS_2 surface. We have shown that the behavior of Fig. 3.16 corresponds approximately to a monolayer level of oxidation and reduction of the surface while the data for the holding experiments correspond to some "penetration" of the degree of oxidation and corresponding increase in the charge for reduction with time, τ_h. It is found that after 'holding,' the electrochemical behavior of the material still remains more or less reversible, at least with respect to the potentials at which the current peaks appear. This is to be contrasted with the situation with oxidation of the noble metals, where the potential of the peak for cathodic

reduction of surface oxide becomes substantially less positive with increasing degree of oxidation of the metal on account of increasing stability of the oxide film as more of it is electrochemically formed and a phase-oxide structure is developed. The holding effect here corresponds, it appears, simply to more matrerial being oxidized with time, but the state of the product remains essentially constant from an electrochemical thermodynamic point of view.

At one point in the work it seemed that metallic iron might be formed in the surface of iron sulfide after reduction at -0.2 V E_H so that the behavior observed in Fig. 3.16 could conceivably be due to formation and reoxidation of this iron on a microscopic scale after reduction. Accordingly, an experiment was conducted in order to define the current-voltage profile in cyclic-voltammetry for pure iron in the same acid medium as that for the experiments on FeS_2. The behavior found was not, in any way, similar to that of Fig. 3.16 and only an oxidation with passivation curve originates, which is not unexpected (cf. 254)

3.3.6 Relation to the Results with PbS

It is clear from the results shown above that there are quite substantial differences between the behavior of FeS_2 and PbS. In particular, a region of reduction processes distinguishable from that of oxidation processes is less clear in the FeS_2 case except at potentials more positive than 0.5 V, and there is much less, if any, evidence for formation of solution-soluble species. This was indicated by experiments with rotating FeS_2 electrodes in which the

current-voltage curves were found to be almost independent of rotation rate, unlike the behavior at PbS.

The i vs V profiles of Fig. 3.16 are to be contrasted with those for PbS, mentioned previously. Notably, no reversible region is observed at PbS. In this respect, the behavior of the latter material is more similar to that of $Fe_{1-x}S$ (Section 3.4).

The interesting reversibility found especially in acidic solution, as in Fig. 3.16, suggests that there may be a reversilbe reduction of the S_2^{2-} ion to two S^{2-} or SH^- ions in the surface of the FeS_2 material. Presumably this could be a fairly facile process without the necessity for much rearrangement, at least locally speaking, of the lattice. Such a process would be reminiscent of the facile reduction/oxidation of the disulfide linkage in organic materials such as cystine (but see Section 3.6).

3.4 COMPARISON OF THE ELECTROCHEMICAL BEHAVIOR OF PYRRHOTITE ($Fe_{1-x}S$)

3.4.1 Cyclic-Voltammetry Results

A further comparison of the behavior of FeS_2 was made with another sulfide, $Fe_{1-x}S$. This material, as the mineral pyrrhotite, differs from FeS_2 in having monomeric S^{2-} ions in the structure rather than disulfide ions, S_2^{2-}. The purpose of this comparison was therefore to examine if the electrochemical reactivity of $Fe_{1-x}S$ was substantially different from that of FeS_2 on account of the change from a disulfide ion structure to a monosulfide one. Especially, the question of reversibility of reduction/oxidation was of interest in relation to the electrochemical behavior of the S_2^{2-} ion in FeS_2.

The behavior of $Fe_{1-x}S$ in pH 1 aqueous $HClO_4$ at sweep rates similar to those for FeS_2 in Fig. 3.16 is substantially different from that of FeS_2. The main electrochemical processes occur over a different potential range, -0.4 to 0.19 V E_H, and are much less reversible than those at FeS_2. Reversals of the cathodic sweep at -0.35, -0.40, and -0.45 V show that the main oxidation peak at -0.2 to -0.15 V in Fig. 3.24 depends on prior reduction of the surface at potentials more negative than -0.35 V.

3.4.2 Irreversibility and Surface Process-Characteristics of $Fe_{1-x}S$

$Fe_{1-x}S$ behaves generally rather less reversibly than FeS_2 under various conditions of pH and a typical i vs V profile is shown in Fig. 3.24 for pH 1. The absence of an effect of electrode rotation indicates again that solution-soluble species are not formed, as was also found with FeS_2. Qualitatively, in this respect, the behavior of $Fe_{1-x}S$ is thus similar to that of FeS_2. As with FeS_2, the peak currents plot out linearly in s and are pH dependent. The peak currents show a general tendency to increase with pH, as with FeS_2, but not in the uniform way found with FeS_2 (Fig. 3.22).

The general structure of the i vs V profiles is, however, substantially different from that for FeS_2; there are four peaks distinguishable over the potential range shown in Fig. 3.24, one of them being reproducibly much larger than the others. No two-peak reversible region, of the type seen in Fig. 3.16 for FeS_2, is observed at $Fe_{1-x}S$. The large anodic peak in Fig. 3.24 for $Fe_{1-x}S$ depends on the potential to which the cathodic sweep has been taken (Fig. 3.25)

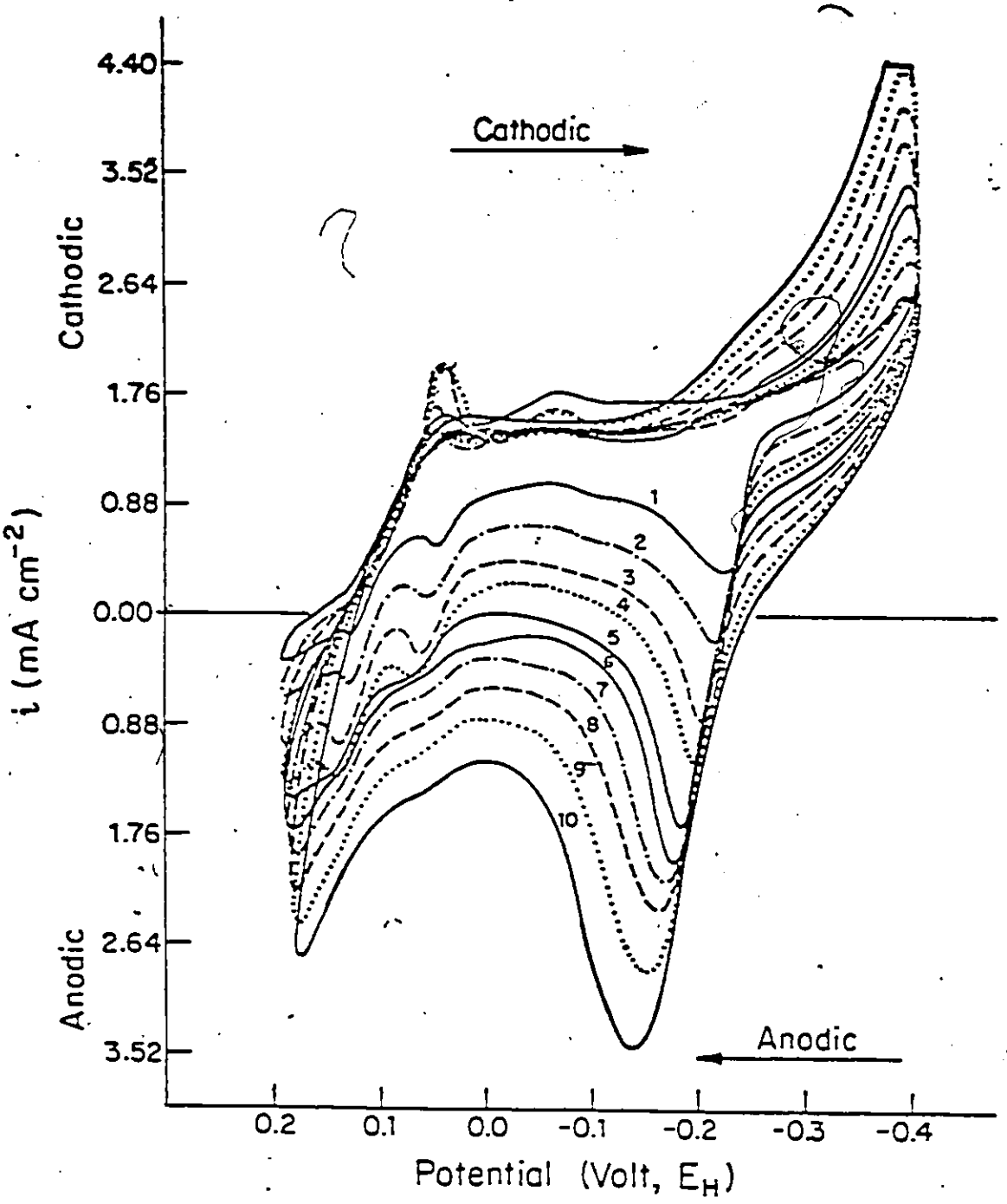

Fig. 3-24: Cyclic voltammetry i vs V profiles for FeS in 0.1 M $HClO_4$. Curves 1-10 for the same respective sweep rates as in the Fig. 3-16, over the potential range -0.40 to +0.20 V E_H.

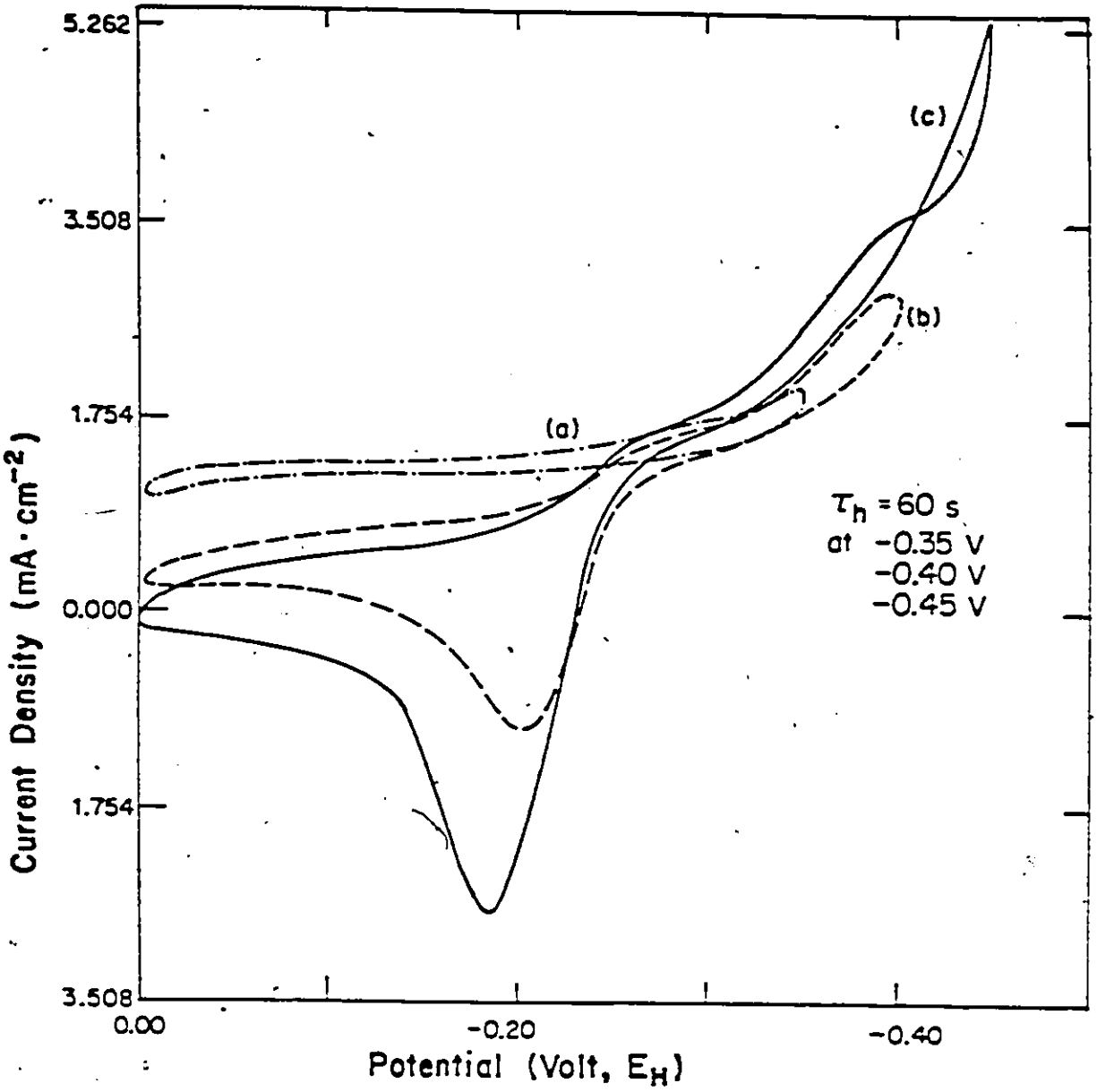

Fig. 3-25: Dependence of main current peak for anodic oxidation of $Fe_{1-x}S$ in 0.1 M $HClO_4$ on potential limit (-0.35, -0.40 and -0.45 V with 60 s holding time) of previous cathodic sweep. Cathodic and anodic sweep rates = 25 mV s^{-1}. Anodic peak is independent of electrode rotation rate.

and thus depends on the prior state of reduction of the surface. The current peak is, however, independent of the electrode rotation rate and is thus not due to solution-soluble S^{2-} or SH^- ions, as was found with PbS.

3.4.3 Comparison of the Behavior with that of PbS

In the experiments carried out in low pH (pH 0, 1, 2 and 3) aqueous solutions it was found that H_2S gas evolves at -0.40 V. This was confirmed by a test with lead acetate paper which turned dark. Referring to the Poubaix disgram (248), this potential is just in the equilibrium range for H_2S stablity. Thus, the reduction current at the most negative end of the potential sweep is associated with the reduction process:

$$FeS + 2\ e \longrightarrow Fe + S^{2-}\ (lattice)$$

and $$S^{2-}\ (lattice) + 2\ H^+ \longrightarrow H_2S \uparrow$$

Here the S^{2-} produced on the lattice or in some other form is not dissolved in solution except in so far as H_2S is formed. Thus, the following large anodic peak in the region, -0.15 to 0.20 V shows no rotation dependence of the current. Since H_2S can evidently actually be formed, and thus also some SH^- and S^{2-} ions, the absence of a rotation dependent current, at $Fe_{1-x}S$ must be due to the lack of reactivity of the $Fe_{1-x}S$ surface for H_2S or sulfide reoxidation.

In high pH solutions the reduction current still arises but there was no detectable H_2S , as may be expected under alkaline conditions.

In case of PbS, we recall that the anodic peak A_1 was affected by electrode rotation, due to formation solution-soluble species which were reoxidized at the PbS surface. The S species formed on the lattice of $Fe_{1-x}S$ appears the same as for FeS_2, as can be observed from the SEM photographs and confirmed by the x-ray analysis results.

3.5 CONCLUSIONS ON REACTIVITY OF MINERAL SULFIDES

The surface and succeeding bulk-phase electrochemical reactions of FeS_2 and $Fe_{1-x}S$ are evidently quite complex and electrochemical studies alone can not provide a full understanding of the reactions which can proceed over various ranges of potential. More work of an analytical kind on coulombic yields of products of oxidation would, for example, be required for a better understanding of the electrochemical reactivity of the iron sulfides to be reached. However, the following can be said about some aspects of the surface processes which can be followed electrochemically at these minerals.

After reduction of the surface of FeS_2 at the initial potential of anodic sweeps, reversible oxidation-reduction processes in two peaks arise, as we have shown in Fig. 3.16, provided the potential in the anodic sweep does not exceed ca. 0.5 V. A similar reversible process is not observed at PbS or $Fe_{1-x}S$.

Since the latter sulfides are structures containing the S^{2-} ion, while FeS_2 contains the S_2^{2-} ion, it seems likely that the reversible surface process at FeS_2 is

$$2\,e + S_2^{2-}\ (\text{lattice}) \rightleftharpoons 2\,S^{2-}\ (\text{lattice}) \qquad (4)$$

Two peaks are observed in the reversible region of the FeS_2 reduction/oxidation i vs V profiles. This is suggestive of two separate, one electron, reduction processes in (4) but the charges under the two peaks do not appear to be quite the same. Polycrystallinity is an obvious possibility for the origin of more than one peak for a surface process (cf. the situation of H electrosorption on Pt (250,255). However, in experiments carried out with single-crystal mineral specimens of FeS_2, the two-peak behavior in the reversible region was still observed.

With PbS, evidently reductive dissolution can occur, [PbS + 2e ⟶ Pb + S^{2-} (soln)], giving rise to solution-soluble SH^- or S^{2-} ions, depending on pH. This is not observed with $Fe_{1-x}S$ or FeS_2 in the time frame of an anodic sweep or else any SH^- or S^{2-} ions that are formed at the negative end of a sweep, or on reductive holding of the potential at that end, are kinetically unreactive, and/or remain fixed as lattice-structured species with regard to their reoxidation at the iron sulfide surfaces.

At potentials more positive than ca. 0.5 V at FeS_2 and $Fe_{1-x}S$, other anodic processes evidently occur (Fig. 3.17(a)) (256), as they do with PbS (Fig. 3.17(b)), leading eventually to substantial, continuous Faradaic currents for oxidation of the bulk material. This can produce such species as SO_3^{2-}, $S_2O_3^{2-}$, SO_4^{2-}, and Fe^{3+} ions. After sufficiently long periods of anodic oxidation in a cell, SO_4^{2-} and Fe^{3+} ions can be chemically detected (reaction with $BaCl_2$ and CNS^- ion, respectively).

Recently, it is to be recorded, FeS_2 has been successfully embodied as a cathode material in a Li/FeS_2 primary battery.

PART II -- INVESTIGATIONS WITH ORGANIC -S-S- AND S-H COMPOUNDS

3.6 CYSTINE: CYCLIC-VOLTAMMETRY BEHAVIOR

3.6.1. Characteristics of the Cyclic-Voltammograms

The cyclic-voltammograms at acid and alkaline pH's (1.3 and 11, repectively) exhibit two current maxima in the cathodic and anodic sweeps with voltage separations of ca. 0.03 V. At neutral pH (7.1), rather more complex peak structures arise, probably on account of the cystine being present in two states of ionization at the electrode interface.

The charge balance between the cathodic and anodic current vs potential profiles is always excessive in the cathodic direction, suggesting irreversibility in the extents of cathodic and anodic reaction and/or diffusion of a cathodically formed product into solution.

The currents are either partly or completely diffusion-controlled as will be shown below, with some indications of a surface reaction process but only under certain conditions. In view of the suggestions and other evidence in the literature (140-143) for surface compound formation with Hg, it is surprizing that the electrochemical behavior is rather largely characterized by diffusion control with peak currents usually being found to be proportional to $s^{\frac{1}{2}}$.

3.6.2 Behavior at Acid pH 1.33

The cyclic-voltammetry behavior at 3 pH's from acid, through neutral to alkaline pH was investigated at various sweep-rates. Typical curves after 10 min initial cycling are shown in Fig. 3.26 for pH 1.33 and at various sweep-rates, s ($V\ s^{-1}$). At this pH, cystine is largely in a positively ionized state, RNH_3^+. Initially, some variation of the shapes of the profiles takes place with successive cycling, as illustrated in Fig. 3.27(a) where it is seen that a second cathodic peak becomes established after a period of cycling (10 min) using initially a fresh electrode and fresh solution. This is the general and reproducible behavior observed in all runs.

An experiment was conducted to examine if the electrochemical response of an adsorbed film only of cystine, uncomplicated by reaction of cystine from the bulk, could be measured. A fresh Hg electrode was dipped into cystine solution for 3 min., then cycled in the electrolyte without any trace of free organic disulfide or thiol; it is found, as in Fig. 3.27(b), that the second cathodic peak, referred to above, is much larger than the first one in the first sweep, but their heights are reversed on the second sweep. The ratios of cathodic (Q_c) to anodic (Q_a) charges over the whole region of curves 1 and 2 of Fig. 3.27(a) are 1.94 and 1.97, respectively. These charges (Q_c) probably contain an appreciable component for cathodic H_2 evolution beyond -0.4 V while over the region 0.45 to -0.05 V, Q_c/Q_a = 0.66 ± 0.05 for both curves. In an experiment (Fig. 3.26) where the cycling itself was only over the range 0.50 to -0.20 V, the Q_c/Q_a ratios are ca. 0.85; they depend somewhat on sweep-rate. The cathodic

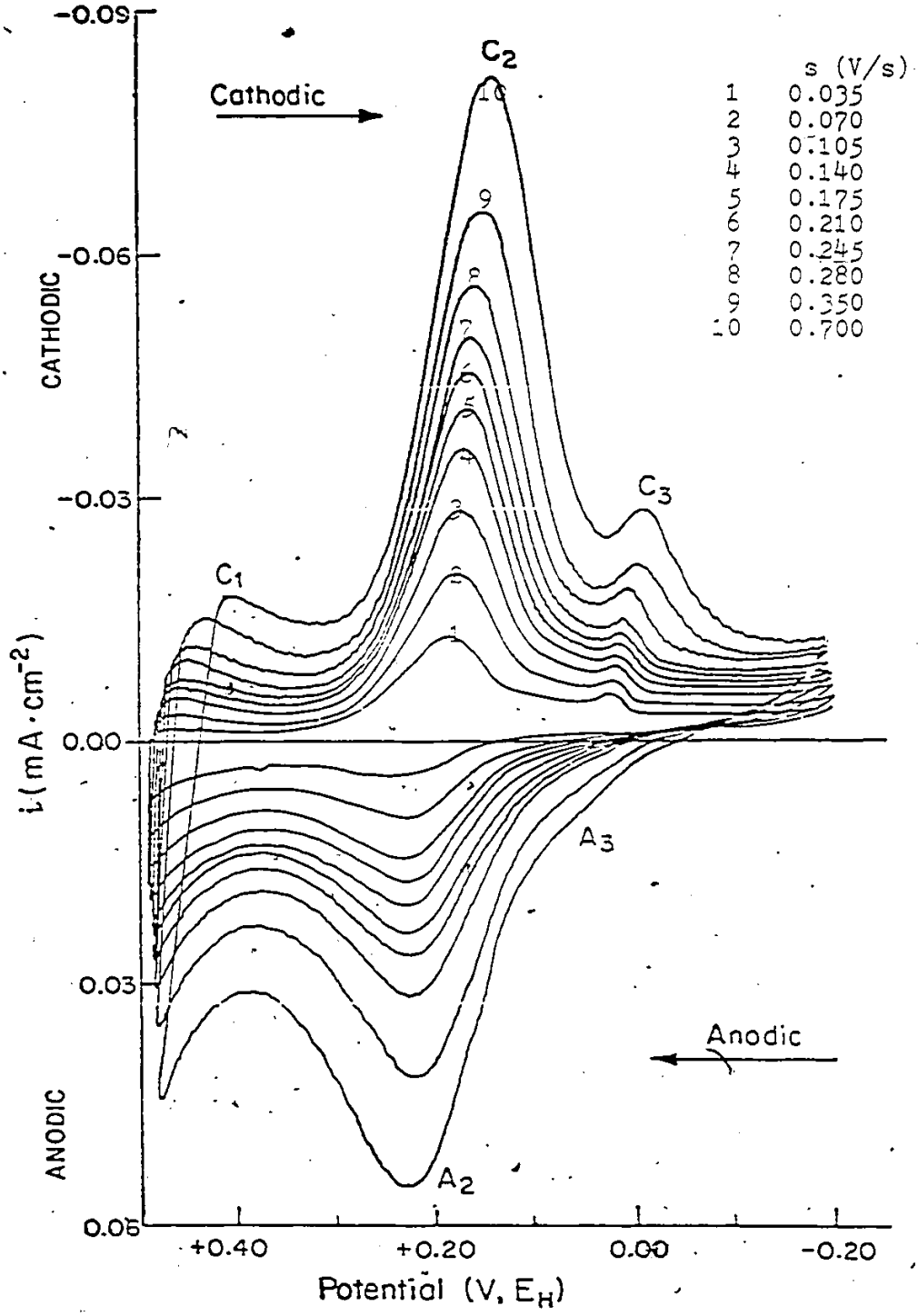

Fig. 3-26: Cyclic voltammetry i vs V profiles of cystine at the Hg electrode at various sweep-rates in pH 1.33 aq solution

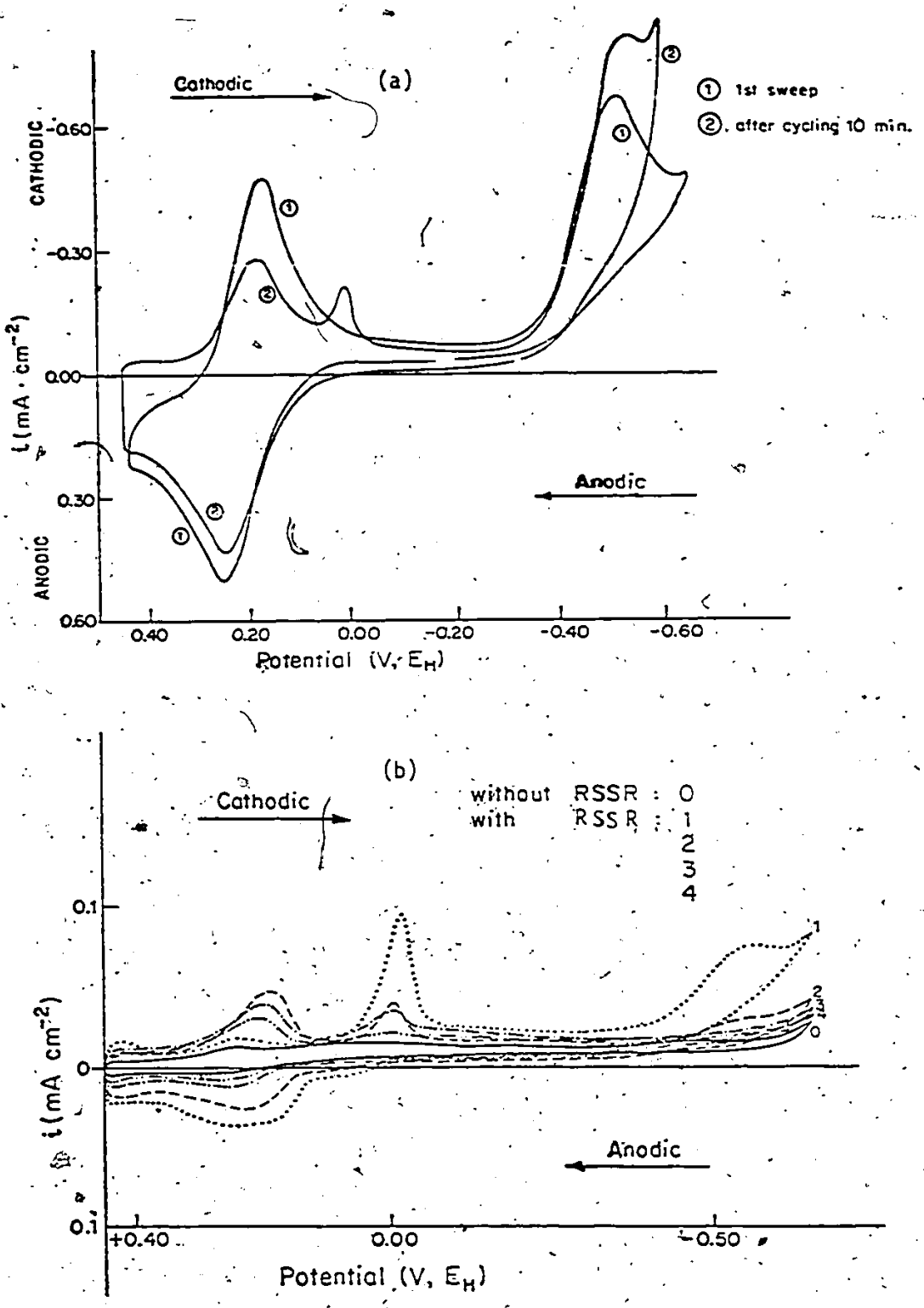

Fig. 3-27: (a) Cyclic voltammetry i vs V profiles of cystine at the Hg electrode in pH 1.33 aq solution showing difference of initial curve (1) from that developed after 10 min of cycling (current peaks at -0.5 V (E_H) appear to be assocoated with H_2 evolution). (b) Fresh Hg electrode dipped into cystine solution for 3 min, then cycled in electrolyte without any trace of free organic disulfide or thiol.

peak C_3 has only a small conjugate anodic component, A_3, visible only as a shoulder on the anodic current profile (Fig. 3.26). However, in $(n\text{-}Bu)_4NClO_4$, added to suppress H_2 evolution, the anodic and cathodic A_3/C_3 peaks are both seen more clearly. Also, at a slow sweep-rate, with sweeps successively reversed at progressively increased cathodic potentials, Fig. 3.28 shows better which peaks on the anodic sweep correspond, respectively, to those on the cathodic side - in our nomenclature, the so-called "cutting" experiment.

The sweep-rate dependence of peak currents, i_p, can distinguish (238,241), in favorable cases, if the electrochemical processes corresponding to these currents are controlled by diffusion ($i_p \propto s^{\frac{1}{2}}$) or originate from a reaction of a chemisorbed species or a surface compound ($i_p \propto s$). Figs. 3.29(a) and (b) show plots of the i_p values for C_2 and C_3 of Fig. 3.26 for regimes of lower and higher sweep-rates; at low s, i_p's are approximately linear in s while at higher s, they are linear in $s^{\frac{1}{2}}$, indicating partcipation both of diffusion-controlled and surface reaction processes.

For parallel surface reaction and diffusion-controlled processes, one can write

$$i_p = k_1 s + k_2 s^{\frac{1}{2}} \qquad [1]$$

which may be expressed either as

$$i_p/s = k_1 + k_2 s^{-\frac{1}{2}} \qquad [2a]$$

or

$$i_p/s^{\frac{1}{2}} = k_1 s^{\frac{1}{2}} + k_2 \qquad [2b]$$

where the k's are some arbitrary proportionality constants but having the correct dimensions. Either eqn. [1] or [2] predicts that i_p will be more characteristic of the surface process at high s than at low. This is contrary to the observed behavior referred to above (Figs. 3.29(a) and (b)) so it seems that the "mixed" sweep-rate dependence which the i_p values exhibit experimentally may better correspond to a "series" relationship between the surface reaction and diffusion-controlled processes, i.e. the surface process is dependent on diffusion to or from the bulk solution phase. This would be represented in terms of impedance by a Faradaic surface reaction resistance in series with a Warburg impedance. For such a situation the corresponding current components, at a given potential, being inversely proportional to the corresponding impedances in series, add in a reciprocal fashion. Thus, at high s, the current is determined by the "$s^{\frac{1}{2}}$" component that increases less rapidly with s than does the "s" component. In the series situation, the reaction and diffusion currents, at any moment, are of course equal.

Plots of the data of Fig. 3.26 and at 10x slower s, according to eqn. (2b), give the relations shown in Fig. 3.30 which illustrate how $i_p/s^{\frac{1}{2}}$ is constant with $s^{\frac{1}{2}}$ only at sufficiently large $s^{\frac{1}{2}}$ values (cf. eqn. 2b), i.e. a behavior contrary to eqn. (2b). Note that for peak C_4 in the H_2 evolution region, diffusion control over the whole range of s is indicated by the constancy of $i_p/s^{\frac{1}{2}}$ with $s^{\frac{1}{2}}$.

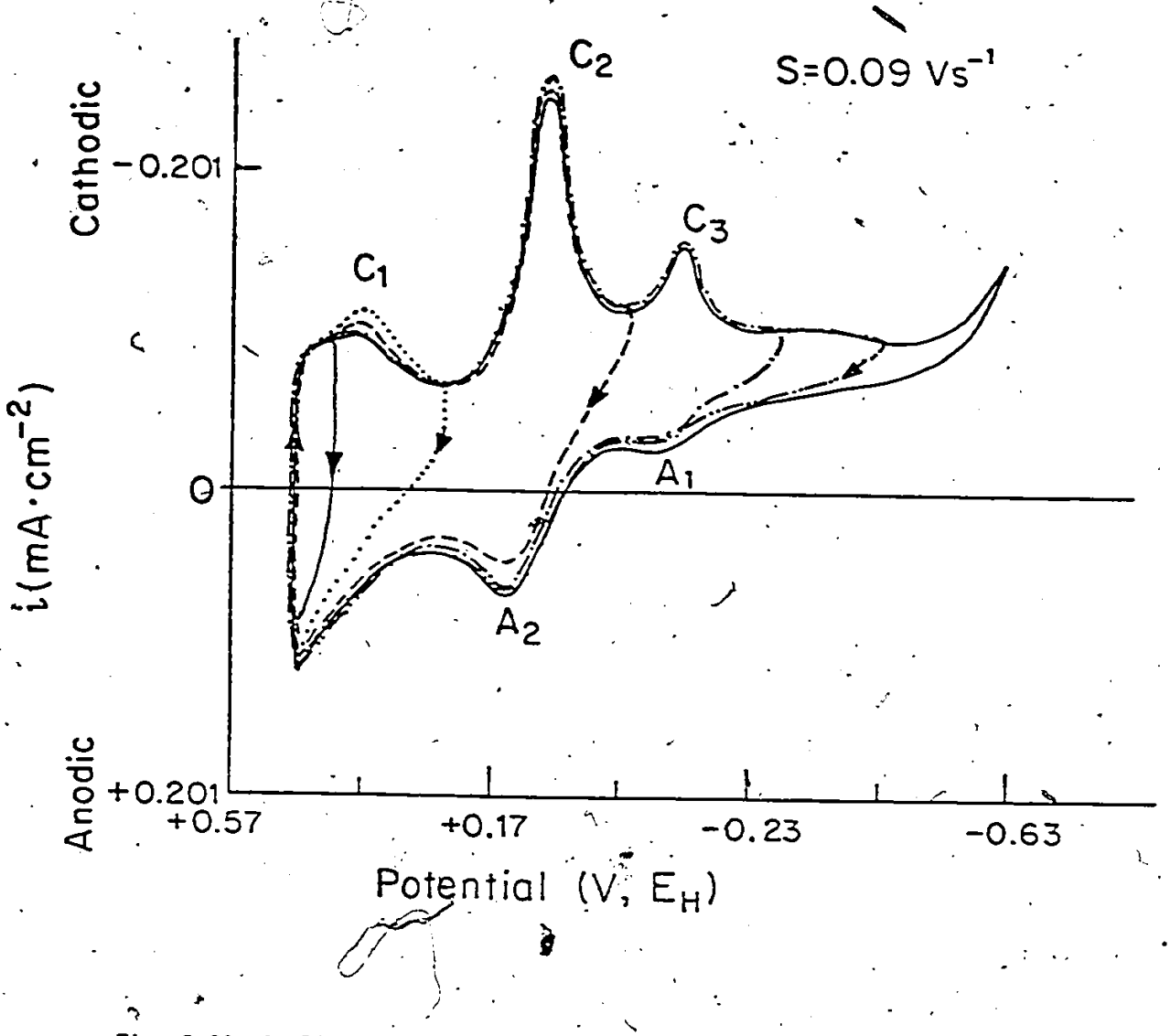

Fig. 3-28: Cyclic voltammetry of cystine at Hg electrode in pH 1.33 aq solution with sweep reversal at several potentials over the reactivity range.

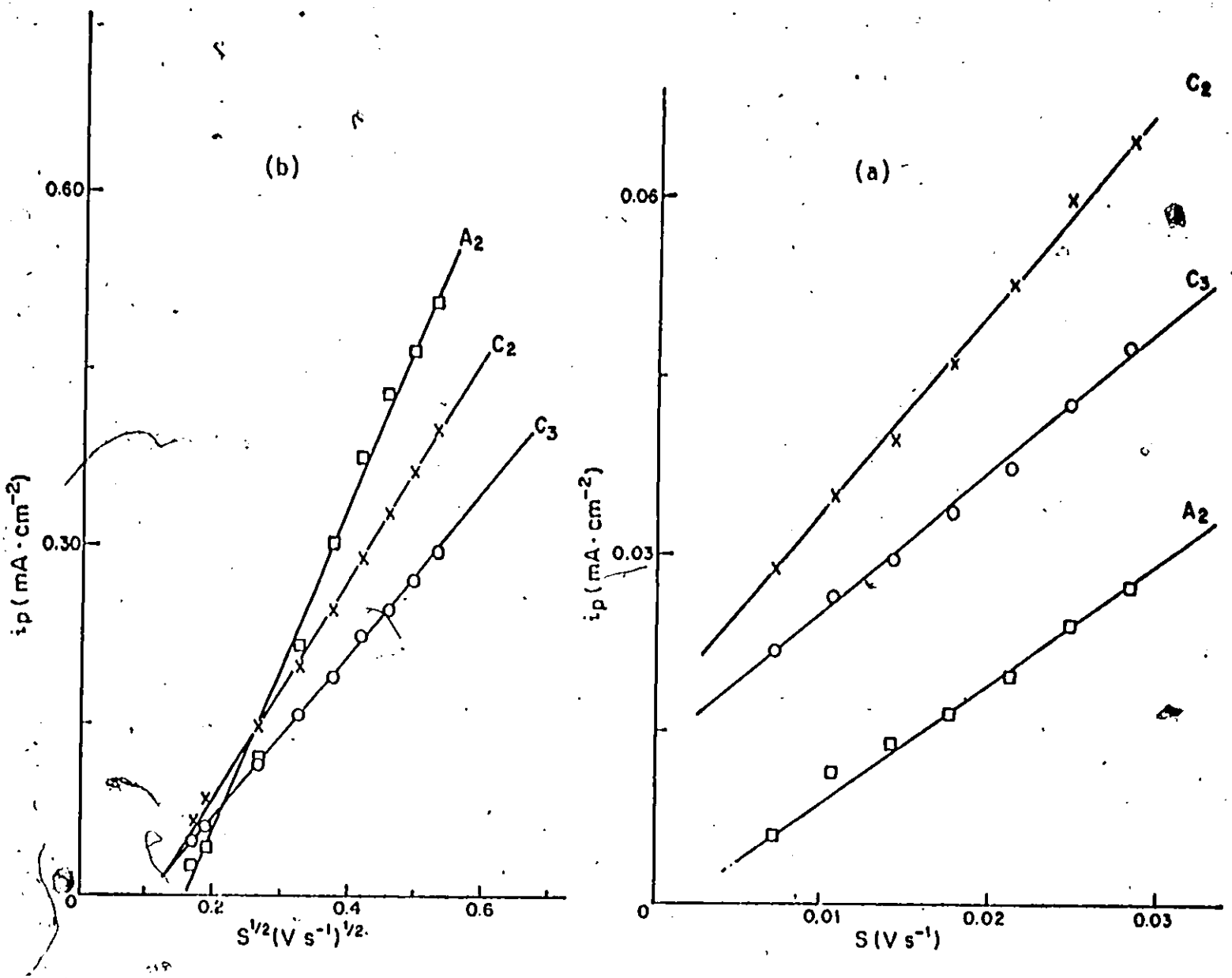

Fig. 3-29: i_p vs s (a) or $s^{\frac{1}{2}}$ (b) plots for cystine at Hg electrode in pH 1.33 aq solution.

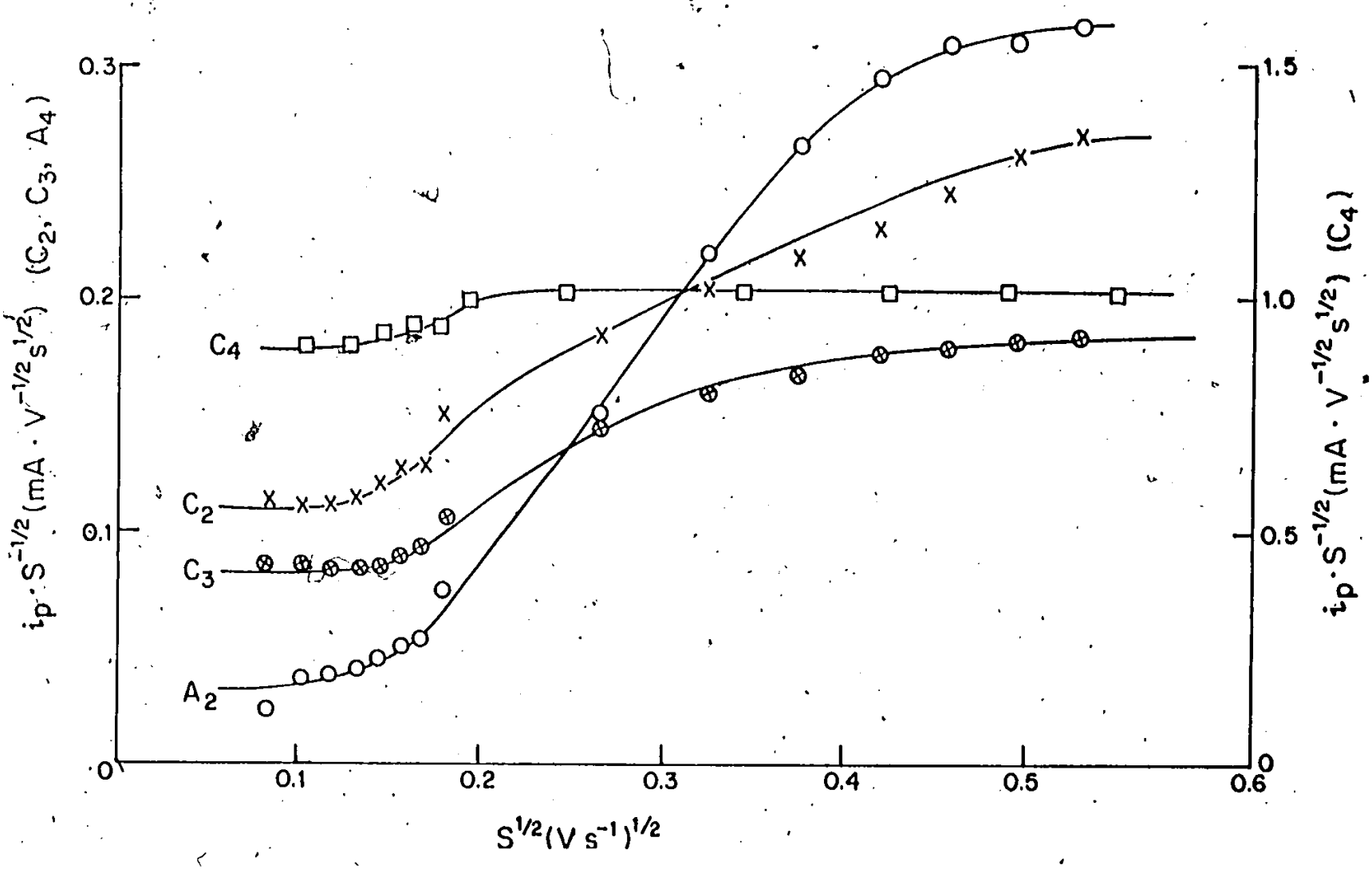

Fig. 3-30: $i_p/s^{\frac{1}{2}}$ vs $s^{\frac{1}{2}}$ for data of Fig. 3-26 and at 10x slower s.

3.6.3 Behavior at Alkaline pH 11

The cyclic-voltammograms for cystine at this pH are shown in Fig. 3.31 for various sweep-rates. At this pH, cystine is largely in the form of a singly charged anion. Again two principal cathodic peaks C_2 and C_3, are observed. The anodic one A_3, conjugate to C_3, is now better resolved than in acid. Also, as in acid solutions, there is some change of the i vs V profile with time of cycling during the initial stages of an experiment; in particular, peak C_3 is initially large and decreases with prolonged cycling. The Q_c/Q_a ratios are 0.78, which values are to be compared with those recorded for the acid solutions referred to in Section (3.6.2). The ratio of i_p values for C_2 and C_3 is also dependent on cycling history since the curves 1 and 9 in Fig. 3.31, taken at the beginning and end of the experiment on sweep-rate dependence, differ significantly but rather little.

The sweep-rate dependence of i_p values for C_2 and C_3 is similar to that in acid in so far as i_p is linear in s for low s but linear in $s^{\frac{1}{2}}$ (diffusion control) for higher s values (Fig. 3.32). The same considerations therefore apply here as were made for the behavior in acid solutions. It is also found that i_p values for A_3 and A_2 on the anodic sweep are linear in $s^{\frac{1}{2}}$ (data from Fig. 3.31).

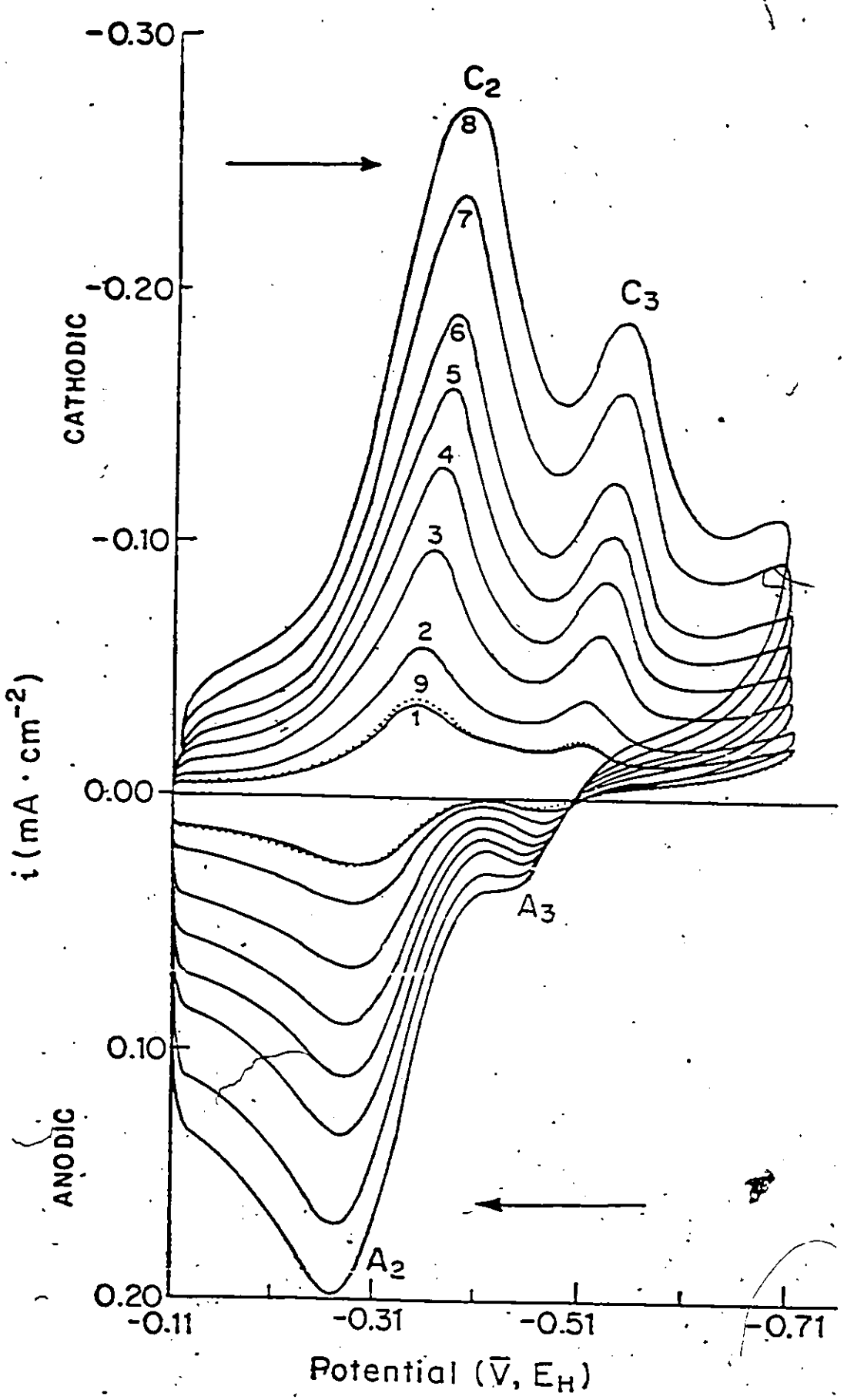

Fig. 3-31: Cyclic voltammetry of cystine at the Hg electrode at various sweep-rates in pH 11 aq solution.

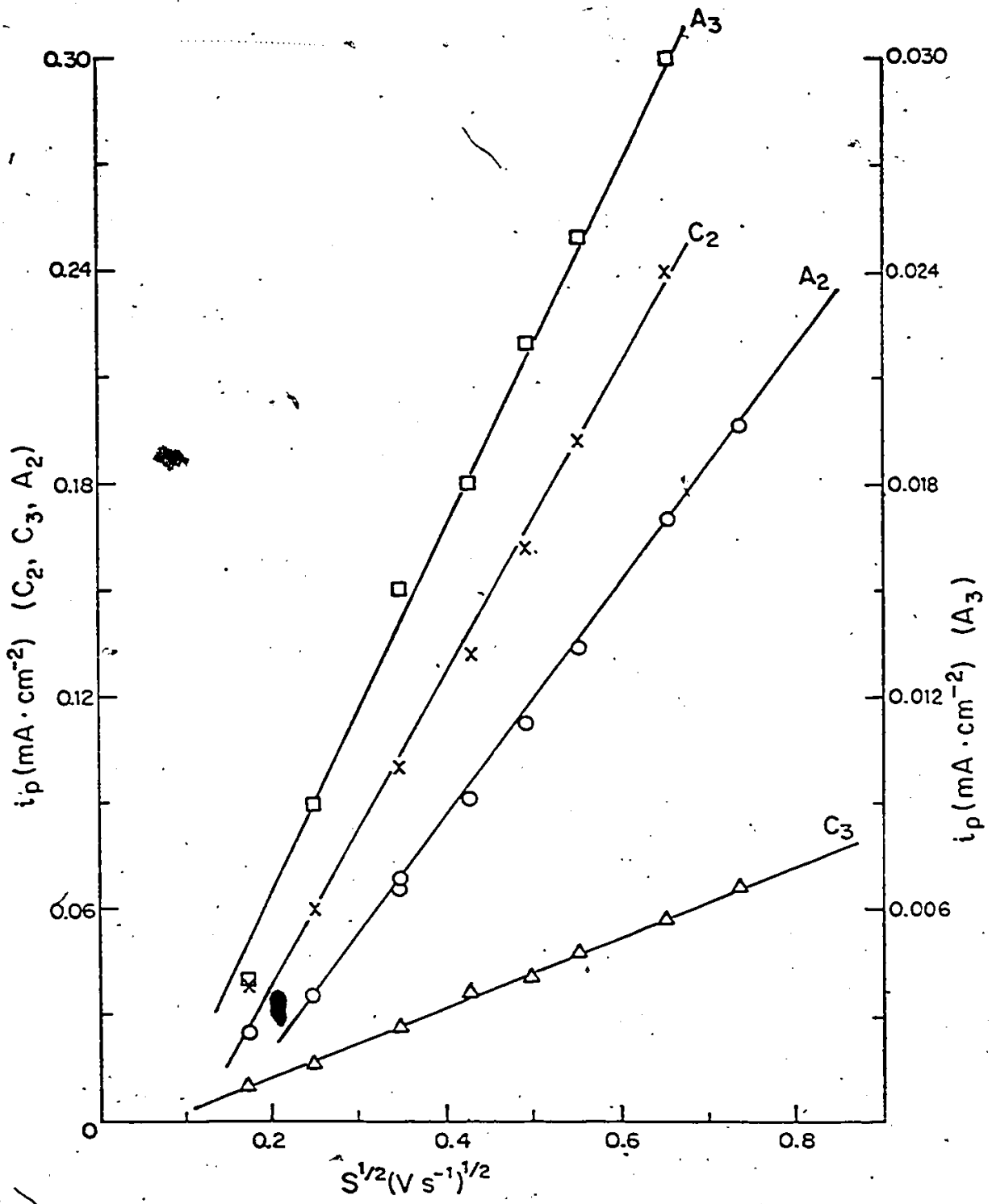

Fig. 3-32: i_p values for the cathodic and anodic peaks of Fig. 3-31 as a function of $S^{1/2}$.

3.6.4 Behavior at Neutral pH, 7.13

The cyclic-voltammetry behavior at neutral pH is shown in Figs. 3.33(a), (b) and (c). The i vs V profiles at various sweep-rates appear to differ substantially from those at acid or alkaline pH's, shown above, in that the region referred to as C_1 in Fig. 3.26 is now developed to a full peak at potentials less cathodic than for C_2 and C_3. There is a corresponding well developed reoxidation region A_1 on the anodic sweep, as is seen in Fig. 3.33(a). However, closer inspection of the behavior in acid solution shows that there is an appreciable current/charge component on the cathodic and anodic sweeps in the region designated as C_1 but no clear peak is developed. The complication here is that if the anodic limit of the sweep is taken any further positive, large anodic Faradaic currents pass, probably due to oxidation of Hg. In the alkaline solution at pH 11, the characteristics of peaks C_2 and C_3, as well as of A_2, are however, rather similar to the corresponding ones of the current peaks observed in acid solution (Figs. 3.26 and 3.33(a)). At low sweep-rates, the peak currents again follow an approximately linear relation with s while at 10x greater rates, the peak currents are neither linear with s nor s .

The ratios of cathodic and anodic charges are as shown in Fig. 3.34; again there is a disbalance of cathodic charge over anodic reoxidation charge with Q_c/Q_a approaching a ratio of 2.0 at the higher sweep-rates. This Q_c/Q_a ratio tends to become quite constant at the value 2.0 with increasing sweep-rate beyond 0.1 V s^{-1} up to the maximum value used, 0.9 V s^{-1}. In acid solution, on the other hand,

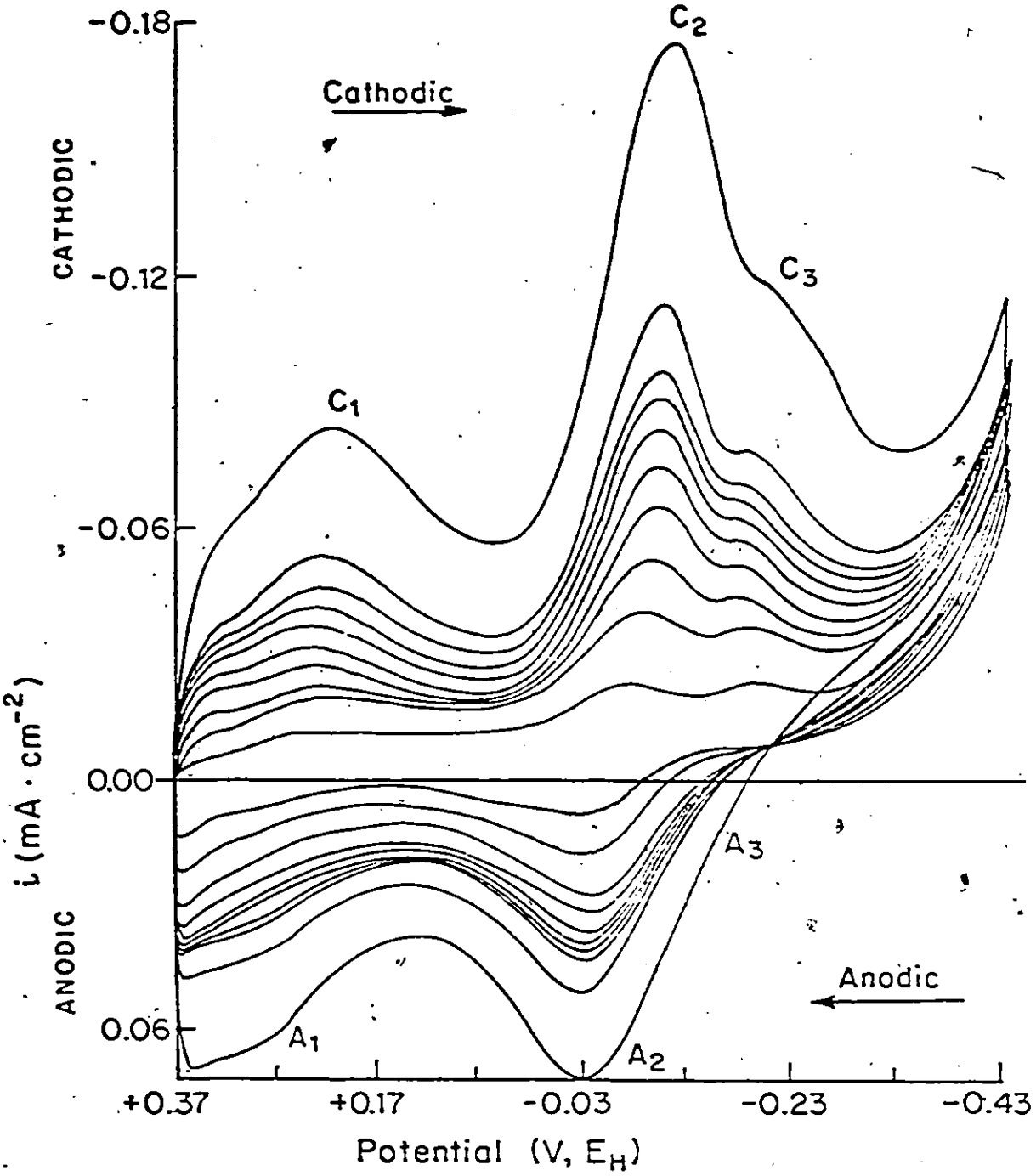

Fig. 3-33: (a) Cyclic voltammetry of cystine at the Hg electrode at various sweep-rates in pH 7.13 aq solution.

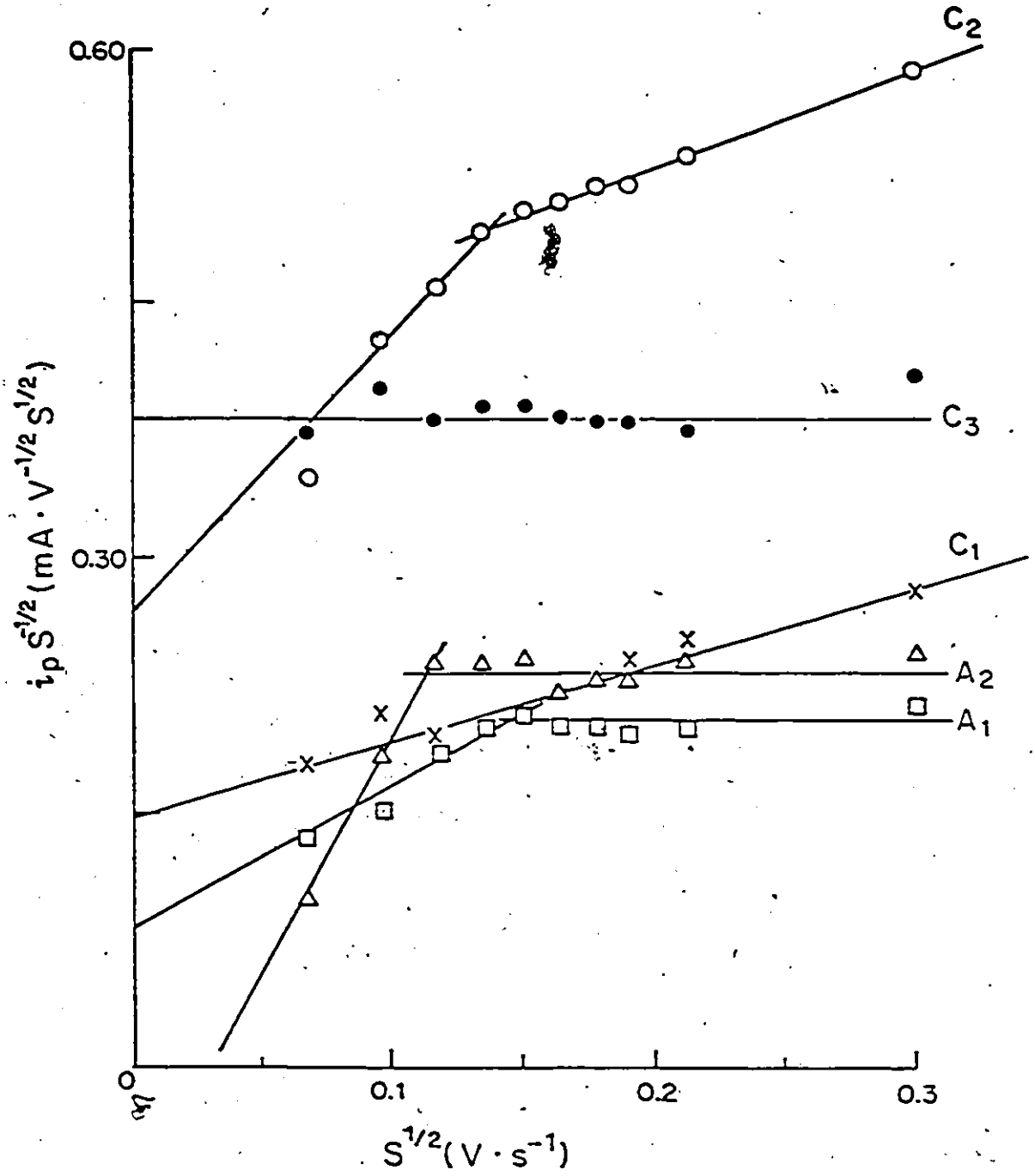

Fig. 3-33: (b) $i_p/s^{\frac{1}{2}}$ vs $s^{\frac{1}{2}}$ for data from (a).

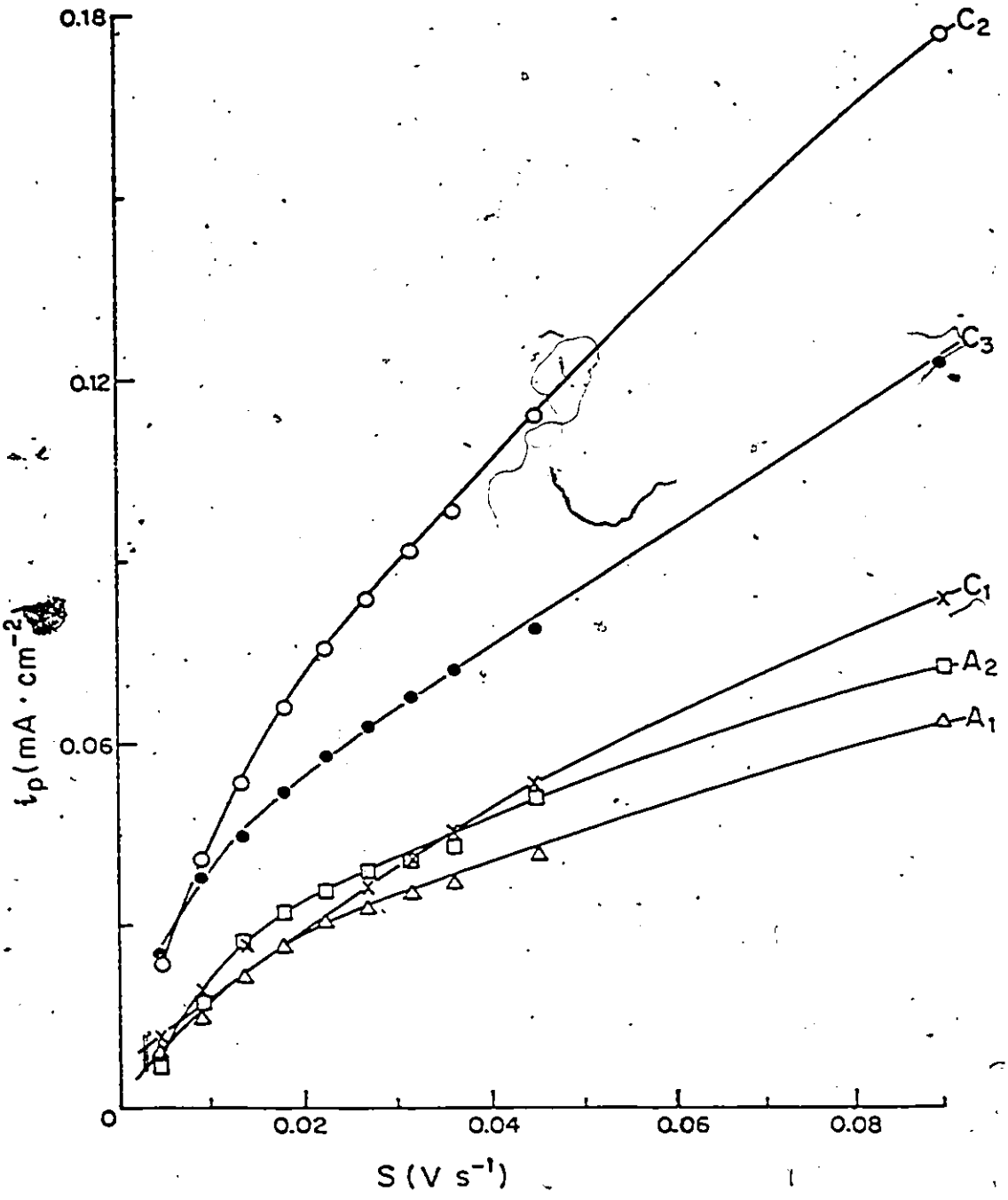

Fig. 3-33: (c) i_p vs s, for data from (a).

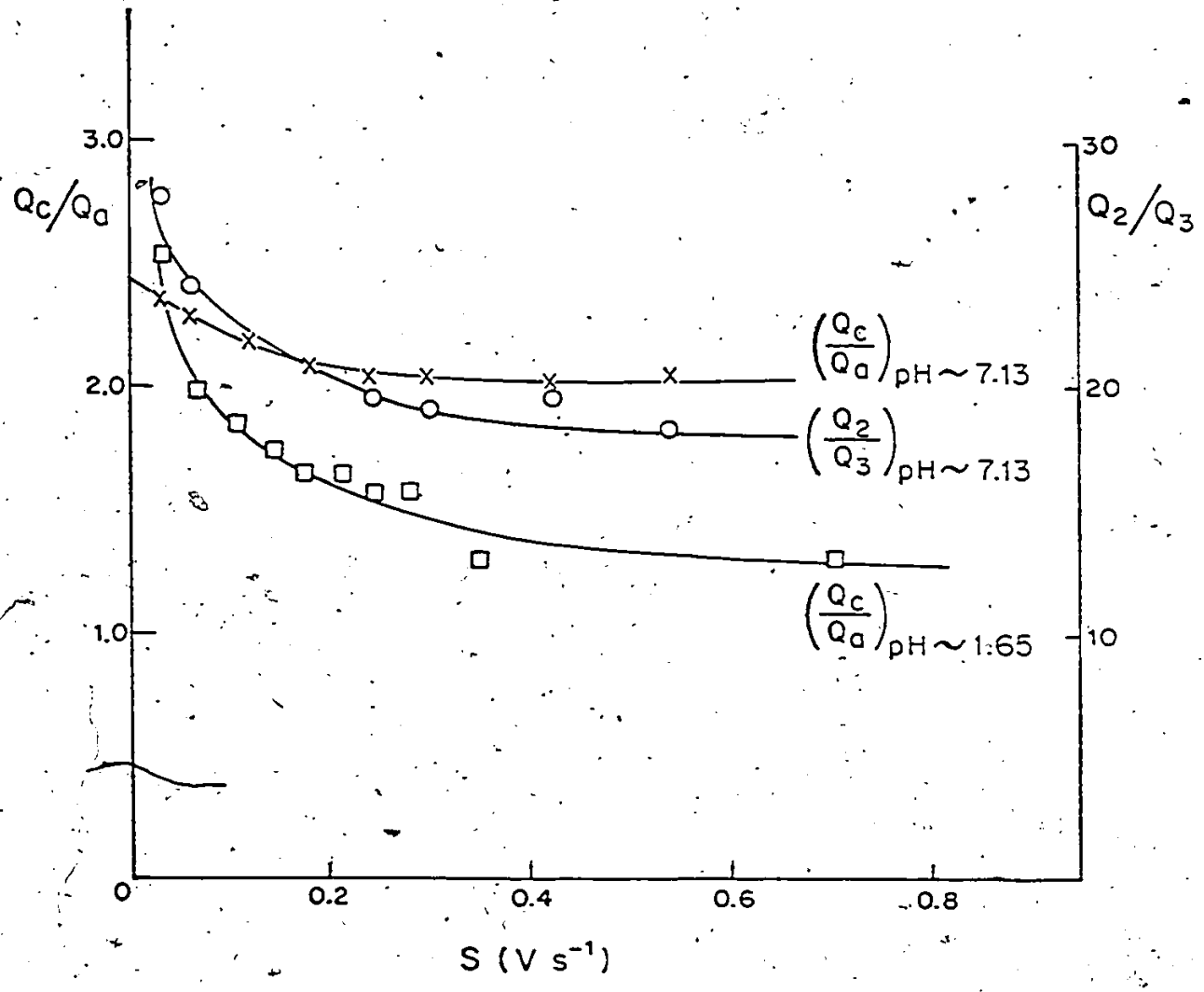

Fig. 3.34: Cathodic to anodic charge ratios, Q_c/Q_a, as a function of sweep-rate at Hg in aq solution of pH 1.33 and 7.13.

Q_c/Q_a, over a similar potential range, approaches a value of 1.3. This suggests or indicates that in alkaline solution the redox process is chemically less reversible and/or that a relatively greater fraction of the reduced species is irreversibly transported into the bulk solution. This difference of behavior may be connected with the changing state of ionization and resultant solvation of the product reduced species as pH is made more alkaline.

The Q_c/Q_a numbers obtained under various conditions are probably not to be interpreted in terms of any exact stoichiometric relation between charges for the reduction and reoxidation of the species in the reaction since diffusion processes are involved and the Q_c/Q_a ratios depend significantly on the sweep-rate and the diffusion conditions.

3.6.5 Concentration Dependence of Peak Currents in Acid Medium

A series of experiments was conducted at 7 concentrations of cystine at pH 1.65. The currents for peaks C_2 and A_2 are shown in Fig. 3.35(a) as a function of concentration for 10 values of s. For all values of s investigated, the i_p values tend toward a limit as the concentration is increased, except for the data at the highest concentration, 6.0 mM. The non-linearity of these plots shows clearly (cf. refs. 239,240) that the peak currents are not simply diffusion-controlled (with an apparent reaction order of unity) as was also the conclusion reached earlier in this section from the i_p vs s or $s^{\frac{1}{2}}$ plots. In fact, the initial approach to limiting values of i_p with increasing concentration suggests the role of approch to a saturation

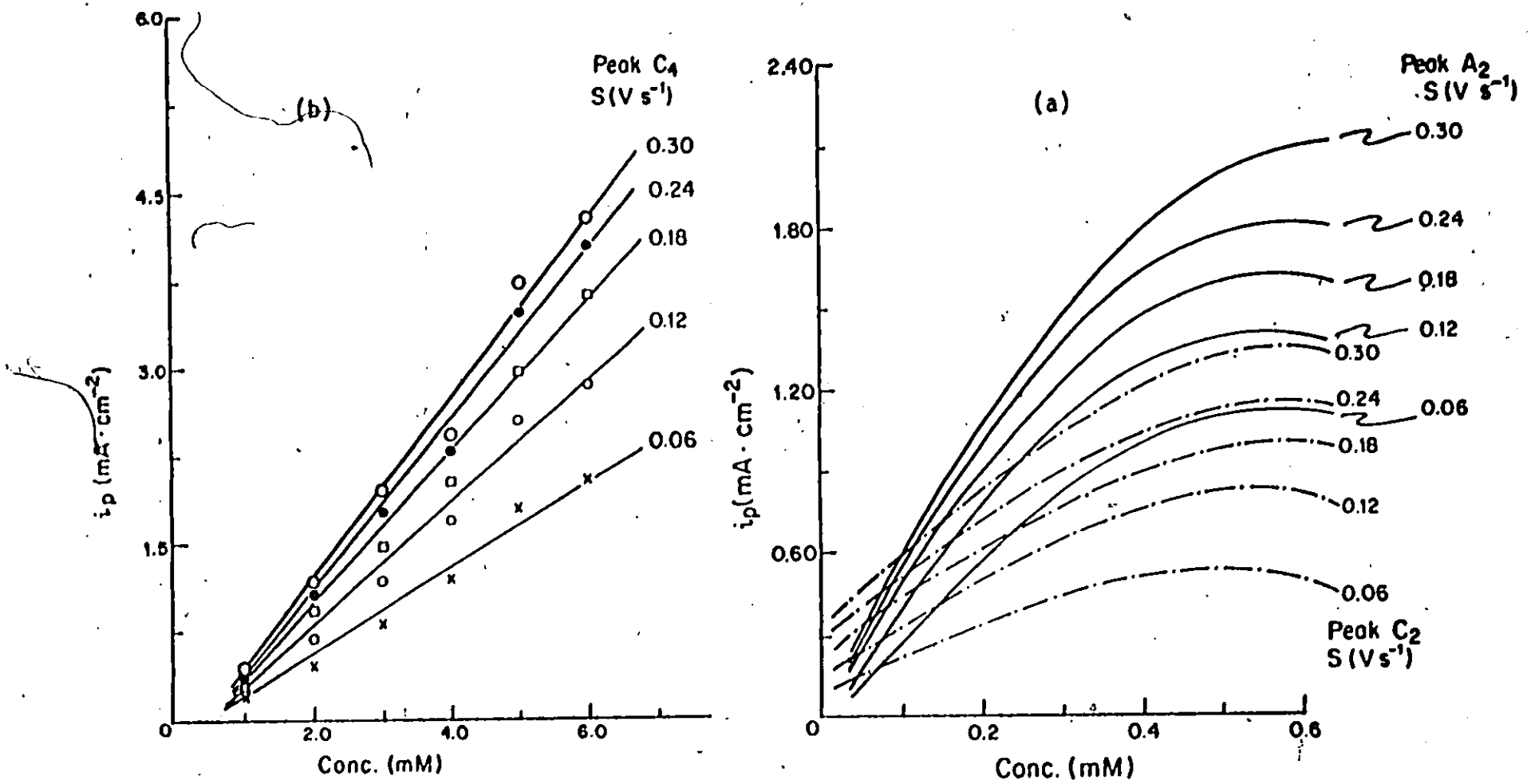

Fig. 3-35: (a) Peak currents for processes C_2 and A_2 in cyclic voltammetry of cystine at Hg in acidic pH 1.65 aq solution, as a function of concentration at various sweep-rates. (b) As in (a), but for the process labelled C_4 in the H_2 evolution.

condition of adsorption at the electrode surface. Possibly the further increase of i_p at the highest concentration is associated with multilayer formation (BET adsorption behavior). Similar curved plots are found for the currents of peak C_3 but that of C_4, in the H_2 evolution region (Fig 3.35(b)), is more linear in concentration over the whole range up to 6.0 mM. This is consistent with the observation that the peak currents in that region are linear with s over all of the s range (see Fig. 3.36), i.e. the process is "more completely" diffusion-controlled with the consequent apparent reaction order of 1.

3.6.6 pH Effect on Peak Potentials

The potentials, V_p, of the distinguishable cathodic and anodic peaks were measured and plotted as a function of pH as shown in Fig. 3.37. It is important to note that the peak potentials plotted are referred, as in the cyclic-voltammograms, to potentials of the H_2/H^+-H_2O electrode in the same solution as the working electrode and thus correspond to the same pH's. The observed slopes of V_p vs pH are 0.065 ± 0.003 V based on data for 3 pH's. The same slopes are found for each of the anodic and cathodic peaks, as follows from the lines drawn in Fig. 3.37.

From these results, it can be concluded that each of the current peaks corresponds to the same type of process as far as the stoichiometric requirements for electron and proton transfer are concerned. In particular, the overall reaction written vs the hydrogen-H^+/H_2O electrode process must involve one net proton transfer per e transferred. Thus it is clear that the potential-determining process (in the limit of reversibility) cannot be, for example,

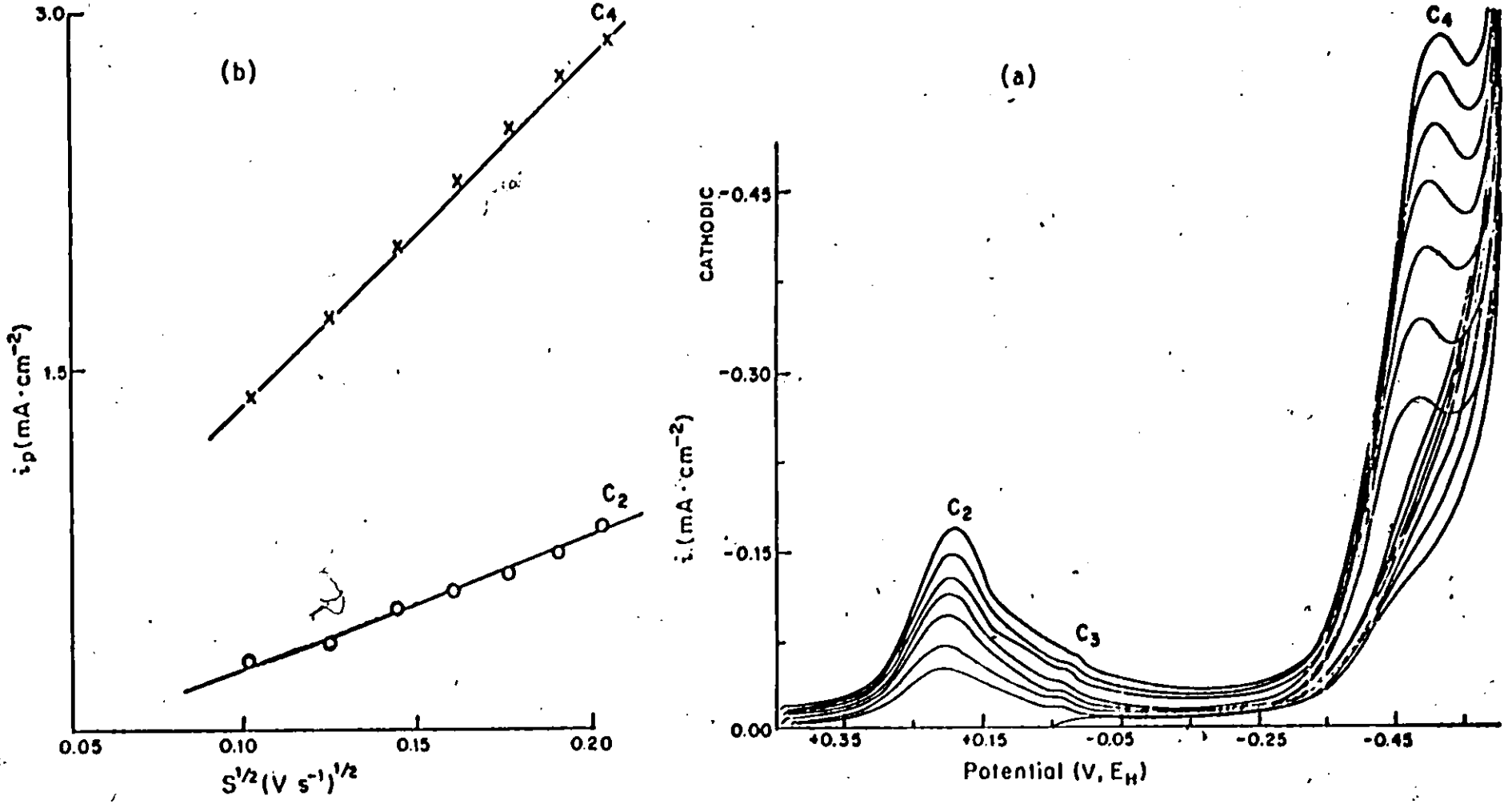

Fig. 3-36: Linearity of i_p with $s^{\frac{1}{2}}$ (b) for the C_4 process with cystine at Hg in pH 1.65 aq solution in H_2 evolution region (a).

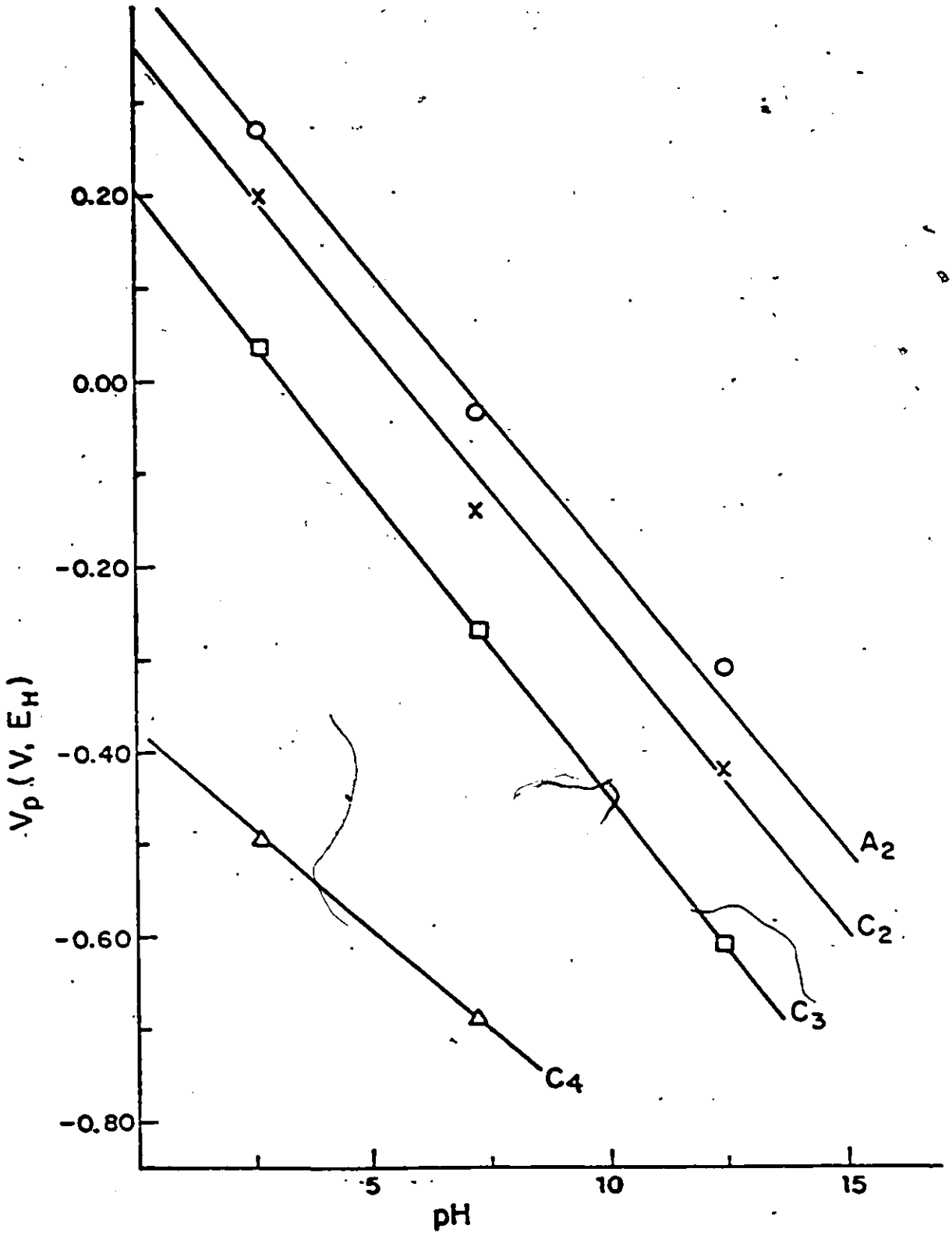

Fig. 3-37: Peaks potentials of cystine at Hg for processes A_2, C_2, C_3 and C_4 as a function of pH.

$$RSSR + 2\ H^+ + 2\ e \longrightarrow 2\ RSH$$

which would have a V_p value that was independent of pH when expressed vs the R.H.E. in the same solution.

A chemical reaction involving Hg (cf. refs. 140,142), followed by an electrochemical equilibrium, could be written formally as

$$RSSR + 2\ Hg \longrightarrow 2\ RSHg$$

$$RSHg + H^+ + e \longrightarrow RSH + Hg \text{ or } RSH(Hg)$$

but this also would lead to no pH effect on V_p expressed relative to the R.H.E. It is clear that any process that involves the same number of electrons and protons in the same elementary reaction will not give the observed behavior. A process such as

$$RSSR + 2\ e \longrightarrow 2\ RS^- \ (+ 2\ H^+ \rightleftharpoons 2\ RSH) \qquad (5)$$

is required. This will lead to a pH dependence of V_p of 0.059 V according to the overall stoichiometric 2e reaction.

$$RSSR + H_2 \rightleftharpoons 2\ RS^- + 2\ H^+ \qquad (6)$$

Similar steps in which the RSSR or RS^- species are complexed with Hg will lead to the same pH dependence as required experimentally.

It must be noted that in the case of cystine or cysteine, two or one ionizable -COOH groups exist in the molecules, respectively, complicating the balance of charge. However, these -COOH groups do not participate directly in the redox process and, at a given acid pH, will remain almost in the same state of ionization before and after

the redox reaction has taken place. However, when cystine in the partially doubly ionized state (pH 11) is reduced to a "monomeric" thiol, the inductive effect between the two $-COO^-$ groups which makes the 1st and 2nd pK_a's of the -COOH groups (which normally differ by ca. 4 units) is lost, each then retaining a pK_a of ca. 4.5. Thus, at pH less than but near 11, we can have the situation

$$2\ ^-OOCR'SSR'COOH + 2\ e \longrightarrow 2\ ^-OOCR'S^- + H^+ \qquad (7)$$

(cf. eqn. 5). Combined with the 2e, $2H^+$, the H_2 electrode reaction, process (7) corresponds to

$$^-OOCR'SSR'COOH + H_2 \longrightarrow 2\ ^-OOCR'S^- + 3\ H^+$$

This would give rise to an unusual pH effect on V_p of (3/2) x 0.059 V, = 0.089 V, a value not observed. Processes (5), (6) are the basis of a preferred explanation of the experimental behavior. Of course, in acid solutions below pH 8, the $-NH_2$ groups of cysteine or cystine become ionized as cation centres involving one or two other proton transfer equilibria while zwitterion states can exist between the $-COO^-$ and $-NH_3^+$ groups on the same C atoms, depending on pH.

The four pK_a's, of cystine and the two of cysteine are recorded in Buckingham's Dictionary of Organic Compounds, together with the pK_a of the -SH group in cysteine (see also ref. 142).

3.7 CYSTEINE: CYCLIC-VOLTAMMETRY BEHAVIOR

3.7.1 General

The electrochemical behavior of cysteine ("RSH") was examined comparatively to that of cystine, reported above, using a similar program of experiments at pH 1.21, 7.1, 11.3 and 13.2. In this case, of course, the oxidation and re-reduction had to be examined by commencing sweeps from an appropriate negative potential but going initially in the positive direction in the first sweep. As before, the cyclic behavior was examined as a function of sweep-rate, pH and concentration.

3.7.2 Behavior at pH 11.3

First will be shown the behavior at pH 11.3 as this is the simplest (Fig. 3.38(a)): apart from a small secondary current component on the cathodic re-reduction side, the whole shape of the anodic/cathodic i vs V profiles is similar to that expected for an irreversible, pure diffusion-controlled process; the peak currents are clearly linear in $s^{\frac{1}{2}}$ as in Fig. 3.38(b) and the anodic/cathodic peak potential separation increases with s. However, the cathodic peak currents are some 20% greater than corresponding anodic ones, for a given sweep-rate.

3.7.3 Behavior at Acidic pH 1.21

At pH 1.21, in dilute solution (0.5 mM), the profiles are again reasonably simple (Fig. 3.39(a)) but with two current components on each side that are linear over some range of s, either in $s^{\frac{1}{2}}$ or s. This is shown by testing the results with the combined plotting function referred to in an earlier section:

$$ip/s^{\frac{1}{2}} = k_1 s^{\frac{1}{2}} + k_2$$

A two-slope graph results for both the main anodic and cathodic peak currents (Fig. 3.39(b)).

At higher concentrations up to 12.5 mM, and already at 2.5 mM (see Fig. 3.40), the profile becomes complicated by a cathodic current component on the anodic sweep and an anodic component on the cathodic sweep. On the anodic sweeps beyond the main current maxima, a sharp shoulder is observed with rapidly decreasing currents. On the following re-reduction sweep, anodic current maxima precede the main cathodic peaks. It seems that the continuing oxidation of RSH on the anodic sweep is inhibited at some critical potential, ca. 120 mV positive of the main maxima, but this inhibition is relieved on the following cathodic sweeps so that current for continuation of an irreversible oxidation of RSH passes on the cathodic sweep over a short range of potentials before the expected (cf. Fig. 3.38(a)) rise of cathodic current in the main peak. The charge balance between the main anodic/cathodic processes is near 1 for the curves of Fig. 3.40. The anomalous behavior shown in this Figure is found to be enhanced at higher concentrations, 4.5, 6.5, 8.5, 10.5 and 12.5 mM, and the sudden

inhibition effect on the anodic sweeps is more pronounced. At the higher concentrations, the i vs V profiles look less and less like those expected for pure diffusion control, though peak currents are still well represented by linear $s^{\frac{1}{2}}$ plots.

3.7.4 Behavior at Neutral pH 7.1

The behavior at pH 7.1 is the most complex and unusual, as shown in Fig. 3.41. Here the "RSH" molecule is mainly in the form of a zwitterion. The first anodic peak is followed by a continuously increasing anodic current with no return to the zero-current line over accessible ranges of potential. The reduction profiles show two or three peaks of comparable current magnitude. Both anodic and cathodic peak currents are again well represented by linear plots in $s^{\frac{1}{2}}$, based on 10 s values, but the overall form of the i vs V profile is clearly not that for a simple diffusion-controlled process.

3.7.5 Concentration Effects

For cysteine oxidation at Hg, the main peak currents at various sweep-rates are almost linear in concentration (Fig. 3.42(a)), as required for a diffusion-controlled process. However, the corresponding re-reduction peak currents are clearly not linear in concentration (Fig. 3.42(b)), indicating the participation of a surface process and/or coupled chemical steps following the initial oxidation process.

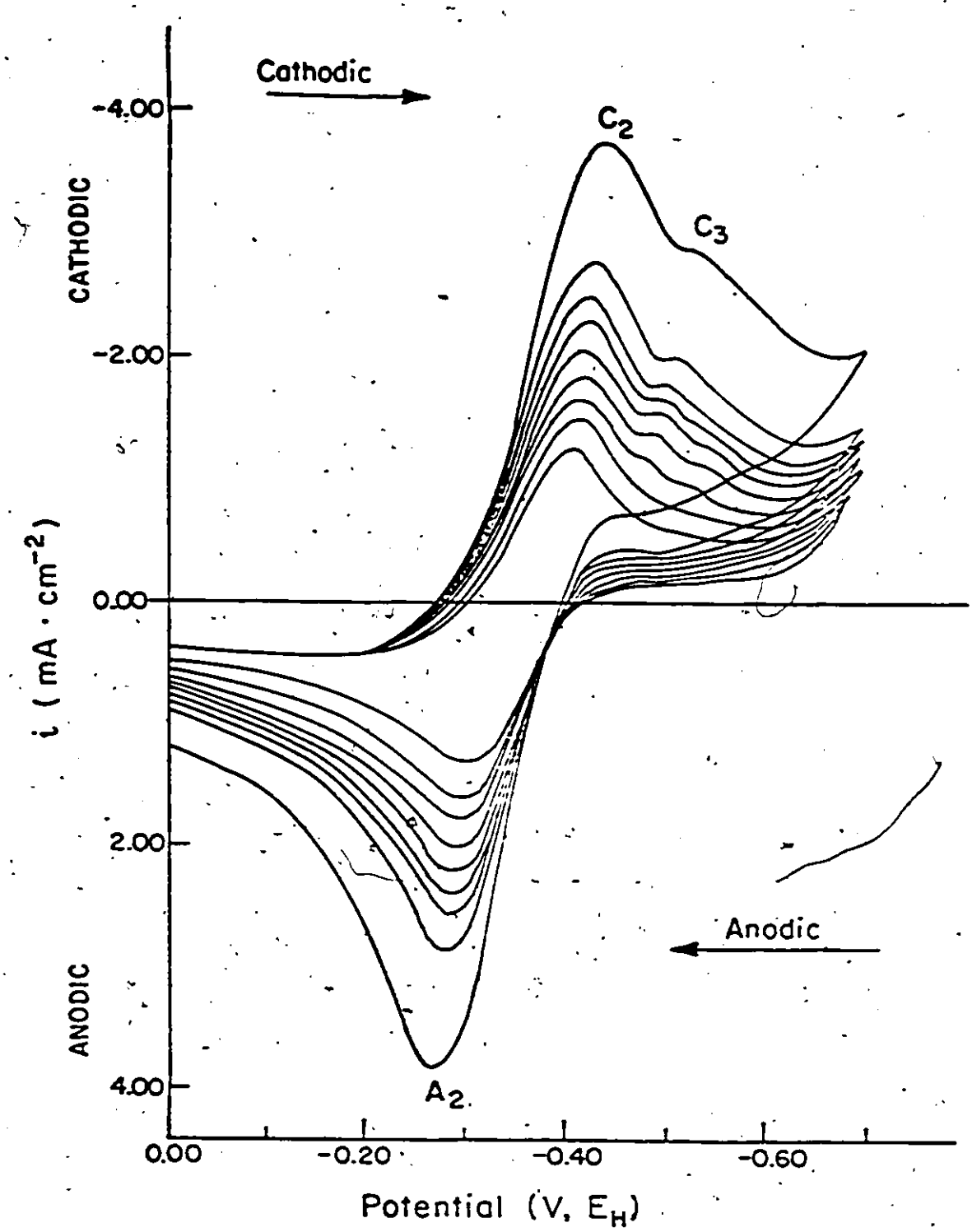

Fig. 3-38: (a) Cyclic voltammetry of cysteine at the Hg electrode at various sweep-rates, in pH 11.3 aq solution.

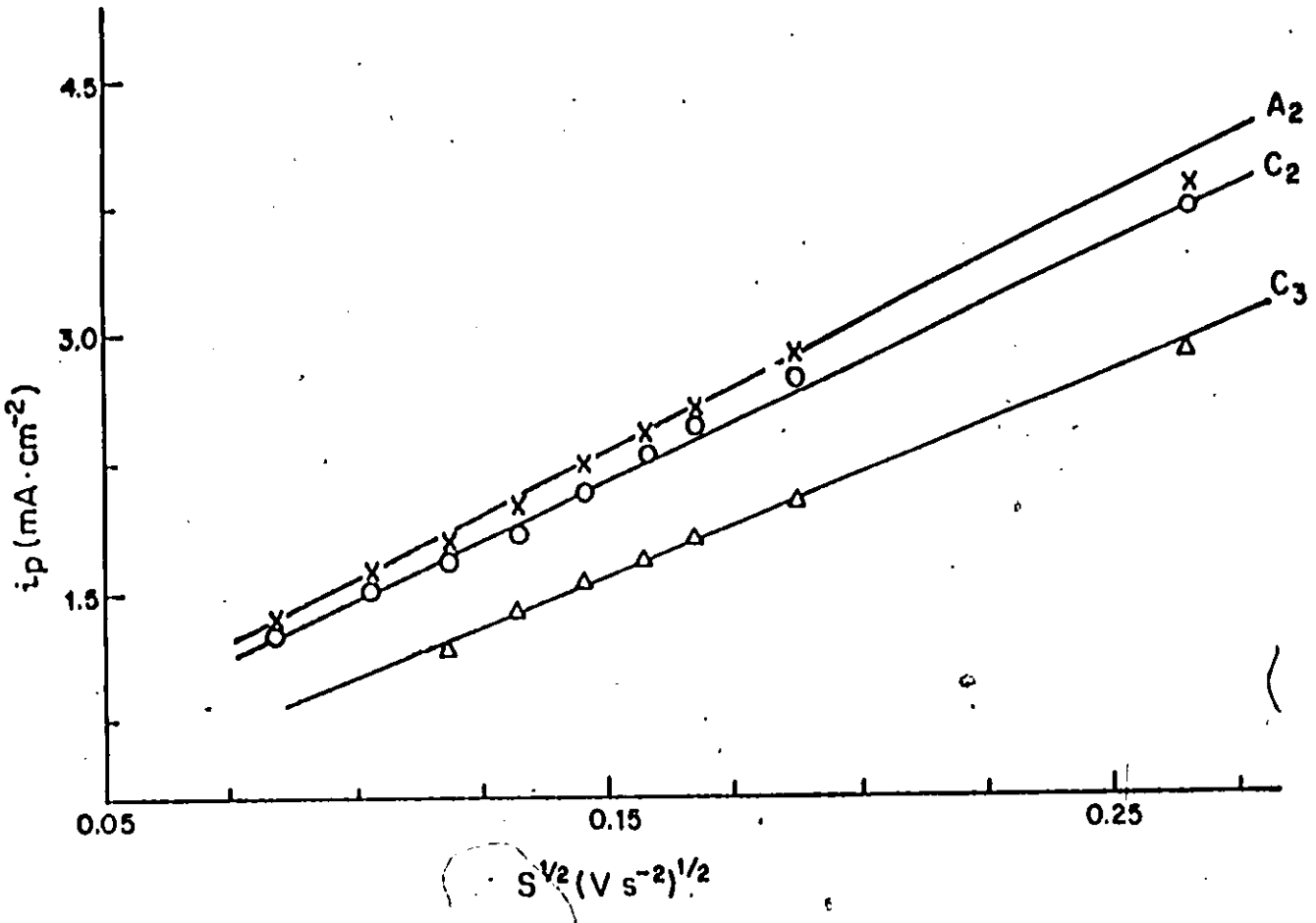

Fig. 3-38: (b) i_p vs $s^{\frac{1}{2}}$ for data from (a).

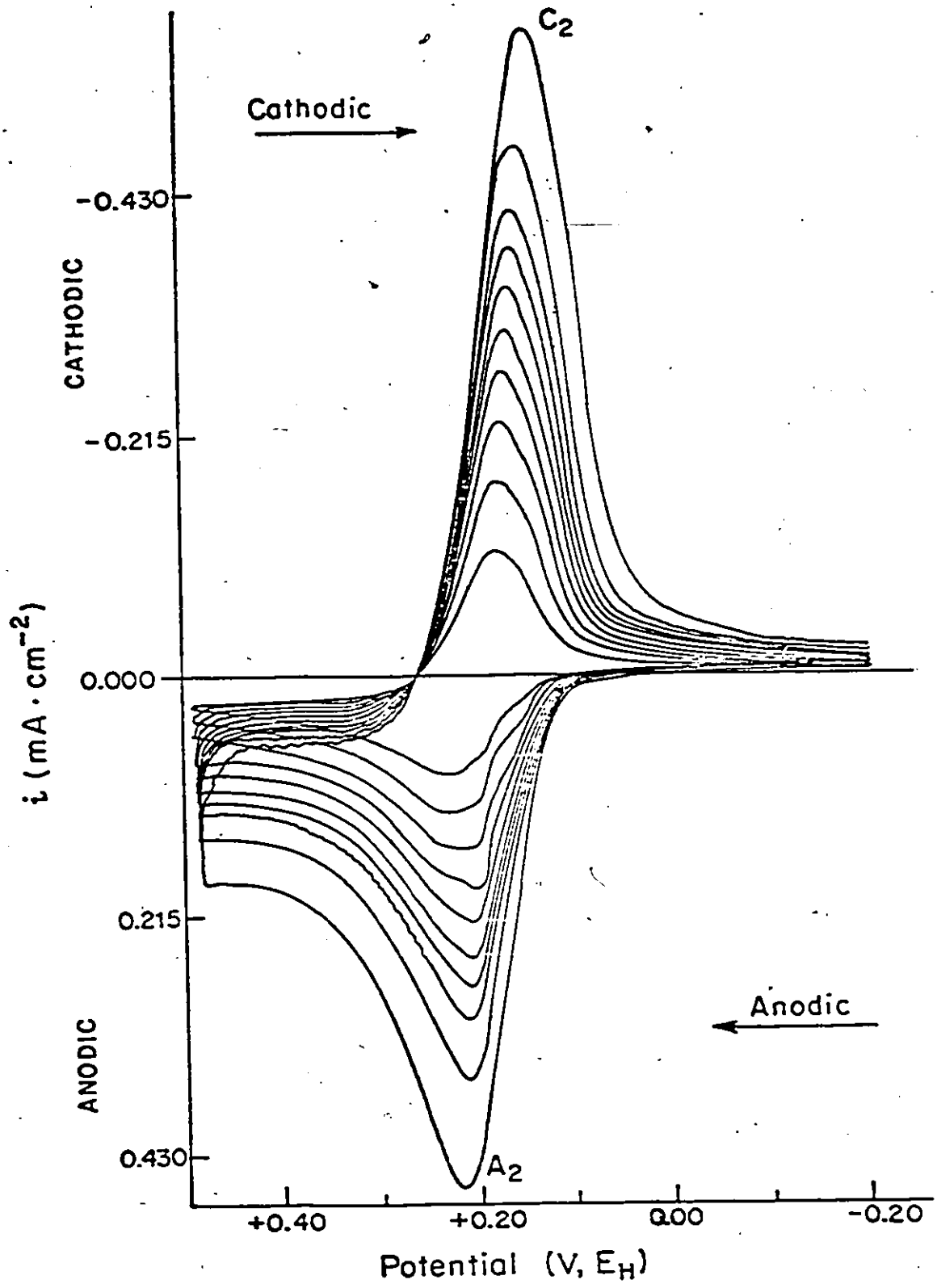

Fig. 3-39: (a) Cyclic voltammetry of 0.5 mM cysteine at the Hg electrode at various sweep-rates in pH 1.21 aq solution.

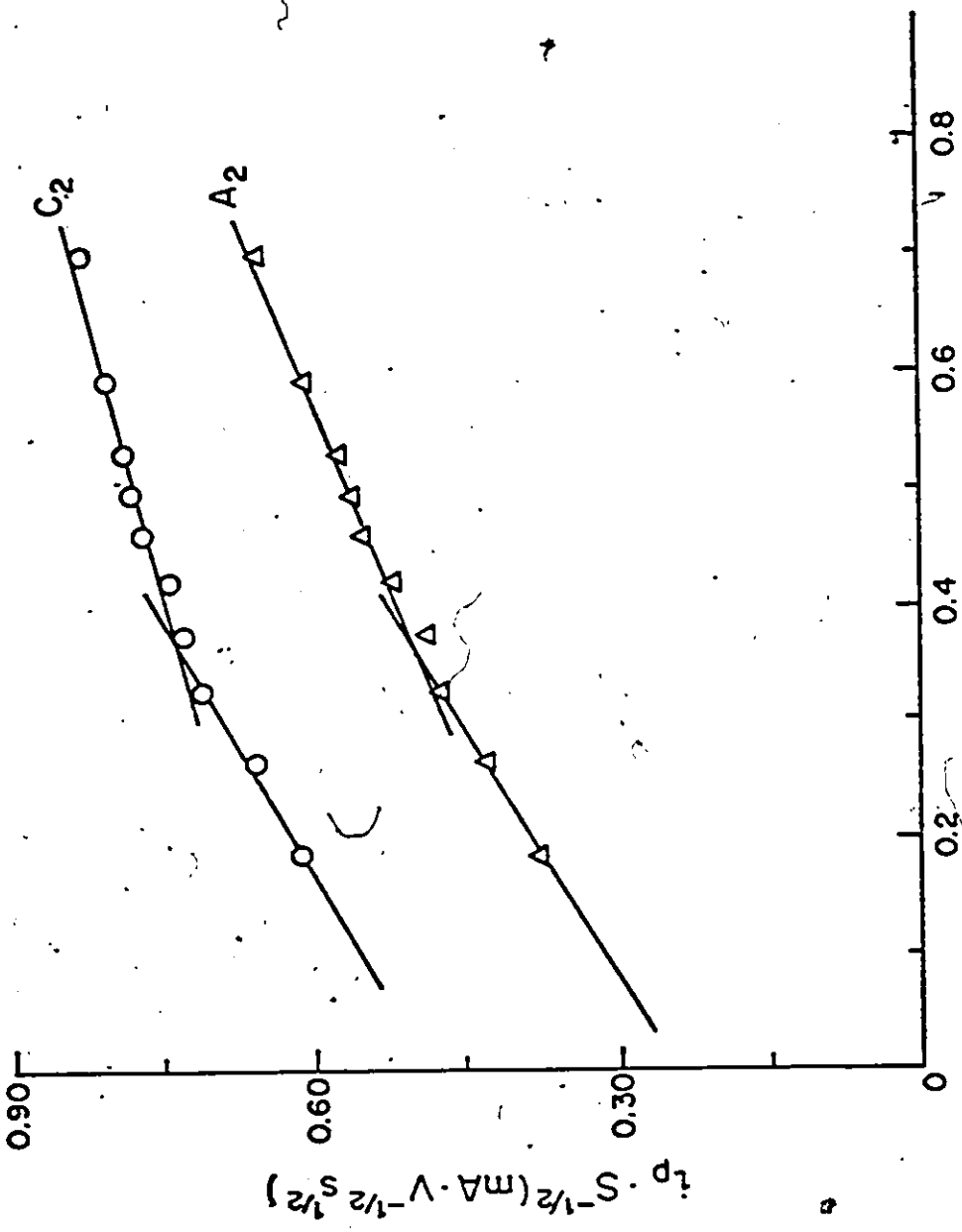

Fig. 3-39: (b) $i_p/s^{\frac{1}{2}}$ vs $s^{\frac{1}{2}}$ for data from (a).

3.8 REACTIVITY OF α-LIPOIC ACID AT Hg

3.8.1 General

The reactivity of α-lipoic acid at Hg was compared with that of cystine and cysteine reported above. The pH's of the solutions were 1.21, 11 and 13. Since this molecule has an ω-COOH group unconjugated with any other functions, it has a normal pK_a so that the molecule is uncharged at pH 1.21 and fully ionized as an anion at the high pH's.

3.8.2 Behavior at pH 1.21

Figs. 3.43(a), (b) and (c) show families of cyclic-voltammetry i vs V profiles at various sweep-rates. Two peaks are evident on both the cathodic and anodic curves, but the relative heights are quite dependent on concentration (compare curves in Fig. 3.43(a) with those in 3.41(b)). The cathodic curves for 0.1 mM branch successively from an almost common ascending current line and similar behavior is seen on both the anodic and cathodic curves at higher concentrations (Fig. 3.43(b) and (c)).

The relation of the cathodic to the anodic curves is interesting in relation to concentration: the charges, Q_c, rise in proportion to concentration (Fig. 3.44) which would be consistent with diffusion control but the Q_a values reach a clear limit of ca. 180 $\mu C\ cm^{-2}$ with increasing concentration above 0.5 mM. This suggests that the anodic curves correspond to reoxidation of an adsorbed complex or surface compound at monolayer saturation (the 180 $\mu C\ cm^{-2}$ is near the charge figure for a 1e process in a monolayer) or that reoxidation is from a

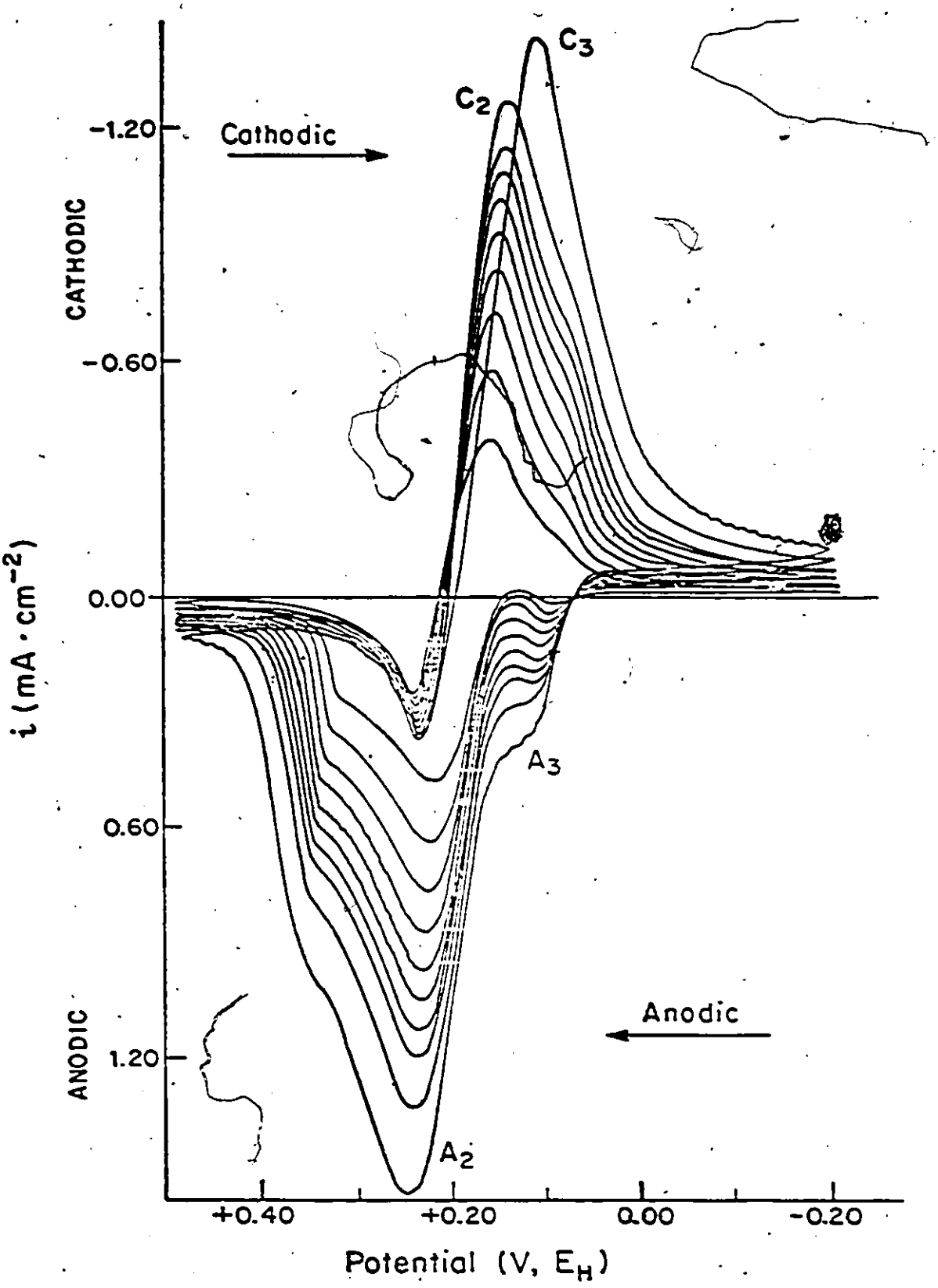

Fig. 3-40: Cyclic voltammetry of 2.5 mM cysteine at Hg electrode at various sweep-rates in pH 1.21 aq solution.

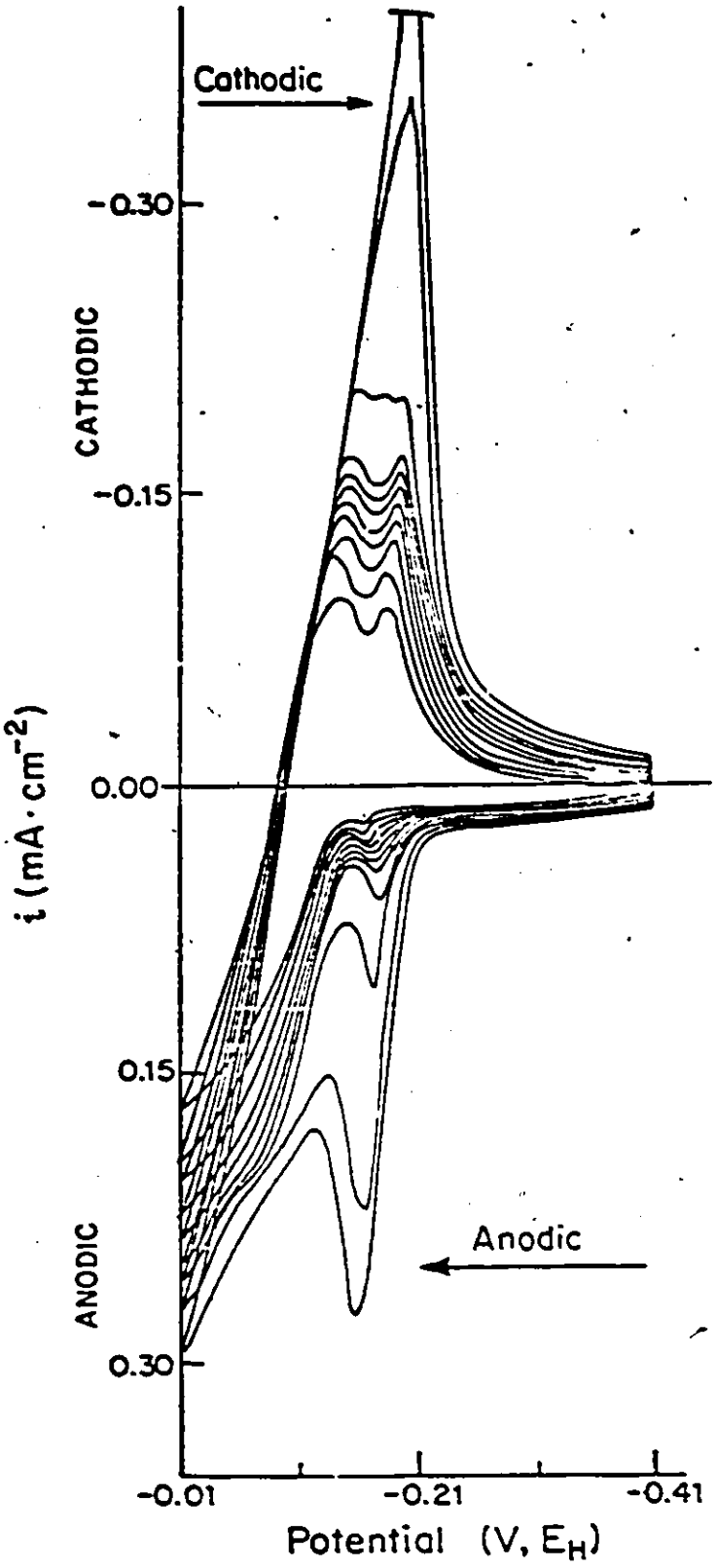

Fig. 3-41: Cyclic voltammetry of 1.2 mM cysteine at Hg electrode in pH 7.10 aq solution.

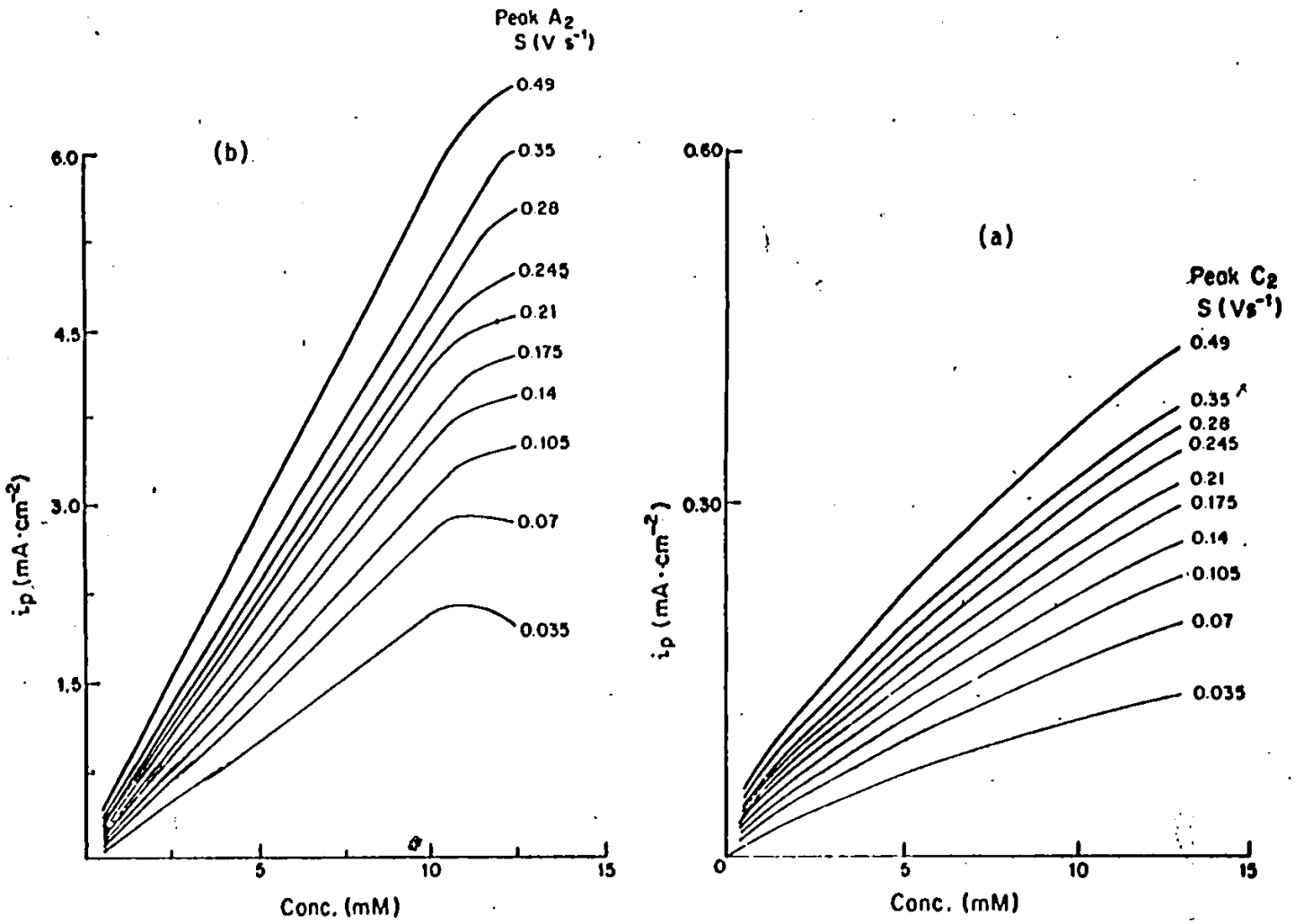

Fig. 3-42: (a) Peak currents for process C_2 in cyclic voltammetry of cysteine at Hg in acidic pH 1.21 aq solution as a function of concentration at various sweep-rates. (b) As in (a) but for A_2 Process.

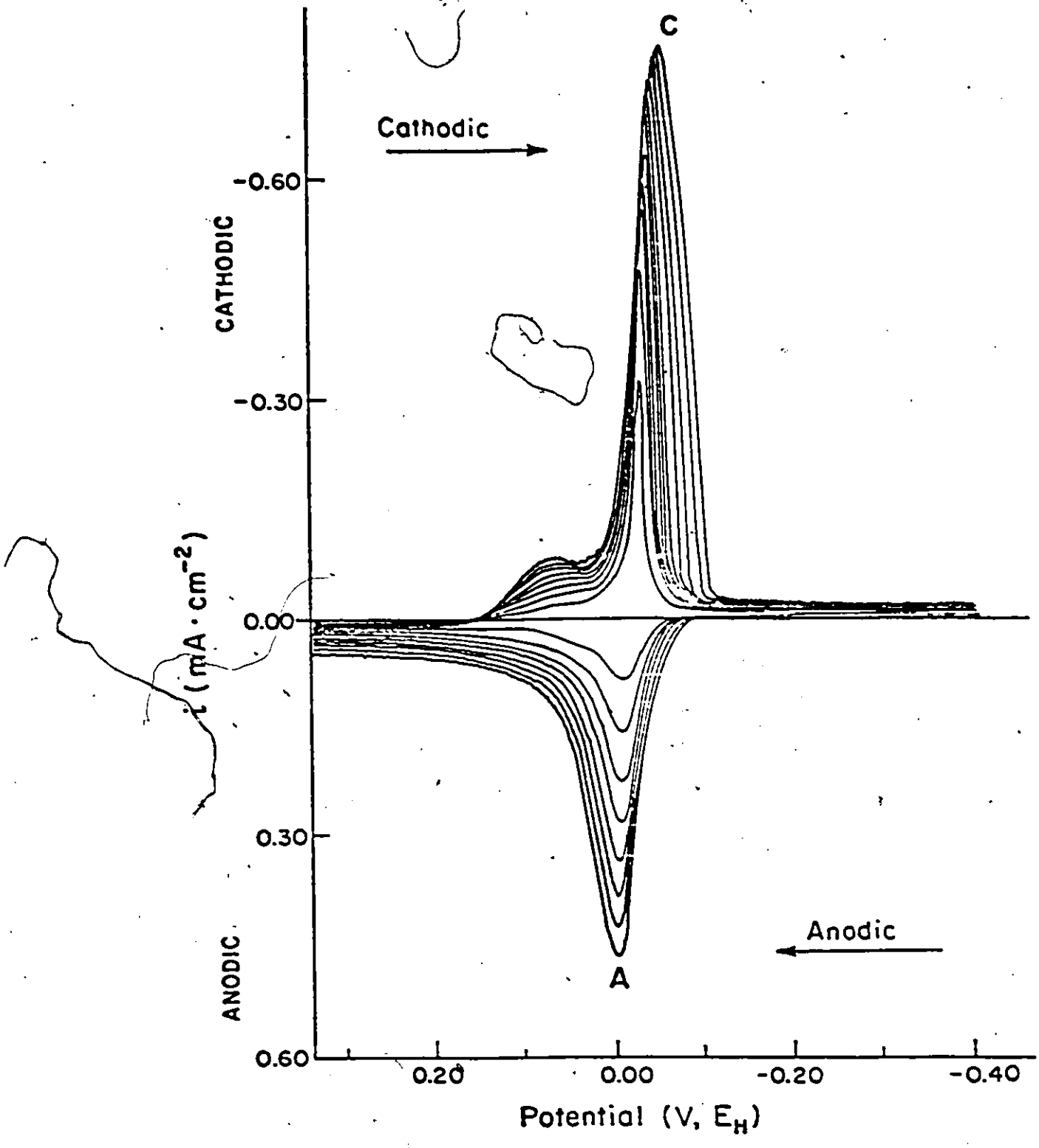

Fig. 3-43: (a) Cyclic voltammetry of 0.1 mM α-lipoic acid at the Hg electrode in pH 1.21 aq solution.

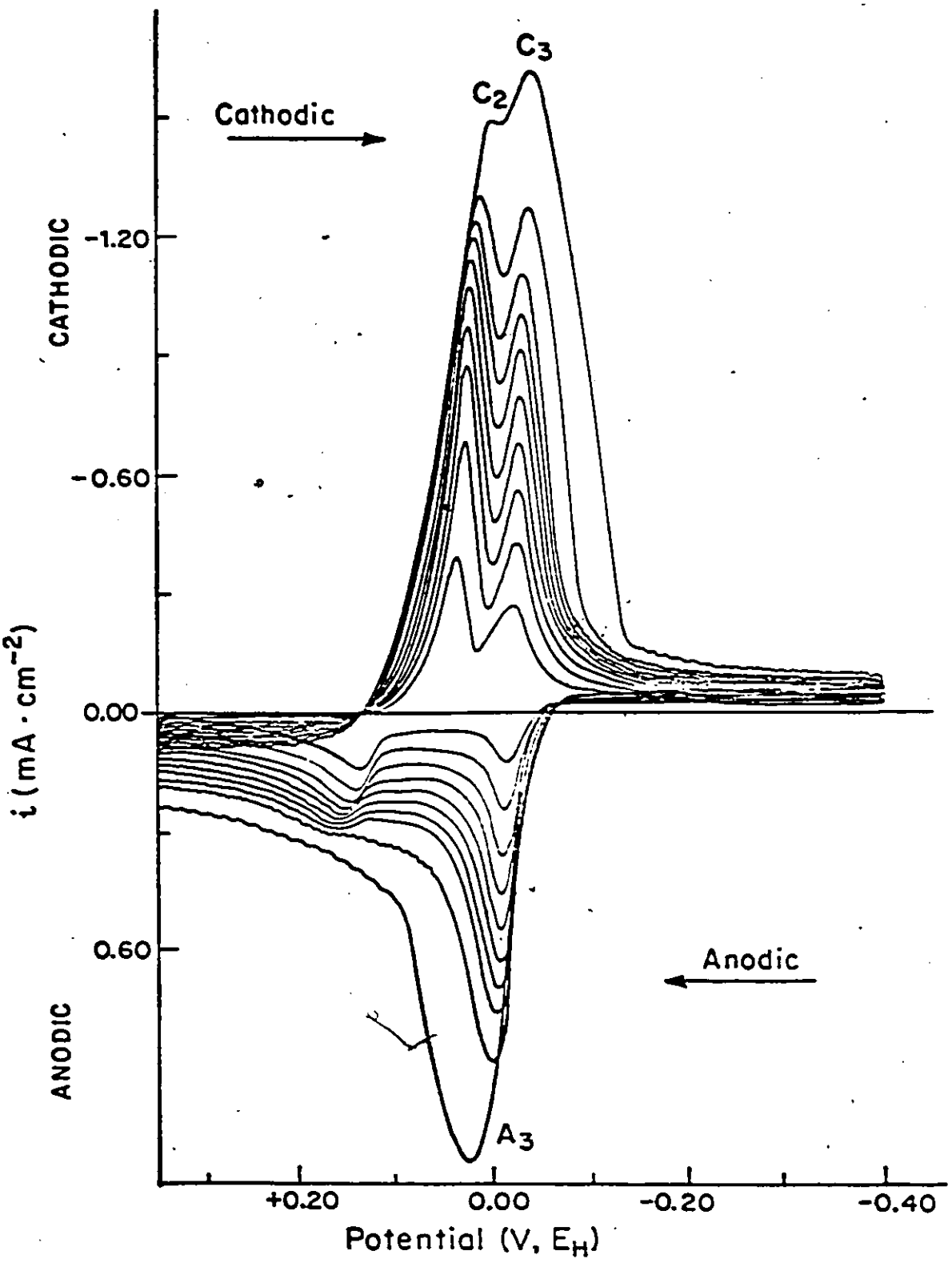

Fig. 3-43: (b) Cyclic voltammetry of 0.5 mM α-lipoic acid at the Hg electrode in pH 1.21 aq solution.

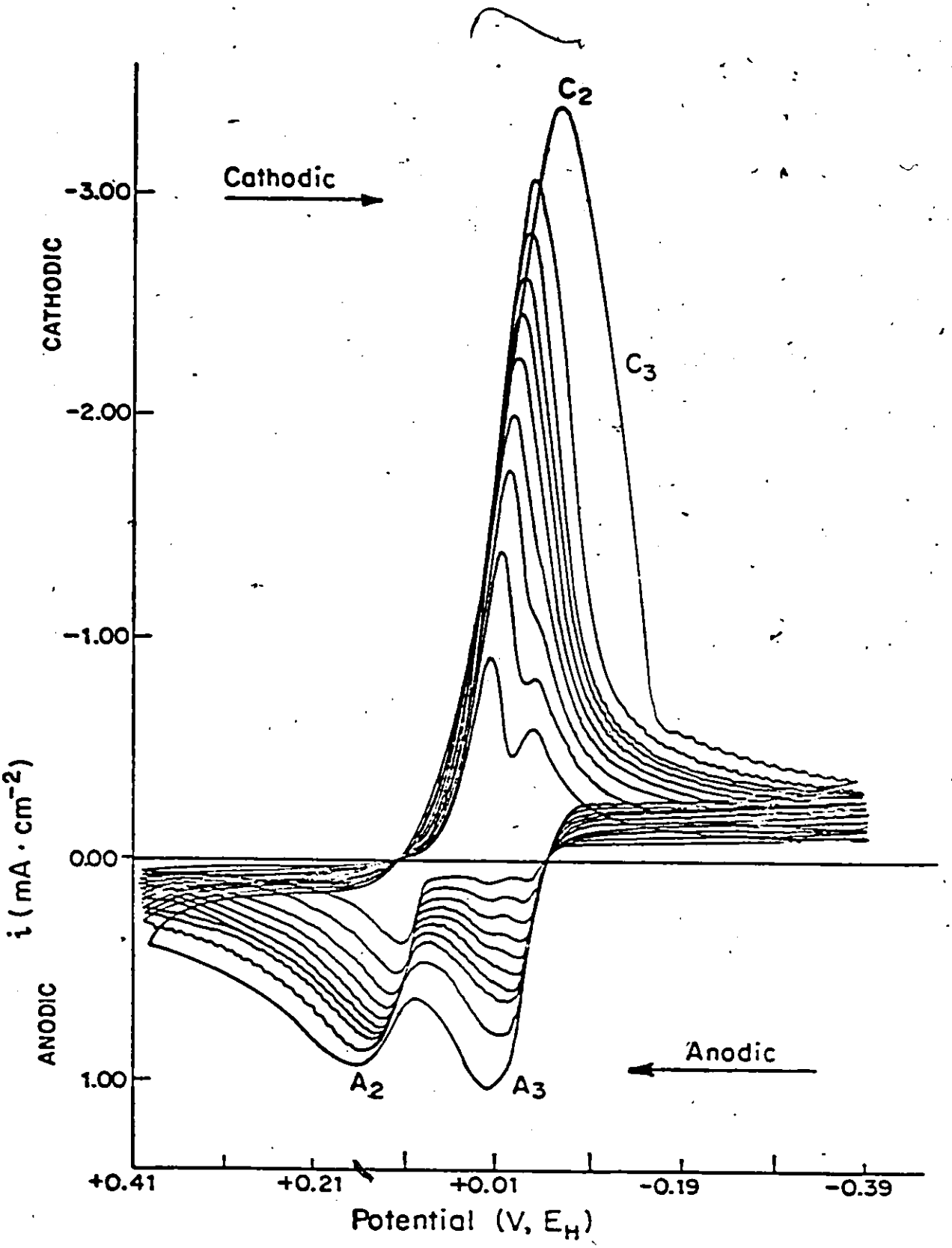

Fig. 3-43: (c) Cyclic voltammetry of 1.5 mM α-lipoic acid at the Hg electrode in pH 1.21 aq solution.

dissolved Hg-complex formed in the cathodic sweep but at saturation solubility in the solution. The latter alternative is consistent with the observation (Fig. 3.45) that the anodic peak currents are, over all of the range of s, linear in $s^{\frac{1}{2}}$. However, the cathodic peak currents reach a plateau limit at high s after increasing with $s^{\frac{1}{2}}$. This is because the curves spread out, rather than increase in height with $s^{\frac{1}{2}}$, as s becomes larger. This is again not consistent with simple diffusion control.

At higher concentration, (Fig. 3.43(b) and (c)) the shapes of the double-peaked curves do not resemble those for either an irreversible or a reversible diffusion-controlled process although, again, currents are more linear in $s^{\frac{1}{2}}$ than in s. Both anodic reoxidation profiles at the higher concentrations break away from common ascending current lines which is a phenomenon not associated with currents arising in a pure diffusion process. The contrast with the anodic profiles for the most dilute solution (0.1 mM) (Fig. 3.43(a)) is particularly noticable; there, in Fig. 3.43(a), the shape is much more like that for a regular diffusion peak. At the higher concentrations, it will be noted that the second peak is much more reversible than the first but the relative heights of the first and second cathodic peaks are now reversed in Fig. 3.43(b) and (c), relative to those in Fig. 3.43(a) for otherwise comparable conditions. This system is very concentration-sensitive in its behavior. Current density vs concentration plots for C_2, A_2, and C_3, A_3 are shown in Figs. 3.46(a), (b), (c) and (d). While there are clearly diffusion-control components in the behavior, other aspects such as reaction through a

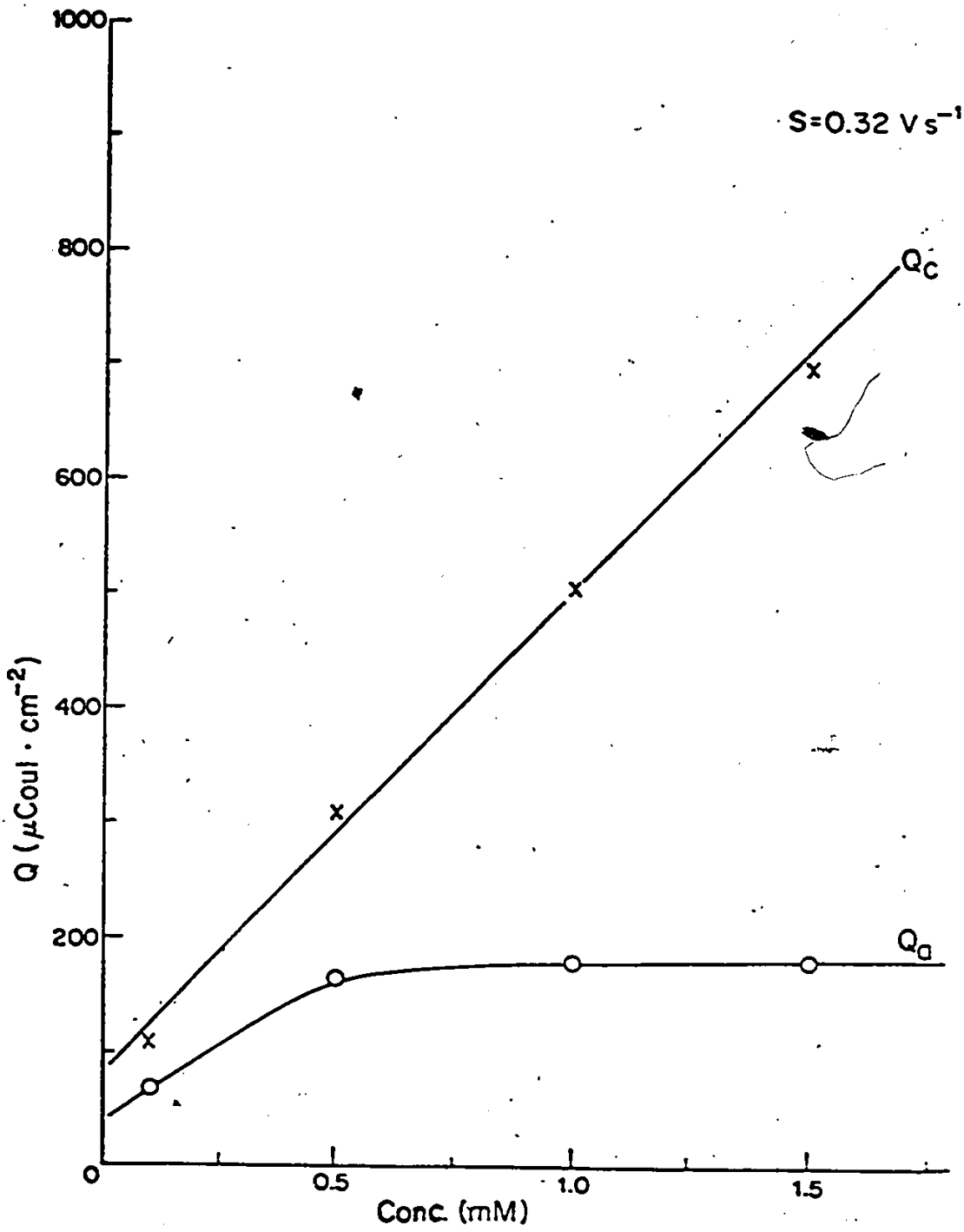

Fig. 3-44: Plots of charges Q_a and Q_c for the anodic and cathodic i vs V profiles for α-lipoic acid at Hg as a function of concentration

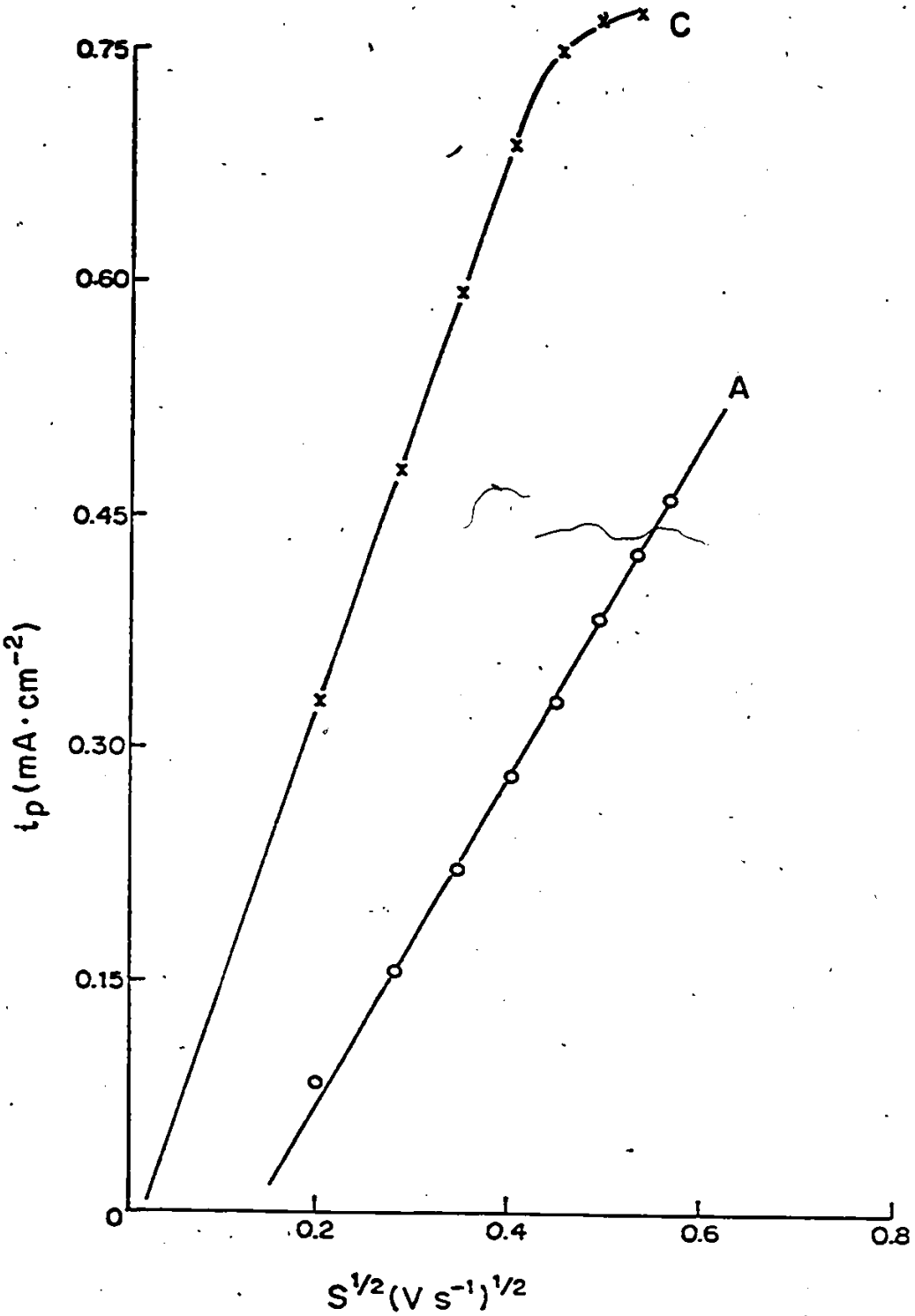

Fig. 3-45: Peak currents as a function of $s^{\frac{1}{2}}$ for the curves of Fig. 3-43(a).

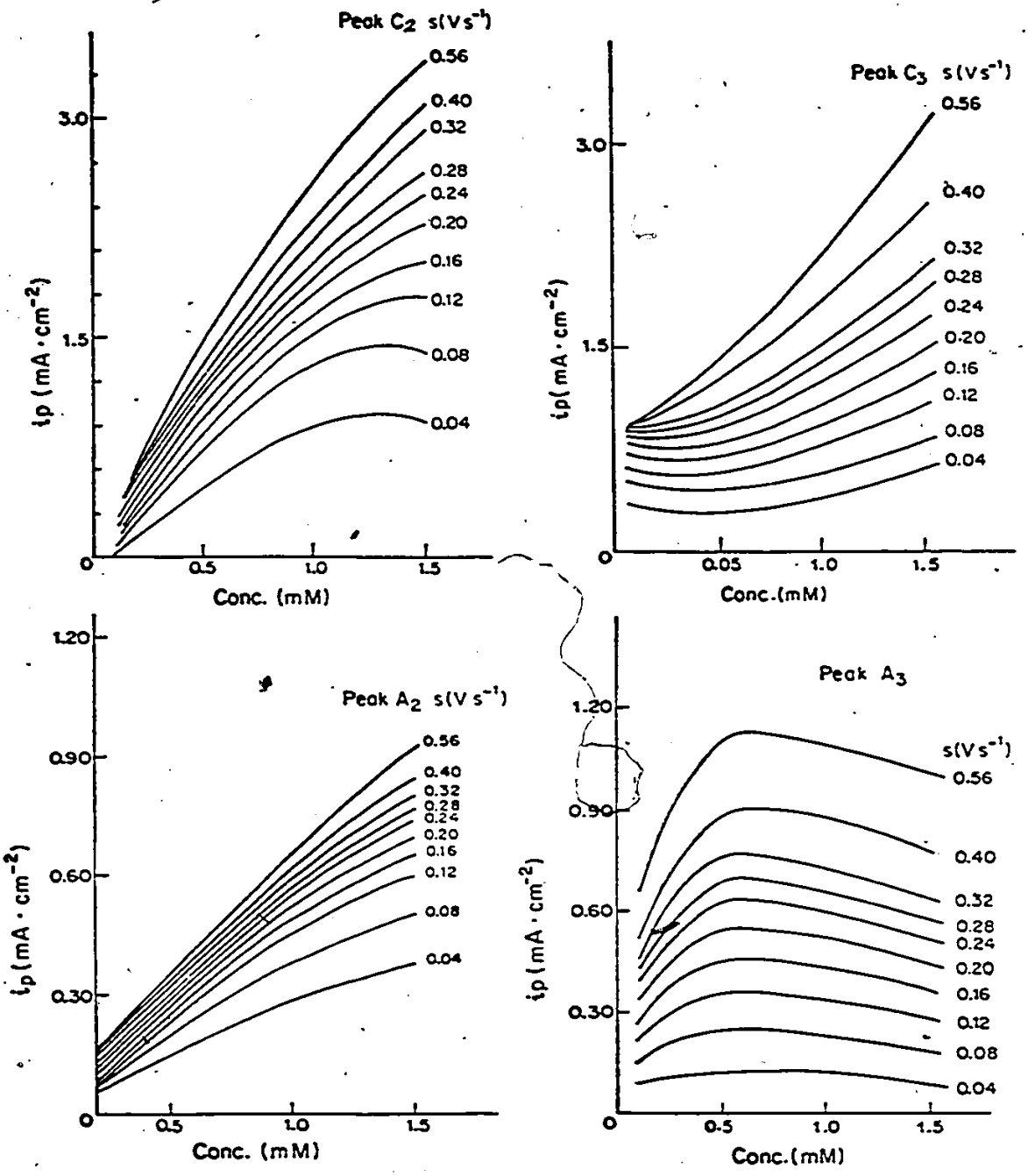

Fig. 3-46: Peak currents for processes C_2, A_2, C_3 and A_3 in cyclic voltammetry of α-lipoic acid at Hg in pH 1.21 aq solution as a function of concentration at various sweep-rates.

surface or adsorbed phase seem to be indicated, as well as two stages that are concentration-dependent.

3.8.3 Behavior at pH 11

The behavior at pH 11 (carbonate buffer) (Fig. 3.47(a)) is quite different from that at acid pH. Three clearly separated current peaks arise on the cathodic sweep but the third of these in the range -0.715 to -0.965 V E_H is almost certainly associated with a catalytic effect of the reduced "RSH" form of α-lipoic acid on the H_2 evolution process which commences at significant rates at these more negative potentials. A small reoxidation current peak is observed on the anodic sweeps and this corresponds to the first peak on the cathodic sweep.

Peak currents can again be represented as linear functions of $s^{\frac{1}{2}}$ (Fig. 3.48(a)) but, in this case, the data for peaks C_4 and C_2 also plot out well as a linear function of s (Fig. 3.48(b)). The plot of V_p vs ln s is shown in Fig. 3.47(b). The cathodic to anodic charge ratio is again 1 based on the 1st and 2nd cathodic peaks. The peak potentials for C_2, C_4 and A_2 vary significantly with s (ca. 30 mV per decade) while those for C_3 are almost independent of s indicating that, for this process, the reaction is hardly polarized over the s range used. However, the process is not in a chemical sense reversible since no corresponding anodic reoxidation region is observed.

The anodic peak region is quite different from those in Figs. 3.43(a), (b) and (c), for pH 1.21 where the forms of the peaks were specially remarked upon in an earlier paragraph (see Section 3.8.2).

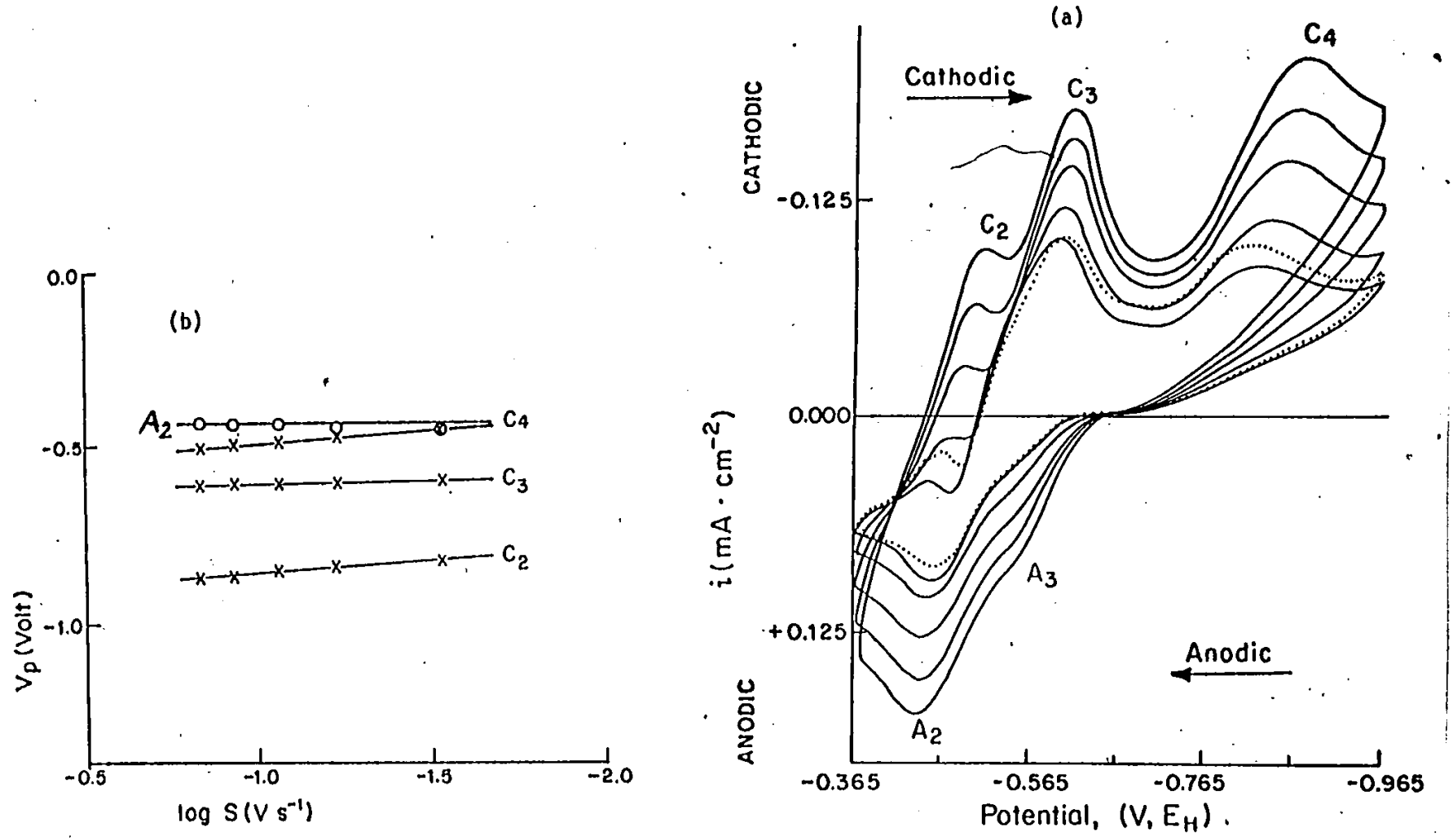

Fig. 3-47: (a) Cyclic voltammetry of α-lipoic acid at the Hg electrode at various sweep-rates in pH 11 aq solution (carbonate buffer). (b) Data from (a) plotted V_p as a function of ln s.

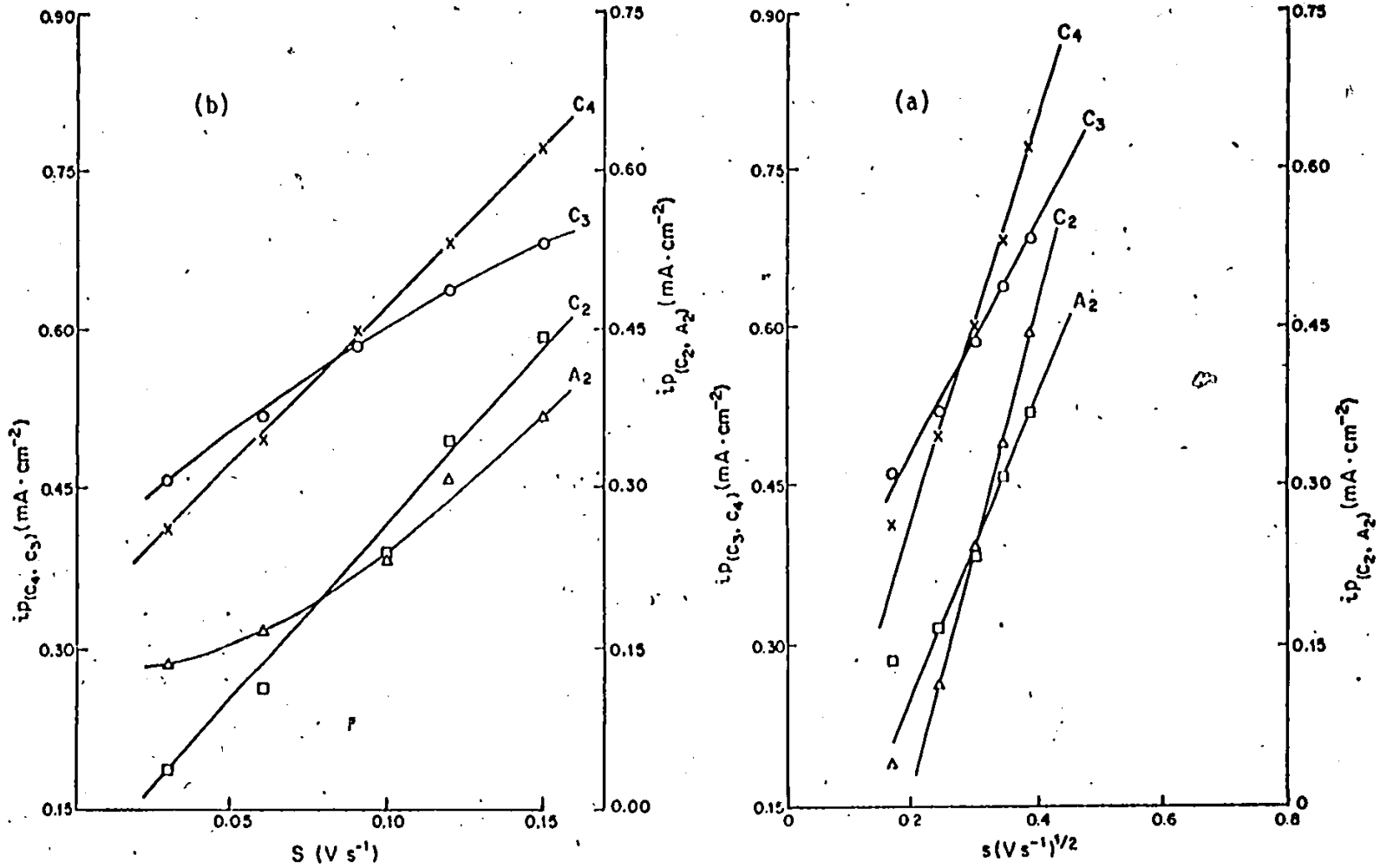

Fig. 3-48: Data from Fig. 3-47 plotted as a function of $s^{\frac{1}{2}}$ (a) or s (b).

The difference of the behavior here from that at pH 1.21 is presumably due to the fact that at pH 11 the molecule and its reduction product(s) are completely ionized as anions so that their adsorption at Hg will tend to be quite different from that at acidic pH's.

3.8.4 Behavior at pH 13

The behavior at pH 13 (NaOH) is shown in Fig. 3.49(a): the i vs V profiles are now again quite complex and surprizingly different from those at pH 11. Initially a single asymmetric cathodic peak is observed, trailing into the H_2 evolution region (-0.895 V,E_H). Sweep reversal results initially in a continuation of the increase of current on the anodic sweep; it seems that this is due, as at pH 11, to catalysis of the cathodic hydrogen evolution reaction by a product of reduction, "RSH", of the α-lipoic acid, as in the cyctine/cysteine case. However, at more anodic potentials in the anodic sweep, almost no anodic peak arises. Consequently, the Q_c/Q_a ratio here is very large and the process is "totally irreversible", i.e. either the product species is electrochemically inactive or its active form is removed by a chemical reaction, e.g., isomerization, complexation, etc.

With further repetitive cycling, a more complex i vs V profile develops (Fig. 3.49(b)) with several cathodic peaks at comparable currents and now a compound anodic reoxidation peak. Again, however, $Q_c >> Q_a$ at all sweep-rates, as was found for acidic pH's.

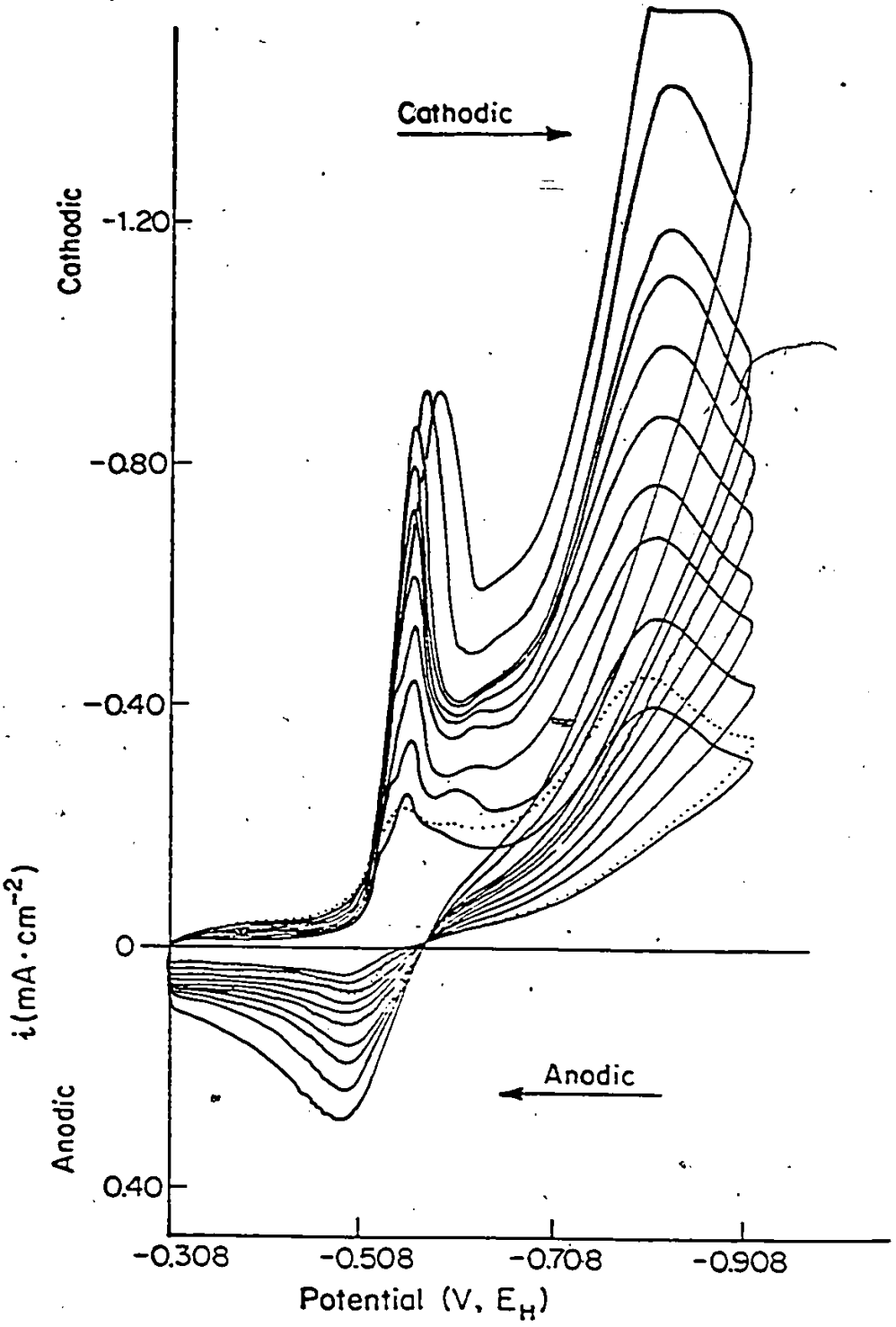

Fig. 3-49: (a) Cyclic voltammetry of α-lipoic acid at the Hg electrode of various sweep-rates in pH 13 (aq NaOH) for initial sweep.

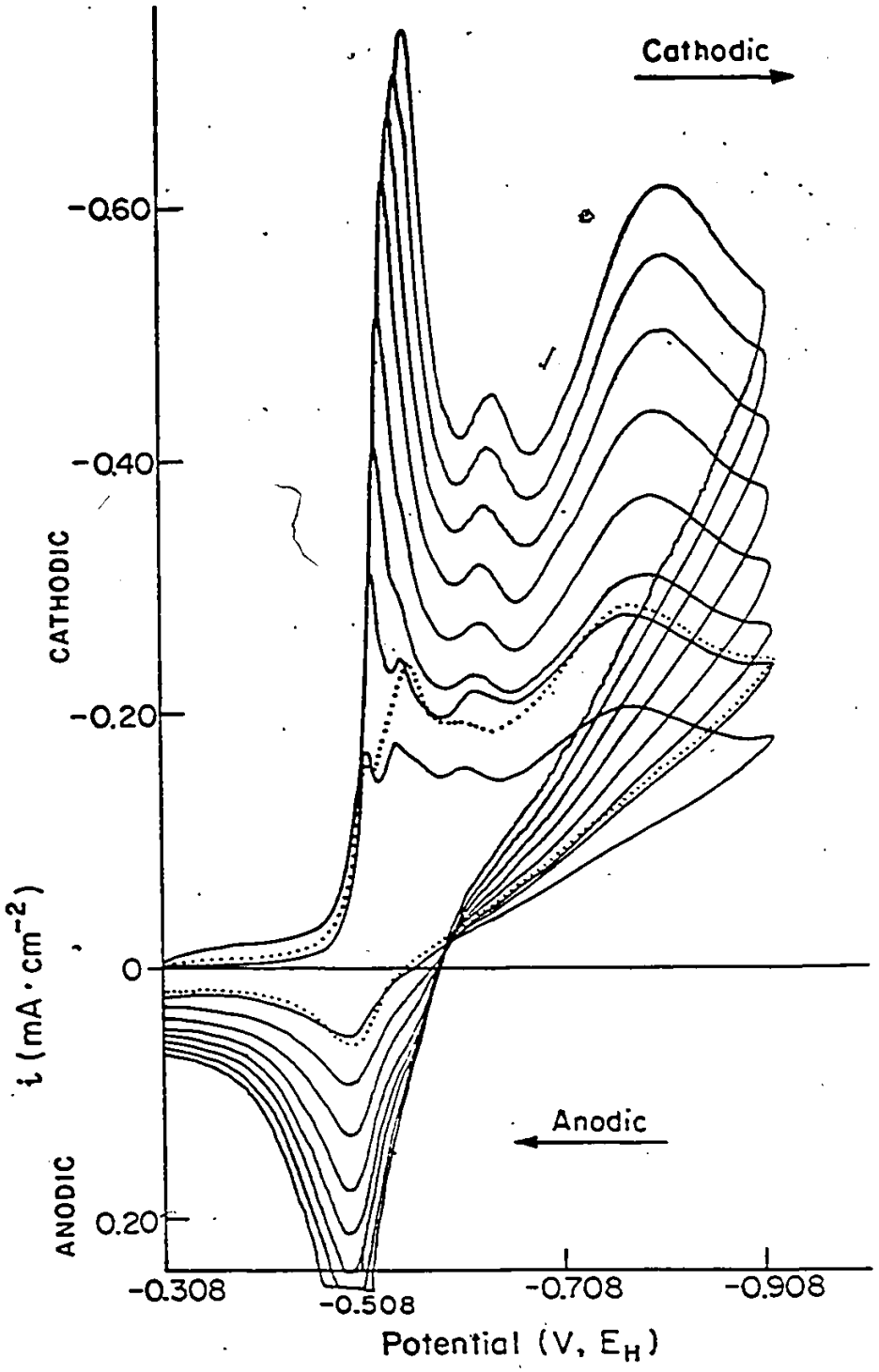

Fig. 3-49: (b) Cyclic voltammetry of α-lipoic acid at the Hg electrode of various sweep-rates in pH 13 (aq NaOH) after a number of repetitive sweep.

Evidently, the processes at alkaline pH are much less reversible than at acid pH, and this may be due, as was suggested above, to the anionic nature of the molecule at alkaline pH's where it would be repelled from the surface at the negative charge densities which obtain over the potential range where the observed currents arise. It can be suggested that the difference from the results at pH 11 (Fig. 3.47) is due to ionization of the -SH group which is formed in the product and, as RS^-, will have different adsorption and reoxidation behavior from that of RSH at lower pH's.

As before, peak currents are predominantly linear in s rather than $\sqrt{s}$.

3.9 GENERAL CONCLUSIONS ON REACTIVITY OF ORGANCIC SULFIDES AT Hg

The reaction of cystine, α-lipoic acid and cysteine at the Hg electrode is not a simple $2H^+$, 2e process. Invariably, several reduction or oxidation peaks arise, which vary in their relative heights depending on concentration and electrochemical cycling history. There is not any systematic 1:1 relationship between the peak currents for two of the peaks that could correspond to two separate electron-transfers at different potentials. Rather it seems that surface processes occur in parallel and consecutively with diffusion-controlled e, H^+ reaction steps which make the i vs V profiles have unusual forms dependent on reactant concentration and cycling history of a given Hg surface in the solution.

In most cases, the current profiles correspond predominantly to apparent diffusion control but the forms of the i vs V profiles are

not of the simple and calculatable form expected for such a process. Thus, some coupled surface and diffusion-controlled reaction steps seem to be involved which give rise to complex electrochemical behavior.

At Pt and Au it is surprizing that over a wide range of potentials no reduction is observed with the linear or cyclic -S-S- molecules and cysteine is only oxidized over the "surface oxidation region" at Pt (> 0.8 V, E_H) or Au (> 1.4 V, E_H, see Fig. 3.50) in acid solutions. These results confirm the earlier suggested importance of complexation with Hg in sulfide or thiol reactivity at the Hg electrode. Similarly, even at Pb, there is no reductive or oxidative activity for disulfides or thiols (Fig. 3.51). The role of specific interaction of the -S-S- or -SH groups with Hg is evidently critical for the reactivity of these types of molecules at an electrode interface.

Unfortunately, the present work shows that the complexity of the interaction with Hg, and the variety of resulting possible intermediate species and coupled chemical and diffusion-controlled reactions that can be involved, makes the electrochemical study of the redox behavior of cystine/cysteine and α-lipoic acid unexpectedly difficult. However, in the present work a systematic phenomenology of the electrochemistry of these materials as a function of pH, concentration, type of electrode metal and sweep-rate conditions has been demonstrated and characterized.

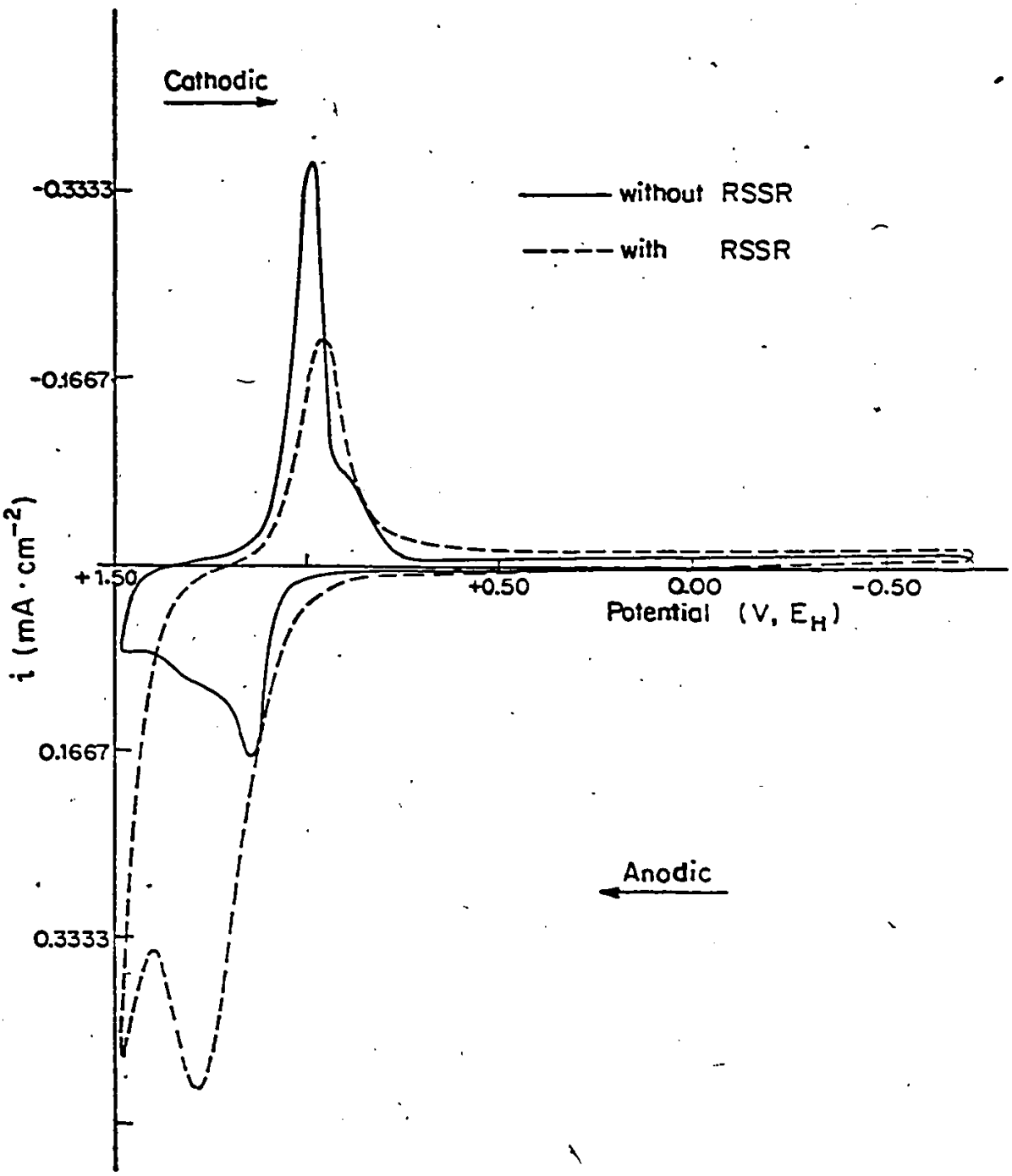

Fig. 3-50: Cyclic voltammetry of cystine at Au electrode in pH 1.22 aq solution, showing only oxidation process occurs at V > +1.4 V_H.

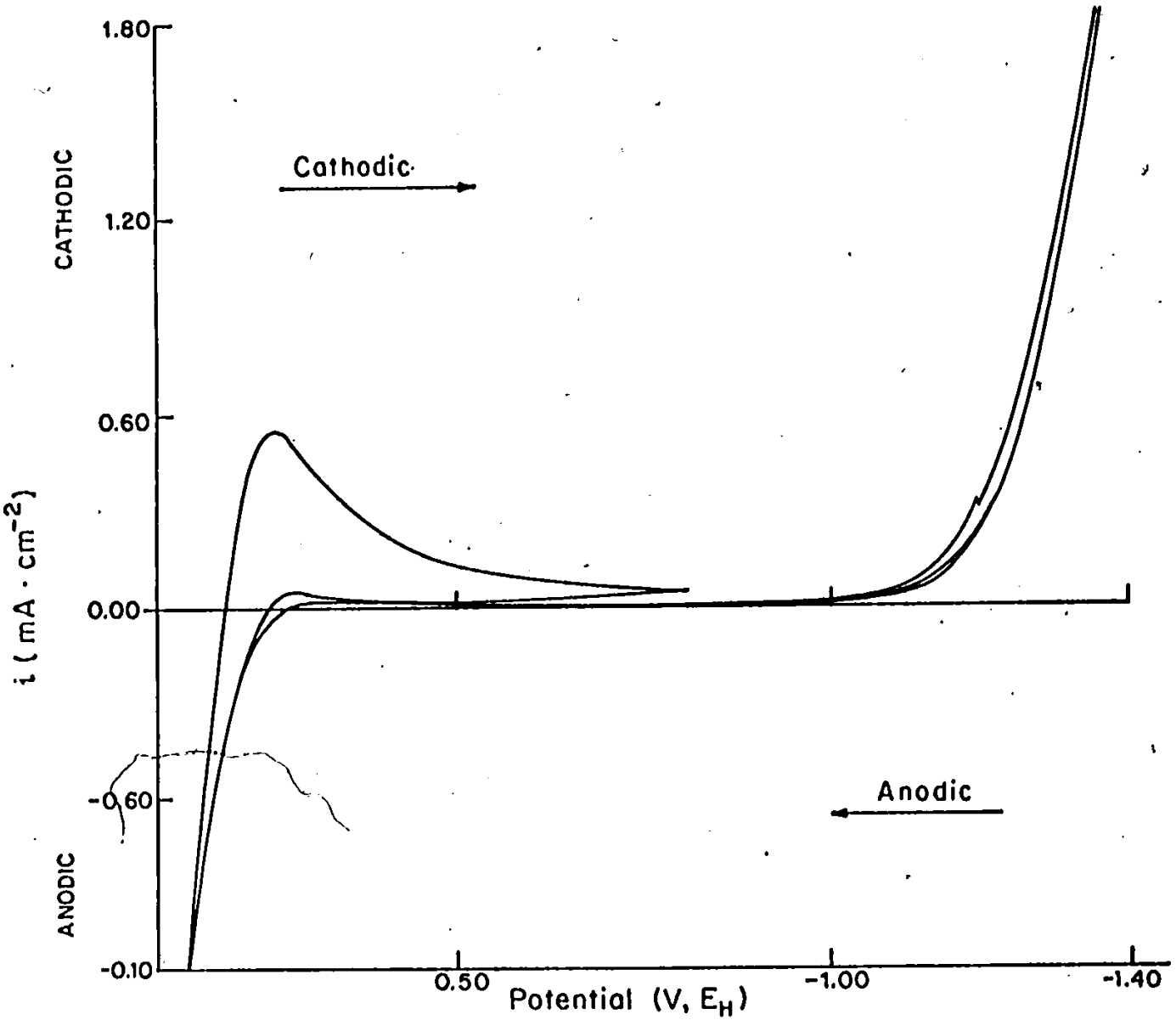

Fig. 3-51: Cyclic voltammetry of cystine at Pb electrode in pH 1.22 aq solution with Bu_4NClO_4, showing no reductive or oxidative activity.

3.10 OVERALL CONCLUSIONS

With pyrite, FeS_2, an electrochemically reversible reduction and re-oxidation process is observed by means of cyclic-voltammetry over a wide pH range. This is attributed to the couple (S-S) + 2 e + 2 H^+ ---> 2 SH^- reacting in the surface structure of the mineral crystal. The absence of diffusion-controlled currents shows that the process occurs at the boundary region of the solid phase FeS_2 without participation or formation of species in solution.

Pyrrhotite, $Fe_{1-x}S$, qualitatively, behaves similarly to pyrite, except with much less reversibility.

For galena, PbS, irreversible reductive dissolution occurs giving rise to solution-soluble SH^- or S^{2-} ion, depending on pH; this is not observed with FeS_2 or $Fe_{1-x}S$.

Comparatively, the redox reactivity of the organic sulfides, cystine, cysteine and α-lipoic acid, are critically dependent on complex formation with Hg, producing an intermediate with the Hg electrode. A mixture of surface reaction and diffusion-controlled processes is involved, and both types of process exhibit reversible and irreversible behavior, dependent on conditions of sweep-rate, concentration and pH. The concentration employed influences the relative current contributions from the diffusion-controlled reaction pathway in comparison with that involving complexes on the Hg surface.

CLAIMS TO ORIGINAL WORK

1. The electrochemical surface reactivity of galena, PbS, has been characterized over a range of electrode potentials, using the techniques of cyclic-voltammetry coupled with rotating electrode instrumentation. The latter allowed the role of formation of solution-soluble electro-active product species, probably sulfide ions, to be identified, and their formation related to holding of the potential constant at various values for controlled times. By examination of the current response to varying rates, s, V s^{-1}, of potential change in cyclic-voltammetry and by use of the rotating electrode technique, surface and diffusion-controlled electrode processes at the PbS interface could be distinguished according to dependence of the currents on s or $s^{\frac{1}{2}}$, and on electrode rotation rate.

2. The above approach was extended to the study of single-crystal surfaces of pyrite, FeS_2, and comparatively pyrrhotite, $Fe_{1-x}S$. It is found that no solution-soluble sulfide species are generated in the electrochemical oxidation or reduction of FeS_2 but a striking region of reversible oxidation/reduction behavior is observed over a potential range of ca., 0.40 V. It is shown that this reversible process involves a species anchored in the surface of the FeS_2 crystal as the currents generated in a cyclic-voltammetry experiment are clearly linear in sweep-rate s, a characteristic criterion for an electrode surface reaction.

3. The currents for the reversible electrode surface reaction arise, it is argued, from the process $S_2^{2-} + 2e \rightleftharpoons 2S^{2-}$ where the S_2^{2-} and the S^{2-} remains, in the case of FeS_2, in the surface structure of the crystal, no diffusion-controlled process being indicated for the currents over the potential range for the reversible process.

4. Support for the identifiction of the reversible process in (3) is based on comparison with the behavior of $Fe_{1-x}S$ where only the monomeric S^{2-} ion is present in the structure so that no dimer/monomer redox reaction is possible. With $Fe_{1-x}S$, no reversible region is observed in cyclic-voltammetry, nor are electro-active solution-soluble species detectably generated.

5. With the FeS_2 mineral, the currents for the reversible process increase by about 10-fold with increasing pH in the range pH = 1 to 11, but after cycling through this pH range, the currents return to the smaller values when the same FeS_2 electrode sample is examined again in the pH 1 solution. This behavior is not fully understood. At pH 1, the charge involved for the reversible surface process is found to correspond approximately to reaction in a monolayer of S_2^{2-} species.

6. SEM examination was made of the mineral surfaces before and after electrochemical cycling; some degradation of the original smooth or polished surface is indicated.

7. With each of the mineral materials, the successive stages of electrochemical reduction, which are indicated by the shapes of the voltammograms, are related to corresponding stages of oxidation in cathodic/anodic sweep cycles. This is referred to as the "cutting

experiment", i.e., a sweep in a given direction is "cut" and reversed at successively more positive or more negative potentials during successive cycles. Only with FeS_2 does this procedure reveal a reversible process over part of the potential range of the sweep.

8. With PbS, relative reflectivity measurements are used to provided a complementary qualitative insight into the changes of surface state of the mineral crystal during electrochemical surface reduction and oxidation. The reflectivity behavior is related to the regions of electrochemical reactivity that are indicated by the cyclic-voltammograms.

9. For each of the mineral sulfides, the electrochemical cathodic and anodic reactivity was examined by progressively increasing the potential limits of voltage sweeps in linear potential-sweep experiments. In some of the experiments, chemical identification of resulting product species, e.g. SO_4^{2-}, Fe^{3+} was made. At cathodic potentials, reduction to H_2S (at acid pH) was identified by the smell of gas generated and by the coloration reaction observed at wet lead acetate paper.

10. Comparative experiments on the reduction/oxidation behavior of two organic disulfides, cystine and α-lipoic acid, and one thiol, cysteine (the conjugate 2e, $2H^+$ reduced form of cystine), were carried out in order to examine if a reversible disulfide/thiol electrode process could be identified, analogous to the disulfide/sulfide reaction at FeS_2. Reduction and oxidation current peaks were demonstrated and characterized, but the processes were shown not to be simple nor to be purely surface reaction controlled. At the Hg

electrode, the reduction of disulfides and the reoxidation of the thiol, cysteine, proceeds via a Hg complex as indicated in work reported in previous literature.

11. Systematic cyclic-voltammetry experiments conducted over a range of sweep-rates showed that the currents arising in reduction and reoxidation processes have invariably an important diffusion-controlled component although, under some conditions, a surface reaction process could be identified and characterized. Generally, "mixed" surface reaction and diffusion-controlled kinetic behavior is observed.

12. A new method for dealing with the mixed reaction control in (11) is proposed and tested: peak currents in cyclic-voltammetry are plotted according either to the equation

$$i_p/s = k_1 + k_2 s^{-\frac{1}{2}}$$

or to

$$i_p/s^{\frac{1}{2}} = k_1 s^{\frac{1}{2}} + k_2$$

where k_2 and k_1 represent constants characteristic of the diffusion-controlled and the surface reaction controlled current components, respectively. This approach, it is shown, helps to clarify the complex mixed reaction control behavior observed with organic sulfide and thiol reactions at the Hg electrode.

13. The importance of complexation with Hg for reactivity of the organic disulfides and the thiol, cysteine, is demonstrated by comparative examination of the electrochemical behavior of these

substances at Pb, Au and Pt electrodes: at Au and Pt, and even at Pb, no reduction takes place over accessible ranges of potential before cathodic hydrogen evolution becomes appreciable in rate, while oxidation only takes place over the surface oxide formation regions at Au and Pt, as with most other organic substances. Evidently, the electrochemical reactivity of the organic sulfides and thiols requires, specifically, complex formation with Hg which acts as a mediator intermediate for the electrochemical redox process with these S-containing organic substances. No reversible redox behavior is observed, as was demonstrated in the case of FeS_2.

14. The forms of the cyclic-voltammograms for redox processes at Hg with cystine, cysteine and α-lipoic acid were characterized over a range of concentrations and of pH's from ca. 1 to ca. 13. pH and concentration effects are substantial, and arise from a) changing state of ionization and adsorbability of the S-compounds with pH and b) changing extent of "surface" and "from bulk" diffusion-controlled reaction of the reagents with increasing concentration. The forms of cyclic-voltammogrms are recognizably not those corresponding to diffusion-controlled reaction from species in bulk solution and only under one or two conditions of pH and concentration are simple forms, characteristic of diffusion-control from bulk, observed. The differences from the diffusion-controlled forms indicates the role of surface reaction processes while the observed non-linear relations between reduction and/or oxidation currents and bulk concentration, support the significant role of surface processes under most conditions. The limited solubility of the sulfide compounds studied

introduces unavoidable diffusion-controlled conditions to signigicant extents.

15. At the most negative potentials, beyond ca. -0.9 V E_H, important "catalytic" effects on the cathodic H_2 evolution reaction at Hg are observed, as were found earlier in polarographic experiments with cysteine by Brdička.

REFERENCES

1. Chander, S. and Fuerstenau, D.W.; Trans. Soc. Mining Eng., AIME, 251, 62 (1972); see also ibid, 256, 193 (1974).

2. Hoover, R.M. and Malhotra, D.; Flotation, 1, 485 (1976).

3. Voskanyan, M.G.; Soversh. Pererab. Mineral'n Syr'ya, M., 38 (1981).

4. Almaev, V.G., Kuznetsova, I.A., Masloboeva, L.V., Nesmelov, V.V., and Osipova, A.V.; Obogasheh. Rud. (Leningrad), 27, 28 (1982).

5. Romanov, A.M., Zelentsov, V.I., Sorokina, V.N., and Nasen'ka L.P.; Elektron. Obrab. Mater., 6, 62 (1974).

6. Rozmdestvenskaya, Z.B., Masalov, I.F., and Mushatova, K.A., V sb., Khimiya i Khim. Tekhnol., 16, 206 (1974).

7. Yashina, G.M., Eliseev, N.I., and Olerskaya, N.L.; Tr. Ural'sk. N.i.i. Proekt In ta Med. Prom-Sti, 18, 131 (1975).

8. Lamache, M., Bauer, D., and Pegouret, J.; Electrochim. Acta., 26, 1845 (1981).

9. Yen, T.F., Wen, C.S., Kwan, J.; U.S. patent 4,043,885; 23 Aug. 1977.

10. Abramov, A.A. and Avdokhin, V.M.; V sb., Obogashch. Rud. (Irkutsk), 3, 35 (1975).

11. Solozhenkin, P.M., Pulatov, G.Yu., and Glembotskii, V.A.; Dokl. Akad. Nauk Tadzh. SSR, 16, 36 (1973).

12. Ahmed, S.M.; Int. J. Min. Process, 5, 163 (1978).

13. Ahmed, S.M.; Int. J. Min. Process, 5, 175 (1978).

14. Tolun, R. and Kitchener, J.A.; Inst. Min. Met. Trans.; 73, 313 (1964).

15. Peters, E. and Majima, H.; Can. Met. Quart., 7, 111 (1968).

16. Fuerstenau, M.C., et al; 'The role of dixanthegen in xanthate flotation of pyrite', presented at the AIME fall meeting, Las Vegas, Nev. Sept. 1957.

17. Majima, H. and Takeda, M.; Trans. Soc. Mining Eng., AIME, 241, 431 (1968).

18. Biegler, T., Rand, D.A.J., and Woods, R.; Electroanal. Chem., 60, 151 (1975).

19. Nicol, M.J., Paul, R.L., and Diggle, T.W.; Electrochim. Acta. 23, 635 (1978).

20. Kishi, T., Shimizu, F., and Nagai, T.; Surf. Technol., 21, 109 (1984); 18, 131 (1975).

21. Kitayama, H., Iwase, Y., Ichino, T., and Osaka, T.; Rikogaku Kenkyusho Hokoku Waseda Daigaku, 104, 9 (1983).

22. Ahmed, S.M., and Gerischer, H.; Electrochim. Acta., 24, 705 (1979).

23. Musuko, N., and Yoshihito, H.; Denki-Kagaku, 31, 967 (1963).

24. Wrabetz, K.E.; Z. Elektrochem., 60, 722 (1956).

25. Sato, M.; Econ. Geol., 55, 1202 (1960).

26. Trampler, G.; Z. Phys. Chem., 99, 9 (1921).

27. Noddack, W., and Wrabetz, K.; Z. Elecktrochem., 59, 96 (1955).

28. Springer, G.; Trans. Inst. Min. Met.; 79, C11 (1970).

29. Seto, M.; Electrochim. Acta.; 11, 361 (1966).

30. Hamilton, I.C., and Woods, R.; J. electroanal. Chem. 118, 327 (1981)

31. Biegler, T., and Swift, D.A.; Electrochim. Acta., 24, 415 (1979).

32. Bailey, L.K., and Peters, E.; Can. Met. Quart., 15, 333 (1976).

33. Meyer, R.E.; J. Electroanal. Chem., 10, 59 (1979).

34. Yashina, G.M., and Olerskaya, N.L.; Fiz.-Tekh. Probl. Razrab. Polezn. Iskop., 6, 113 (1979).

35. Hillrichs, E., and Bertram, R.; Hydrometal., 11, 195 (1983).

36. Hillrichs, E., and Bertram, R,; Hydrometal., 11, 181 (1983).

37. Hillrichs E., Greulich, H., and Bertram, R., Hydromet. Res. Dev. and Plant Prat., pp. 277, Ed. by Osseo-Asene, K., and Miller, J.D., Conf. Proc. Met. Soc. of AIME, 1983.

38. Ammou-Chokroum, M., Sen, P.K., and Fouques, F.; Dev. Miner. Process. 2, 759 (1981).

39. Baur, J.P., Gibbs, H.L., and Wadsworth, M.E.; U.S. Bureau of Mines, R.I. 7823, 1974.

40. Jones, D.L.; Ph.D. Disser, Dept. of Met., Univ. of Brit. Colum., Vancourver, B.C., 1974.

41. Warren, G.W., Wadsworth, M.E., and El-Raghy, S.M.; Hydromet. Res. Dev. and Plant Pract., pp. 261, Ed. by Osseo-Asene K., and Miller, J.D., Conf. Proc. Met. Soc. of AIME, 1983.

42. Parker, A.J., Paul, R.L., and Power, G.P.; J. Electroanal. Chem., 118, 305 (1981).

43. Johnson, J.W., Chang, J., Narasagouder, R., and O'Keefe, J.J.; J. Appl. Electrochem., 8, 25 (1978).

44. Skewes, H.R.; Proc. Aust. Inst. Min. Met.; 244, 35 (1972).

45. Paul, R.L., Nicol, M.J., Diggle, J.W., and Saunders, A.P.; Electrochim. Acta., 23, 625 (1978).

46. Ghali, E., and Dandapani, B.; J. Appl. Electrochem. 10, 325 (1980).

47. Dandapani, B., and Ghali, E.; J. Electrochem. Soc., 129, 271 (1982).

48. Dandapani, B., and Ghali, E.; Hydromet. Res. Dev. and Plant Pract., pp. 213, Ed. by Osseo-Asene, K., and Miller, J.D., Conf. Proc. Met. Soc. of AIME, 1983.

49. Mazalov, I.F., Rozhdestvenskaya, Z.B., Simon, T.P., and Ponomarenko, P.L.; Khim. Khim. Tekhnol. (Alma-Ata),13, 172 (1972).

50. Garden, J.R., and Woods, R.; J. Electroanal. Chem. 100, 447 (1979).

51. Power, G.P.; Aust. J. Chem., 34, 2287 (1981).

52. Power, G.P.; Electrochim. Acta., 27, 359 (1982).

53. Price, D.C., and Davenport, W.P.; J. Appl. Electrochem., 12, 281 (1982).

54. Krishraswamy, P., and Fuerstenau, D.W.; Hydromet. Res. and Dev. Plant Pract., pp. 227, Ed. by Osseo-Asene, K., and Miller, J.D., Conf. Proc. Met. Soc. of AIME, 1983.

55. Peters, E., and Bailey, L.K.; 'Electrochemstry of molybdenite' paper no. 36, 7th Annual Hydromet. meeting, Vancourver, B.C., Aug. 1977.

56. Green, M.; 'Electrochemistry of the semiconductor-electrolyte interface', Modern Aspects Electrochemistry, no. 2, pp 343. Ed. by Bockris, J.O'M., and Conway, B.E., plenum Press, New York.

57. Gerischer, H.; Adv. Electrochem. Electrochem. Eng. 1, 139 (1961).

58. Kunori, S., and Ishii, F.; J. Min. Met. Inst. Jap., 79, 785 (1963).

59. Biegler, T.; J. Electroanal. Chem., 70, 265 (1976).

60. Biegler, T., and Swift, D.A.; Electrochim. Acta., 24, 415 (1979).

61. Gerischer, H.; J. Electrochem. Soc., 113, 1174 (1966).

62. Tyagai, V.A.; Elektrokhimiya, 4, 387 (1965). Tyagai, V.A.; and Kolbasov, G.Ya.; Surf. Sci., 28, 423 (1971).

63. Gerischer, H.; Surf. Sci., 13, 265 (1969); see also J. Vac. Sci. Technol., 15, 1422 (1978).

64. Healy, T.W.; Australasian Inst. Min. Met., Melbourne, 1973, p477.

65. Eadington, P., and Prosser, A.P.; Trans. Inst. Min. Met. 78, C74 (1969).

66. Simkovich, G., and Wagner, J.B.; J. Electrochem. Soc., 110, 513 (1963).

67. Richardson, P.E., and Maust Jr, E.E.; Trends Electrochem. plenary invited contrib., Aust. Electrochem. Conf. 4th, 1976 (pub. 1977), p.317, Ed. by Bockris, J'OM., Rand, D.A.J., and welch, B.J.; Plenum, New York, 1977.

68. Phillips, M.L., and Spitler, M.T.; J. Electrochem. Soc., 128, 2137 (1981).

69. Wilson, J.R., and Park, S.M.; J. Electrochem. Soc., 129, 149 (1982).

70. Tenne, R.; J. Electrochem. Soc., 129, 143 (1982).

71. An Chiling, and She Weimin; Taiyangneng Xuebao, 2, 298 (1981). Xiao Yihong, Wang Chouchen, Chang Junling; ibid, 2, 342 (1981).

72. Rothwarf, A., and Barnett, A.M.; IEEE, Trans. Electron Devices, ED24, 381, (1977).

73. Tributsch, H.; J. Electrochem. Soc., 128, 1261 (1981).

74. Calabrese, G.S., and Wrighton, M.S.; J. Am. Chem. Soc., 103, 6273 (1981).

75. Nakamura, M.; Ger. Offen., 3,044,547, 02, Jul. 1981.

76. Simon, R.A., Ricco, A.J., Harrison, D.J., and Wrighton, M.S.; J. Phys. Chem., 87, 4446 (1983).

77. Tributsch, H.; Ber. Bunsenges. Phys. Chem., 81, 361 (1977).

78. Tributsch, H., and Bennett, J.C.; J. Electroanal. Chem., 81, 97 (1977).

79. Tributsch, H.; Z. Naturforsch; 32A, 972, (1977).

80. Gerischer, H.; Am. Chem. Soc. Symp. Ser., 146, 1 (1981).

81. Kubiak, C.P., Schneemeyer, L.F., and Wrighton, M.S.; Report 1980, TR-22, order no. AD-A088606, 13pp.
Avail NTIS, From Gov. Rep. Announce Index (U.S.) 81, 61 (1981).

82. DeMichelis-Quiriconi, R., and Astier, M.L.; Fr. Demande, 2,469,436, 22, May 1981.

83. Fornarini, L., Stirpe, F., Scrosati, B., and Razzini, G.; Sol. Energy Mater. 5, 107 (1981).

84. Audas, R., and Irwin, J.C.; J. Appl. Phys., 52, 6954 (1981).

85. Djemal, G., Mueller, N., Lachish, U., and cahen, D.; Sol. Energy Mater. 5, 403 (1981).

86. Fujishima, A., Noguchi, Y., Honda, K., and Loo, B.H.; Bull. Chem. Soc. Jap.; 55, 17 (1982).

87. Kautek, W., and Gerischer, H.; Surf. Sci., 119, 46 (1982).

88. Ahmed, S.M., Electrochim. Acta., 27, 707 (1982).

89. Schneemeyer, L.F., and Cohen, U.; J. Electrochem. Soc., 130, 1536 (1983).

90. Thompson, L.K.; Diss. Abstr. Inst., B44, 1108 (1983).

91. Parkinson, B.A., Kam, K.K., Kline, G., and Levy, C.; Nov. 81, 77P IS-4784, Contract W-7405-ENG-82, DE82006287, DCA05/MFA01 NTIS.

92. Tributsch, H.; J. Electrochem. Soc., 125, 1086 (1978).

93. Gobrecht, J., Tributsch, H., and Gerischer, H.; J. Electrochem. Soc. 125, 2085 (1978).

94. Whittingham, M.S.; Mater. Res. Bull., 9, 1981 (1974).

95. Denis, M.B.; Mater. Res. Bull., 10, 287, (1975). U.S. Patent, 3,933,688, 1976.

96. Whittingham, M.S., and Gamble, F.M.; Mater. Res. Bull., 10, 363 (1975).

97. Whittingham, M.S.; J. Electrochem. Soc., 123, 315 (1976).

98. Silbernagel, B.G.; Solid State commun., 13, 1911 (1975).

99. Silbernagel, B.G., and Whittingham, M.S.; Mater. Res. Bull., 11, 29 (1976).

100. Whittingham, M.S.; Sci., 192, 1126 (1976).

101. Whittingham, M.S.; Belgian patent, 819,672, 1973.

102. Bichon, J., et al; C. R. Acad. Sci. Paris, Serie C, t.276, 1283 (1973).

103. Chianelli, R.R.; et al; Mat. Res. Bull., 10, 1379 (1975).

104. Riekel, C., and Schollhorn, R.; Mat. Res. Bull., 10, 629 (1975).

105. Lablanc-Sorean, et al; Mat. Res. Bull., 9, 191 (1974).

106. Winn, D.A.; Ph.D. Disser., Dept. of Material Sci., Imperial College, London, 1975.

107. Marmaduke, B.A., and Donaghey, L.F.; 11th IECEC Proc. 1, 467 (1976).

108. Winn, D.A., and Steele, B.C.H.; J. Electrochem. Soc., 122, 68C (1975).

109. Besenhard, J.O., Meyer, H., and Schoellhorn, R.; Z. Naturforsch, B. Anorg. Chem., Org. Chem., 31B, 907 (1976).

110. Haering, R.R., and Stiles, J.A.R.; Can. Patent, 1,081,320; 08, July, 1980.

111. Suib, S.L., Faulkner, L.R., Stucky, G.D., and Blattner, R.J.; Anal. Chem., 51, 1060 (1979).

112. Jacobson, A.J., Chianelli, R.R., and Whittingham, M.S.; 'Chem. uses molybdenite', Proc. Int. Conf., 3rd 1979, p209, Ed. by Barry, H.F., and Mitchell, P.C.H..

113. Kumagai, N., Tanno, K., and Kumagai, N.; Electrochim. Acta., 27, 1087 (1982).

114. Johnson, W.B., and Worrell, W.L.; Solid State Ionics, 5, 367 (1981).

115. Zanini, M., Shaw, J.L., and Tennenhouse, G.J.; Solid State Ionics, 5, 371 (1981).

116. Eibschuetz, M., Murphy, D.W., and Disalvo, F.J.; Physica B plus C, 99(1/4), 145 (1980). (Int. Conf. on layered materials and intercalates. Nijmega, Netherlands, Aug. 1979)

117. Patriarca, M., Voso, M.A., Scrosati, B., Bonino, F., and Lazzari, M.; Solid State Ionics, 6, 15 (1982).

118. Cairns, E.J., and Shimotake, H.; Sci., 164, 1347 (1969).

119. Nelson, P.A., et al; Progress Report for the peroid July-Dec. 1974, ANL-75-1, ANL, 1975.

120. Steunenberg, R.K., and Roche, M.F.; Report 1977, CONF-770531-1, pp. 24, avail. NTIS, Fr Energy Abstr. 2, 1977, no. 51952.

121. McCoy, L.R., and Heredy, L.A.; 11th IECEC, Proc. 1, 485 (1976).

122. Dunning, J.S., Bradley, T.G., and Zeitner, E.J.; 11th IECEC, Proc., 1, 491 (1976).

123. Inoue, T., and Koura, N.; Denki Kagaku Oyobi Kogyo Butsuri Kagaku, 49, 761 (1981).

124. Mrazek, F.C., and Battles, J.E.; Progress Report for the peroid Jan-June 1974, ANL-8109, pp. 72, ANL, 1975.

125. Steunenberg, R.K., Martin, A.E., and Tomczuk, Z.; U.S. Patent, 3,941,612; Mar.1976.

126. Shimotake, H., and Bartholme, L.G.; Progress Report for the peroid July-Dec 1974, ANL-75-1, p32, ANL, 1975.

127. Elliott, R.C., and Cooper, T.O.; Extended Abstr. of Battery Electronics Division, Electrochemical Society, Toronto, Canada, May 11-16, 1975. Vol. 75-1 (1975).

128. Shimotake, H., Walsh, W.J., Carr, E.S., and Bartholme, L.G.; 11th IECEC, 1, 471 (1976).

129. Elliott, R.C., and Cooper, T.C.; Progress Report for the peroid of Jan-June 1975, ANL-75-36, p24, ANL, 1976.

130. McPheeters, C.C., Schertz, W.W., and Yao, N.P.; Extended Abstr. of Battery Division, Electrochemical Society, Dallas, Taxas, Oct. 5-10, 1975. (Vol. 75-2, 1975).

131. Brec, R., Dugast, A., and Le Mehaute, A.; Mater. Res. Bull., 15, 619 (1980).

132. Takahashi, S., Koura, N.; Denki Kagaku Oyobi Kogyo Butsuri Kagaku, 49, 62 (1981).

133. Evans, W.P., Leger, V.Z.; Eur. Pat. Appl. Ep 68,476 (cl.H01M4/58) 05 Jan 1983; U.S. Appl. 278,896, 29 Jun 1981.

134. McKee, D.W., and Pak, M.S.; U.S. Patent, 3,573,988, 06 Apr. 1971.

135. Hodes, G., Manassen, J., and Cahen, D.; Ger. Offen. 3,004,262, 04 Sept. 1980.

136. Brdička, R.; Coll. Czech. Chem. Comm., 5, 112 and 238 (1933).

137. Bockris, J. O'M., and Conway, B.E.; J. Phys. Coll. Chem., 53, 527 (1949).

138. Conway, B.E., Bockris, J.O'M., and Lovrecek, B.; Proc. CITCE Meeting, Poitiers, 1956, Butterworths Sci. Publ.

139. Brdička, R.; Coll. Czech. Chem. Comm.; 8, 366 (1936).

140. Kolthoff, I.M., and Barnum, C.; J. Amer. Chem. Soc., 62, 3061 (1940).

141. Kolthoff, I.M., and Barnum, C.; J. Amer. Chem. Soc., 63, 520 (1941).

142. Stankovich, M., and Bard, A.J.; J. Electroanal. Chem., 75, 487 (1977).

143. Moiroux, J., Fleury, M.B., and Deycard, S.; Biochem. and Bioenerg. 3, 404 (1976).

144. Schapinck, F.W., and Oudeman, M., Leu, K.W., and Helle, J.N.; Trans. Farad. Soc., 56, 415 (1961).

145. Mairesse-Ducarmois, C.A., Patriarche, G.J., and Vandenbalck, J.L.; J. Pharma. Belg., 31, 169 (1976).

146. Mairesse-Ducarmois, C.A., Patriarche, G.J., and Vandenbalck, J.L.; Anal. Chim. Acta., 71, 165 (1974).

147. Mairesse-Ducarmois, C.A., Patriarche, G.J., and Vandenbalck, J.L.; Anal. Chim. Acta., 88, 47 (1977).

148. Toropova, V.F., Polyakov, Yu. N., and Naumova, E.A.; Deposited Doc. 1974, VINITI 816-75, 15pp.

149. Almagro, V., Gomez, M.M., and Sancho, J.; An. Quim., 72, 414 (1976).

150. Roque da Silva, A.S., and Roque da Silva, A.M.; Rev. Port. Farm., 31, 52 (1981).

151. Walsh, E.O'F.; An Introduction to Biochemistry, pp. 28-29; 58-59; 137; 230-231; 401-403, English Universities Press, London (1953).

152. Cipris, D., and Pouli, D.; U.S. Patent, 4,072,584; 07, Feb. 1978.

153. Wong, C.H., and Wang, K.T.; J. Chin. Chem. Soc. (Taipei), 25, 149 (1978).

154. Khusainov, M.A., and Rafikov, R.K.; Tezisy. Dokl.-Vses. Soveshch. Polyarogr., 7th 1978, 64. Ed. by Feoktistov, L.G., Izd. Nauka, Moscow, USSR.

155. Toropova, V.F., Budnikov, G.K., and Medyantseva, E.P.; Elektrokhimiya, 11, 393 (1975).

156. Medyantseva, E.P.; Sb Aspirantsk. Rabot. Kazan. Un-t. Estestv. N. Biol. Khimiya, 241, (1975).

157. Lamache-Duhameaux, M.; J. Electroanal. Chem., 97, 117 (1979).

158. Kadlecek, J., and Kalous, V.; J. Electroanal. Chem., 105, 225 (1979).

159. Rogers, G.T., and Mallett, D.N.; Bioelectrochem. and Bioenerg., 10, 269 (1983) (section of J. Electroanal. Chem., 155, (1983)).

160. Samec, Z., Malysheva, Zh.N., and Koryta, J.; J. Electroanal. Chem., 65, 573 (1975).

161. Pradac, J., and Koryta, J.; J. Electroanal. Chem., 17, 167 (1968).

162. Pradac, J., and Koryta, J.; J. Electroanal. Chem., 17, 177 (1968).

163. Brdička, R.; Coll. Czech. Chem. Comm., 5, 148; 112 (1933).

164. Roncato, A.; Arch. Sci. Riol., 20, 146 (1934).

165. Reddy, S.J., and Krishnan, V.R.; Trans. SAEST, 15, 99 (1980).

166. Bianco, P., and Haladjian, J.; J. Eletroanal. Chem., 72, 347 (1976).

167. Zagal, J., Fierro, C., and Rozas, R.; J. Electroanal. Chem., 119, 403 (1981).

168. Nikulin, V.N., Khusainov, M.A., and Pavlichenko, L.A.; Novosti. Elektrokhim. Org. Soedin., Tezisy. Dokl. Vses. Soveshch. Elektrokhim. Org. Sodin., 8th 1973, 57-8. Ed. by Feoktistov, L.G., 'Zinatne' Riga, USSR.

169. Nygard, B.; Arkiv. Kemi., 28, 650 (1967).

170. Trudinger, P.A., Lambert, I.B., and Skyring, G.W.; Econ. Geol., 67, 1114, (1972).

171. Harvey, R.D.; Econ. Geol., 23, 778 (1928).

172. Keller, G.V., and Frischknecht, F.C.: 'Electrical Methods in Geophysical Prospecting', pp. 519, Pergamon Press, New York, 1967.

173. Parasnis, D.S.: 'Mining Geophysics' 2nd ed., pp. 395, Elsevier, Amsterdam, 1973.

174. Goudin, A.M.: 'Flotation' 2nd ed., pp 573, McGraw-Hill, New York, 1957.

175. Ney, P.: 'Zeta-Potentiale und Flotierbarkeit von Meneralen', pp. 214, Springer-Verlag, Wien and New York, 1973.

176. Dewald, J.R., Semiconductor electrodes. In: 'Semiconductors' Ed. by Hannay, N.B., pp. 727, Reinhold, New York, 1959.

177. Karasev, A.P., Krasnikov, V.I., Seyfullin, R.S., and Sychugov, V.S.; Izv. Phys. Solid Earth, 121 (1971).

178. Pleskov, Y.V., Electrical double-layer of the semiconductor-electrolyte interface. In: 'Progress in Surface and Membrane Science', vol. 7, pp. 57, Ed. by Danielli, J.F., Rosenberg, M.D., and Cadenhead, D.A., Academic press, New York, 1973.

179. Bragg, W.L.; Proc. Roy. Soc., A89, 468 (1914), also Elliott, N.; Chem. Phys., 33, 903 (1960).

180. Brostigen, G., and Kjekshus, A.; Acta. Chem. Scand., 23, 2186 (1969).

181. Miyahara, S., and Teranishi, T.; J. Appl. Phys., 39, 896 (1968).

182. Bither, T.A., Bouchard, R.J., Cloud, W.H., Donohue, P.C., and Siemons, W.J.; Inorg, Chem., 7, 2208 (1968).

183. Li, E.K., Johnson, K.H., Eastman, D.E., and Freeouf, J.L.; Phys. Rev. Lett., 32, 470 (1974).

184. Fukui, T., Miyadai, T., and Miyahara, S.; J. Phys. Soc. Jap., 31, 1277 (1971).

185. Marinace, J.C.; Phys. Rev., 96, 593 (1954).

186. Sasaki, A.; Mineral. Jour., 1, 290 (1955).

187. Horita, H.; Jap. J. Appl. Phys.,12, 617 (1973).

188. Agayev, Ya, and Erniyazov, Kh.; Izv. Akad. Nauk. Turkm. SSR, ser. Fiz-Tek. 5, 104 (1963).

189. Kiriev, P.S., Korovin, A.P., Krasnikov, V.I., Muravieinik, N.A., Pantaev, V.D., Sychugov., V.S., Seifullin, R.S., and Favorov, V.A.; Izv. Akad. Nauk. SSSR, ser. Geolog., 6, 75 (1969).

190. Ovchinnikov, I.K., and Krivoshein, A.A.; Izv. Phys. Solid Earth, 86 (1972).

191. Pridmore, D.F., and Shuey, R.T.; Amer. Mineral, 61, 248 (1976).

192. Fleischer, M.; Econ. Geol., 50th Anniv. Vol., 970 (1955).

193. Hewley, J.E.; Econ. Geol. 47, 260 (1952).

194. Fischer, M., and Hiller, J.E.; Neues Jb. Mineral., 89, 281 (1956).

195. Favorov, V.A., Krasnikov, V.I., and Sychugov, V.S.; Izv. Akad. Nauk. SSSR, ser. Geolog., 11, 72 (1972).

196. Suziki, T.; Sci. Rept. Tohoku Univ., ser. 3, 8, 317 (1962).

197. Smith, F.G.; Econ. Geol., 42, 515 (1947).

198. Karasev, A.P., Krasnikov, V.I., Pantaev, V.D., Seifullin, R.S., Sychugov, V.S., Favorov, V.A.; Akad. Nauk. SSSR, Sibirskoe Otdelenie, Geologiya i Geofizika, 5, 64 (1972).

199. Carpenter, R.H., and Desborough, G.A.; Amer. Mineral., 49, 1350 (1964).

200. Arnold. R.G.; Can. Mineral., 9, 31 (1967).

201. Vaughan, D.J., Schwarz, E.J., and Owens, D.R.; Econ. Geol. 66, 1131 (1971).

202. Evens, H.T., Sci., 167, 621 (1970).

203. Bertaut, E.F.; C. R. Acad. Sci., Paris, 234, 1295 (1952).

204. Toknami, M., Nishiguchi, K., and Morimoto, N.; Amer. Mineral. 57, 1066 (1972).

205. Fleet, M.E.; Acta. Crystallogr., B27, 1864 (1971).

206. Parasnis, D.S.; Geophys. Prosp., 4, 249 (1956).

207. Semenov and Malchevskiy; Razvedka Nedr., 9, 35 (1939); reference 40 in Keller, G.V.; 'Electrical Properties of Rocks and Minerals', In: 'Handbook of Physical Constants', Ed. by Clark, S.P., Geological Soc. of America, Memoir 97, 1966.

208. Hirahara, E., and Murakami, M.; J. Phys. Chem. Solids, 7, 281 (1958).

209. Hihara, T.; J. Sci. Hiroshima Univ., A24, 31 (1960).

210. Suchet, J.P.; 'Crystal Chemistry and Semiconductor in Transition Metal Binary Compounds', pp. 380, Academic Press, New York, 1971.

211. Fujime, S., MurakAmi, M., and Hirahara, E; J. Phys. Soc. Jap., 16, 183 (1961).

212. Theodossiou, A.; Phys. Rev., A137, 1321 (1965).

213. Bin, M., and Pauthenet, R.; J. Appl. Phys., 34, 1161 (1963).

214. Levinson, L.M., and Treves, D.; J. Phys. Chem. Solids, 29, 2227 (1968).

215. Vaughan, D.J., and Tossell, J.A.; Sci. 179, 375 (1973).

216. Gehlen, K. Von, and Piller, H.; Mineral. Mag., 35, 335 (1965).

217. Kaplan, H.I., and Worrell, W.L.; 'The variation of the electrical conductivity of FeS with sulfur pressure at temperatures between 670 and 900 C', In: 'The chemistry and Extended Defects in Non-Metallic Solids', pp. 672, Ed. by Eyring, L., and O'Keefe, M., North-Holland, Amsterdam, 1970.

218. Wyckoff, R.W.G.: 'Crystal Structures', 2nd ed. vol. 1, pp.92, Wiley-Interscience, New York, 1963.

219. Scanlon, W.W., 'Polar Semiconductors', in: 'Solid State Physics', Vol. 9, pp. 83, Ed. by Seitz, F., and Turnbull, D., Academic Press, 1958.

220. Krebs, H.; Acta. Cryst., 9, 95 (1956).

221. Overhof, H., and Rossler, U.; Phys. Stat. Sol., 37, 691 (1970).

222. Weinberg, I., and Callaway, J.; Nuovo Cimento, 24, 190 (1962).

223. Paul, W., and Jones, R.V., Proc. Phys. Soc., B66, 194 (1953).

224. Moss, T.S.; Proc. Phys. Soc., B66, 993 (1953).

225. Scanlon, W.W.; Phys. Rev., 92, 1573 (1953).

226. Buckingham, J., 'Dictionary of Organic Compounds', 5th ed. Chapman, New York, 1982.

227. Reinmuth, W.H.; Anal. Chem., 32, 1509 (1960).

228. Conway, B.E., Angerstein-Kozlowska, H., Sharp, W.B.A., and Criddle, E.E.; Anal Chem., 45, 1331 (1973).

229. Sharp, W.B.A.; Ph.D. thesis, Univ. of Ottawa, 1976.

230. Conway, B.E.; Proc. Roy. Soc. (London), 256A, 128 (1960).

231. Azzam, A.M., Bockris, J.'OM, Conway, B.E., and Rosenberg, H.; Trans Far. Soc., 46, 924 (1950).

232. MacDonald, J.J., and Conway, B.E.; Proc. Roy. Soc. (London), 269A, 419 (1962).

233. Feltham, A.M., and Spiro, M.; Chem. Rev., 71, 177 (1971).

234. Bates, R.G.; 'Determination of pH', 2nd ed. pp.294, Wiley-Interscience, New York, 1973.

235. Hills, G.J., and Ives, D.J.G.; 'The Hydrogen Electrode' in: 'Reference Electrodes', pp. 92, Ed. by Ives, D.J.G., and Janz, G.J., Academic Press, New York, 1961.

236. Sevčik, A.; Coll. Czeck. Chem. Comm., 13, 349 (1948); see also Randles, J.E.B.; Trans. Far. Soc., 44, 327 (1948)

237. Delahay, P., ans Perkins, G.; J. Phys. Coll. Chem., 55, 586; 1146 (1951).

238. Nicholson, R.S., and Shain, I.; Anal. Chem., 36, 706 (1964).

239. Delahay, P.; J. Amer. Chem. Soc., 75, 1190 (1953); see also Berzins, T., and Delahay, P.; ibid, 75, 555 (1953).

240. Delahay, P.; 'New Instrumental Method in Electrochemistry', chap. 6, John Wiley and Sons, New York, 1954.

241. Angerstein-Kozlowska, H., Conway, B.E., and Klinger, J.; J. Electroanal. Chem., 87, 301 (1978).

242. Laviron E.; Bull. Soc. Chim., France, 2256, (1968).

243. Ronillier, L., and Laviron, E.; J. Electroanal. Chem., 157, 193 (1983).

244. Tessier, D.F., and Conway, B.E.; to be published.

245. Angerstein-Kozlowska, H., Klinger, J., and Conway, B.E.; J. Electroanal. 75, 45 (1977).

246. Conway, B.E., Angerstein-Kozlowska, H., and Ho, F.C.; J. Vac. Sci. Technol. 14, 351 (1977).

247. Garrels, R.M., and Christ, C.M.,; 'Solutions, Minerals and Equilibria', Harper and Row, New York, 1965.

248. Pourbaix, M.; 'Atlas of Electrochemical Equilibria', CEBELCOR, Brussels, Belgium, 1974.

249. Angerstein-Kozlowska, H., and Conway, B.E.; J. Electroanal. Chem., 95, 1 (1979).

250. Angerstein-Kozlowska, H., Conway, B.E., and Sharp, W.B.A.; J. Electroanal. Chem., 43, 9 (1973).

251. Hadži-Jordanov, S., Angerstein-Kozlowska, H., and Conway, B.E.; J. Electroanal. Chem., 125, 1471 (1978).

252. Böld, W., and Breiter, M.W.; Electrochim. Acta., 5, 145 (1961); see also Gilman, S.; Electrochim. Acta., 9, 1025 (1964).

253. Gileadi, E., and Conway, B.E.; Can. J. Chem., 42, 90 (1964); see also Trans. Far. Soc., 58, 2493 (1962).

254. MacDonald, D., in 'Modern Aspects of Electrochemistry', Vol. II, pp. 141, Ed. by Conway, B.E., and Bockris, J.O'M., Plenum, New York, 1975.

255. Kolb, D.M., in 'Advances in Electrochemistry and Electrochemical Engineering', Vol. II, pp. 127, Ed. by Gerischer, H., and Tobias, C., Interscience, New York, 1978.

256. Tributsch, H.; Bunsenges. Phys. Chem., 79, 570; 580 (1975); 80, 323 (1976); see also J. Bacteriol. 134, 310 (1978).

257. Woods, R.; "Electrochemistry of Sulphide Flotation" in "Flotation ", A.M. Gaudin Memorial Vol., Vol. 1, ed. M.C. Fuerstenau, AIME. New York, 1976,p 298.

258. Poling G.W.; "Reactions Between Thiol Reagents and Sulphide Minerals", ibid., p. 334.

259. Richardson, P.E. and Maust, E.E. Jr., "Surface Chemistry of Galena in Aqueous Electrolytes and its Effects on Xanthate Interactions", ibid., p. 364.

260. Leja, J.; "Surface Chemistry of Froth Flotation", Plenum Press, New York, 1982.

261. Roger, J.; "Principles of Sulphide Mineral Flotation" in "Froth Flotation", Rocky Mountain Fund Series, 50th Anniversary Vol., ed., D.W. Fuerstenau, AIME, New York, 1962, p. 139-169.

262. Ahmed, S.M., "Electrochemical Studies of Metal Sulphides in Relation to Flotation", Ch. 8 in "Recent Developments in Seperation Science", Vol. V, ed., N.N. Li, J.S. Dranoff, J.S. Schultz and P. Somasunderan, CRC Press Inc., 1979, p. 96-133.

263. Memming, R.; "charge Transfer Processes at Semiconductor Electrodes" in "Electrochemistry, A Series of Advances", Vol. 11, Ch. 1, ed., A.J. Bard, Marcel Dekken Inc., New York, 1980, p. 2.

264. Gerisher, H.; "Electron Transfer and Electrocatalysis" in "Electrocatalysis on Non-Metallic Surfaces", Proceedings of the Workshop, NBS. Gaithersburg, Maryland, Dec. 1975, ed., A.D. Franklin.

265. Gerisher H.; J. Electroanal. Chem., 150, 553, (1983).

266. Rajeshwar, K., Singh, P. and Dubow, J.; J. Electrochim Acta 23, 1117, (1978).

267. Harris, L.A. and Wilson, R.H.; Ann. Rev. Mater. Sci., 8, 99, (1978).

268. Nozik, A.J.; "Photoelectochemical Cells", Phil. Trans. R. Soc., Lond. A295, 453, (1980).

269. Morrison, S.R.; "Electrochemistry at Semiconductor and oxidised Electrodes", Plenum Press, New York, 1980.

270. Memming, R; Ber Bunsengers. Phys. Chem., 81, 733, (1977).

271. Gerisher, H. and Gobrecht, J.; Ber Bunsengers. Phys. Chem. 82, 520, (1978).